

Dynamic Evaluation of the New FOIL Instrumented Rigid Pole: FOIL Test Numbers 96F008 Through 96F015

PUBLICATION NO. FHWA-RD-99-026

DECEMBER 1998



PB99-130270

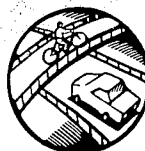


U.S. Department of Transportation
Federal Highway Administration

Research and Development
Turner-Fairbank Highway Research Center
6300 Georgetown Pike
McLean, VA 22101-2296

REPRODUCED BY:
U.S. Department of Commerce
National Technical Information Service
Springfield, Virginia 22161

NTIS



FOREWORD

The Federal Highway Administration (FHWA) Federal Outdoor Impact Laboratory (FOIL) has always had a unique feature in its instrumented rigid pole, which was designed to measure frontal and side-impact crush characteristics of small passenger vehicles. With the adoption of the National Cooperative Highway Research Program Report Number 350 (NCHRP 350) as the new crash test standard, and an increasing interest in vehicle collisions with narrow objects, the need developed for computer-generated finite element models (FEM) of full-size pickup trucks. This necessitated the need for a new, larger capacity rigid pole. A new, taller, stouter rigid pole was designed and fabricated. This report documents the test procedures and test results from seven frontal full-scale vehicle crash tests between FOIL's new rigid pole and test vehicles ranging in size from FOIL's surrogate bogie to a full-size Chevrolet C2500 pickup truck.

This report (FHWA-RD-99-026) contains test data, photographs taken with high-speed film, and a summary of the test results.

This report will be of interest to all State departments of transportation, FHWA headquarters, region and division personnel, and highway safety researchers interested in the crashworthiness of roadside safety hardware.




A. George Ostensen, Director
Office of Safety and Traffic
Operations Research and Development

NOTICE

This document is disseminated under the sponsorship of the Department of Transportation in the interest of information exchange. The United States Government assumes no liability for its contents or use thereof. This report does not constitute a standard, specification, or regulation.

The United States Government does not endorse products or manufacturers. Trade and manufacturers' names appear in this report only because they are considered essential to the object of the document.

1. Report No. FHWA-RD-99-026	2. Government Accession No.	3. Recipient's Catalog No.	
4. Title and Subtitle DYNAMIC EVALUATION OF THE NEW FOIL INSTRUMENTED RIGID POLE: FOIL TEST NUMBERS 96F008 THROUGH 96F015		5. Report Date December 1998	
		6. Performing Organization Code	
7. Author(s) Christopher M. Brown	 PB99-130270	8. Performing Organization Report No.	
9. Performing Organization Name and Address MiTech Incorporated 8484 Georgia Avenue, Suite 950 Silver Spring, MD 20910		10. Work Unit No. (TRAIS) 3A5F3142	
		11. Contract or Grant No. DTFH61-94-C-00008	
12. Sponsoring Agency Name and Address Office of Safety and Traffic Operations R&D Federal Highway Administration 6300 Georgetown Pike McLean, VA 22101-2296		13. Type of Report and Period Covered Test Report, March-July 1996	
		14. Sponsoring Agency Code	
15. Supplementary Notes Contracting Officer's Technical Representative (COTR)- Richard King, HSR-20			
16. Abstract This report contains the test procedures, test setup followed, and the test results from seven frontal full-scale vehicle crash tests conducted at the Federal Outdoor Impact Laboratory (FOIL) located at the Turner-Fairbank Highway Research Center in McLean, Virginia. The frontal collisions were between FOIL's new, larger capacity rigid pole and test vehicles ranging in size from FOIL's surrogate bogie vehicle to a full-size Chevrolet C2500 pickup truck. Two FOIL bogies, two Ford Festiva's, one Volkswagen Rabbit, one Ford pickup truck, and one Chevrolet pickup truck were accelerated to varying speeds before striking the large rigid pole. This series of seven crash tests served multiple purposes, with the main objective being to get the new, larger capacity rigid pole operational. The results from the crash tests indicated that the new rigid pole was operational and structurally sound.			
17. Key Words Rigid pole, FOIL, frontal, C2500 pickup, bogie, Festiva, VW, F150, FEM		18. Distribution Statement No restrictions. This document is available to the public through the National Technical Information Service, Springfield, VA 22161.	
19. Security Classif. (of this report) Unclassified	20. Security Classif. (of this page) Unclassified	21. No. of Pages 155	22. Price

SI* (MODERN METRIC) CONVERSION FACTORS

APPROXIMATE CONVERSIONS TO SI UNITS

APPROXIMATE CONVERSIONS FROM SI UNITS

Symbol	When You Know	Multiply By	To Find	Symbol	When You Know	Multiply By	To Find	Symbol
LENGTH								
in	inches	25.4	millimeters	mm	millimeters	0.039	inches	in
ft	feet	0.305	meters	m	meters	3.28	feet	ft
yd	yards	0.914	meters	m	meters	1.09	yards	yd
mi	miles	1.61	kilometers	km	kilometers	0.621	miles	mi
AREA								
in ²	square inches	645.2	square millimeters	mm ²	square millimeters	0.0016	square inches	in ²
ft ²	square feet	0.093	square meters	m ²	square meters	10.764	square feet	ft ²
yd ²	square yards	0.836	square meters	m ²	square meters	1.195	square yards	yd ²
ac	acres	0.405	hectares	ha	hectares	2.47	acres	ac
mi ²	square miles	2.59	square kilometers	km ²	square kilometers	0.386	square miles	mi ²
VOLUME								
fl oz	fluid ounces	29.57	milliliters	mL	milliliters	0.034	fluid ounces	fl oz
gal	gallons	3.785	liters	L	liters	0.264	gallons	gal
ft ³	cubic feet	0.028	cubic meters	m ³	cubic meters	35.71	cubic feet	ft ³
yd ³	cubic yards	0.765	cubic meters	m ³	cubic meters	1.307	cubic yards	yd ³
MASS								
oz	ounces	28.35	grams	g	grams	0.035	ounces	oz
lb	pounds	0.454	kilograms	kg	kilograms	2.202	pounds	lb
T	short tons (2000 lb)	0.907	megagrams (or "metric ton")	Mg (or "t")	megagrams (or "metric ton")	1.103	short tons (2000 lb)	T
TEMPERATURE (exact)								
°F	Fahrenheit temperature	5(F-32)/9 or (F-32)/1.8	Celcius temperature	°C	Celcius temperature	1.8C + 32	Fahrenheit temperature	°F
ILLUMINATION								
fc	foot-candles	10.76	lux	lx	lux	0.0929	foot-candles	fc
fl	foot-Lamberts	3.426	candela/m ²	cd/m ²	candela/m ²	0.2919	foot-Lamberts	fl
FORCE and PRESSURE or STRESS								
lbf	poundforce	4.45	newtons	N	newtons	0.225	poundforce	lbf
lbf/in ²	poundforce per square inch	6.89	kilopascals	kPa	kilopascals	0.145	poundforce per square inch	lbf/in ²

NOTE: Volumes greater than 1000 l shall be shown in m³.

* SI is the symbol for the International System of Units. Appropriate rounding should be made to comply with Section 4 of ASTM E380.

TABLE OF CONTENTS

<u>Section</u>	<u>Page</u>
BACKGROUND	1
SCOPE	1
TEST MATRIX	2
TEST VEHICLES	3
300K RIGID POLE	11
INSTRUMENTATION	21
<u>Speed trap</u>	21
<u>Transducer data</u>	21
<u>High-speed photography</u>	23
DATA ANALYSIS	26
<u>Speed trap</u>	26
<u>Transducer data package</u>	26
<u>High-speed photography</u>	27
RESULTS	27
CONCLUSIONS	29
APPENDIX A. DATA PLOTS	40
APPENDIX B. TEST PHOTOGRAPHS	126
REFERENCES	147

PROTECTED UNDER INTERNATIONAL COPYRIGHT
ALL RIGHTS RESERVED.
NATIONAL TECHNICAL INFORMATION SERVICE
U.S. DEPARTMENT OF COMMERCE

LIST OF FIGURES

<u>Figure No.</u>	<u>Page</u>
1. Sketch of the bogie vehicle	4
2. Sketch of low-speed honeycomb configuration	5
3. Vehicle properties for test 96F010	7
4. Vehicle properties for tests 96F011 and 96F012	8
5. Vehicle properties for test 96F014	9
6. Vehicle properties for test 96F015	10
7. Sketch of new 300K rigid pole	14
8. Sketch of old rigid pole	16
9. Photographs of new 300K rigid pole frontal configuration	18
10. Photographs of old rigid pole frontal configuration and side-impact configuration	20
11. Layout of the test setup	25
12. Comparison of bogie testing, acceleration vs. time (load cell), tests 92F028 and 96F008	31
13. Comparison of bogie testing, velocity vs. time (load cell), tests 92F028 and 96F008	32
14. Comparison of bogie testing, displacement vs. time (load cell), tests 92F028 and 96F008	33
15. Comparison of bogie testing, force vs. displacement (load cell), tests 92F028 and 96F008	34
16. Comparison of Festiva testing, acceleration vs. time (load cell), tests 94F011 and 96F011	35
17. Comparison of Festiva testing, displacement vs. time (load cell), tests 94F011 and 96F011	36
18. Comparison of Festiva testing, energy vs. displacement (load cell), tests 94F011 and 96F011	37
19. Comparison of Festiva testing, force vs. displacement (load cell), tests 94F011 and 96F011	38
20. Visual comparison of the Ford Festiva, tests 94F011 and 96F011	39
21. Acceleration vs. time, test 96F008	40
22. Nose acceleration vs. time, test 96F008	41
23. Velocity vs. time, accelerometer data, test 96F008	42
24. Displacement vs. time, accelerometer data, test 96F008	43
25. Force vs. time, load-cell data, test 96F008	44
26. Force vs. displacement, load-cell data, test 96F008	45
27. Energy vs. displacement, load-cell data, test 96F008	46
28. Resultant load height vs. time, test 96F008	47
29. Acceleration vs time, test 96F009	48
30. Nose acceleration vs. time, test 96F009	49
31. Velocity vs. time, test 96F009	50
32. Displacement vs. time, test 96F009	51
33. Force vs. time, load-cell data, test 96F009	52
34. Force vs. displacement, load-cell data, test 96F009	53
35. Energy vs. displacement, load-cell data, test 96F009	54
36. Resultant load height vs. time, test 96F009	55
37. Acceleration vs. time, test 96F010	56
38. Velocity vs. time, test 96F010	57
39. Displacement vs. time, test 96F010	58

LIST OF FIGURES (Continued)

<u>Figure No.</u>		<u>Page</u>
40.	Force vs. time, load-cell data, test 96F010	59
41.	Force vs. displacement, load-cell data, test 96F010 . . .	60
42.	Energy vs. displacement, load-cell data, test 96F010 . .	61
43.	Acceleration vs. time, Y-axis, test 96F010	62
44.	Acceleration vs. time, Z-axis, test 96F010	63
45.	Acceleration vs. time, test 96F011	64
46.	Velocity vs. time, test 96F011	65
47.	Displacement vs. time, test 96F011	66
48.	Force vs. time, load-cell data, test 96F011	67
49.	Force vs. displacement, test 96F011	68
50.	Energy vs. displacement, load-cell data, test 96F011 . .	69
51.	Acceleration vs. time, Y-axis, test 96F011	70
52.	Acceleration vs. time, Z-axis, test 96F011	71
53.	Resultant load height vs. time, test 96F011	72
54.	Acceleration vs. time, top of engine, test 96F011 . . .	73
55.	Acceleration vs. time, bottom of engine, test 96F011 . .	74
56.	Acceleration vs. time, left control arm, test 96F011 . .	75
57.	Acceleration vs. time, right control arm, test 96F011 . .	76
58.	Acceleration vs. time, instrument panel, test 96F011 . .	77
59.	Acceleration vs. time, left-rear seat, test 96F011 . . .	78
60.	Acceleration vs. time, right-rear seat, test 96F011 . . .	79
61.	Acceleration vs. time, test 96F012	80
62.	Velocity vs. time, test 96F012	81
63.	Displacement vs. time, test 96F012	82
64.	Force vs. time, load-cell data, test 96F012	83
65.	Force vs. displacement, load-cell data, test 96F012 . . .	84
66.	Energy vs. displacement, load-cell data, test 96F012 . .	85
67.	Acceleration vs. time, Y-axis, test 96F012	86
68.	Acceleration vs. time, Z-axis, test 96F012	87
69.	Resultant load height vs. time, test 96F012	88
70.	Acceleration vs. time, top of engine, test 96F012	89
71.	Acceleration vs. time, bottom of engine, test 96F012 . .	90
72.	Acceleration vs. time, left control arm, test 96F012 . .	91
73.	Acceleration vs. time, right control arm, test 96F012 . .	92
74.	Acceleration vs. time, instrument panel, test 96F012 . .	93
75.	Acceleration vs. time, left-rear seat, test 96F012 . . .	94
76.	Acceleration vs. time, right-rear seat, 96F012	95
77.	Acceleration vs. time, test 96F014	96
78.	Velocity vs. time, test 96F014	97
79.	Displacement vs. time, test 96F014	98
80.	Force vs. time, load-cell data, test 96F014	99
81.	Force vs. displacement, load-cell data, test 96F014 . . .	100
82.	Energy vs. displacement, load-cell data, test 96F014 . .	101
83.	Acceleration vs. time, Y-axis, test 96F014	102
84.	Acceleration vs. time, Z-axis, test 96F014	103
85.	Resultant load height vs. time, test 96F014	104
86.	Acceleration vs. time, top of engine, test 96F014	105
87.	Acceleration vs. time, bottom of engine, test 96F014 . .	106
88.	Acceleration vs. time, left control arm, test 96F014 . .	107
89.	Acceleration vs. time, instrument panel, test 96F014 . .	108
90.	Acceleration vs. time, left-rear seat, test 96F014 . . .	109

LIST OF FIGURES (Continued)

<u>Figure No.</u>	<u>Page</u>
91. Acceleration vs. time, right-rear seat, test 96F014 . .	110
92. Acceleration vs. time, test 96F015	111
93. Velocity vs. time, test 96F015	112
94. Displacement vs. time, test 96F015	113
95. Force vs. time, load-cell data, test 96F015	114
96. Force vs. displacement, load-cell data, test 96F015 . .	115
97. Energy vs. displacement, load-cell data, test 96F015 .	116
98. Acceleration vs. time, Y-axis, test 96F015	117
99. Acceleration vs. time, Z-axis, test 96F015	118
100. Resultant load height vs. time, test 96F015	119
101. Acceleration vs. time, top of engine, test 96F015 . .	120
102. Acceleration vs. time, bottom of engine, test 96F015 .	121
103. Acceleration vs. time, left control arm, test 96F015 .	122
104. Acceleration vs. time, right control arm, test 96F015 .	123
105. Acceleration vs. time, instrument panel, test 96F015 .	124
106. Acceleration vs. time, left-rear seat, test 96F015 . .	125
107. Test photographs during impact, test 96F008	126
108. Test photographs during impact, test 96F009	127
109. Test photographs during impact, test 96F010	128
110. Test photographs during impact, test 96F011	129
111. Test photographs during impact, test 96F012	130
112. Test photographs during impact, test 96F014	131
113. Test photographs during impact, test 96F015	132
114. Pretest photographs, test 96F008	133
115. Post-test photographs, test 96F008	134
116. Pretest photographs, test 96F009	135
117. Post-test photographs, test 96F009	136
118. Pretest photographs, test 96F010	137
119. Post-test photographs, test 96F010	138
120. Pretest photographs, test 96F011	139
121. Post-test photographs, test 96F011	140
122. Pretest photographs, test 96F012	141
123. Post-test photographs, test 96F012	142
124. Pretest photographs, test 96F014	143
125. Post-test photographs, test 96F014	144
126. Pretest photographs, test 96F015	145
127. Post-test photographs, test 96F015	146

LIST OF TABLES

<u>Table No.</u>	<u>Page</u>
1. Test matrix for the 300K rigid pole	3
2. Rigid pole comparison summary	11
3. FMVSS 208 instrumentation, Ford Festiva tests	22
4. FMVSS 208 instrumentation, Chevrolet C2500 truck	22
5. Summary of camera placement	24
6. Summary of results for 300K rigid pole testing	28

BACKGROUND

One unique feature of the Federal Highway Administration's (FHWA) Federal Outdoor Impact Laboratory (FOIL) has been its instrumented rigid pole. The rigid pole was designed to measure frontal and side-impact crush characteristics of small passenger vehicles. The data were used to develop surrogate test vehicles, finite element vehicle models, and vehicle safety standards. The primary design parameter for the rigid pole was based on impacts with small vehicles (820 kg) and 222,000 N striking the pole at 760 mm above its base. With the adoption of the National Cooperative Highway Research Program Report Number 350 (NCHRP Report 350)⁽¹⁾ as the new crash test standard for roadside safety features and an increasing interest in vehicle collisions with narrow objects, the need developed for computer-generated finite element models (FEM) of full-size pickup trucks. The first step was to collect frontal and side-impact crash test data to develop and validate the truck FEMs. This necessitated the need for a new, larger capacity rigid pole. The original FOIL rigid pole was too short to accommodate side-impacts with vehicles standing taller than 1.5 m, and not stout enough to withstand a frontal collision from a full-size pickup truck. A new, taller, stouter rigid pole was designed and fabricated in order to conduct narrow-object frontal and broadside collisions using minivans, sport utility vehicles, and pickup trucks. The design parameters for the new rigid pole were to be able to capture the taller profiles of pickup trucks during a broadside collision and to withstand the force from a 2000-kg pickup truck traveling at 55 km/h, or the force required to exhaust the energy-absorbing capacity of a pickup truck's front end (i.e., bumper, radiator, engine compartment, firewall, etc.). The design load capacity chosen was 1.3 MN.

SCOPE

This report documents the test procedures and test setup followed, and the test results from seven frontal full-scale vehicle crash tests conducted at FHWA's FOIL, located at the Turner-Fairbank Highway Research Center (TFHRC) in McLean, Virginia. The frontal collisions were between FOIL's new large instrumented rigid pole and test vehicles ranging in size from FOIL's surrogate bogie vehicle to a full-size Chevrolet C2500 pickup truck. Two FOIL bogies, two Ford Festiva's, one Volkswagen Rabbit, one Ford pickup truck, and one Chevrolet pickup truck were accelerated to varying speeds before striking the large rigid pole. The series of seven crash tests served multiple purposes, with the main objective being to get the new larger capacity rigid pole operational. The multiple objectives of these tests were as follows:

- To verify that the delivered rigid pole met the design specifications visually and structurally and that all sensors delivered with the pole were in working condition.
- To ensure that the larger diameter of the frontal impact face did not produce different crush characteristics in vehicles previously tested against the old, smaller rigid pole.
- To gradually build up the force on the rigid pole using increasingly heavier, faster vehicles. This was to observe different components of the pole to ensure their ability to withstand the peak design load.
- To collect force-deflection or crush characteristic data for a Chevrolet C2500 pickup truck. Force-deflection data are used by the FEM simulation community to develop and validate vehicle FEMs.

The results from the crash tests indicated that the rigid pole was operational and structurally sound. The two FOIL bogie tests and two Ford Festiva tests showed that the new, larger diameter pole did not drastically change the force-deflection characteristic of each respective vehicle. The pickup truck tests showed that their front-end energy-absorbing capacity was exhausted at a test speed of 48 km/h. The large rigid pole was capable of withstanding the force from this collision and the data supplied simulation engineers with the information needed to develop and validate a FEM of a full-size pickup truck.

TEST MATRIX

Seven crash tests were conducted on FOIL's new, higher capacity rigid pole. The tests were conducted using vehicles that varied in size and weight and were traveling at different speeds. Table 1 is the test matrix for the seven rigid pole tests. The two FOIL bogie tests were conducted as a means to impart the first dynamic load on the rigid pole. They were also conducted to ensure that the force-deflection characteristic produced did not differ from previously conducted bogie tests on the old rigid pole. Following this rationale, the two Ford Festiva tests were conducted. A centerline test and a $\frac{1}{4}$ -point test were conducted to ensure that force-deflection characteristics at different locations were not affected by the increased diameter of the new rigid pole. The Volkswagen Rabbit test was conducted as a means to impart a greater dynamic load on the rigid pole. The Rabbit was ballasted up to 907 kg and was accelerated to a nominal speed of 53 km/h. The heavier, faster Rabbit imparted a force on the rigid pole greater than that produced from the lighter, slower bogie and the Festiva vehicles. After verification that the rigid pole withstood the collisions, the pickup truck tests were conducted. The first truck, a Ford F150, was ballasted to 1941 kg and was accelerated to a nominal

speed of 45 km/h. The rigid pole withstood the impact and the Chevrolet pickup truck test was conducted. Because the Ford F150's front end was completely collapsed by the rigid pole, only a slight increase in speed was implemented during the Chevrolet C2500 pickup truck test. The Chevrolet C2500 pickup truck had a mass of 2051 kg. An uninstrumented dummy was placed in the driver's seat of the Chevrolet C2500. This was done to observe the dummy kinematics during an impact with a narrow fixed object. A dummy was not used in the previous six tests.

Table 1. Test matrix for the 300K rigid pole.					
Test Number	Test Date	Test Vehicle	Test Speed (km/h)	Vehicle Mass (kg)	Location of Impact
96F008	4-24-96	FOIL bogie	35	839	Center
96F009	5-15-96	FOIL bogie	37	839	Center
96F010	5-22-96	Volkswagen Rabbit	53	907	Center
96F011	6-05-96	Ford Festiva	35	820	Center
96F012	6-18-96	Ford Festiva	35	816	Driver ¼-point
96F014	7-11-96	Ford F150 pickup	45	1941	Center
96F015	7-26-96	Chevrolet C2500 pickup	48	2051	Center

TEST VEHICLES

The test vehicles included the FOIL surrogate bogie vehicle, a 1979 Volkswagen (VW) Rabbit, a 1988 and a 1990 Ford Festiva, a 1981 Ford F150 pickup truck, and a 1994 Chevrolet C2500 pickup truck.

The FOIL bogie vehicle uses a honeycomb material in a sliding nose to simulate the crush characteristics of an 839-kg small vehicle — more specifically, a 1979 VW Rabbit.⁽²⁾ The height of the bogie vehicle's nose was 444 mm, which corresponds to the bumper height of a VW Rabbit. Figure 1 is a sketch of the bogie vehicle. Figure 2 depicts the honeycomb configuration used in the two bogie tests.

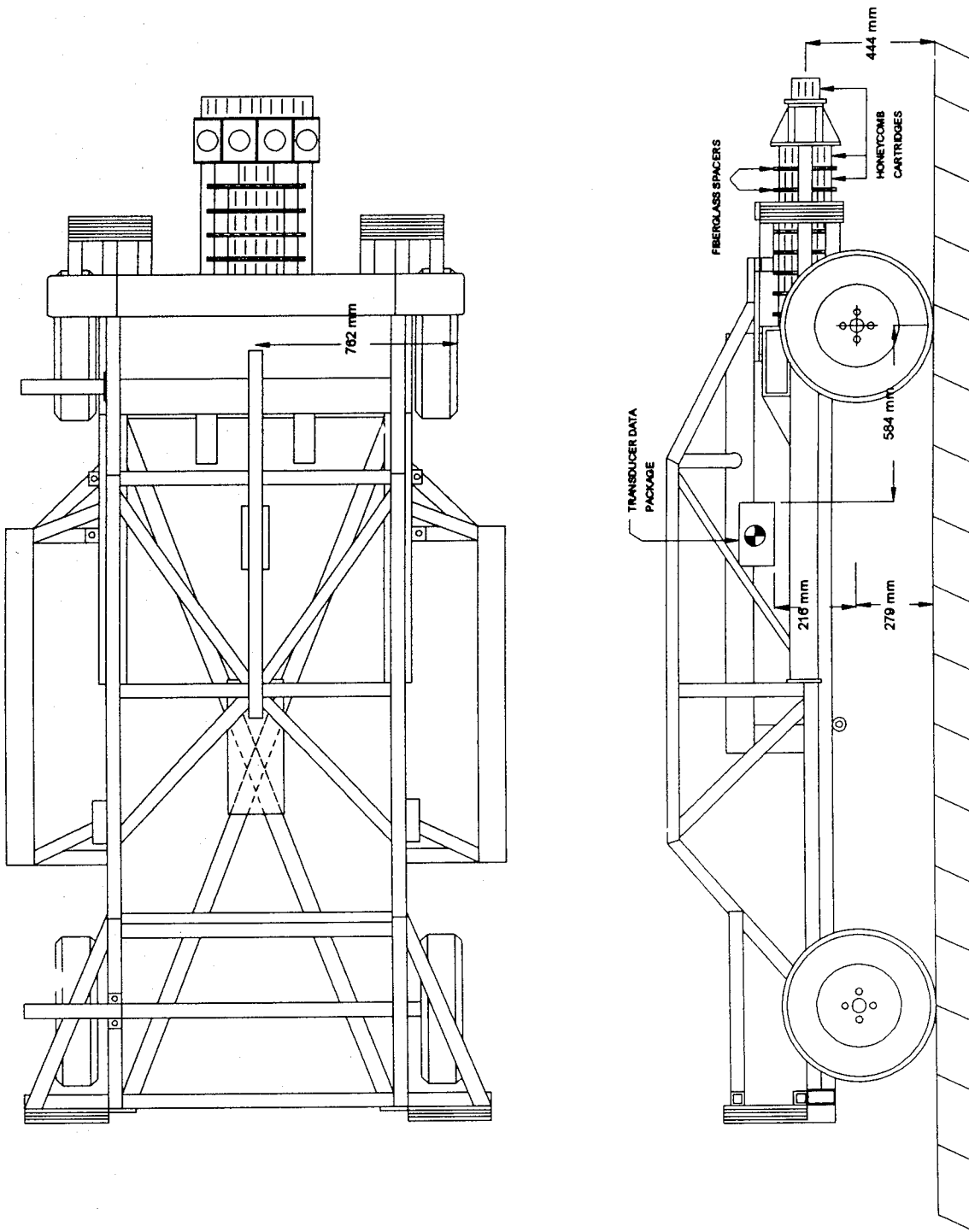
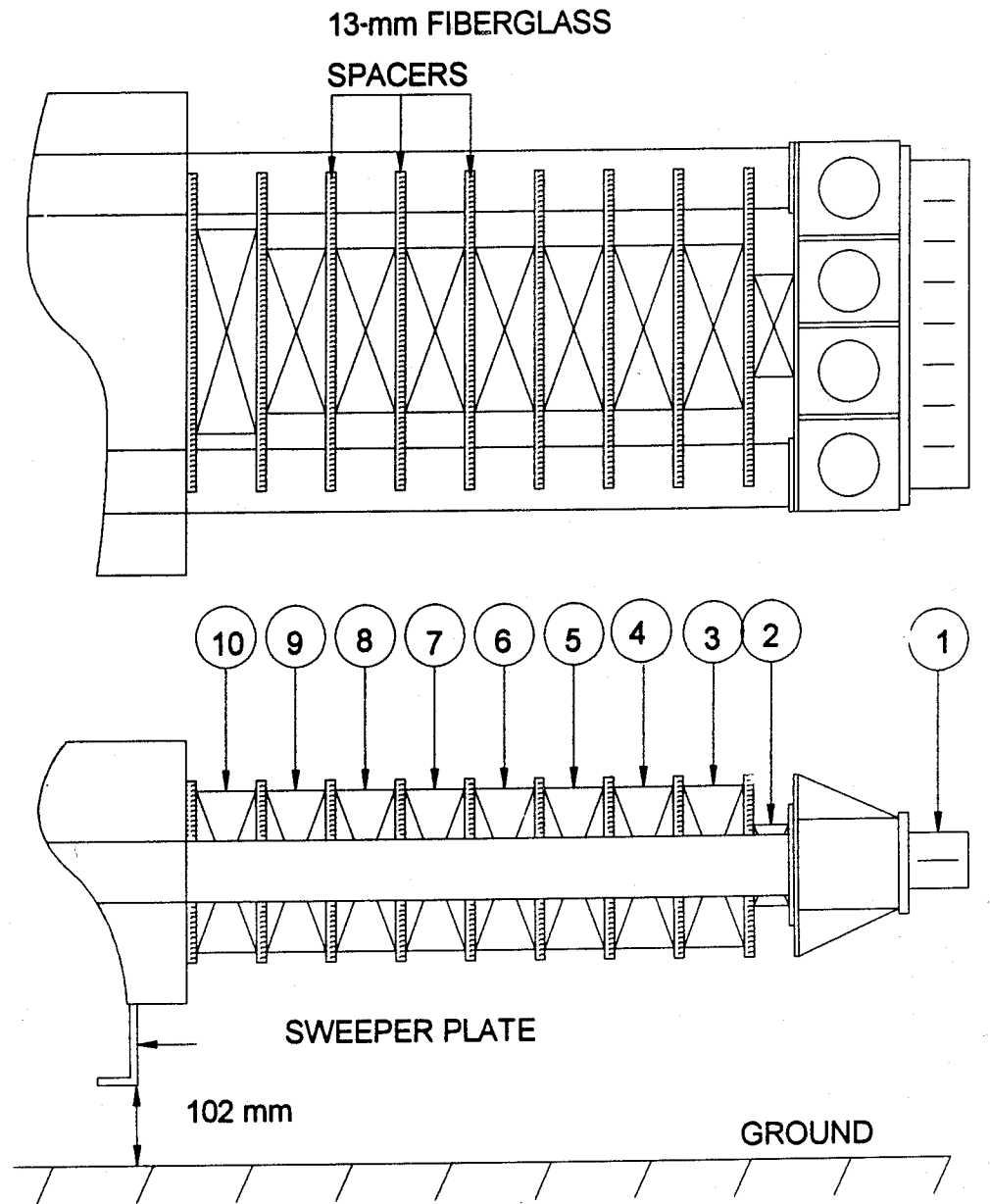


Figure 1. Sketch of the bogie vehicle.



Cartridge Number	Size (mm) / punch (mm ²)	Static Crush Strength(kPa)
1	70 x 406 x 76	896
2	102 x 127 x 51	172
3	203 x 203 x 76 / 13,545	896
4	203 x 203 x 76 / 9,675	1,585
5	203 x 203 x 76 / 3,870	1,585
6	203 x 203 x 76	1,585
7	203 x 203 x 76 / 13,545	2,756
8	203 x 203 x 76 / 7,740	2,756
9	203 x 203 x 76	2,756
10	203 x 254 x 76	2,756

Figure 2. Sketch of low-speed honeycomb configuration.

An old, rusted 1979 VW Rabbit was used as a means to impart a high dynamic load on the new rigid pole. All fluids were drained prior to testing. No vehicle components were removed from the vehicle. Data acquisition equipment, sensors, guidance system components, and ballast were added to the vehicle with the final mass of the Rabbit equaling 907 kg. The bumper height of the Rabbit was 444 mm. Figure 3 is a sketch showing the physical parameters of the VW Rabbit.

The 1988 and 1990 Ford Festiva's were two-door hatchbacks with manual transmissions. Prior to testing, all fluids were drained. The vehicles were stripped of certain components to allow for the installation of data acquisition equipment, sensors, a remote braking system, and guidance system components. No components were removed from the engine compartment. The target test mass for the vehicles was 820 kg. An anthropomorphic dummy was not placed in the vehicle. Figure 4 shows the physical properties and dimensions of both model years.

The Ford F150 pickup truck was used as a means to impart a higher dynamic load on the rigid pole than typically observed by passenger sedans at low speeds. The fluids were drained and the longitudinal and lateral location of the center of gravity (c.g.) was determined prior to and again after instrumentation. No components were removed from the truck. Data acquisition equipment, sensors, and guidance system components were installed in the truck and the final weight was determined. The target weight was 1950 kg. The weight is greater than passenger sedans, but lower than a full-size pickup truck as specified in NCHRP 350. Figure 5 lists some physical parameters of the Ford F150 pickup truck.

The truck specified in NCHRP 350 has a test weight of 2000 kg. A 1994 Chevrolet C2500 pickup truck was used to load the rigid pole with a higher peak force than the Ford F150. The fluids were drained and the longitudinal and lateral location of the c.g. was determined prior to and again after instrumentation. No components were removed from the truck. Data acquisition equipment, sensors, and guidance system components were installed in the truck and the final weight was determined. A dummy was placed in the driver position and was restrained using the belt restraining system within the truck. The dummy was not instrumented; it was used for ballast and to observe occupant kinematics. The target test weight was 2000 kg. Fully instrumented, the Chevrolet C2500 weighed 2051 kg. With one uninstrumented dummy, the test weight of the vehicle was 2128 kg. Figure 6 shows the physical parameters of the Chevrolet C2500 pickup truck.

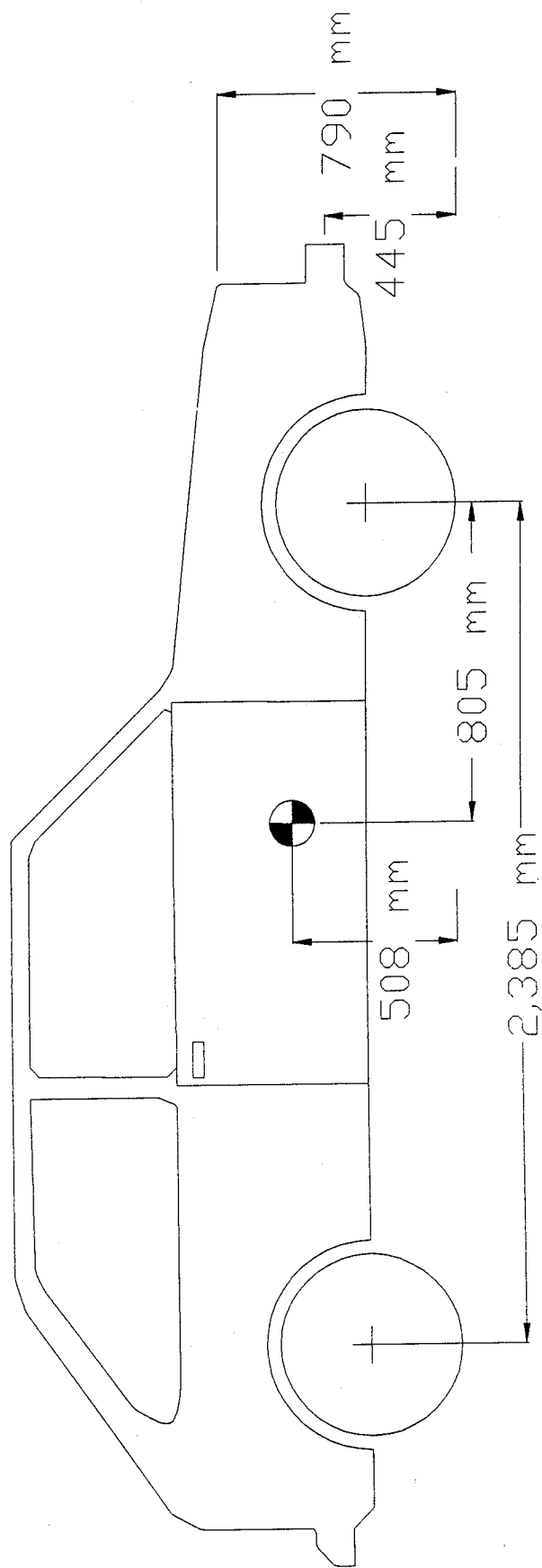
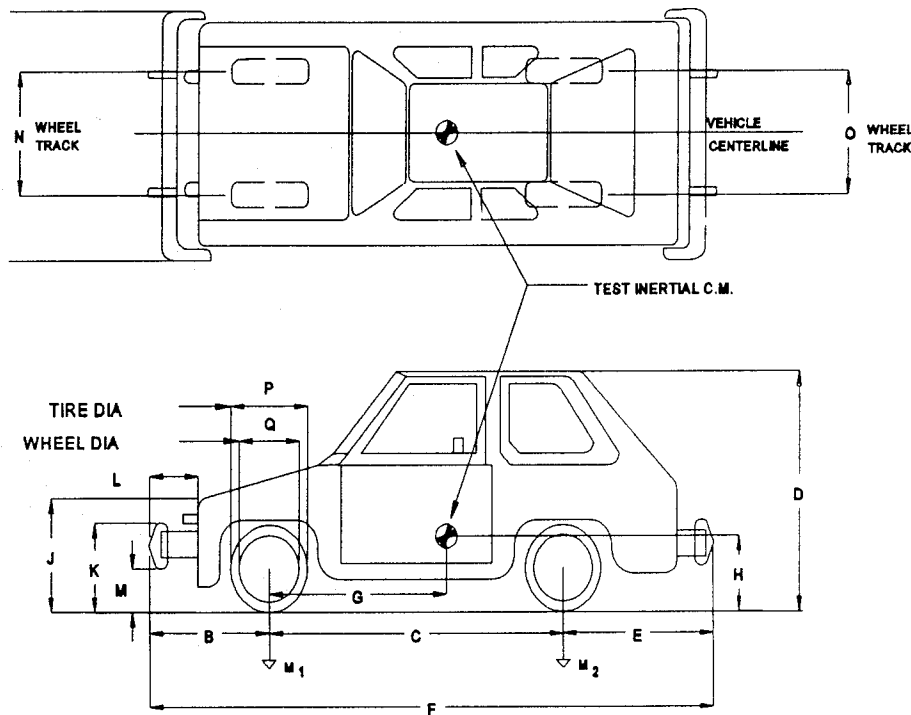


Figure 3. Vehicle properties for test 96F010.

DATES: JUNE 15 AND 22, 1996 TEST NUMBERS: 96F011/96F012 MAKE: FORD
 MODEL: FESTIVA YEAR: 1988 AND 1990 ODOMETER: _____ GVW: _____
 TIRE SIZE: _____ VIN NUMBER: _____ TREAD TYPE: _____
 MASS DISTRIBUTION: CURB: LF 241 RF 231 LR 144 RR 127
 TEST INERTIAL: LF 238 RF 262 LR 147 RR 173

DESCRIBE ANY DAMAGE TO VEHICLE PRIOR TO TEST:



ENGINE TYPE: 4 CYLINDER

ENGINE CID: _____

TRANSMISSION TYPE:

 AUTO

 X MANUAL

OPTIONAL EQUIPMENT:

DUMMY DATA:

TYPE: _____

MASS: _____

SEAT POSITION: _____

GEOMETRY

A <u>1556</u>	E <u>521</u>	J <u>953</u>	N <u>1397</u>	R _____
B <u>673</u>	F <u>3531</u>	K <u>546</u>	O <u>1403</u>	S _____
C <u>2305</u>	G <u>876</u>	L <u>102</u>	P <u>533</u>	T _____
D <u>1454</u>	H <u>533</u>	M <u>406</u>	Q <u>305</u>	U _____

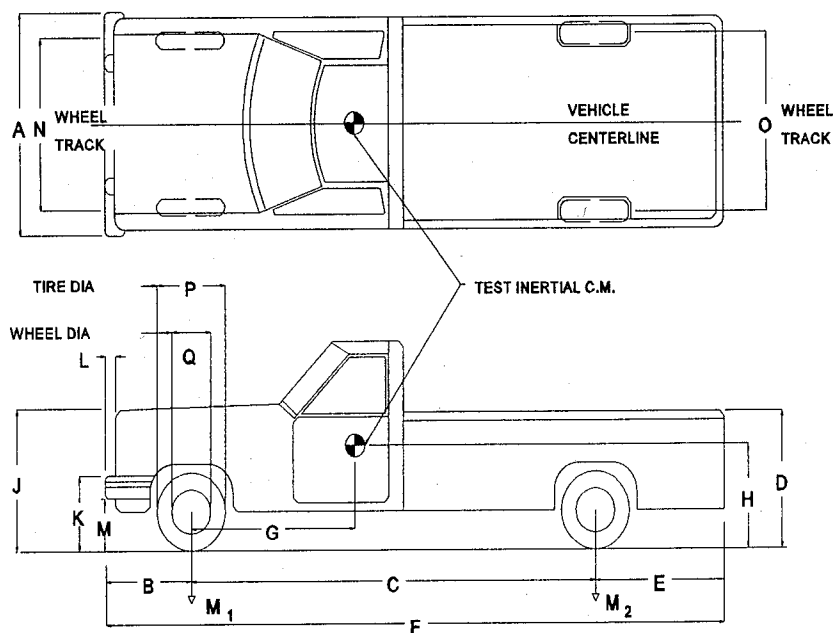
<u>MASS</u>	<u>CURB</u>	<u>TEST</u> <u>INERTIAL</u>	<u>GROSS</u> <u>STATIC</u>
M_1	<u>472</u>	<u>500</u>	_____
M_2	<u>271</u>	<u>320</u>	_____
M_T	<u>743</u>	<u>820</u>	_____

Figure 4. Vehicle properties for tests 96F011 and 96F012.

DATE: JULY 11, 1996 TEST NO: 96F014 TIRE PRESSURE: 50 psi MAKE: FORD
 MODEL: F-150 YEAR: 1981 ODOMETER: 163,415 km GVW: 2766 kg
 TIRE SIZE: 10R15 VIN NUMBER: 1FTEF1SE9BNA23216 TREAD TYPE: ALL-TERRAIN
 MASS DISTRIBUTION: CURB: LF _____ RF _____ LR _____ RR _____
 TEST INERTIAL: LF _____ RF _____ LR _____ RR _____

DESCRIBE ANY DAMAGE TO VEHICLE PRIOR TO TEST:

RUST



ENGINE TYPE: IN-LINE 6 CYL

ENGINE CID: 4.9 LITER

TRANSMISSION TYPE:

 AUTO

 X MANUAL

OPTIONAL EQUIPMENT:

DUMMY DATA:

TYPE: N/A

MASS: N/A

SEAT POSITION: N/A

GEOMETRY

A	<u>1905</u>	E	<u>135</u>	J	<u>1145</u>	N	<u>1640</u>	R	<u> </u>
B	<u>790</u>	F	<u>4305</u>	K	<u>585</u>	O	<u>1640</u>	S	<u> </u>
C	<u>3380</u>	G	<u>N/A</u>	L	<u>890</u>	P	<u>735</u>	T	<u> </u>
D	<u>1165</u>	H	<u>N/A</u>	M	<u>335</u>	Q	<u>380</u>	U	<u> </u>

<u>MASS</u>	<u>CURB</u>	<u>TEST INERTIAL</u>	<u>GROSS STATIC</u>
M ₁	<u> </u>	<u> </u>	<u> </u>
M ₂	<u> </u>	<u> </u>	<u> </u>
M _T	<u> </u>	<u>1946</u>	<u>1946</u>

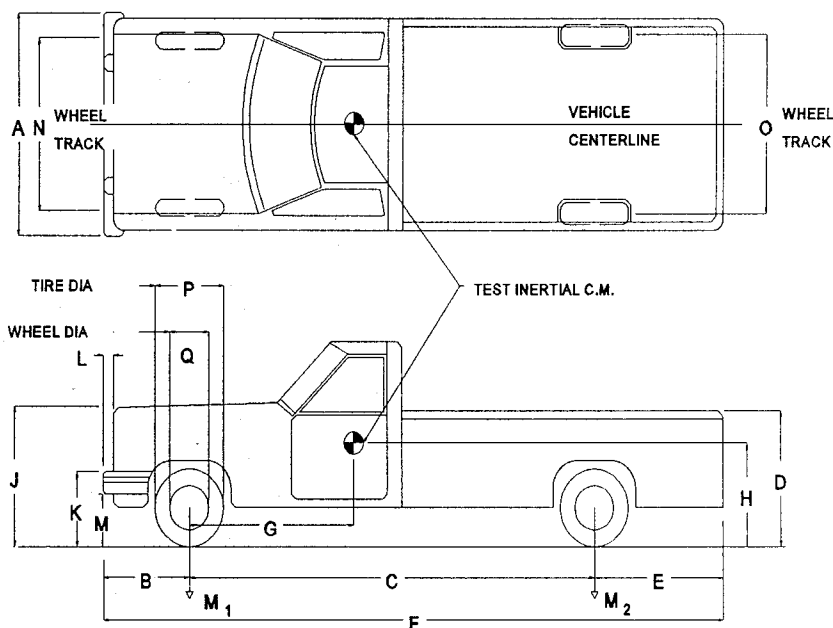
1 psi = 6.89 kPa

Figure 5. Vehicle properties for test 96F014.

DATE: 7-17-96 TEST NO: 96F015 TIRE PRESSURE: 40 psi MAKE: CHEVROLET
 MODEL: C2500 YEAR: 1994 ODOMETER: 35,667 km GVW: 4473 CURB
 TIRE SIZE: 275/80-16 VIN NUMBER: 1GCGC24K3RE102616 TREAD TYPE: SMOOTH
 MASS DISTRIBUTION: CURB: LF 601 RF 537 LR 383 RR 508
 TEST INERTIAL: LF 522 RF 645 LR 541 RR 344

DESCRIBE ANY DAMAGE TO VEHICLE PRIOR TO TEST:

TAILGATE HAS 2 DENTS IN TOP



ENGINE TYPE: GAS V8

ENGINE CID: 350

TRANSMISSION TYPE:

AUTO

X MANUAL

OPTIONAL EQUIPMENT:

AC, CARGO LIGHT

TOW PACKAGE

DUMMY DATA:

TYPE: UNINSTALLED FRONTAL

IMPACT DUMMY

MASS: 77 KG

SEAT POSITION: DRIVER

GEOMETRY

A <u>1835</u>	E <u>1295</u>	J <u>1168</u>	N <u>1607</u>	R _____
B <u>895</u>	F <u>5556</u>	K <u>648</u>	O <u>1607</u>	S _____
C <u>3391</u>	G <u>1473</u>	L <u>95</u>	P <u>737</u>	T _____
D <u>1842</u>	H _____	M <u>432</u>	Q <u>432</u>	U _____

MASS	CURB	TEST INERTIAL	GROSS STATIC
M ₁	<u>1138</u>	<u>1167</u>	<u>1210</u>
M ₂	<u>891</u>	<u>885</u>	<u>919</u>
M _T	<u>2029</u>	<u>2051</u>	<u>2128</u>

1 psi = 6.89 kPa

Figure 6. Vehicle properties for test 96F015.

300K RIGID POLE

The functional purpose of the new rigid pole remained the same as that of the older, smaller rigid pole. The poles were fabricated to measure vehicle crush properties. Frontal and side crush characteristics can be determined using either rigid pole. However, the older, smaller rigid pole was not tall enough to capture the side profile of trucks, vans, and sport utility vehicles, nor was it stout enough to withstand a frontal impact from the same larger vehicles. The design load for the older rigid pole was 222 kN, striking the pole 760 mm above ground. A new, taller, higher load capacity rigid pole was designed and fabricated. Using computer simulation analysis, the design load chosen for the new pole was 1.3 MN, striking the rigid pole 890 mm above ground. The new rigid pole design utilized the same design concepts of the old rigid pole. Each pole consisted of four major structural components: (1) the impact faces (frontal and side-impact configuration); (2) the connecting rods to transfer the load from the impact faces to the load cells; (3) a vertical box beam, which is the main structural element; and (4) a rear brace and strut to tie the main concrete foundation to an auxiliary concrete foundation. The old rigid pole was constructed using ASTM A36 steel, while the new pole was almost entirely constructed from ASTM A572 steel (a 39-percent increase in the steel yield strength). Each rigid pole utilized Interface, Incorporated load cells to measure the forces on the rigid poles. The side-impact configuration of the rigid pole can use either 111-kN or 222-kN capacity load cells at any location, as in the old rigid pole. The old rigid pole used the same load cells in the frontal configuration. However, the capacity of the load cells used on the new rigid pole in the frontal impact configuration had to be increased to 445 kN to accommodate the anticipated dynamic load from a full-size pickup truck. Table 2 summarizes the differences between the two rigid poles.

Table 2. Rigid pole comparison summary.						
	Height (mm)	Pole system weight(kg) frontal	Design load height (mm)	Design load(kN)	Number of impact faces and load cells	
					Frontal	Side- impact
Old rigid pole	1525	695	760	222	1 / 2	3 / 6
300K rigid pole	2135	1860	890	1335	1 / 2	4 / 8

The old rigid pole's frontal and side-impact configuration impact faces were comprised of reinforced semicircular 205-mm extra-heavy-walled steel pipe (220-mm outer diameter). Three faces were used for the side-impact mode and one longer face was

used for frontal impacts. The cross-sectional area of the faces was 4032 mm^2 . Each face had a shear strength of 605 kN (using 250-N/mm² steel, ASTM A36). The new rigid pole was designed using 255-mm-diameter solid semicircular steel impact faces for side-impact and a 205-mm x 125-mm steel block nested inside a notched 305-mm-diameter solid semicircular face for frontal impacts. The cross-sections for the new pole's impact faces were $25,160 \text{ mm}^2$ (side-impact) and $52,000 \text{ mm}^2$ (frontal). The shear strength for the new pole's faces increased to 5.2 MN (side-impact) and 10.8 MN (frontal), using 345-N/mm² steel (ASTM A572).

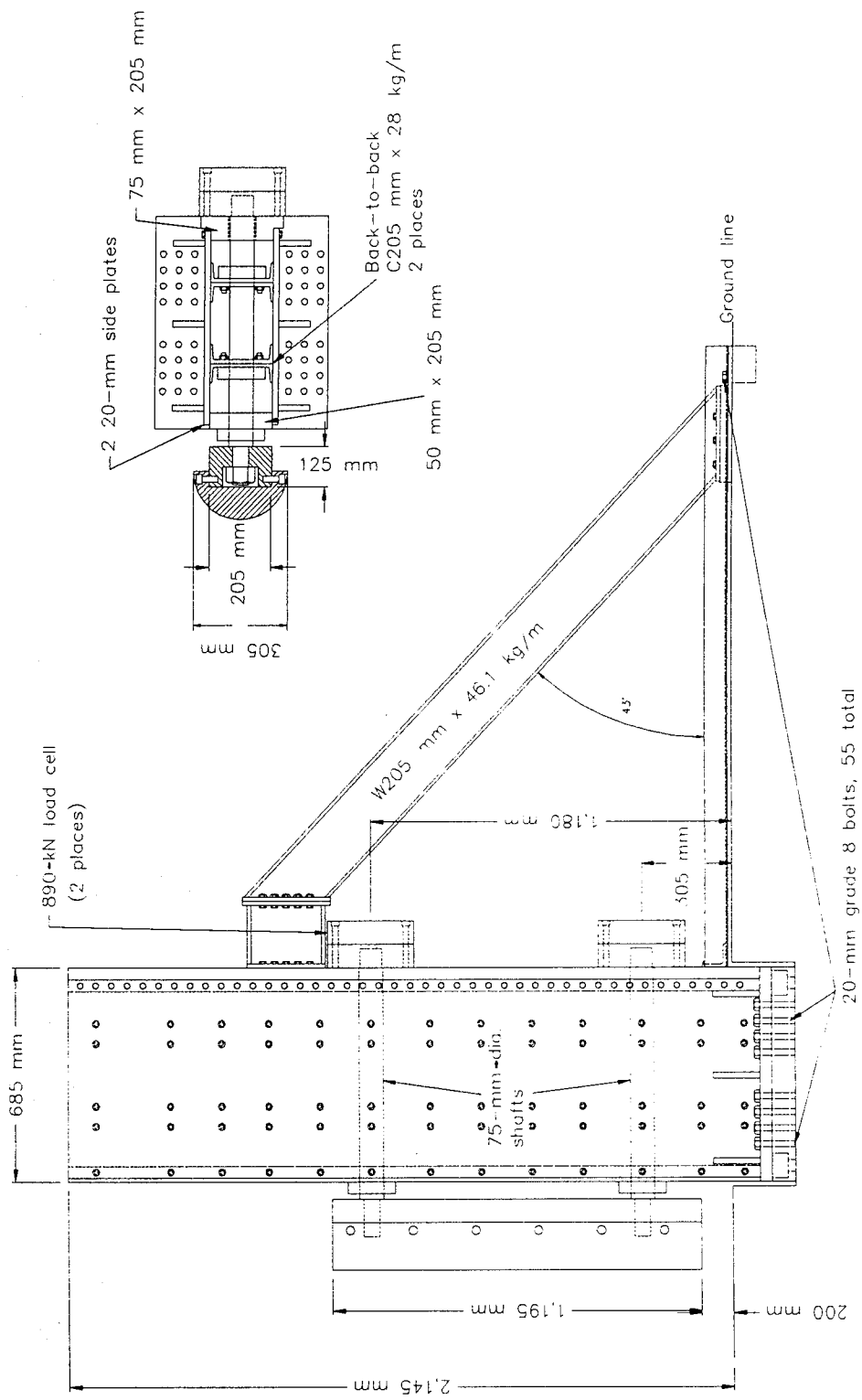
Two connecting rods per impact face were used to transfer the impact load from the impact faces back to the load cell attached to the rear of the rigid poles. The old pole utilized 50-mm-diameter rods for both frontal and side-impacts. The new pole utilized longer 50-mm-diameter rods for side-impact and 75-mm-diameter rods for frontal impact configurations. The critical buckling stress (F_c) for the side-impact rods in the new pole was 248 N/mm^2 for a load capacity of 500 kN per rod. The 75-mm rod used for frontal impacts in the new pole had an F_c equal to 293 N/mm^2 for a total load capacity of 1.3 MN per rod. All rods in the new rigid pole were fabricated using ASTM A572 steel. The load capacity of the rods was sufficient to withstand the anticipated load from the Chevrolet C2500.

The vertical box beam is the main structure for both rigid poles. The vertical box beam of the old rigid pole was constructed from two 12-mm steel side plates welded and bolted to four C180-mm x 14.6-kg/m channels. The cross-sectional area and area moment of inertia (I_s) of the box section was approximately $21,290 \text{ mm}^2$ and $4.2 \times 10^6 \text{ mm}^4$, respectively. All steel used to fabricate the old vertical box beam was ASTM A36 steel. The vertical box section of the new rigid pole retained the general concept. However, the side plates were fabricated from 20-mm-thick plate, and the end channels were replaced using a 50-mm x 205-mm plate in the front and a 75-mm x 205-mm plate in the rear. Each of the inside channels of the old pole design were replaced using two back-to-back C205-mm x 28-kg/m channels. The cross-sectional area and I_s for the new pole design increased to $64,200 \text{ mm}^2$ and $3.5 \times 10^9 \text{ mm}^4$. The maximum bending stress on the vertical box beam from a 1.3-MN load at an elevation of 890 mm was 50 N/mm^2 . The shear capacity of the vertical box beam is 13.3 MN.

To reduce the overturning moment on the vertical box beam, a rear brace was fastened to the beam and the rear auxiliary concrete foundation. The two foundations were tied together using a heavy C section span between the bottom of the vertical box beam and the rear foundation. The old pole design used a W205-mm x 22.3-kg/m brace and a C305-mm x 30.8-kg/m foundation strut. The new design increased the size of the brace and strut to W205 mm x 46.1 kg/m and C380 mm x 50.4 kg/m, respectively.

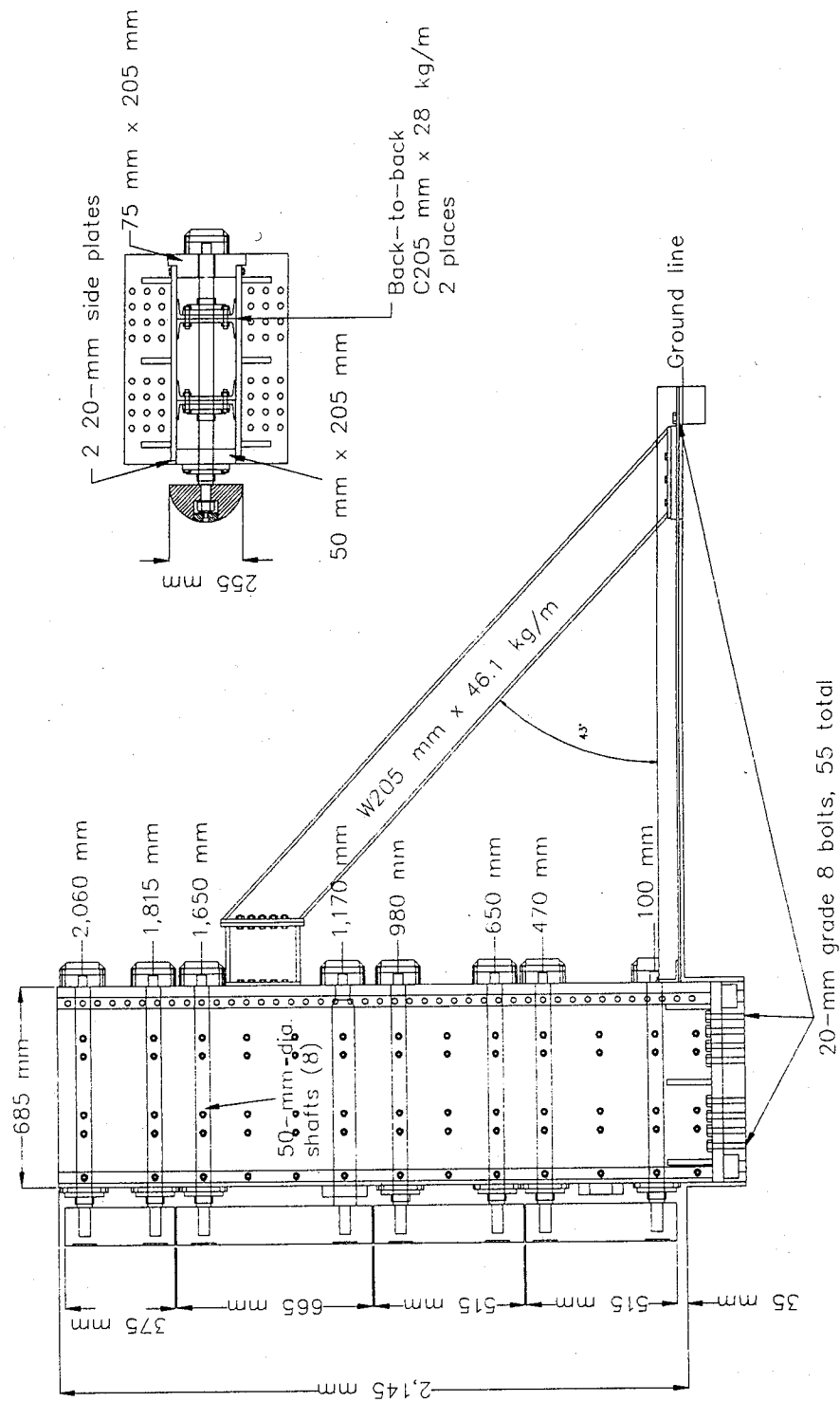
The base of the new rigid pole's vertical box-beam assembly was bolted to the FOIL runway foundation using 48 20-mm grade 8 bolts torqued to 475 N·m. Seven additional bolts were used to bolt the rear strut to the auxiliary foundation. The old rigid pole used 12 20-mm grade 5 bolts total.

Sketches of the new and old rigid poles are shown in figures 7 and 8, respectively. Photographs of each pole are shown in figures 9 and 10.



FOIL 300K rigid pole, frontal impact layout.

Figure 7. Sketch of new 300K rigid pole.



FOIL 300K rigid pole, side-impact layout.

Figure 7. Sketch of new 300K rigid pole (continued).

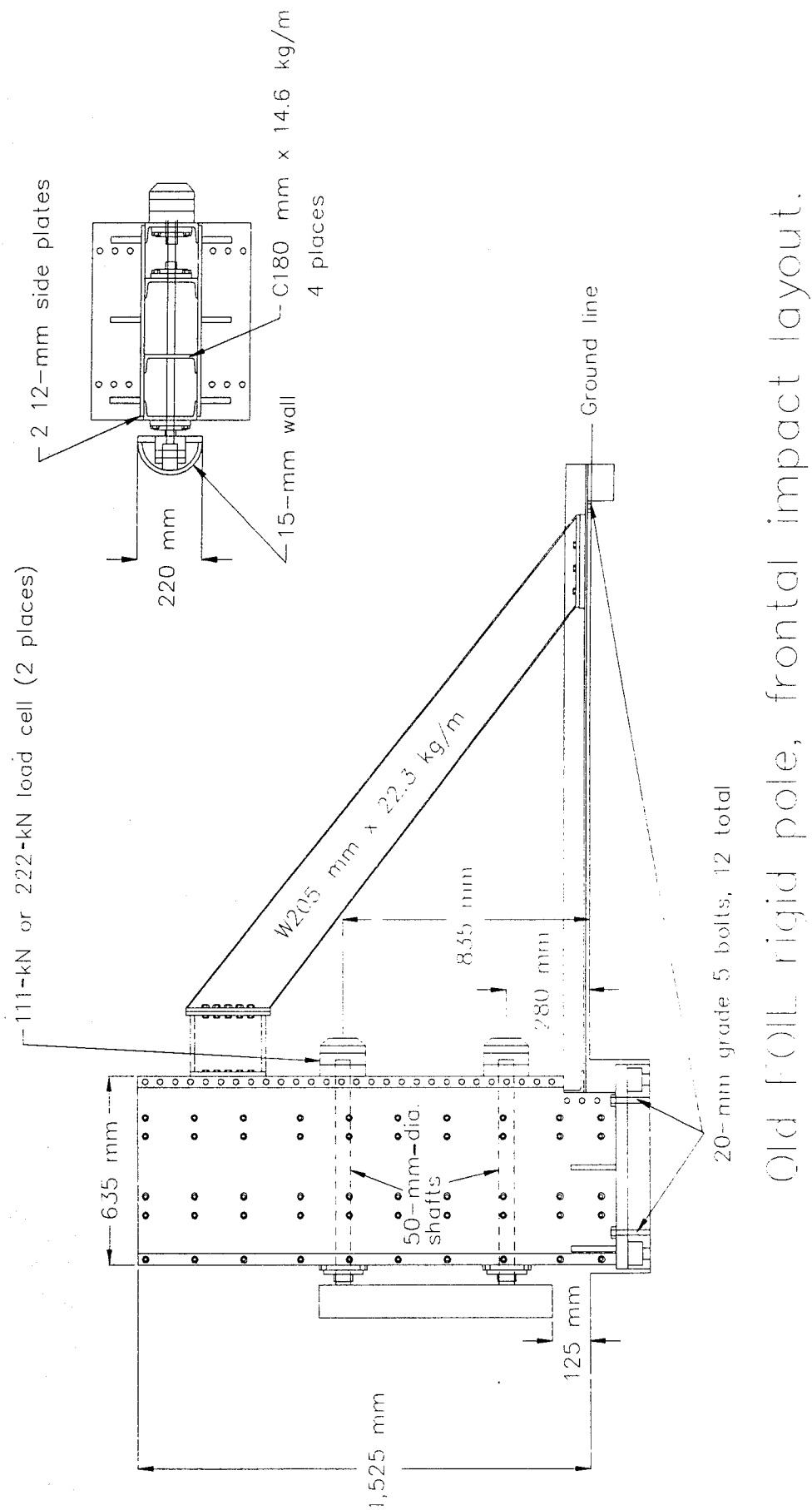
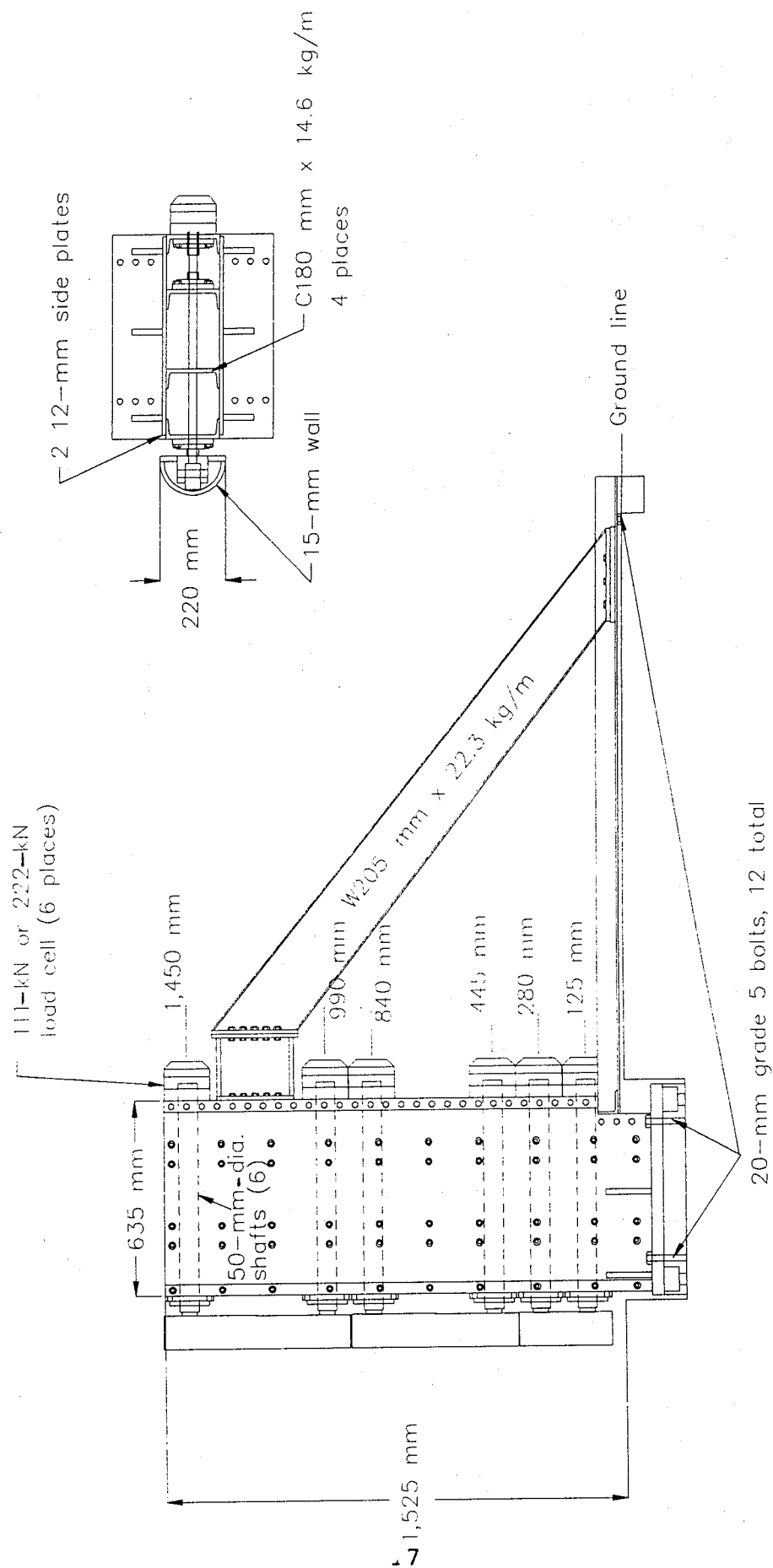


Figure 8. Sketch of old rigid pole.



Old FOIL rigid pole, side-impact layout.

Figure 8. Sketch of old rigid pole (continued).

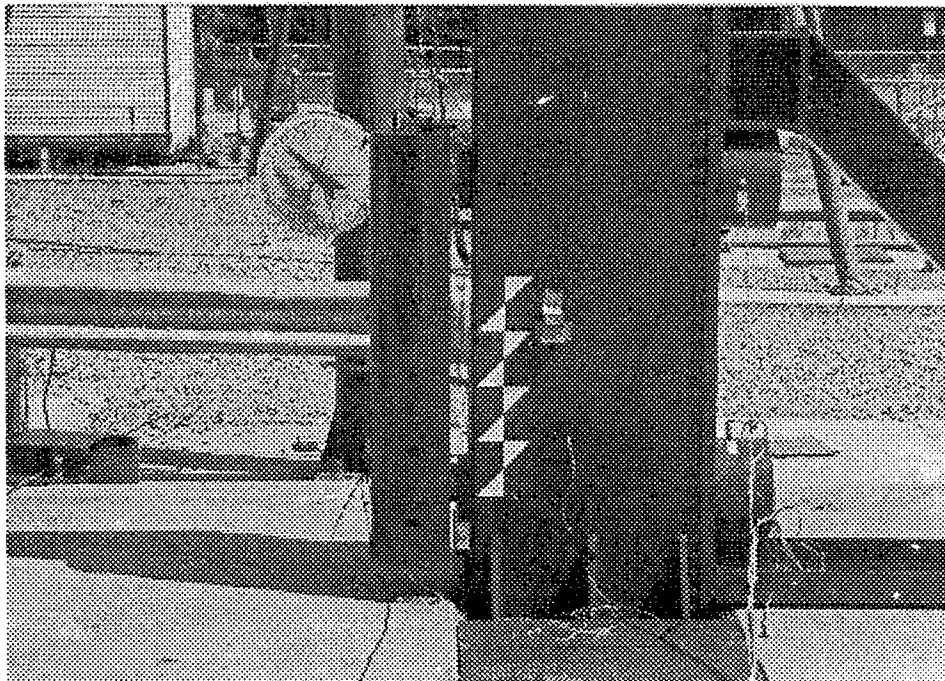
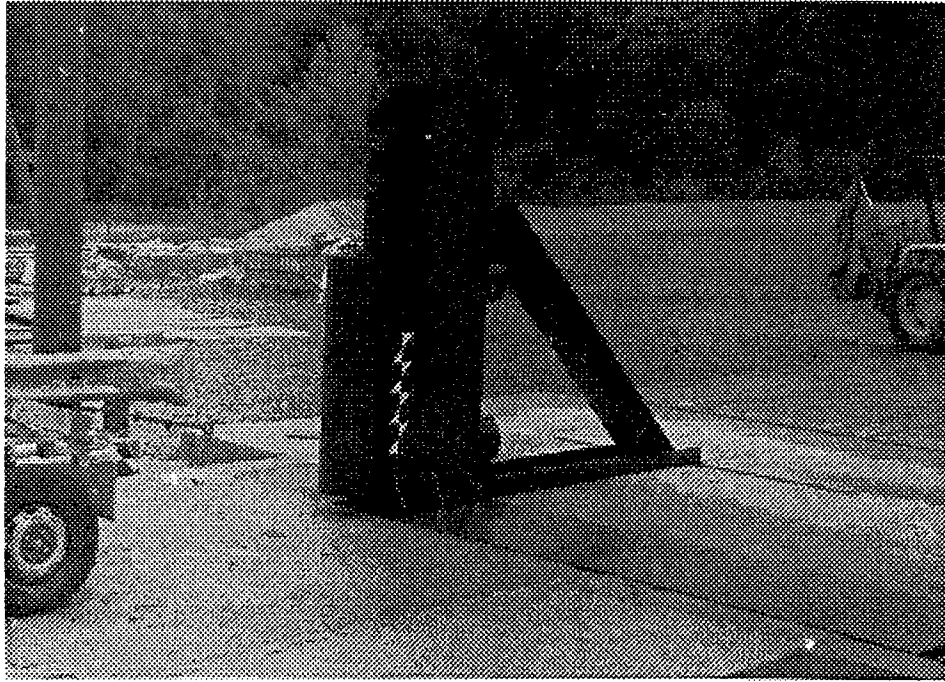


Figure 9. Photographs of new 300K rigid pole frontal configuration.



Figure 9. Photographs of new 300K rigid pole side-impact configuration (continued).

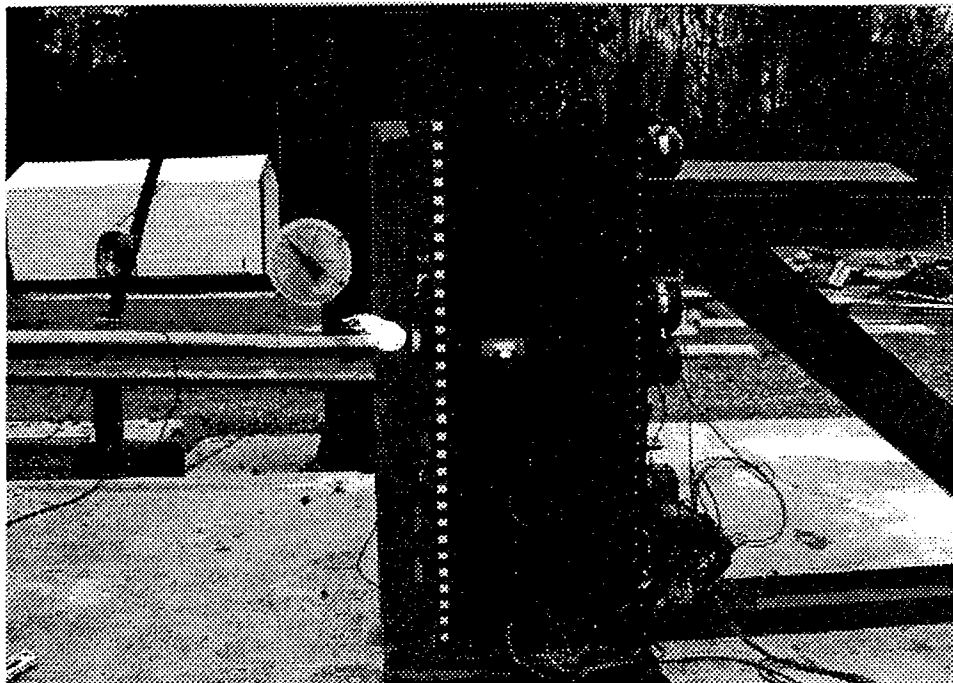
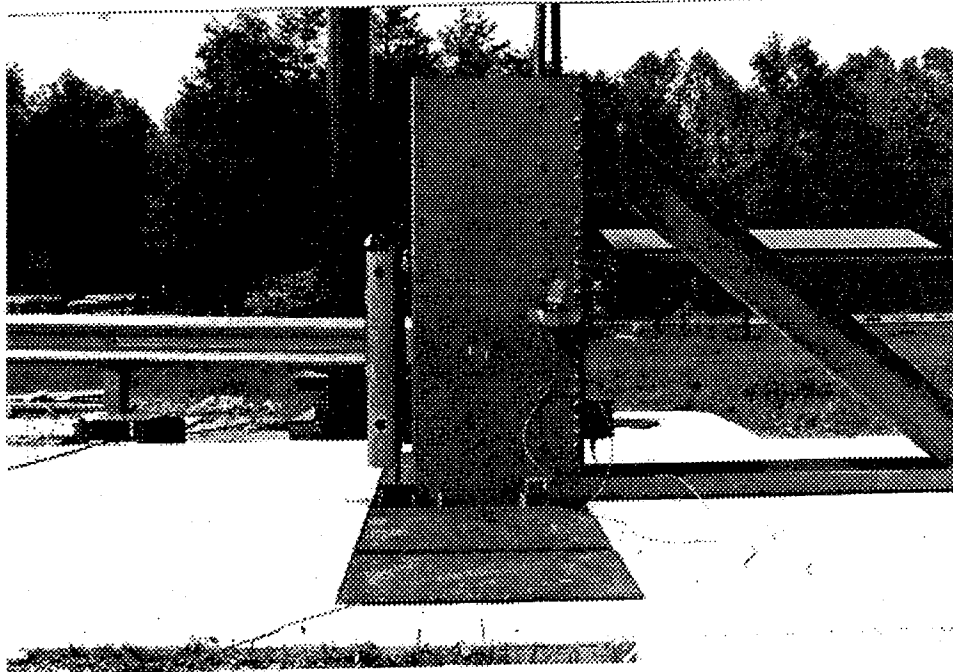


Figure 10. Photographs of old rigid pole frontal configuration (above) and side-impact configuration (below).

INSTRUMENTATION

For each test, speed-trap, accelerometer, load-cell, and high-speed film data were collected to measure the peak load on the 300K rigid pole and to obtain frontal crush characteristic or force-deflection data from a Chevrolet C2500 pickup truck.

Speed trap. The speed trap was used to determine each vehicle's speed just prior to contact with the rigid pole. The center of the speed trap was placed approximately 3.7 m before the rigid pole. The speed trap consisted of a set of five contact switches fastened to the runway at 0.3-m intervals. As the vehicles passed over the switches, electronic pulses were recorded on analog tape.

Transducer data. The minimum instrumentation used consisted of the two load cells attached to the rigid pole, a triaxial c.g. accelerometer, and a triaxial rate transducer at the vehicle's c.g. The minimum instrumentation was used during the bogie and VW Rabbit tests. The bogie vehicle tests also utilized one high-g accelerometer inside the sliding nose weldment. In addition to the minimum instrumentation, the Ford Festiva's, Ford F150 pickup truck, and the Chevrolet C2500 pickup truck were instrumented as described in Federal Motor Vehicle Safety Standard (FMVSS) 208.⁽³⁾ The data from the transducers were recorded by two data acquisition systems: the onboard data acquisition system (ODAS) III and an umbilical cable tape recorder system. Table 3 describes the FMVSS 208 instrumentation, including accelerometer locations used during tests 96F011 and 96F012 (Ford Festiva tests). The location coordinates were referenced from the right-front wheel hub, which was 255 mm above ground. Table 4 describes the FMVSS 208 instrumentation, including accelerometer locations used during test 96F015 (Chevrolet pickup truck test). The location coordinates were referenced from the right-front wheel hub, which was 370 mm above ground.

The ODAS III is a self-contained system. The output from the sensors was prefiltered, digitally sampled, and digitally stored within the ODAS units mounted directly to the test vehicle inside the occupant compartment. The ODAS units are factory set with a 4000-Hz analog prefilter and a digital sampling rate of 12,500 Hz. FMVSS 208 accelerometer and rate transducer data were collected via the ODAS III system.

The FOIL umbilical cable system utilizes a 90-m cable between vehicle transducers, rigid pole load cells, or other sensors and a rack of signal conditioning amplifiers. The output from the amplifiers was recorded on 25-mm magnetic tape via a Honeywell 5600E tape recorder. After the test, the tape is played back through anti-aliasing filters, then input to a Data Translation analog-to-digital converter (ADC). The sample rate was set to 4000 Hz. The umbilical cable system recorded c.g. acceleration data, bogie nose acceleration data, and rigid pole load-cell data.

Table 3. FMVSS 208 instrumentation, Ford Festiva tests.

Location	Data	Full scale	(X,Y,Z) position* (mm)
1	Top of motor	2000 g	203, 648, 495
2	Bottom of motor	2000 g	200, 750, 10
3	Right control arm	2000 g	127, 64, 25
4	Left control arm	2000 g	127, 1435, 25
5	Top of instrument	2000 g	-520, 750, 584
6	Right side under rear	2000 g	-1778, 394, 140
7	Left side under rear	2000 g	-1778, 1105, 140
c.g.	Triaxial rate transducer, pitch, roll, yaw	500 deg/s	-787, 750, 216
c.g.	Longitudinal	100 g	-787, 750, 51
c.g.	Lateral acceleration	100 g	-813, 660, 51
c.g.	Vertical acceleration	100 g	-813, 750, 102
c.g.	Longitudinal	100 g	-787, 750, 76
Pole	Load cell, pole force	890 kN	Upper load cell 1180 mm above ground
Pole	Load cell, pole force	890 kN	Lower load cell 305 mm above ground
NA	Tape switches	1.5	Runway
* Referenced from the center of the right wheel hub.			

Table 4. FMVSS 208 instrumentation, Chevrolet C2500 truck.

Location	Data	Full scale	(X,Y,Z) position* (mm)
1	Top of motor	2000 g	0, 890, 597
2	Bottom of motor	2000 g	125, 840, -75
3	Right control arm	2000 g	138, 138, 0
4	Left control arm	2000 g	138, 1510, 0
5	Instrument panel	2000 g	-660, 915, 890
6	Left side in bed	2000 g	-3390, 1384, 460

Table 4. FMVSS 208 instrumentation, Chevrolet C2500 truck (continued).			
Location	Data	Full scale	(X,Y,Z) position* (mm)
7	Right side in bed	2000 g	-3390, 290, 460
c.g.	Triaxial rate transducer, pitch, roll, yaw	500 deg/s	-2260, 840, 395
c.g.	Longitudinal	100 g	-2260, 840, 395
c.g.	Lateral acceleration	100 g	-2260, 840, 395
c.g.	Vertical acceleration	100 g	-2260, 840, 395
c.g.	Longitudinal	100 g	-2260, 840, 395
Pole	Load cell, pole force	890 kN	Upper load cell 1180 mm above ground
Pole	Load cell, pole force	890 kN	Lower load cell 305 mm above ground
NA	Tape switches	1.5	Runway
* Referenced from the center of the right wheel hub.			

High-speed photography. The crash tests were photographed using five high-speed cameras with an operating speed of 500 frames/s. All high-speed cameras used Kodak 2253 daylight film. The high-speed film was analyzed for impact speed and acceleration data. In addition to the high-speed cameras, one real-time camera loaded with Kodak 7239 daylight film and two 35-mm still cameras were used to document the test. Table 5 summarizes the cameras used and their respective placements. An overhead layout of the test setup is shown in figure 11. A pickup truck is shown in the figure; however, all seven tests were set up in the same manner. The camera numbers in table 5 are included in figure 11.

Table 5. Summary of camera placement.				
Camera	Type	Film speed frames/s	Lens (mm)	Location
1	LOCAM II	500	100	Right 90° to impact
2	LOCAM II	500	75	Right 90° to impact
3	LOCAM II	500	50	Right side 45° to impact
4	LOCAM II	500	50	Left side 45° to impact
5	LOCAM II	500	10	Overhead
6	BOLEX	24	ZOOM	Documentary
7	CANNON AE-1	still	ZOOM	Documentary
8	CANNON AE-1	still	ZOOM	Documentary

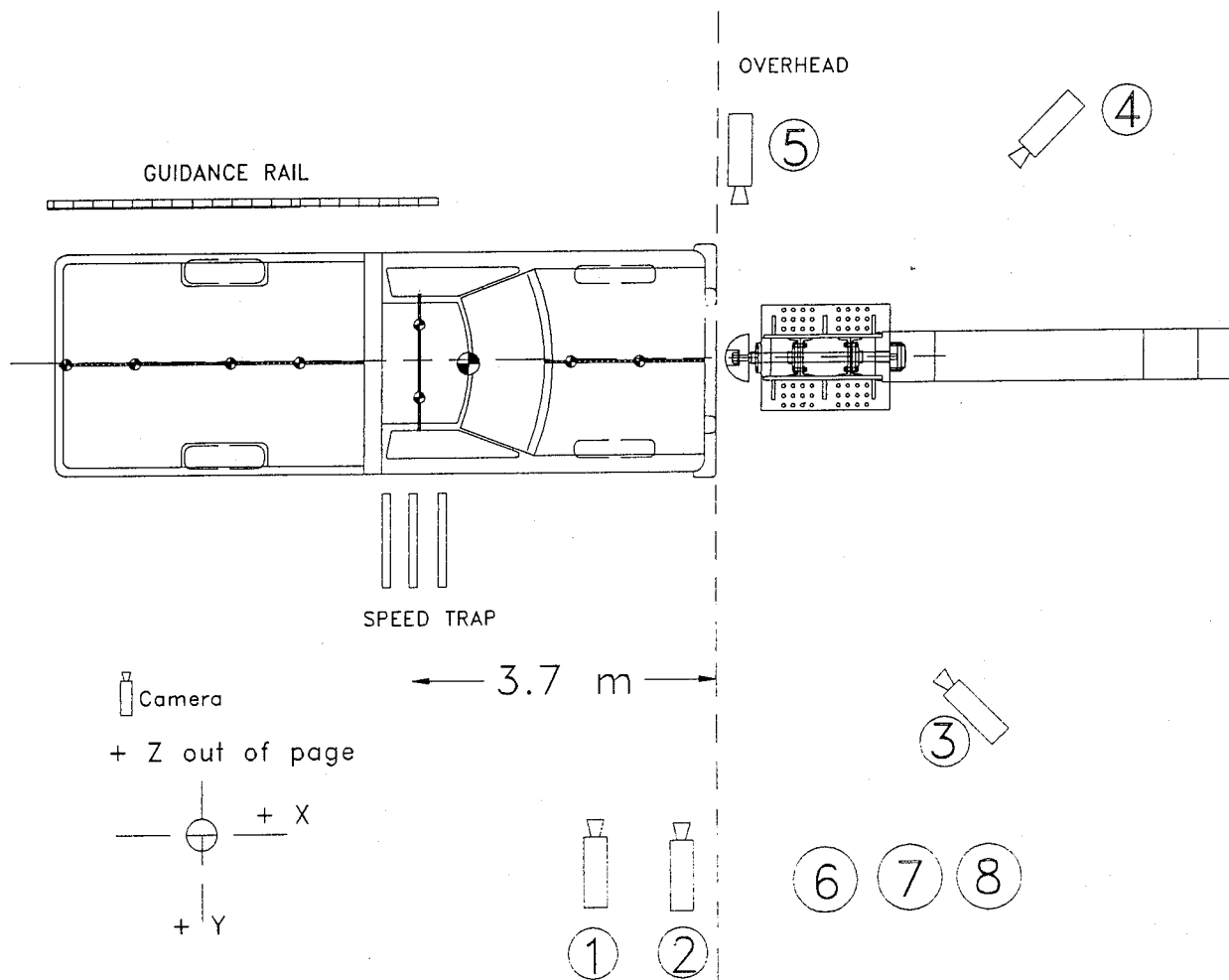


Figure 11. Layout of the test setup.

DATA ANALYSIS

Data were collected via the FOIL analog tape recorder system, including speed-trap data, the FOIL ODAS III, and high-speed film.

Speed trap. As the vehicles passed over the speed trap, electronic pulses from the five contact switches were recorded to analog tape. The tape was played back through a Data Translation ADC inside a desktop computer. The time intervals between the first pulse and each of the subsequent four pulses were then obtained using the analysis software provided with the ADC. The displacement vs. time data were then entered into a computer spreadsheet and a linear regression was performed to determine the best-line fit of the data points. The impact velocity was then determined from the slope of the best-line fit of the displacement vs. time curve.

Transducer data package. After the test, data were digitally converted and stored. The data from the tape recorder system and the ODAS III system were converted to the ASCII format, zero bias was removed, and data were digitally filtered using a digital Butterworth low-pass filter. The data from the crash tests were digitally filtered with a cutoff frequency of 300 Hz. The data were transferred to a spreadsheet for analysis.

The c.g. acceleration data were integrated twice to produce velocity and displacement traces. A force vs. time trace was generated by multiplying the acceleration data by the mass of the vehicle and plotting the product with time. Acceleration vs. time traces were plotted for all FMVSS 208 accelerometers.

The load cells measured forces at two separate locations on the rigid pole. The two forces obtained were summed together to generate the entire force for the event. Using the force vs. time trace, an acceleration trace was produced by dividing the force vs. time trace by the mass of the vehicle. Velocity and displacement traces were generated by a single and double integration of the acceleration trace. A force vs. displacement trace was generated from the load-cell data. The force vs. displacement trace depicts the frontal crush characteristic of a vehicle for the given impact location. An energy vs. displacement trace was derived from integrating the force vs. displacement trace. The energy curve verifies the conservation of energy during the test and shows the amount of energy consumed for a given amount of deformation.

The load cells measured the forces on the rigid pole at two separate locations. The two load cells were attached to a single, common rigid pole impact face. Using torque equations, a resultant load height on the rigid pole vs. displacement (crush) was generated. This plot is important because it depicts the location (height) on the vehicle that was producing the load. The resultant load height varied as the vehicle crushed inward.

As contact between different structures in the vehicle occurred, the resultant load's vertical location shifted.

High-speed photography. Each crash event was recorded on 16-mm film by five high-speed cameras. The camera perpendicular to the vehicle trajectory, with a 50-mm lens, was the only camera used for high-speed film analysis. Analysis of each crash event was performed using an NAC Film Motion Analyzer model 160-F in conjunction with a desktop personal computer. The motion analyzer digitized the 16-mm film, reducing the image to Cartesian coordinates. The Cartesian coordinate data were then imported into a computer spreadsheet for analysis. Using the Cartesian coordinate data, a displacement vs. time history of each test was obtained. A linear regression was performed on the first 20 data points of the displacement vs. time traces to determine the impact velocities of the vehicles. The film was used to verify data obtained from the speed trap and rate transducer and could be used in the event of transducer malfunction. The film was used to observe roll, pitch, and yaw angular displacements. The speed trap, accelerometer, and load-cell data were used as the primary sources of data.

RESULTS

In each of the rigid pole crash tests, the test vehicles were accelerated to within 1 km/h of the target impact speed. The vehicles struck the rigid pole within 20 mm of the target impact location. A summary of the test results is presented in table 6. In each bogie vehicle test, the crushable honeycomb nose collapsed and the bogie rebounded with a small negative velocity. The VW Rabbit and Ford Festiva's struck the rigid pole and the bumper, grill, and engine compartment collapsed. The engines were forced into the firewall. Each vehicle's front wheel assemblies were damaged, diminishing the amount of rebound. Little or no rebound was observed during the pickup truck tests. The trucks were severely damaged, the engine mounts and frame were buckled. The frame and transmission mounts buckled downward enough to make contact with the ground. The lowest load recorded by the rigid pole load cells was 150,000 N during the off-center Ford Festiva test, while the highest load was recorded during the full-size Chevrolet pickup truck test (658,000 N).

Data plots from each crash test are presented in appendix A. Photographs of the crash test taken from high-speed film and pre- and post-test photographs are presented in Appendix B.

Table 6. Summary of results for 300K rigid pole testing.							
Data / Test number	96F008	96F009	96F010	96F011	96F012	96F014	96F015
Vehicle	FOIL Bogie	FOIL Bogie	VW Rabbit	Ford Festiva	Ford Festiva	Ford F150 Pickup	Chevrolet C2500 Pickup
Inertial Weight (kg)	839	839	907	816	820	1941	2051
Speed(m/s)	10.3	10.5	14.8	10.1	10.3	12.4	13.3
Initial Energy (kJ)	44.2	46.7	99.3	42.2	43.1	150.3	181.8
Peak Acceleration (g's): Accelerometer	23.1	30.5	63.3	37.5	35.1	130.7	32.7
Load Cell	24.5	27.6	44.1	23.6	18.8	35.0	43.0
Peak Force (kN): Accelerometer	190	251	564	303	281	2489	658
Load Cell	201	227	393	190	150	673	864
Displacement (mm): Accelerometer	660	660	850	520	530	1790	920
Load Cell	590	680	750	490	500	790	800
Film	688	685	784	361	538	888	830
Static	622	630	790	370	546	875	815
Work F•d (kJ): Accelerometer	43.8	46.2	97.5	40.9	41.9	143.4	179.9
Load Cell	43.8	46.7	97.4	41.2	42.8	149.5	180.3

CONCLUSIONS

The contractor delivered the rigid pole assembled in the side-impact configuration. The pole was installed in the FOIL foundation pit to ensure proper alignment and fit with the existing FOIL foundation. The pole was unassembled, then assembled again in the frontal configuration. The rigid pole parts came apart and fit together well. Each load cell delivered with the rigid pole mounted correctly and was in good working condition. The new, larger capacity rigid pole met the specified fabrication criteria.

The crash tests into the rigid pole used vehicles varying in size and weight. The test speeds for the tests varied from 35 km/h to 48 km/h. The force on the pole varied with the weight and speed of the test vehicle. The speed and weight of the test vehicle were increased from test to test to gradually build up the forces on the pole. The pole withstood the impact forces from all vehicles. The impact speed required to exhaust the energy-absorbing capacity of a full-size pickup truck was determined to be 48 km/h. The peak force observed during this test was 658,000 N, half the design load. The pole was unassembled and inspected after the seven crash tests. No structural damage, bent parts, cracks, or loose bolts were observed. The load cells were in good operating condition after completion of the tests. The rigid pole withstood the impact of a full-size pickup truck without approaching the design limit.

The data plots and results indicate that the new, larger diameter (305-mm) rigid pole does not significantly affect the crush characteristics of vehicles previously tested using the smaller diameter pole (220 mm). The frontal crush characteristic of a vehicle when striking a narrow object is dependant upon the time and sequence of deformation to structures within the vehicles. The 85-mm increase in pole diameter was not enough to produce a dissimilar energy-absorbing characteristic to that of the same vehicles impacting a smaller pole. The increase in diameter was too small to change the time and sequence of structural deformation. This was anticipated for the bogie vehicle, considering the consistent performance of the honeycomb nose. The nose would collapse in the same manner when striking a rigid wall. Data plots that illustrate the similar bogie vehicle behavior are presented in figures 12 through 15. Differences in peak acceleration and displacements may be attributed to the difference in initial energy. The impact speed of test 92F028 was lower than that of test 96F008. Additional data from test 92F028 are contained in the report *Validation of the ENSCO Surrogate Bogie Vehicle, FOIL Test Numbers 92F028, 92F029, 92F030, and 92F031.*⁽⁴⁾ Two center-impact Ford Festiva crash tests are compared in figures 16 through 19. Test 94F011 involved a Ford Festiva striking the old rigid pole at 35 km/h. Test 96F011 was similar to test 94F011, although the Ford Festiva struck the new, larger rigid pole. The data plots show that the increase in pole diameter did not significantly alter the crush

characteristics of the Ford Festiva. A visual comparison of the Ford Festiva tests is shown in figure 20. Additional data from test 94F011 are presented in the report *Ford Festiva Collisions With Narrow Objects*.⁽⁵⁾

The electronic data and high-speed film will assist simulation engineers in developing and validating a finite element model for a Chevrolet C2500 pickup truck.

Test no. 92F028 & 96F008

Acceleration vs. time (load cell)

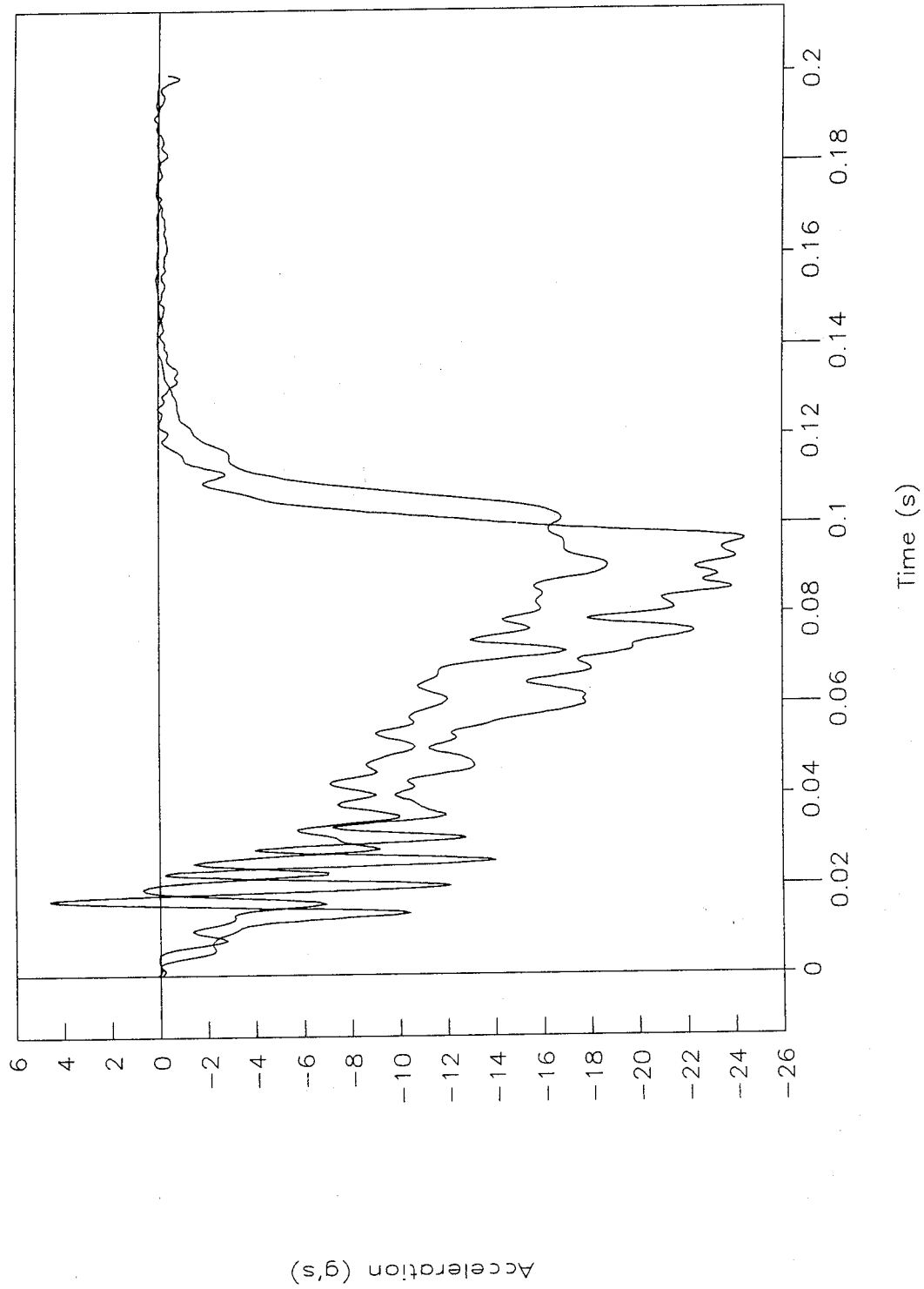


Figure 12. Comparison of bogie testing, acceleration vs. time (load cell), tests 92F028 and 96F008.

Test no. 92F028 & 96F008

Velocity vs. time (load cell)

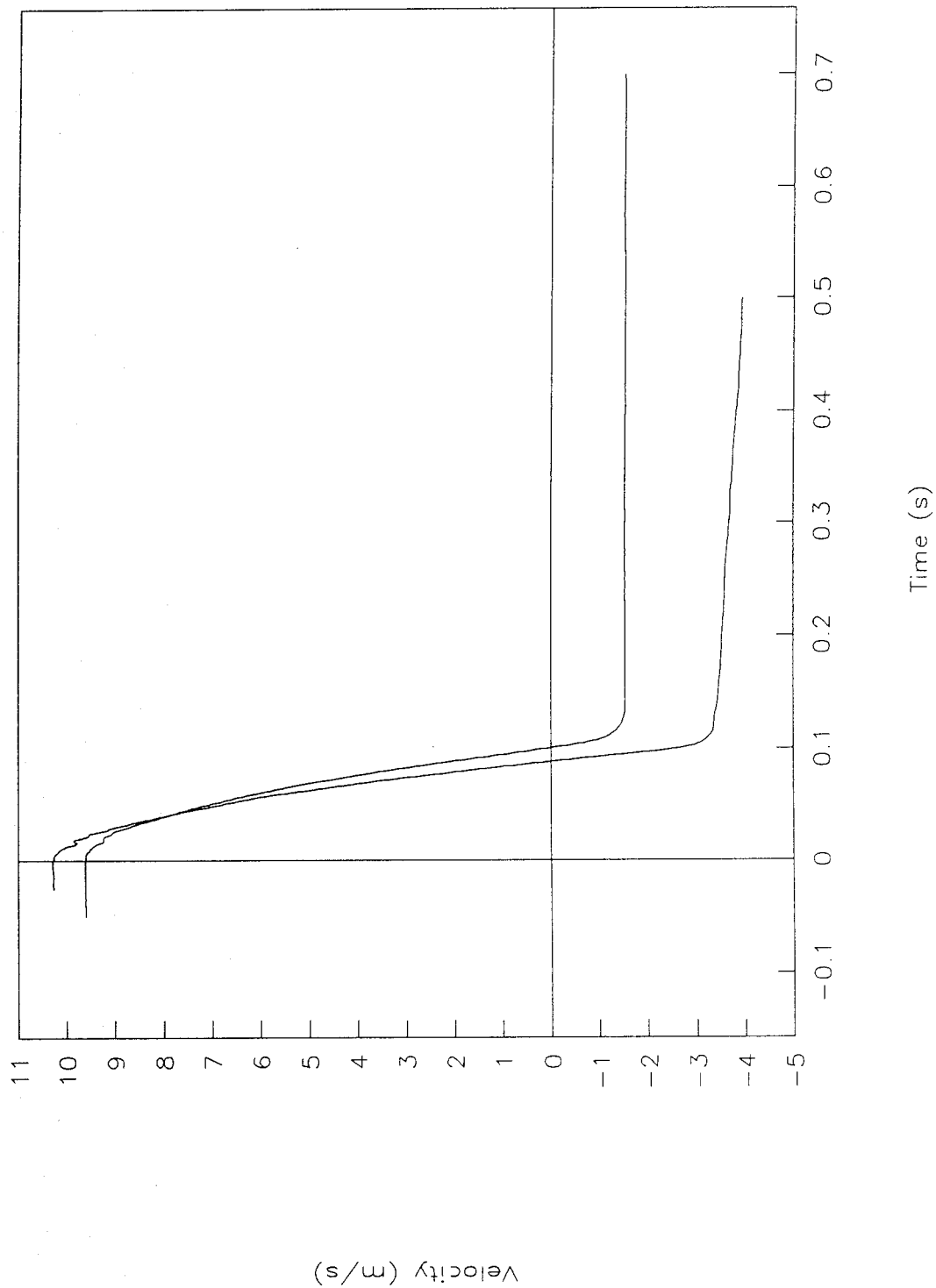


Figure 13. Comparison of bogie testing, velocity vs. time (load cell), tests 92F028 and 96F008.

Test no. 92F028 & 96F008

Displacement vs. time (load cell)

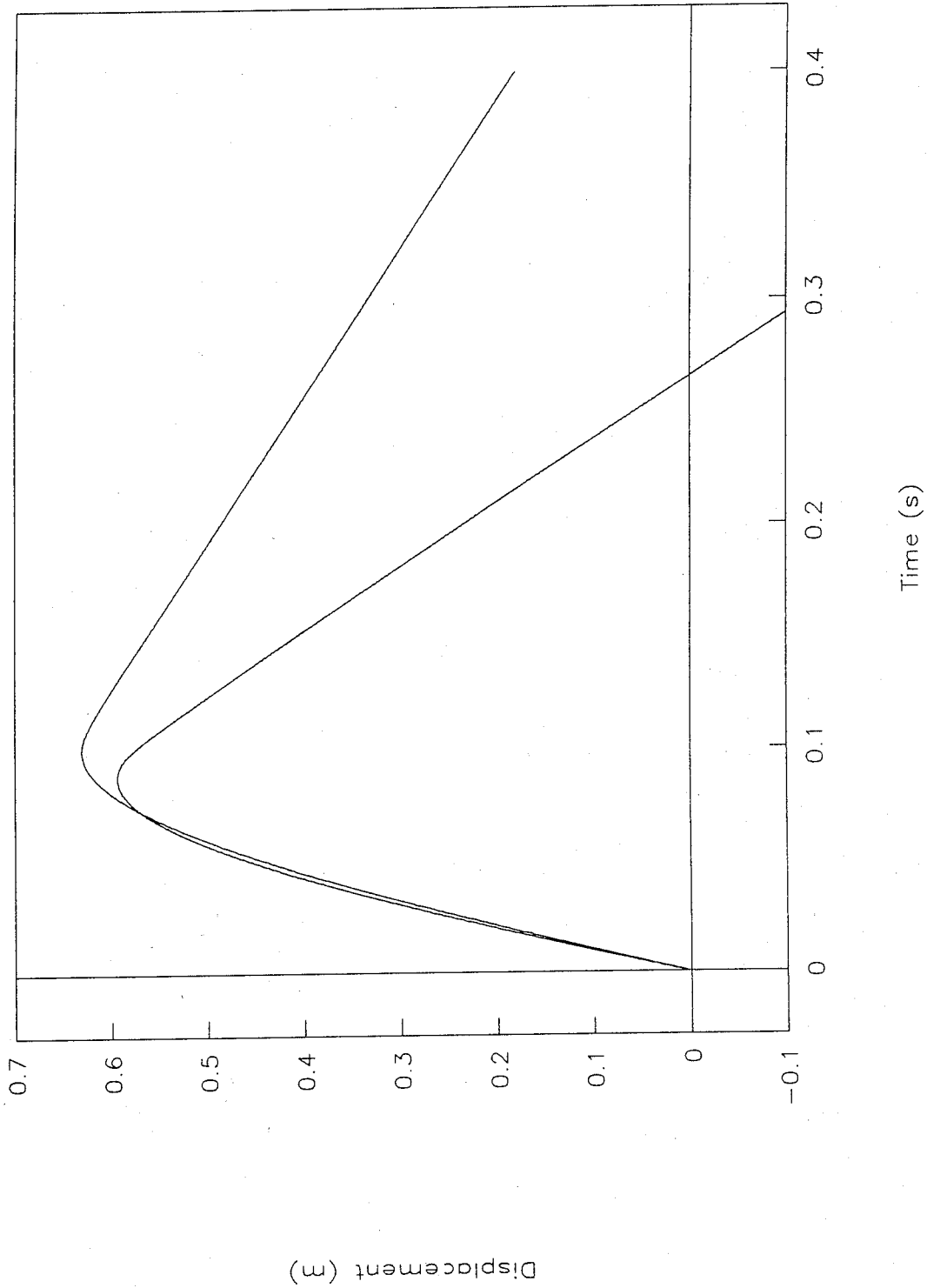


Figure 14. Comparison of bogie testing, displacement vs. time (load cell), tests 92F028 and 96F008.

Test no. 92F028 & 96F008

Force vs. displacement (load cell)

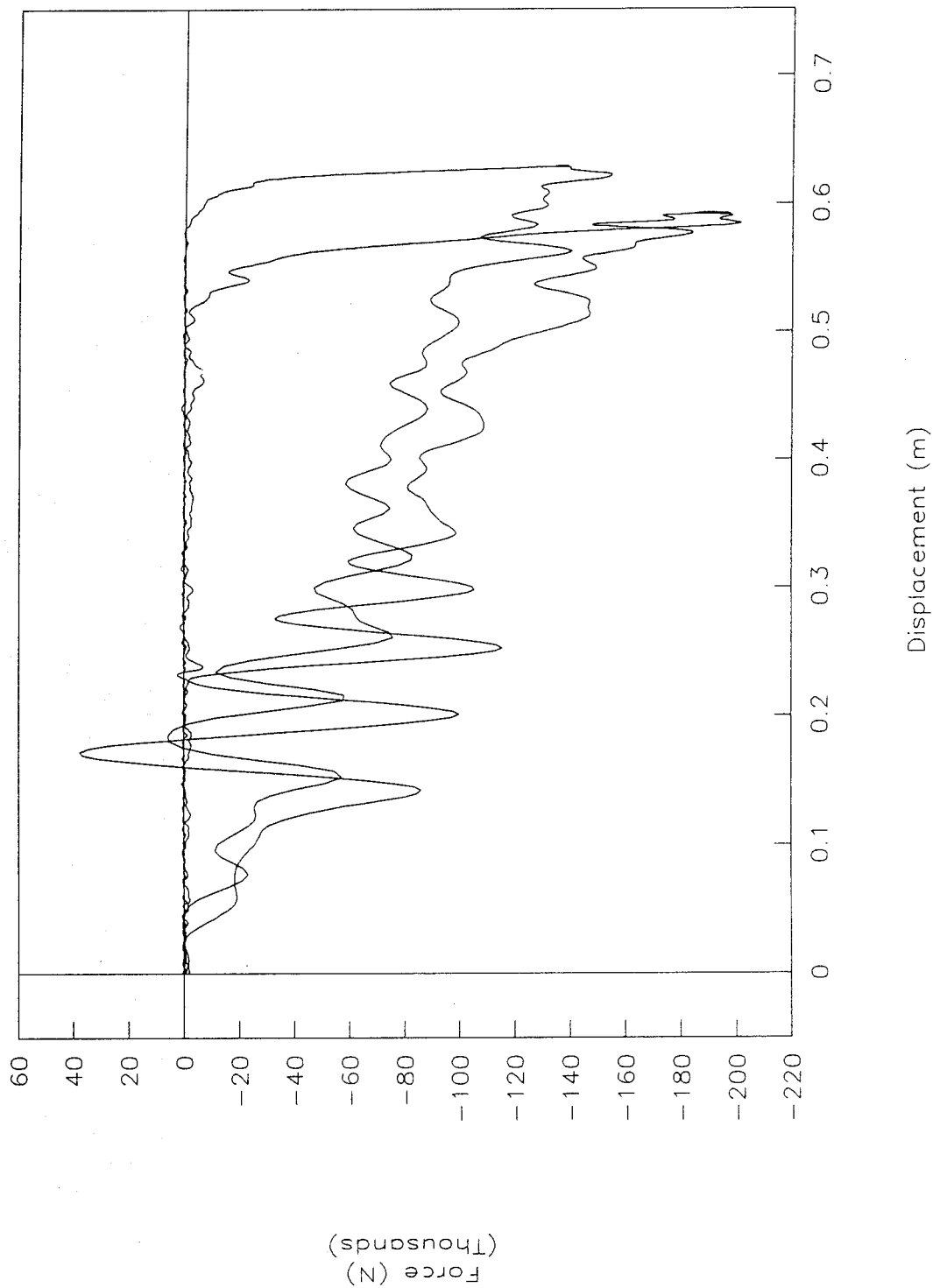


Figure 15. Comparison of bogie testing, force vs. displacement (load cell), tests 92F028 and 96F008.

Test no. 94F011 & 96F011

Acceleration vs. time (load cell)

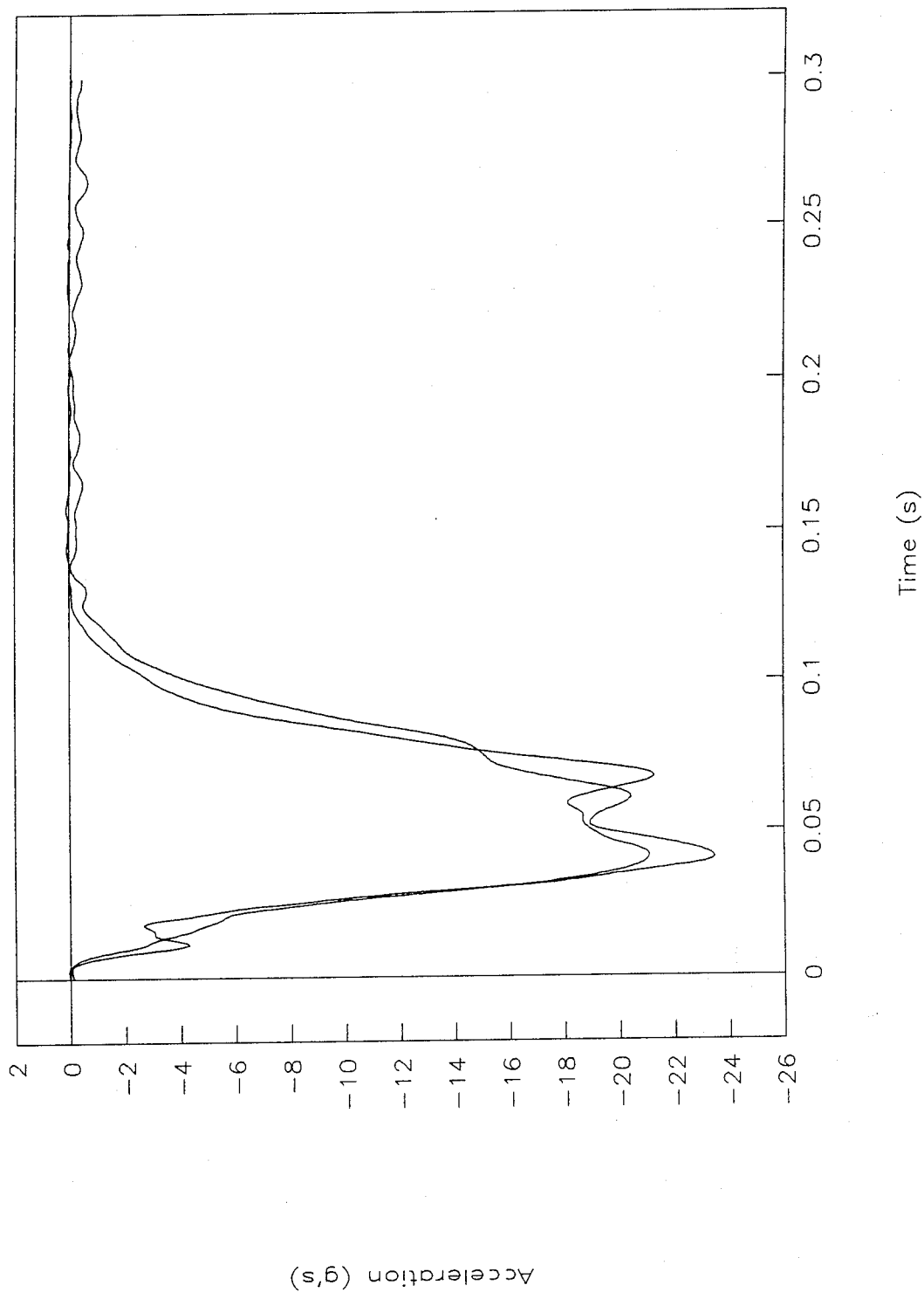


Figure 16. Comparison of Festiva testing, acceleration vs. time (load cell), tests 94F011 and 96F011.

Test no. 94F011 & 96F011

Displacement vs. time (load cell)

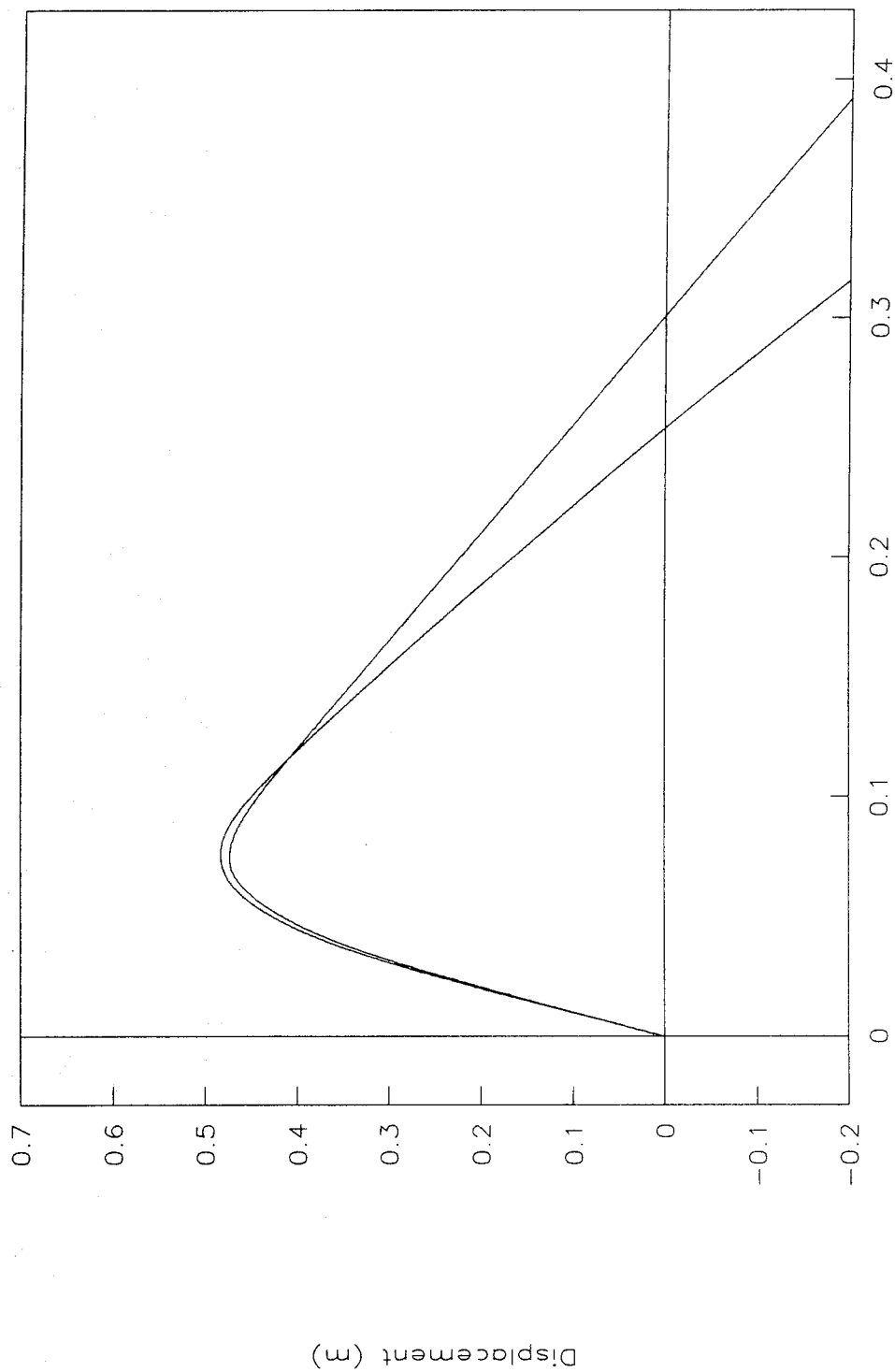


Figure 17. Comparison of Festiva testing, displacement vs. time (load cell), tests 94F011 and 96F011.

Test no. 94F011 & 96F011

Energy vs. displacement (load cell)

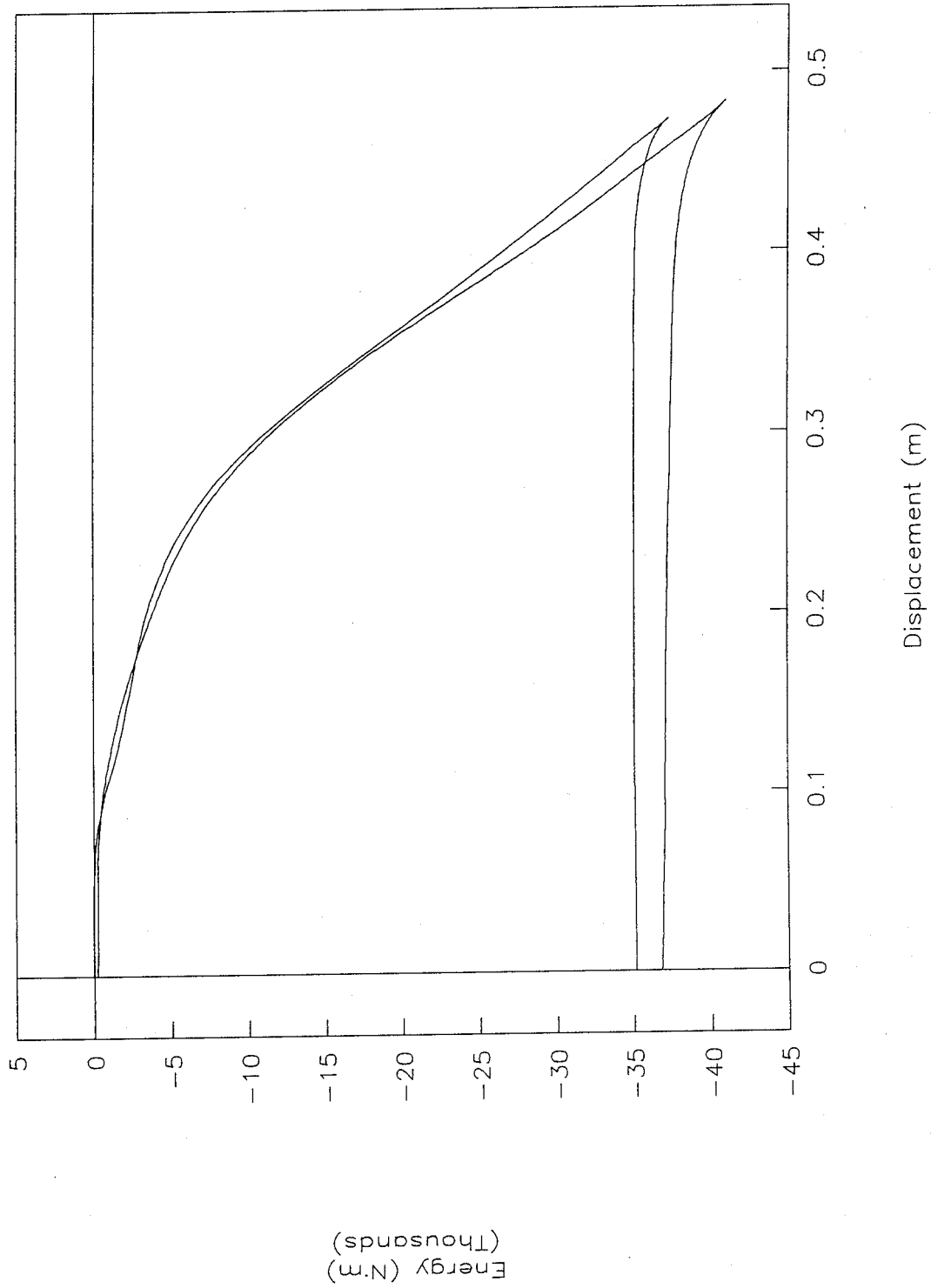


Figure 18. Comparison of Festiva testing, energy vs. displacement (load cell), tests 94F011 and 96F011.

Test no. 94F011 & 96F011

Force vs. displacement (load cell)

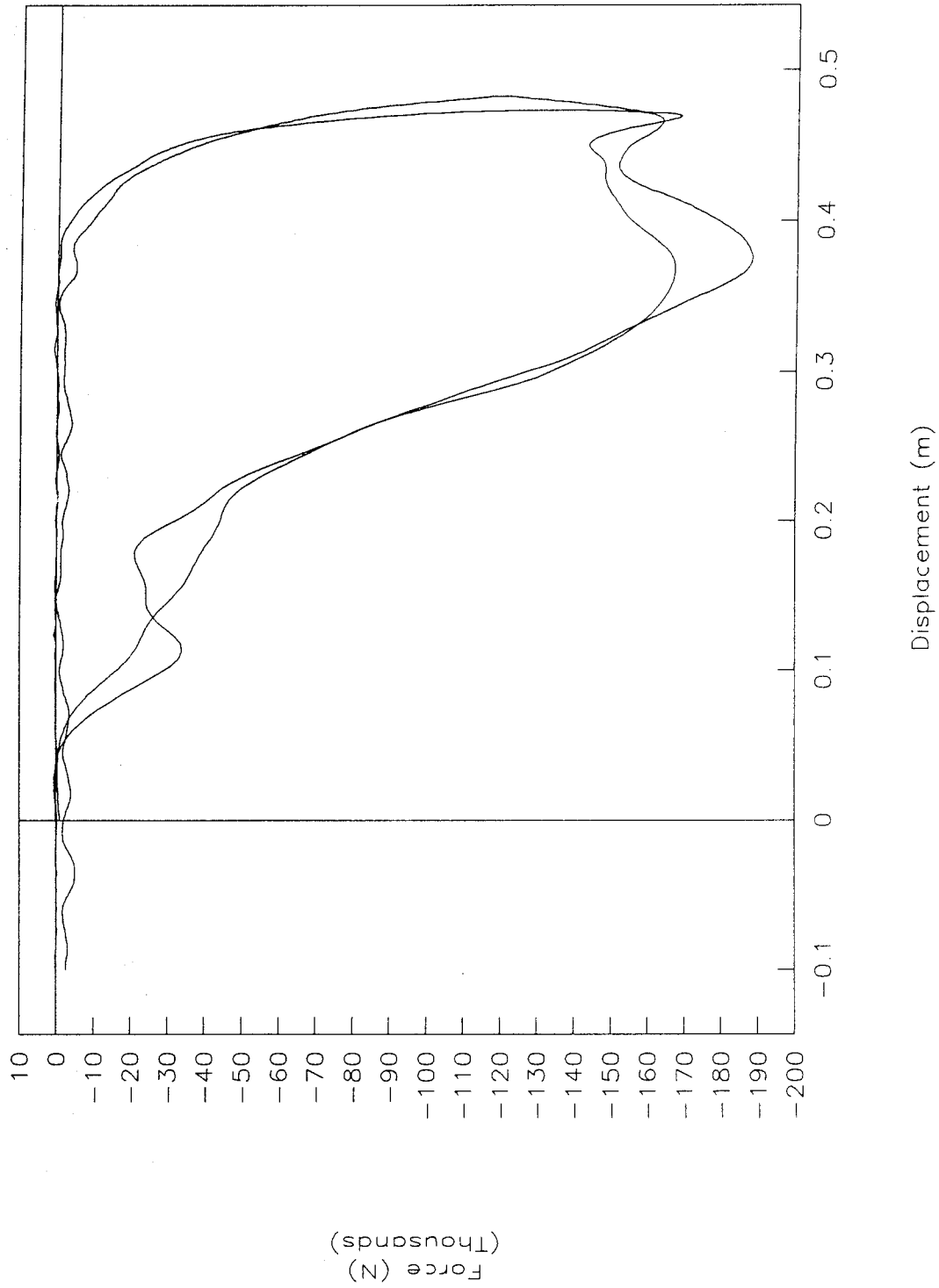


Figure 19. Comparison of Festiva testing, force vs. displacement (load cell), tests 94F011 and 96F011.

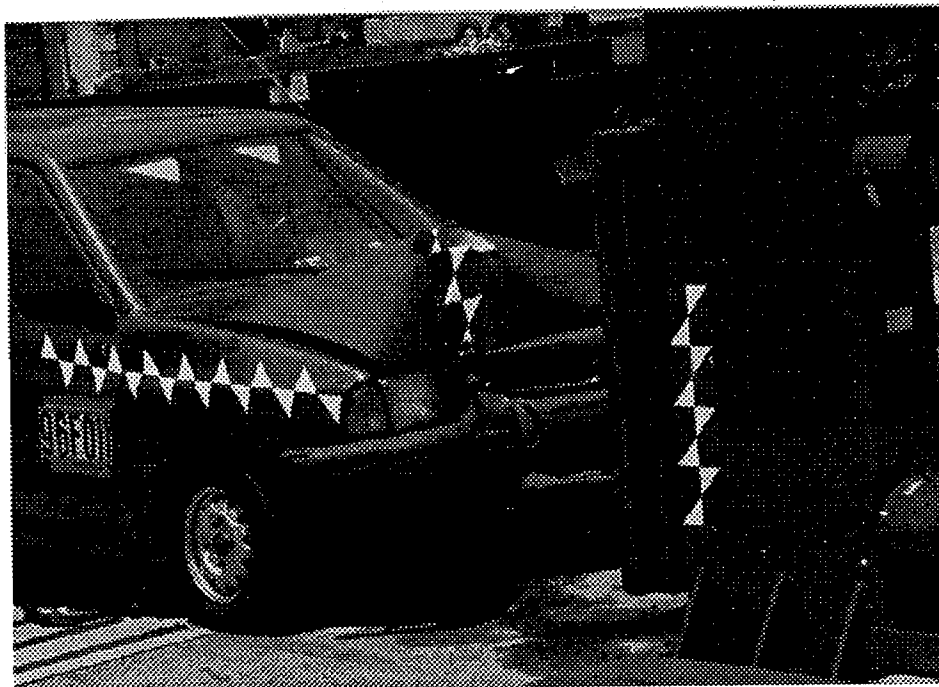


Figure 20. Visual comparison of the Ford Festiva tests, 94F011 (above) and 96F011 (below).

APPENDIX A. DATA PLOTS

Test No. 96F008

Acceleration vs. time

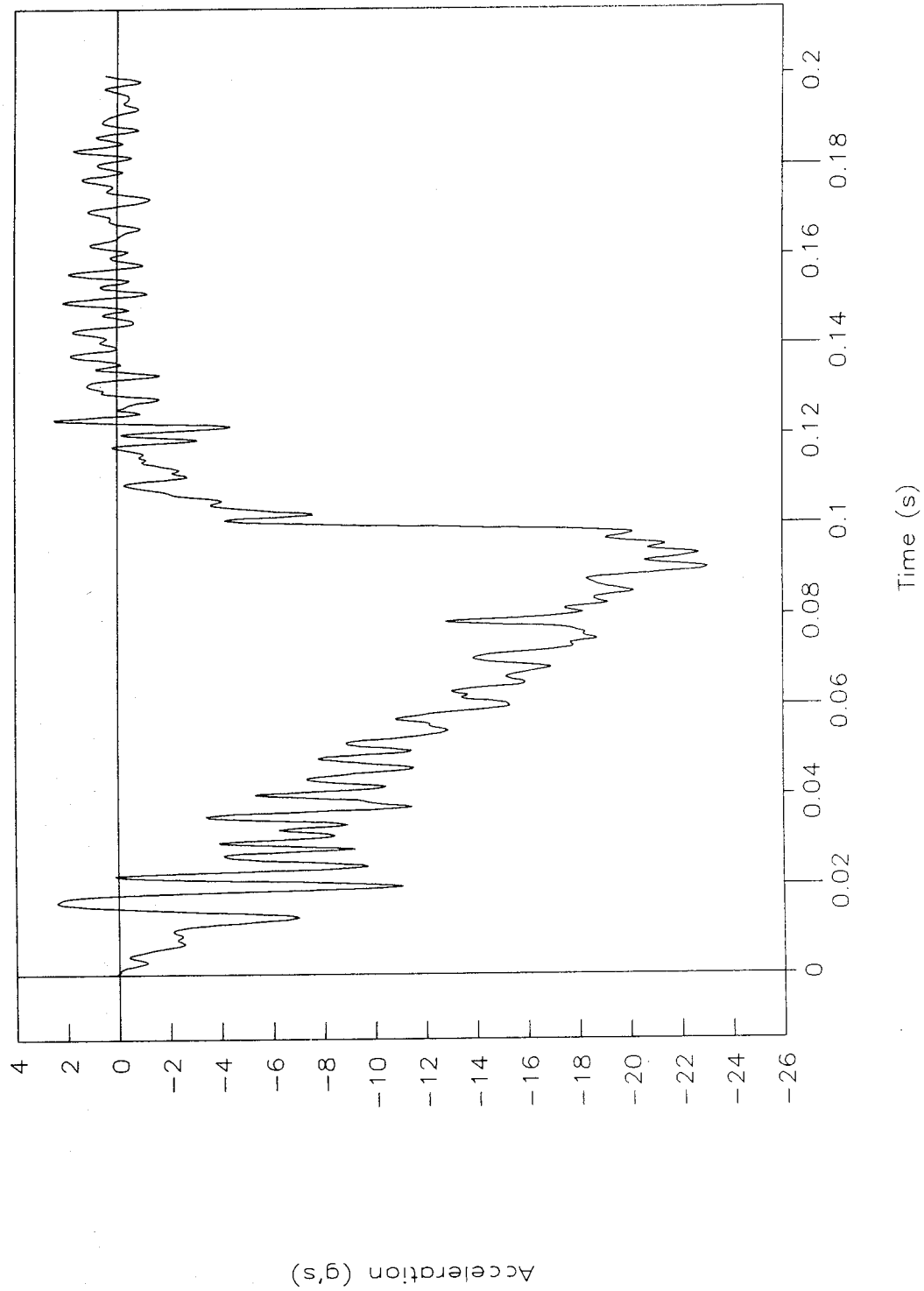


Figure 21. Acceleration vs. time, test 96F008.

Test No. 96F008

Nose acceleration vs. time

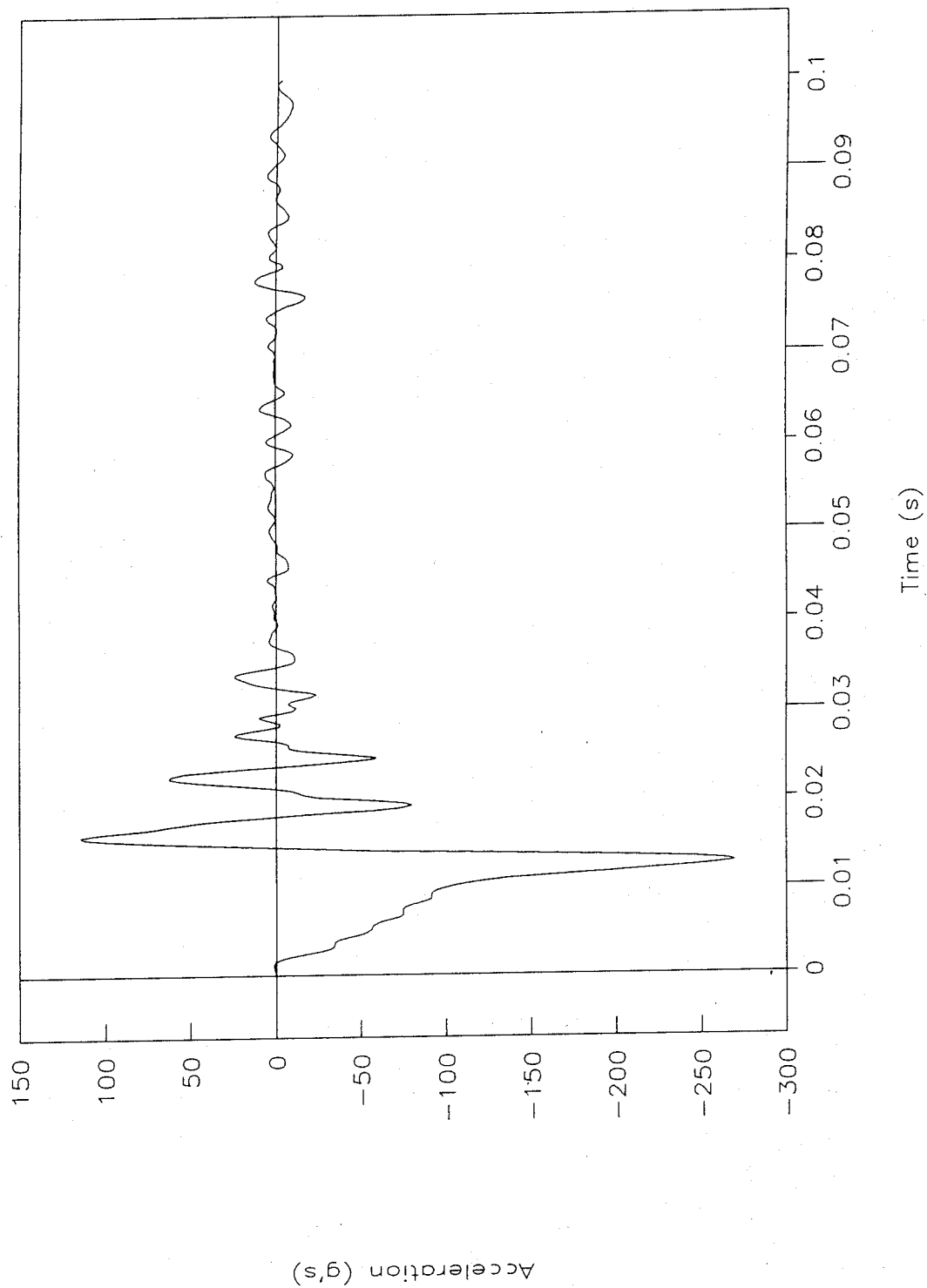


Figure 22. Nose acceleration vs. time, test 96F008.

Test No. 96F008

Velocity vs. time, accelerometer data

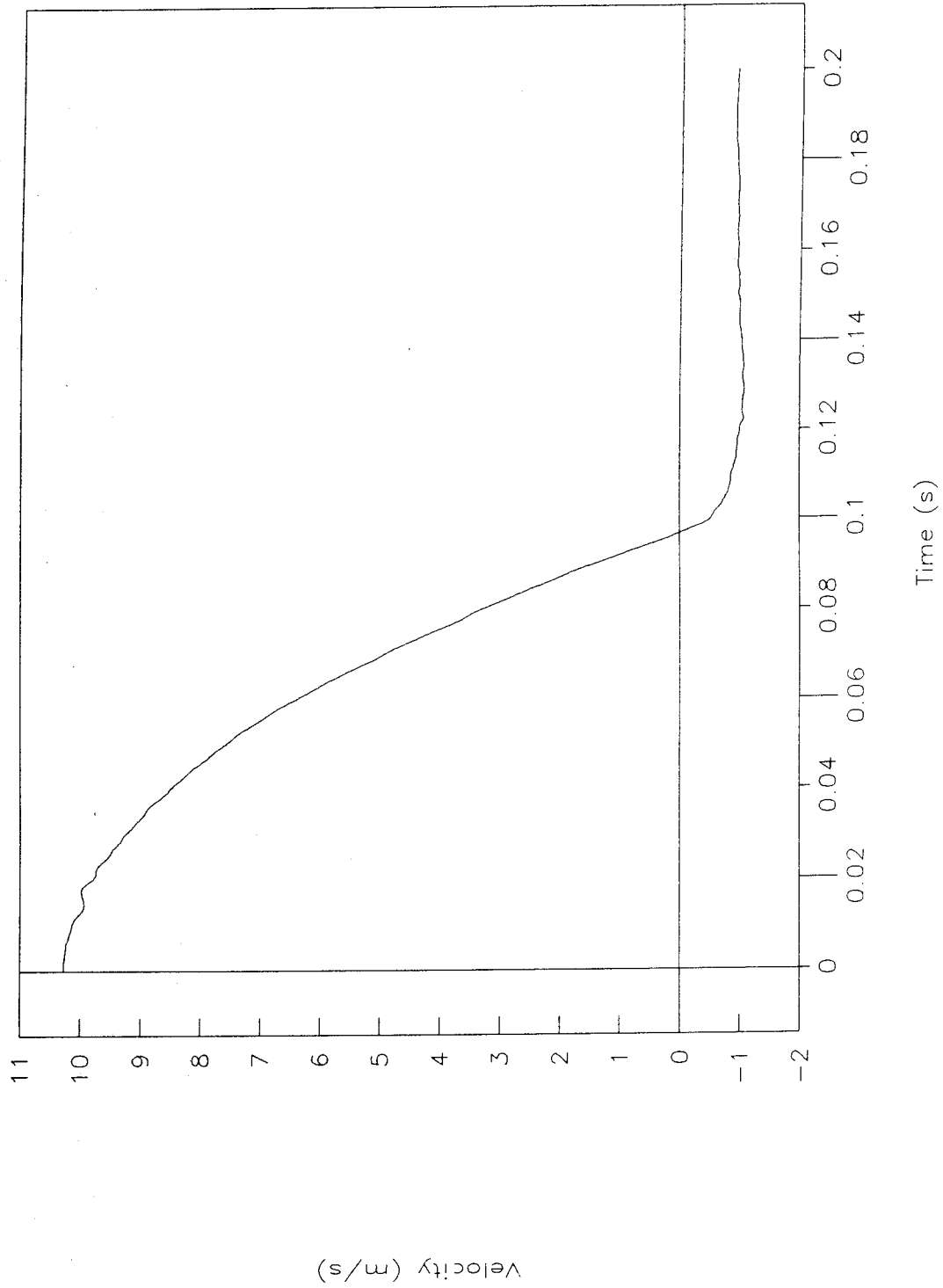


Figure 23. Velocity vs. time, accelerometer data, test 96F008.

Test No. 96F008

Displacement vs. time accelerometer data

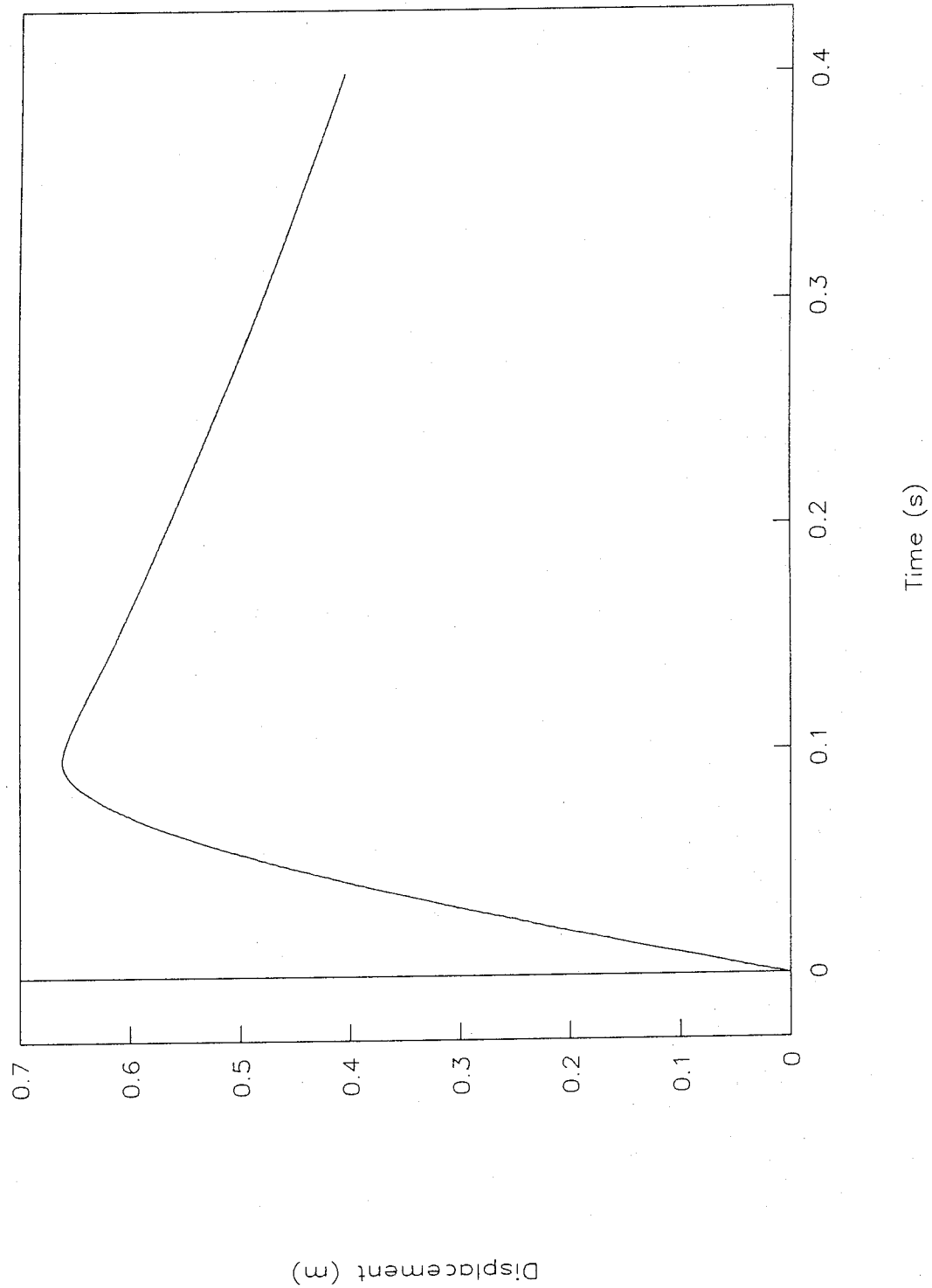


Figure 24. Displacement vs. time, accelerometer data, test 96F008.

Test No. 96F008

Force vs. time, load-cell data

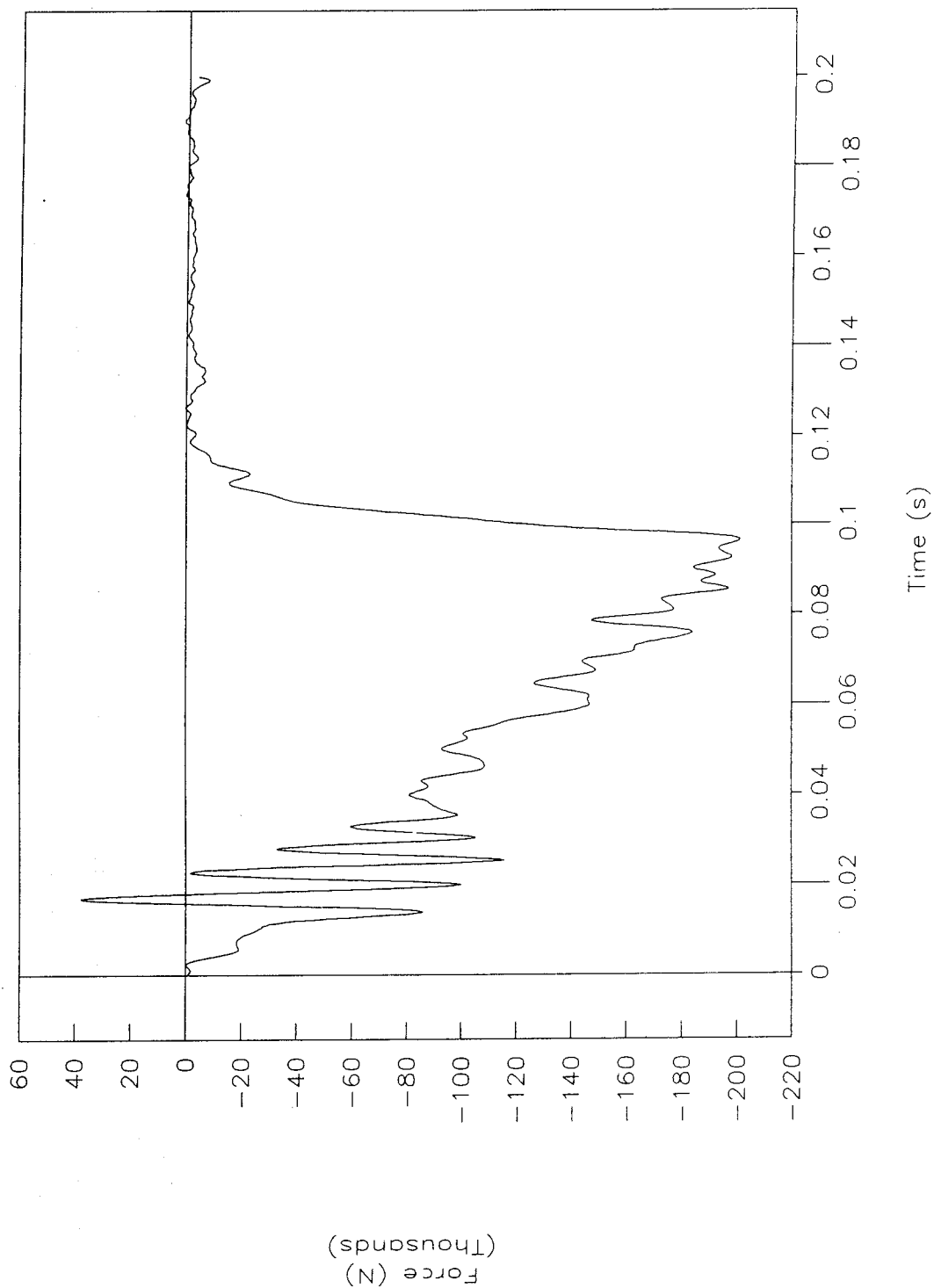


Figure 25. Force vs. time, load-cell data, test 96F008.

Test No. 96F008

Force vs. displacement, load-cell data

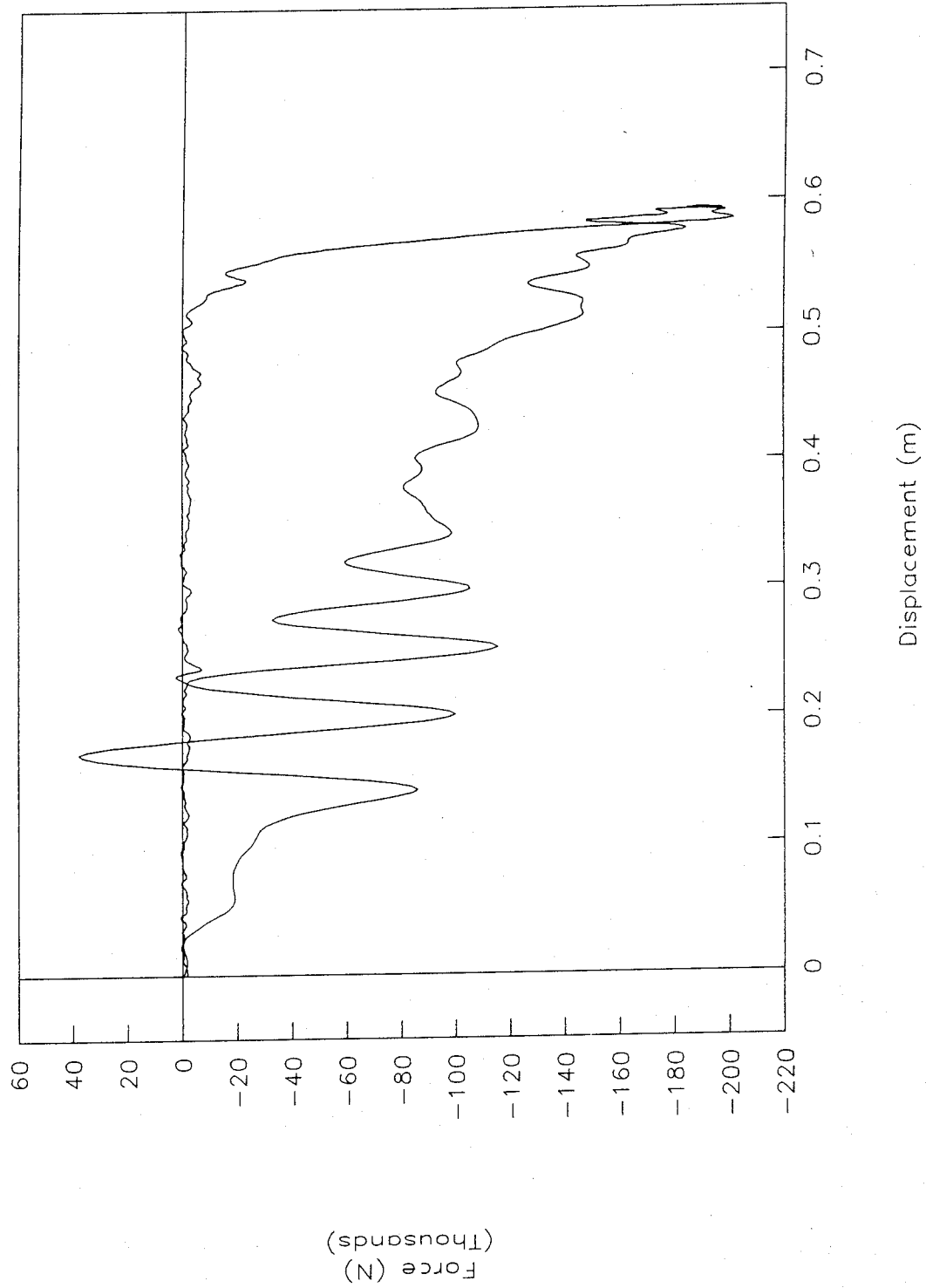


Figure 26. Force vs. displacement, load-cell data, test 96F008.

Test No. 96F008

Energy vs. displacement, load-cell data

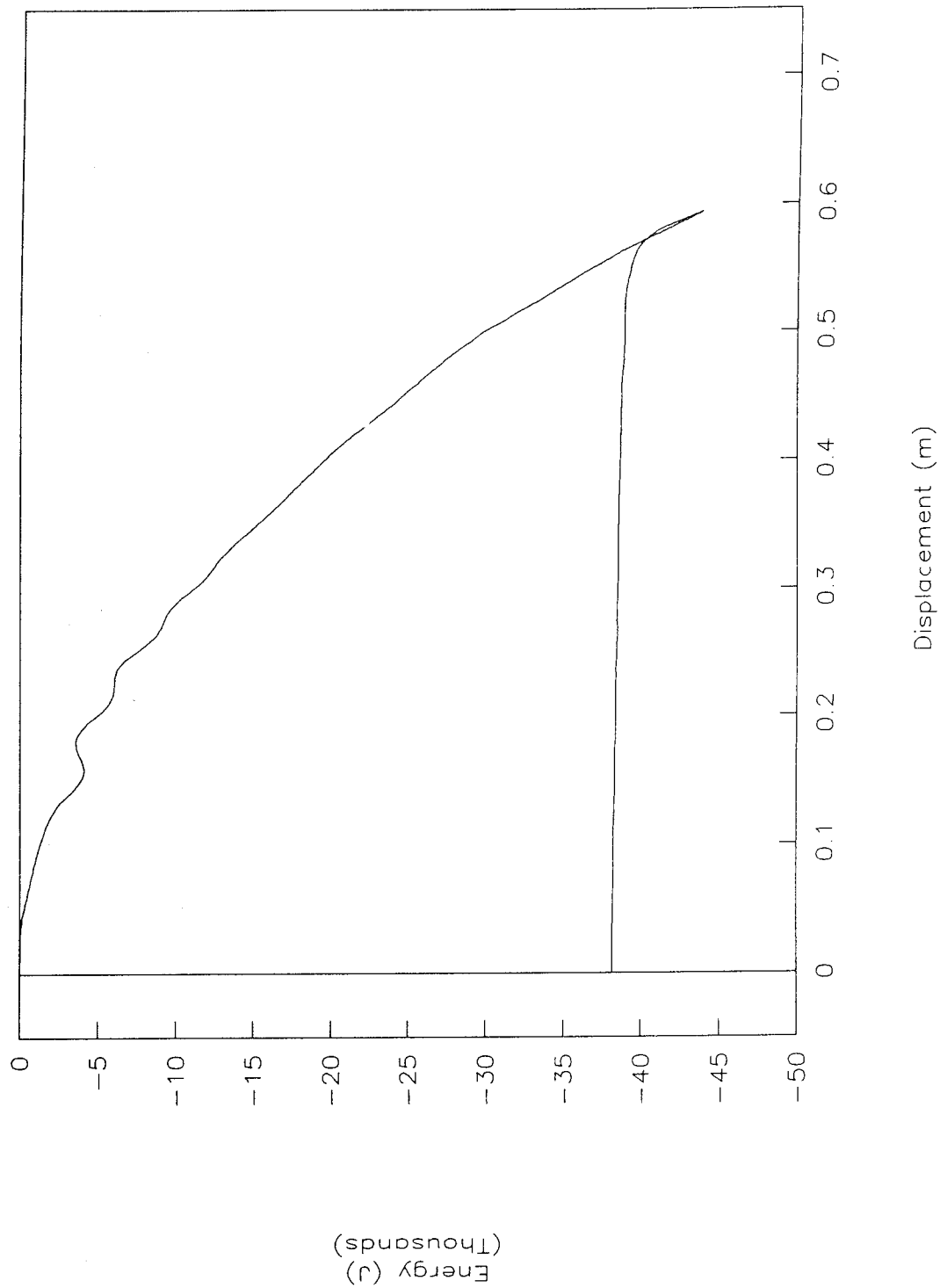


Figure 27. Energy vs. displacement, load-cell data, test 96F008.

Test No. 96F008

Resultant load height vs. time

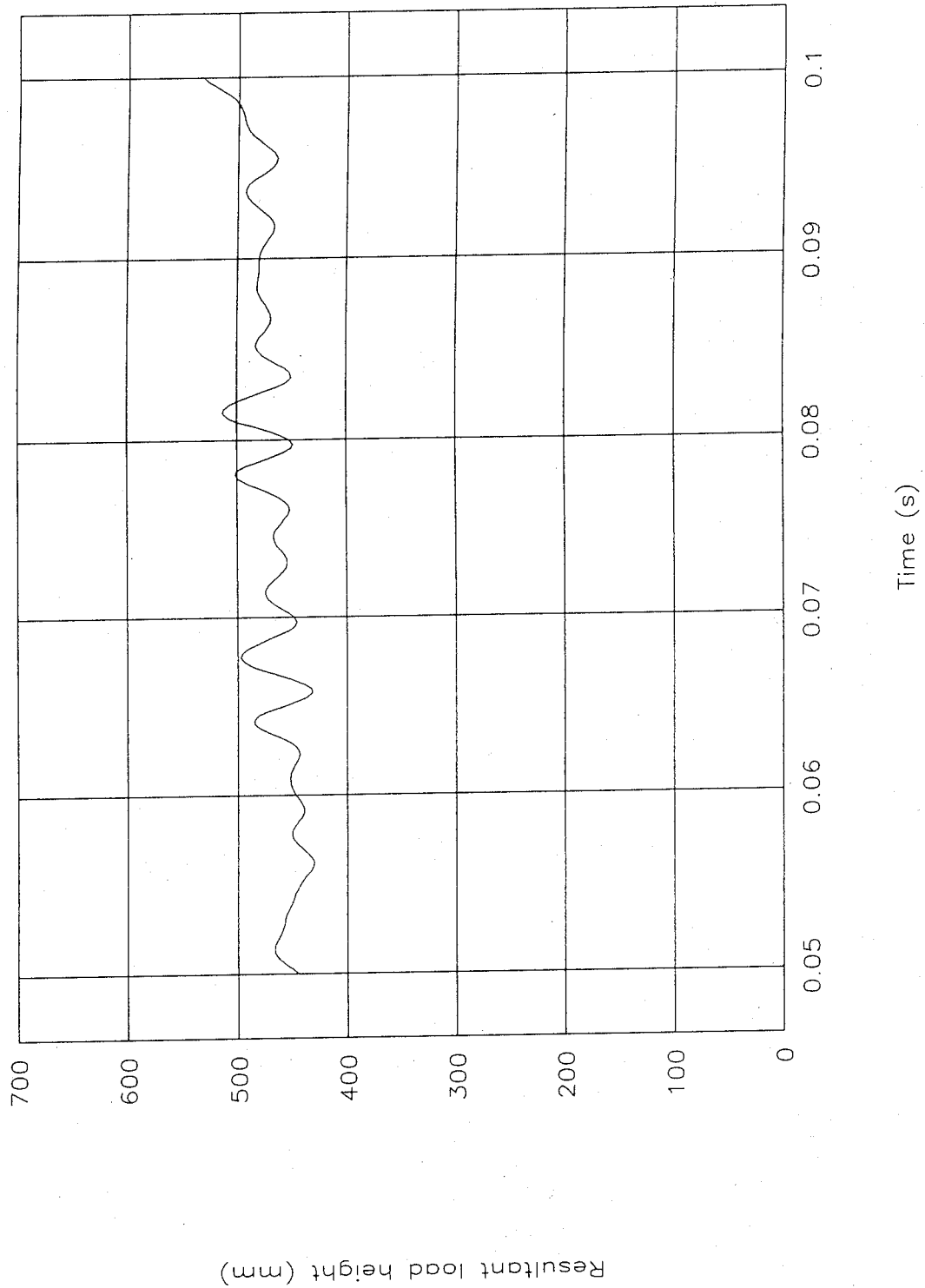


Figure 28. Resultant load height vs. time, test 96F008.

Test No. 96F009

Acceleration vs. time

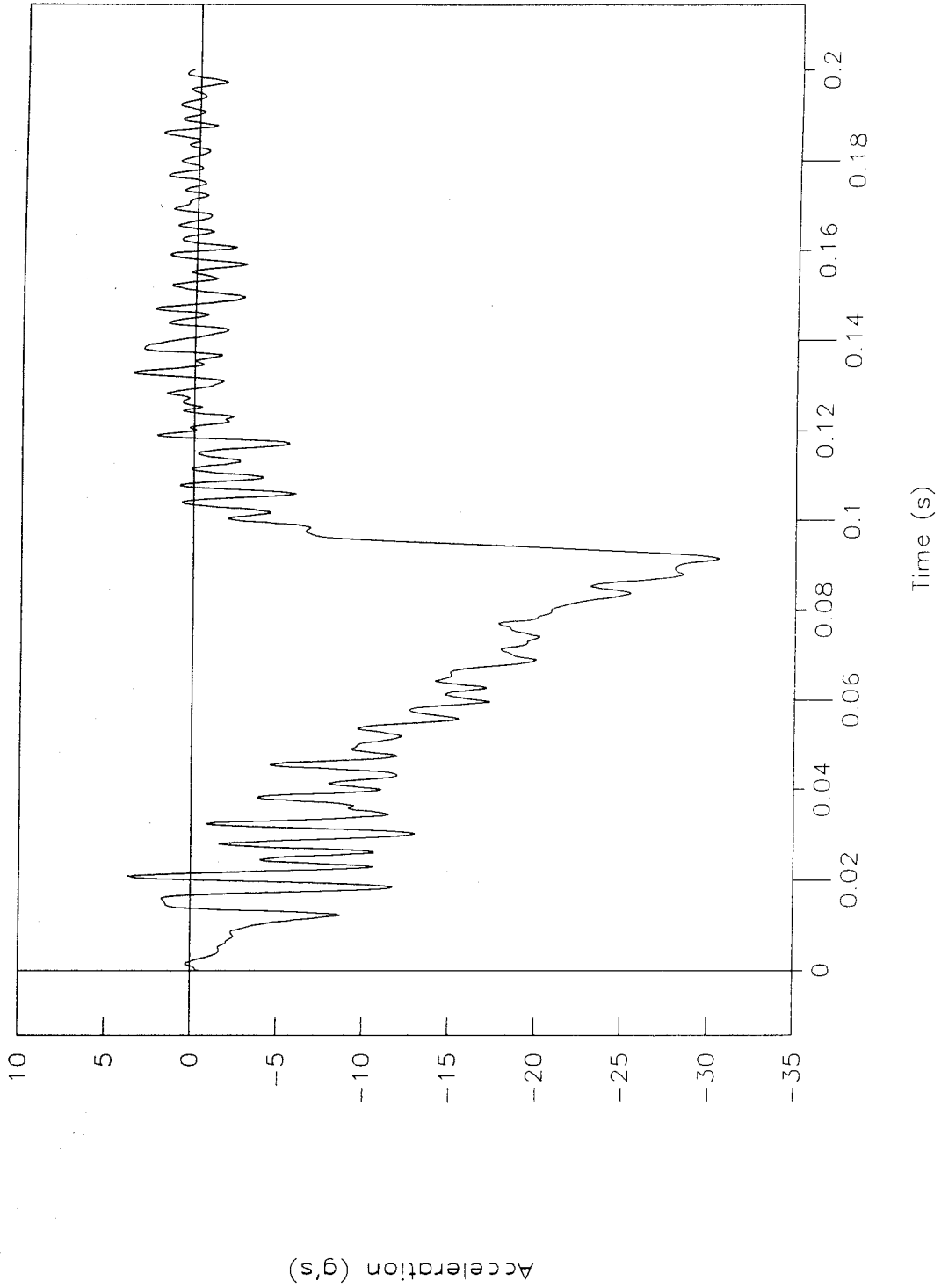


Figure 29. Acceleration vs time, test 96F009.

Test No. 96F009

Nose acceleration vs. time

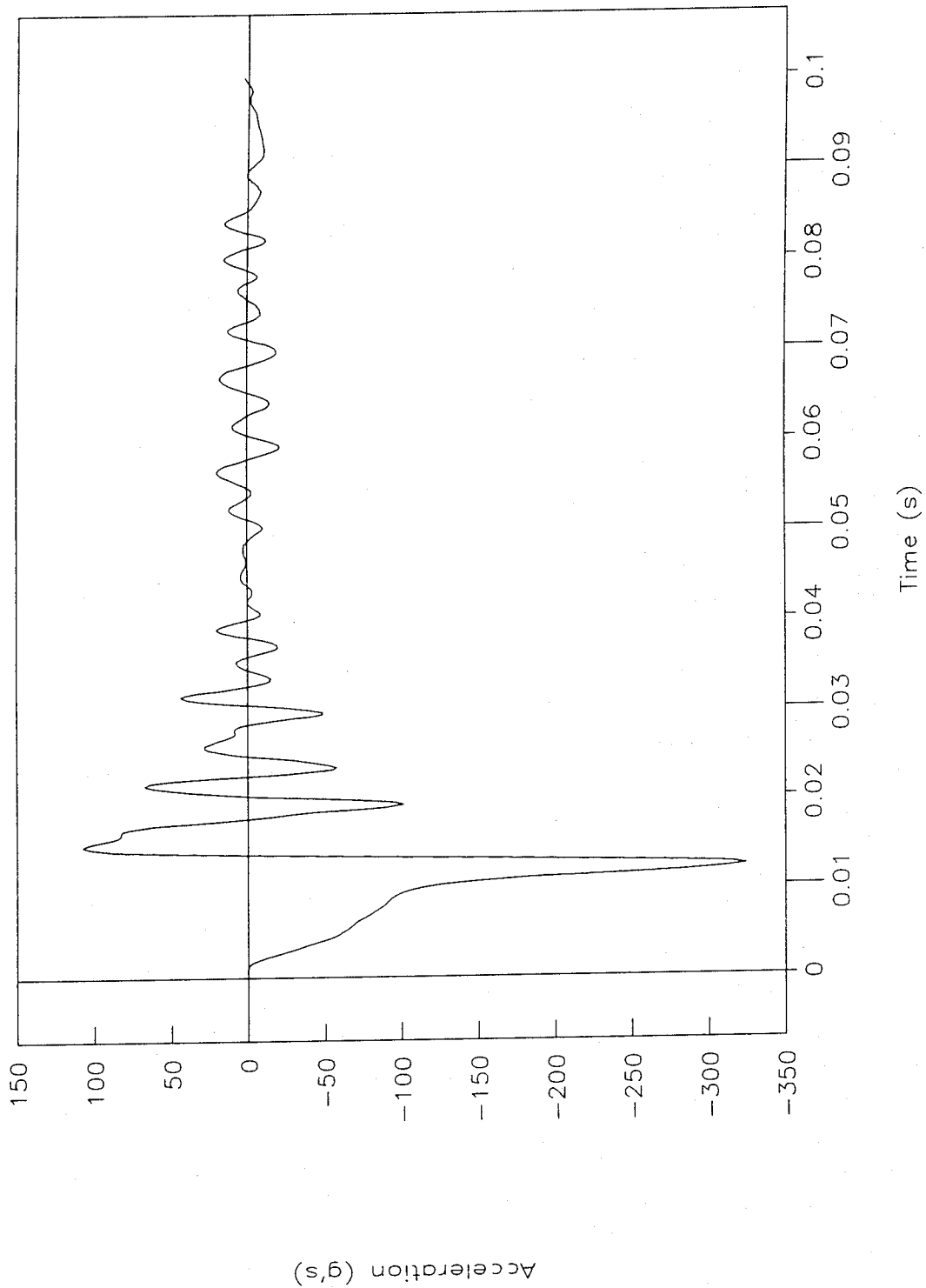


Figure 30. Nose acceleration vs. time, test 96F009.

Test No. 96F009

Velocity vs. time

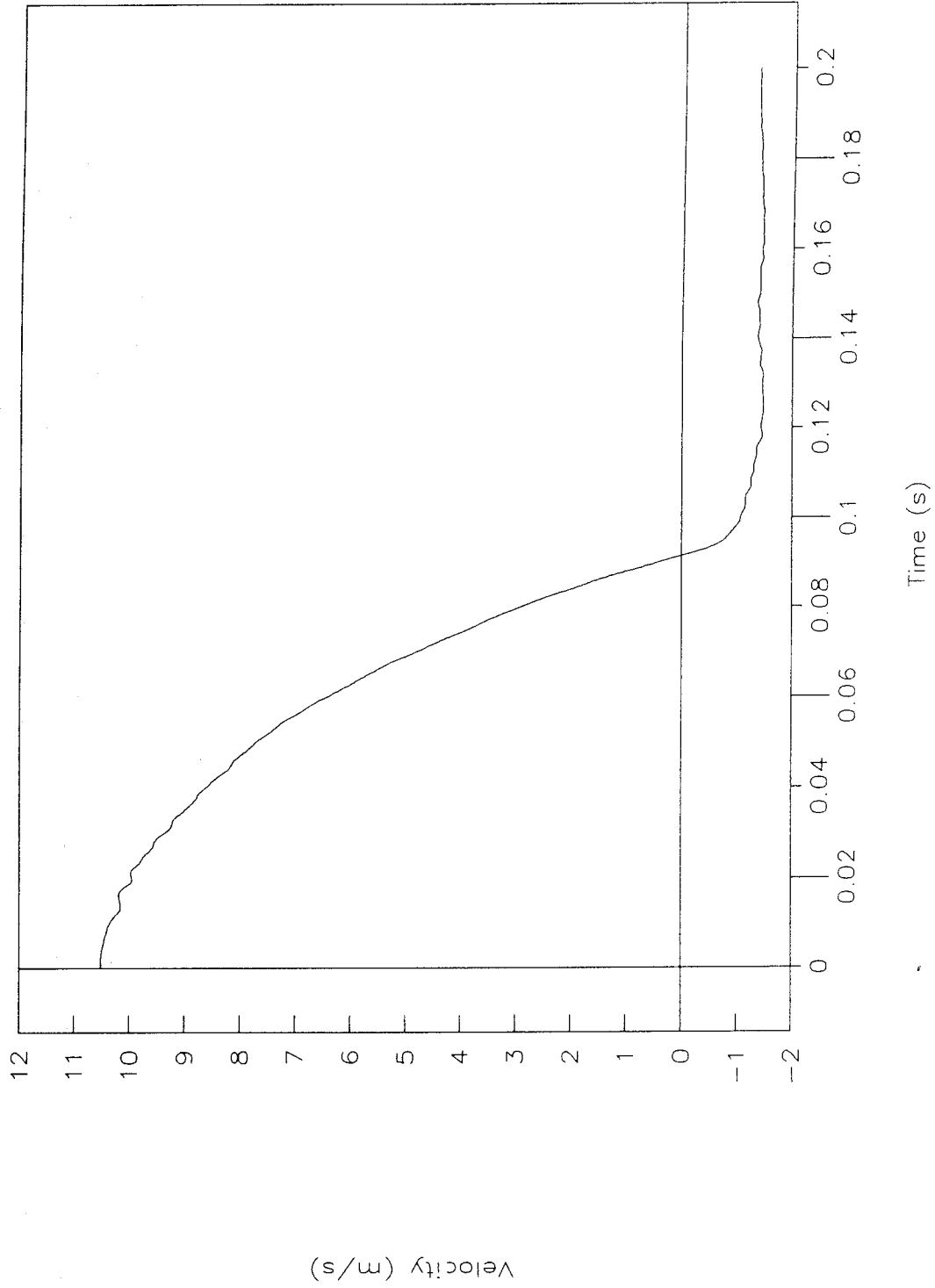


Figure 31. Velocity vs. time, test 96F009.

Test No. 96F009

Displacement vs. time

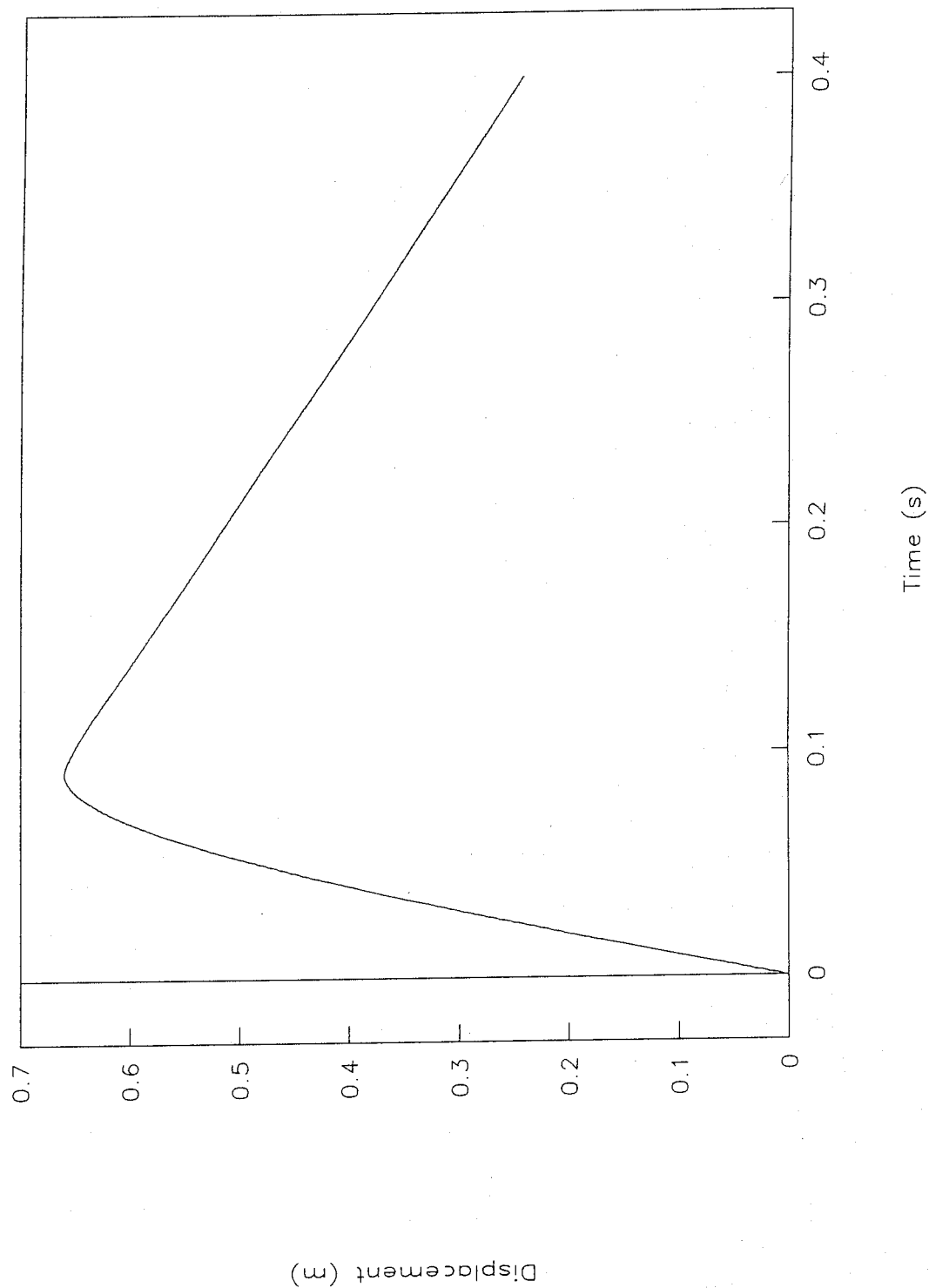


Figure 32. Displacement vs. time, test 96F009.

Test No. 96F009

Force vs. time, load-cell data

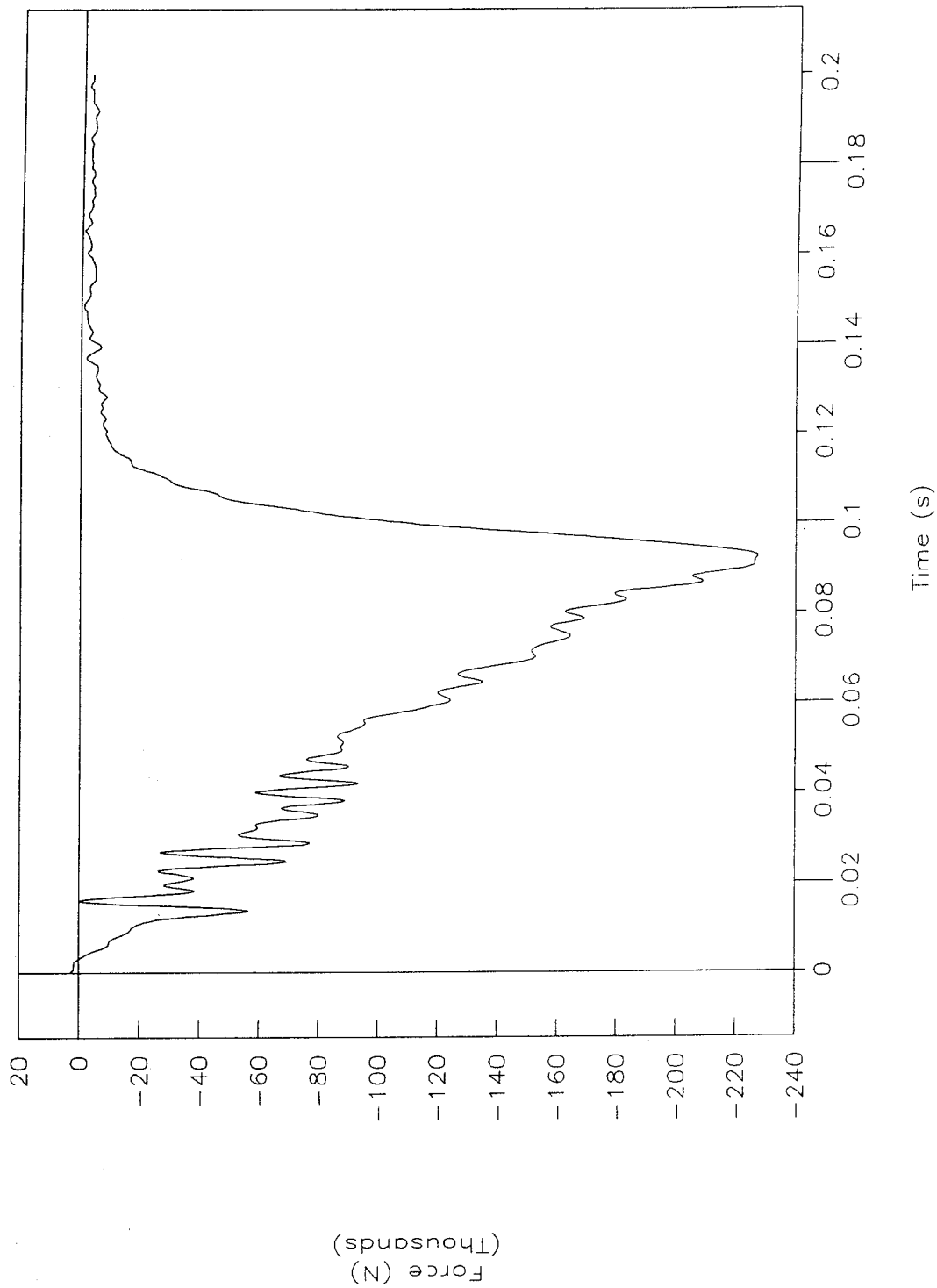


Figure 33. Force vs. time, load-cell data, test 96F009.

Test No. 96F009

Force vs. displacement, load-cell data

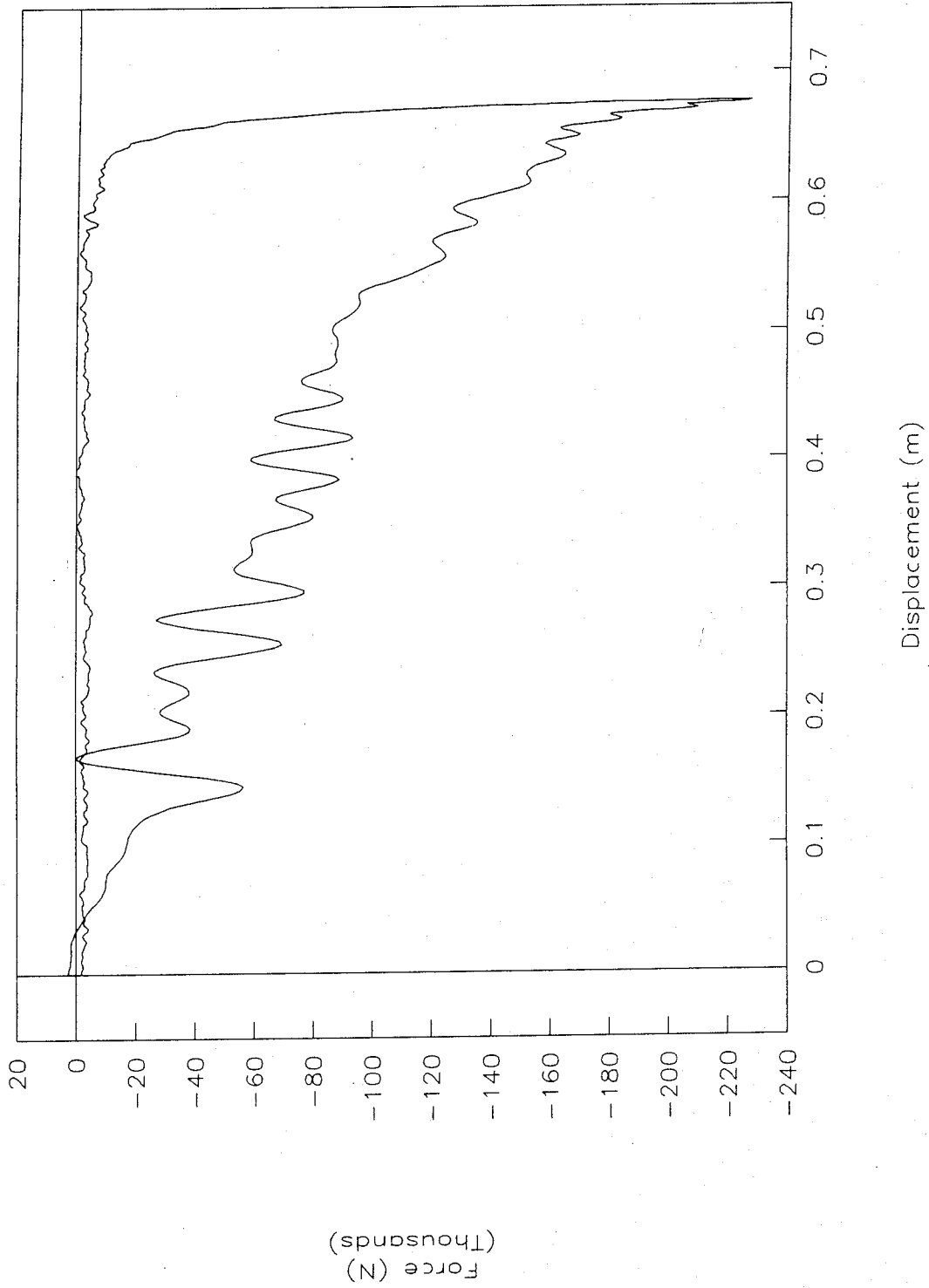


Figure 34. Force vs. displacement, load-cell data, test 96F009.

Test No. 96F009

Energy vs. displacement, load-cell data

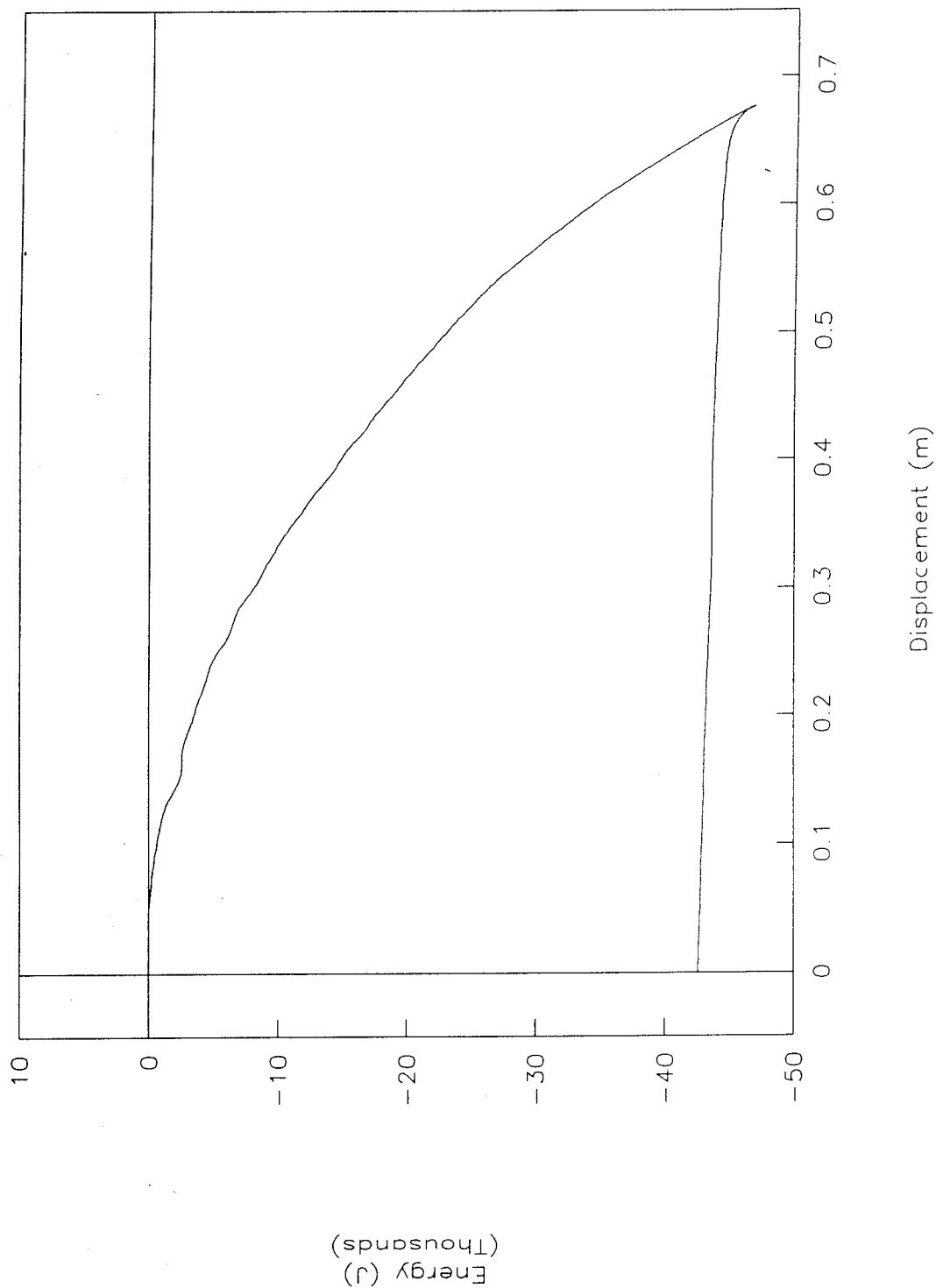


Figure 35. Energy vs. displacement, load-cell data, test 96F009.

Test No. 96F009

Resultant load height vs. time

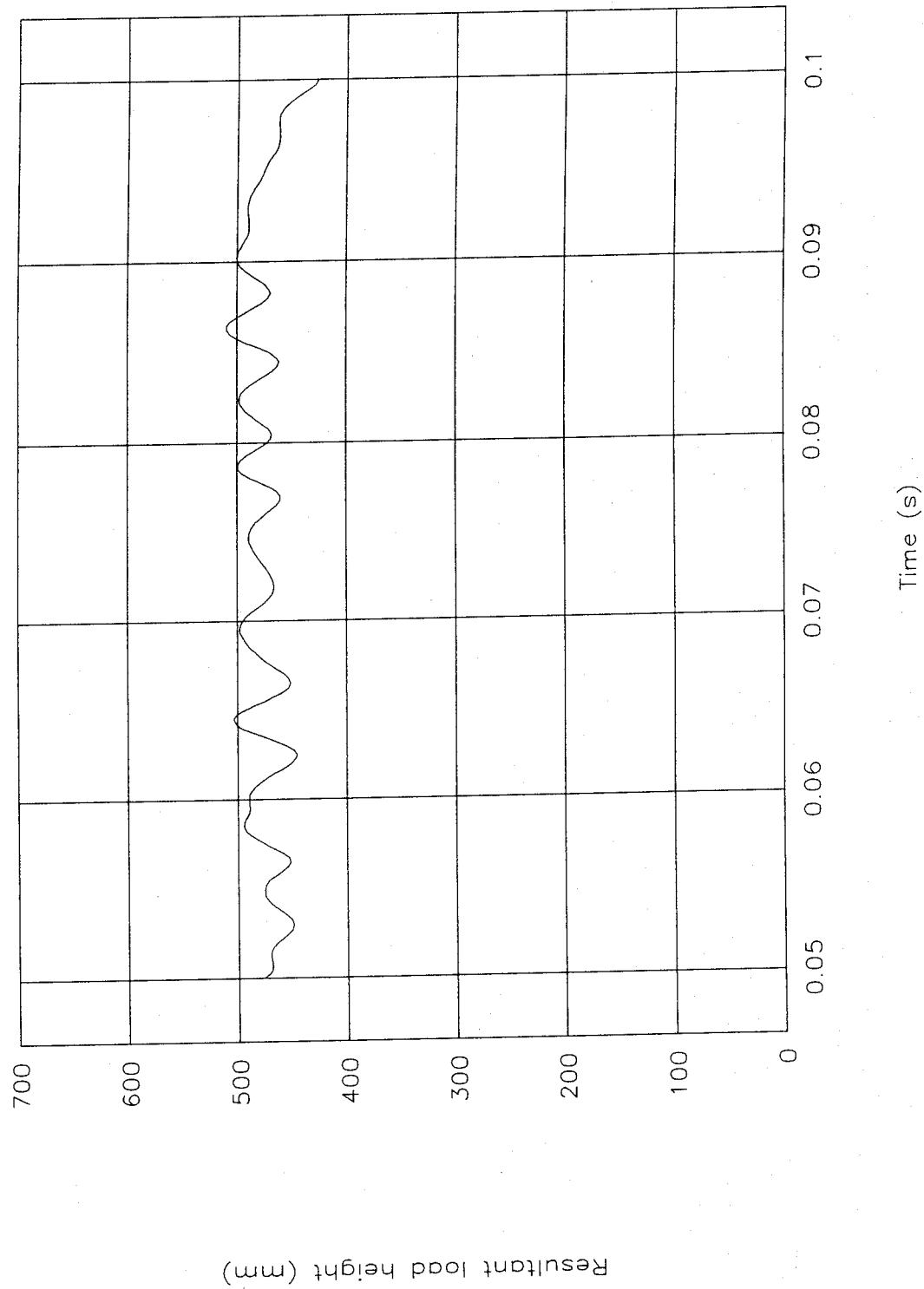


Figure 36. Resultant load height vs. time, test 96F009.

Test No. 96F010

Acceleration vs. time

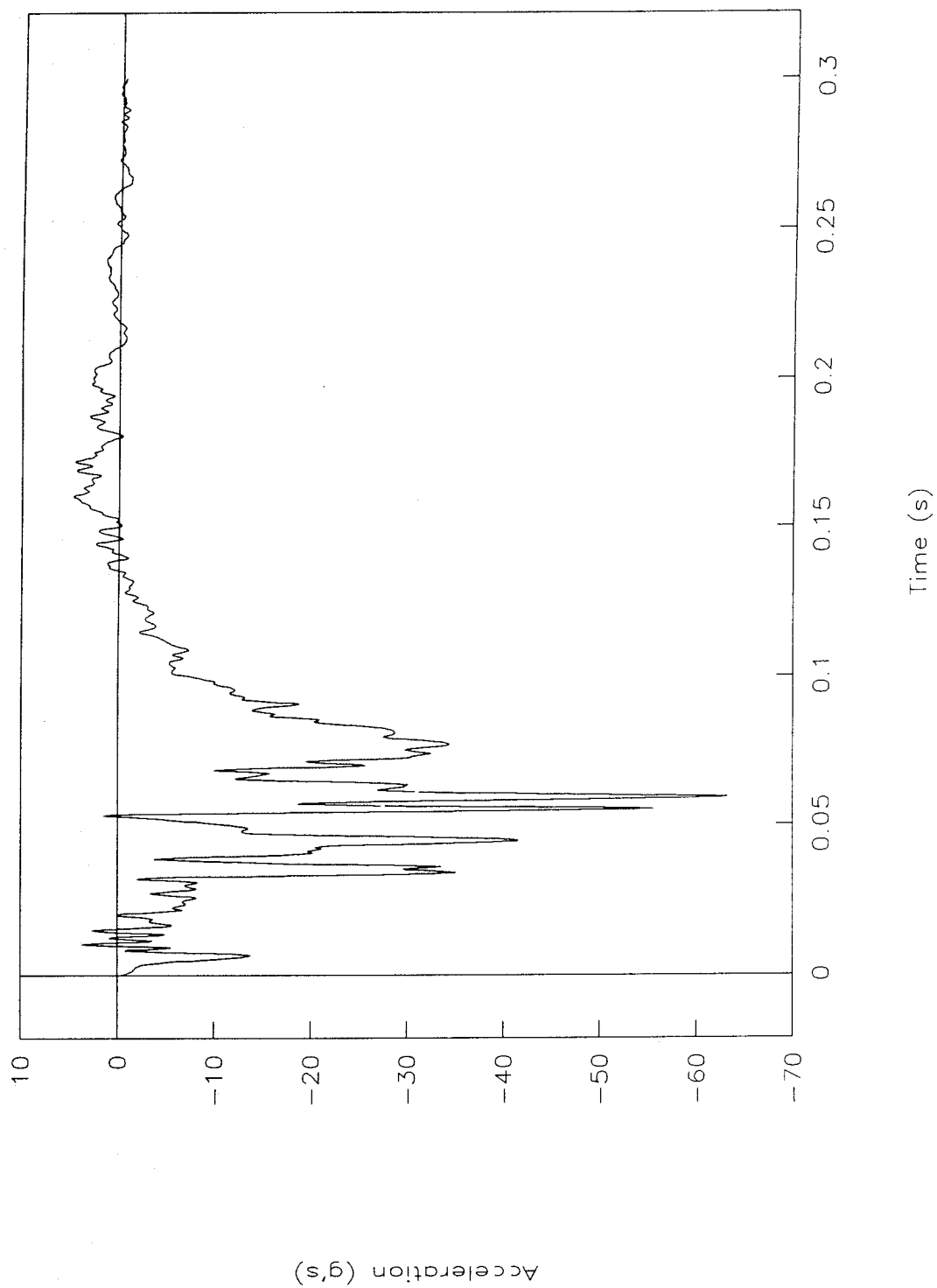


Figure 37. Acceleration vs. time, test 96F010.

Test No. 96F010

Velocity vs. time

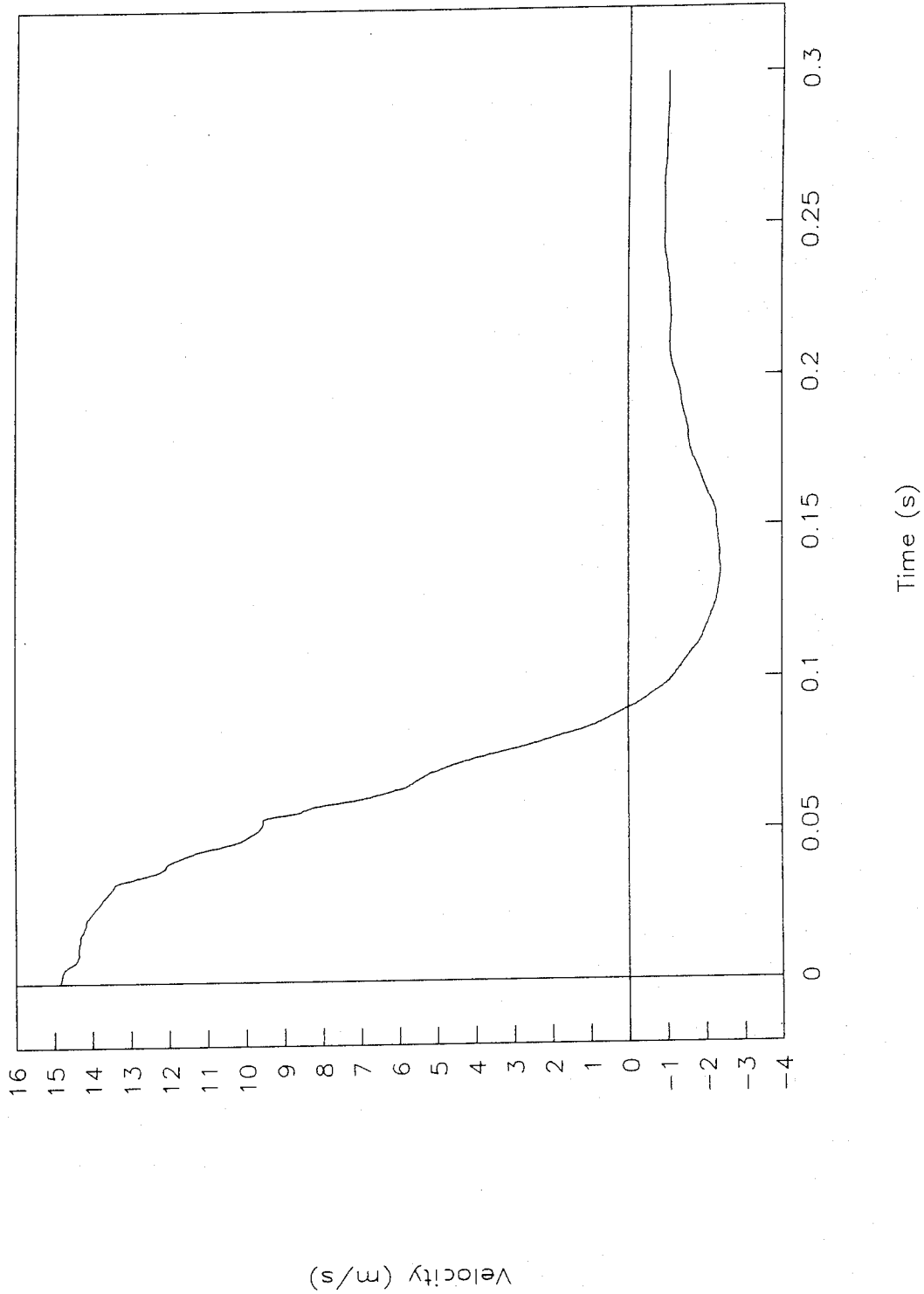


Figure 38. Velocity vs. time, test 96F010.

Test No. 96F010

Displacement vs. time

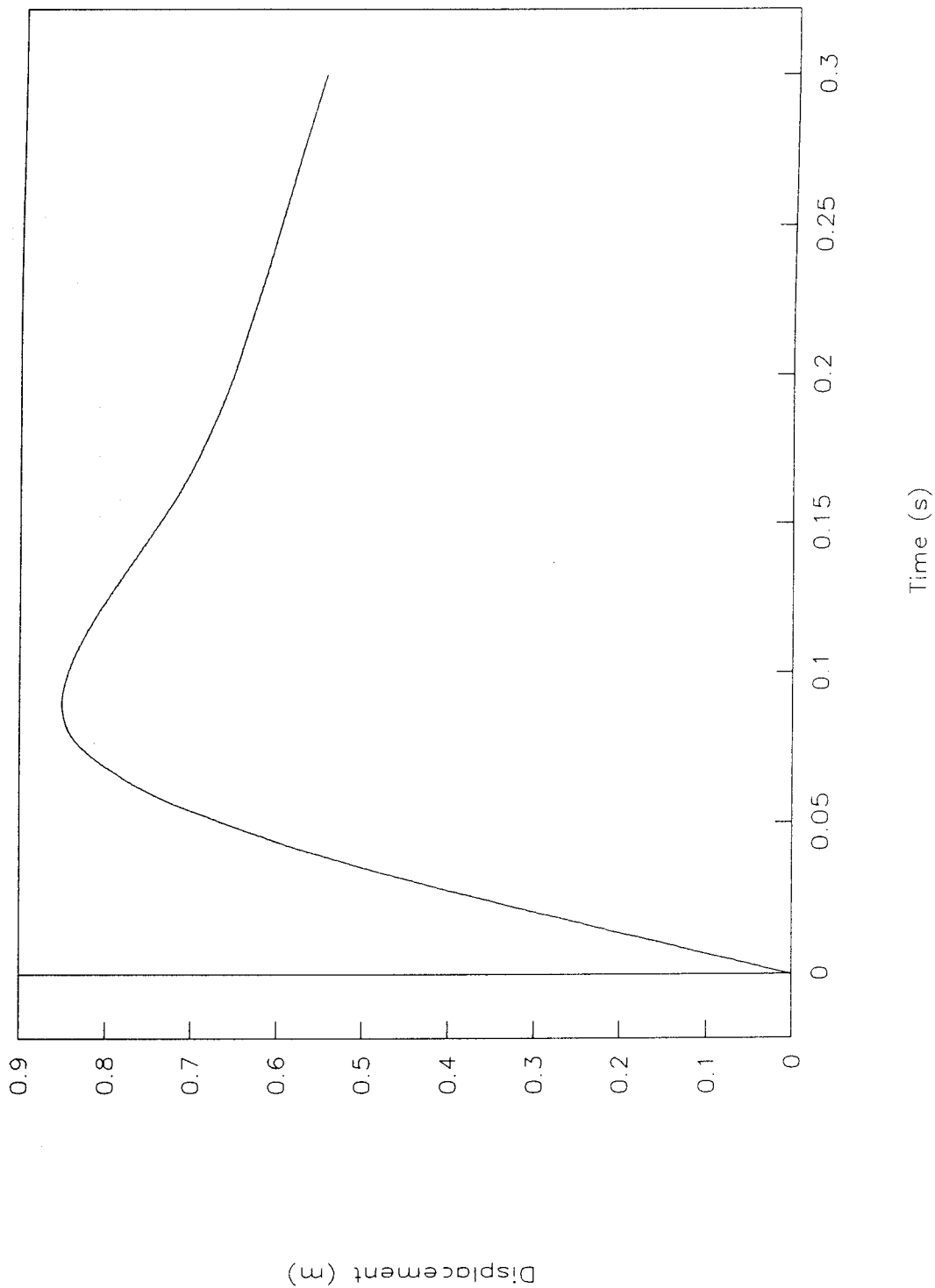


Figure 39. Displacement vs. time, test 96F010.

Test No. 96F010

Force vs. time, load-cell data

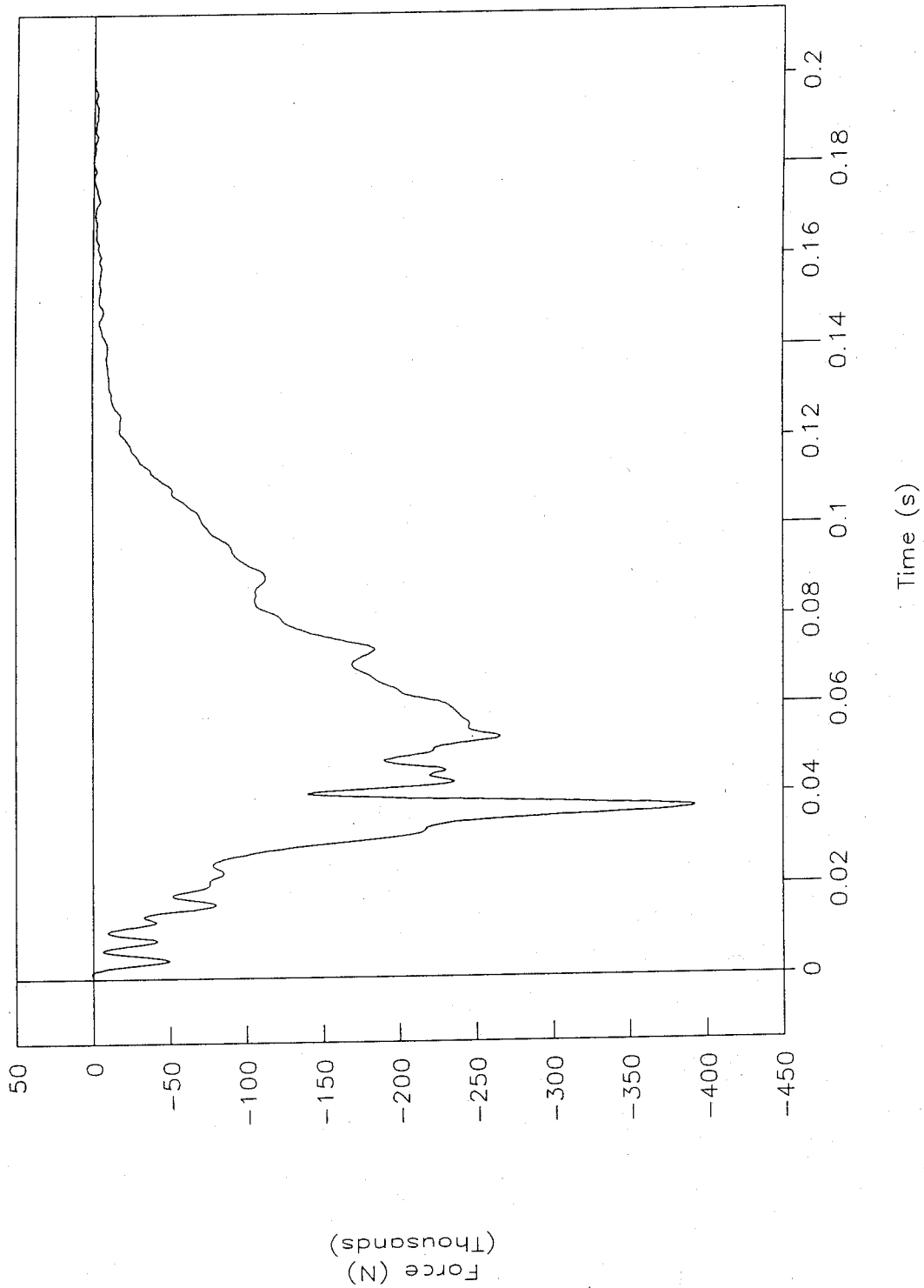


Figure 40. Force vs. time, load-cell data, test 96F010.

Test No. 96F010

Force vs. displacement, load-cell data

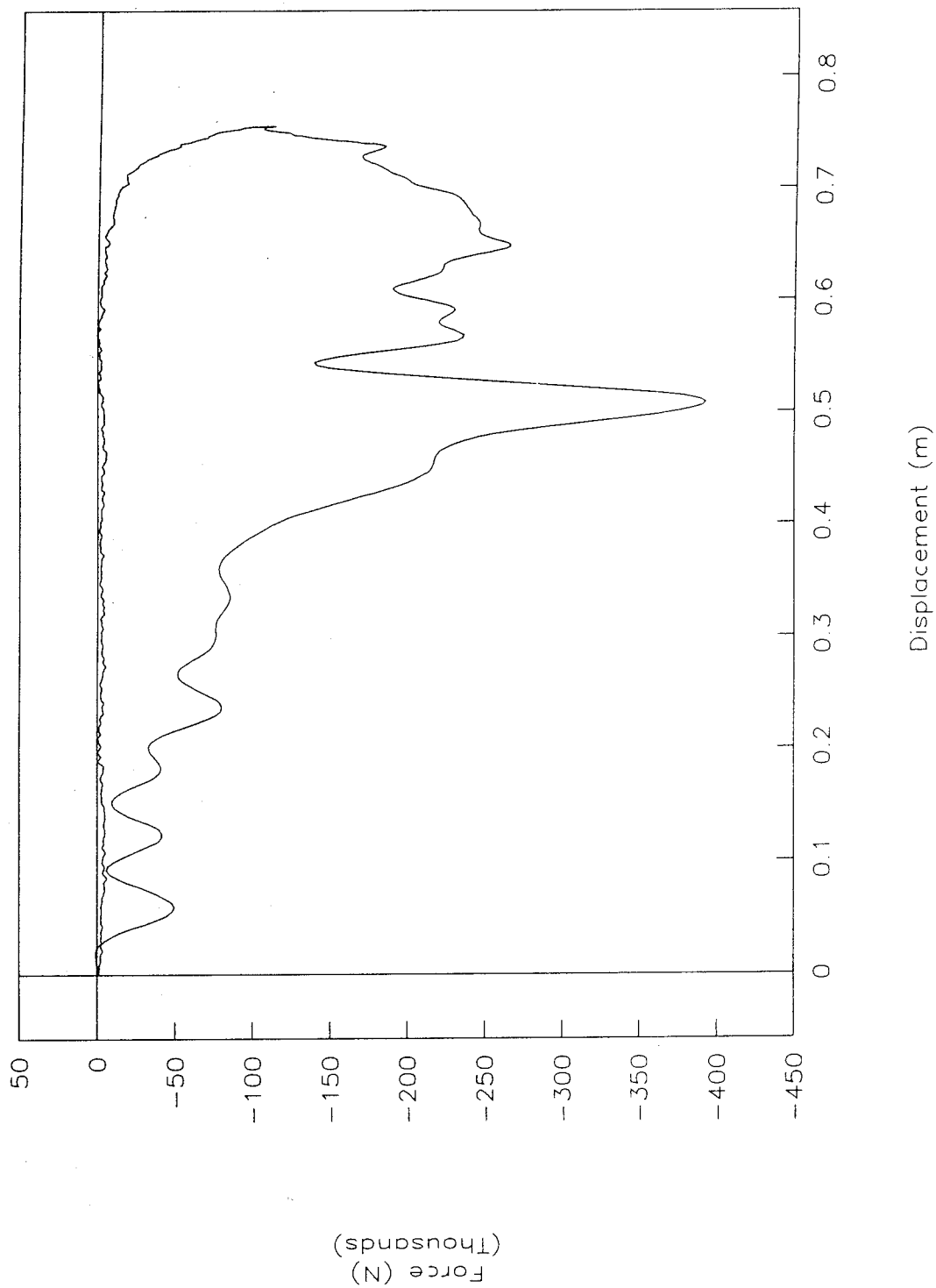


Figure 41. Force vs. displacement, load-cell data, test 96F010.

Test No. 96F010

Energy vs. displacement, load-cell data

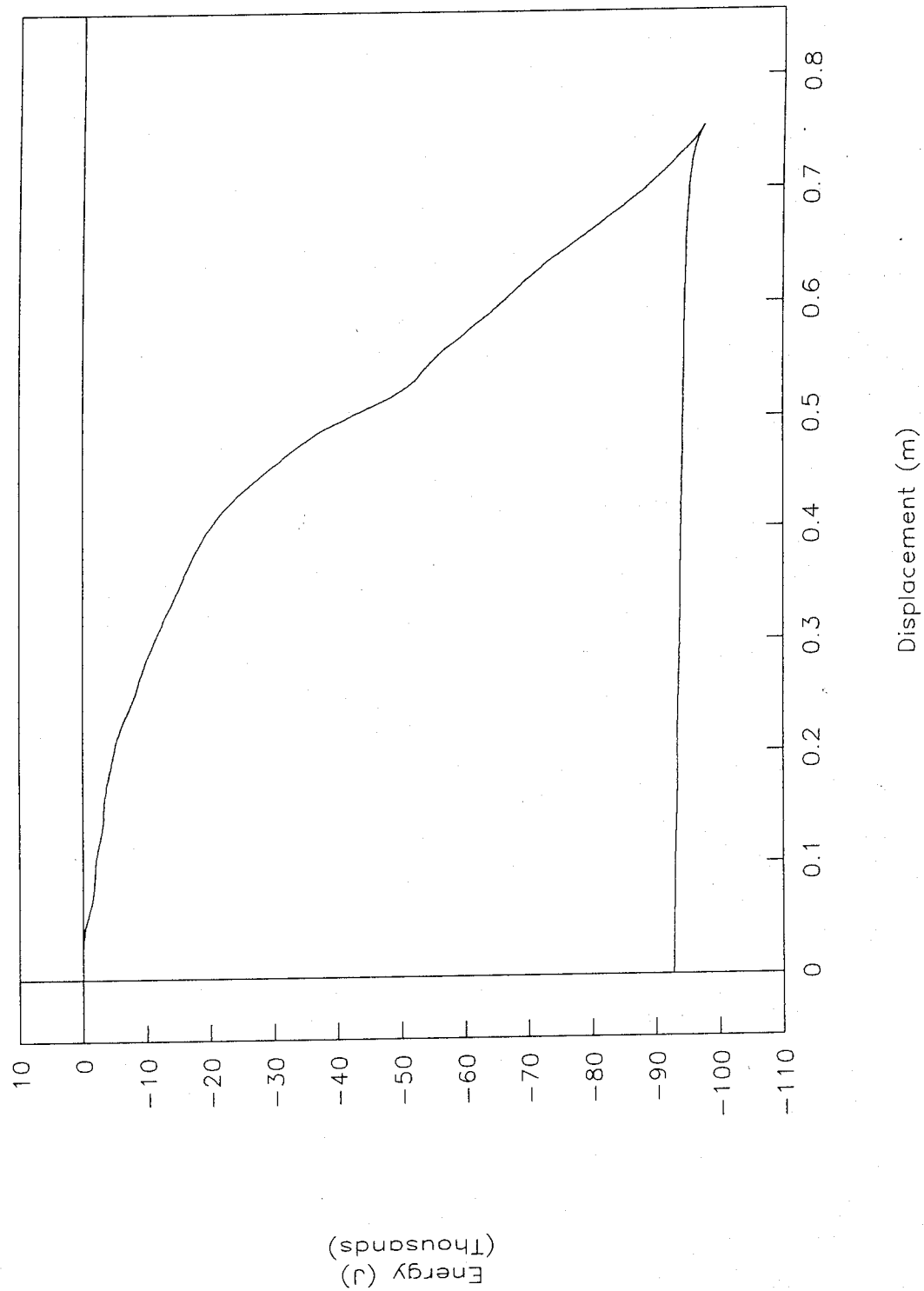


Figure 42. Energy vs. displacement, load-cell data, test 96F010.

Test No. 96F010

Acceleration vs. time, Y-axis

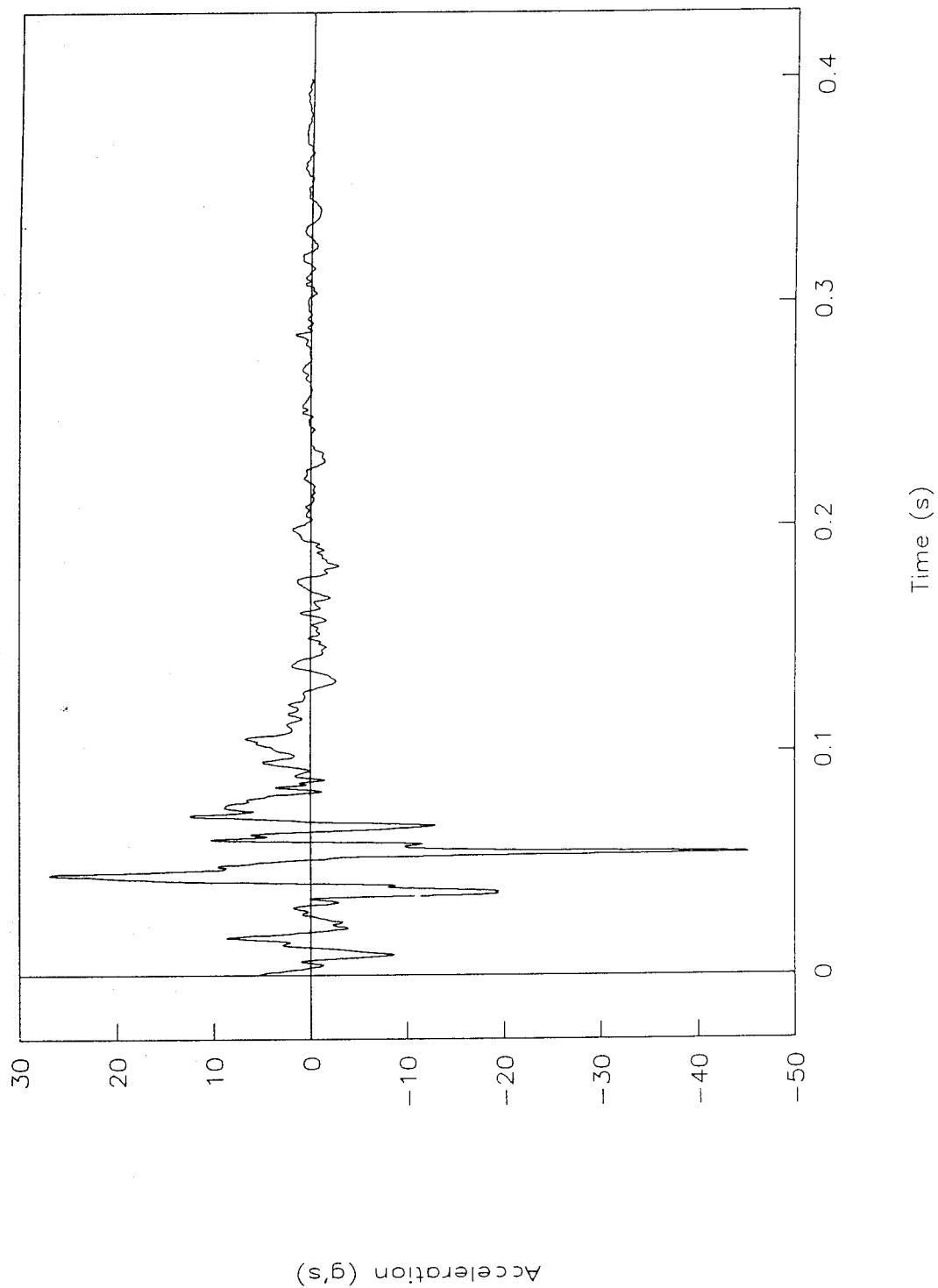


Figure 43. Acceleration vs. time, Y-axis, test 96F010.

Test No. 96F010

Acceleration vs. time, Z-axis

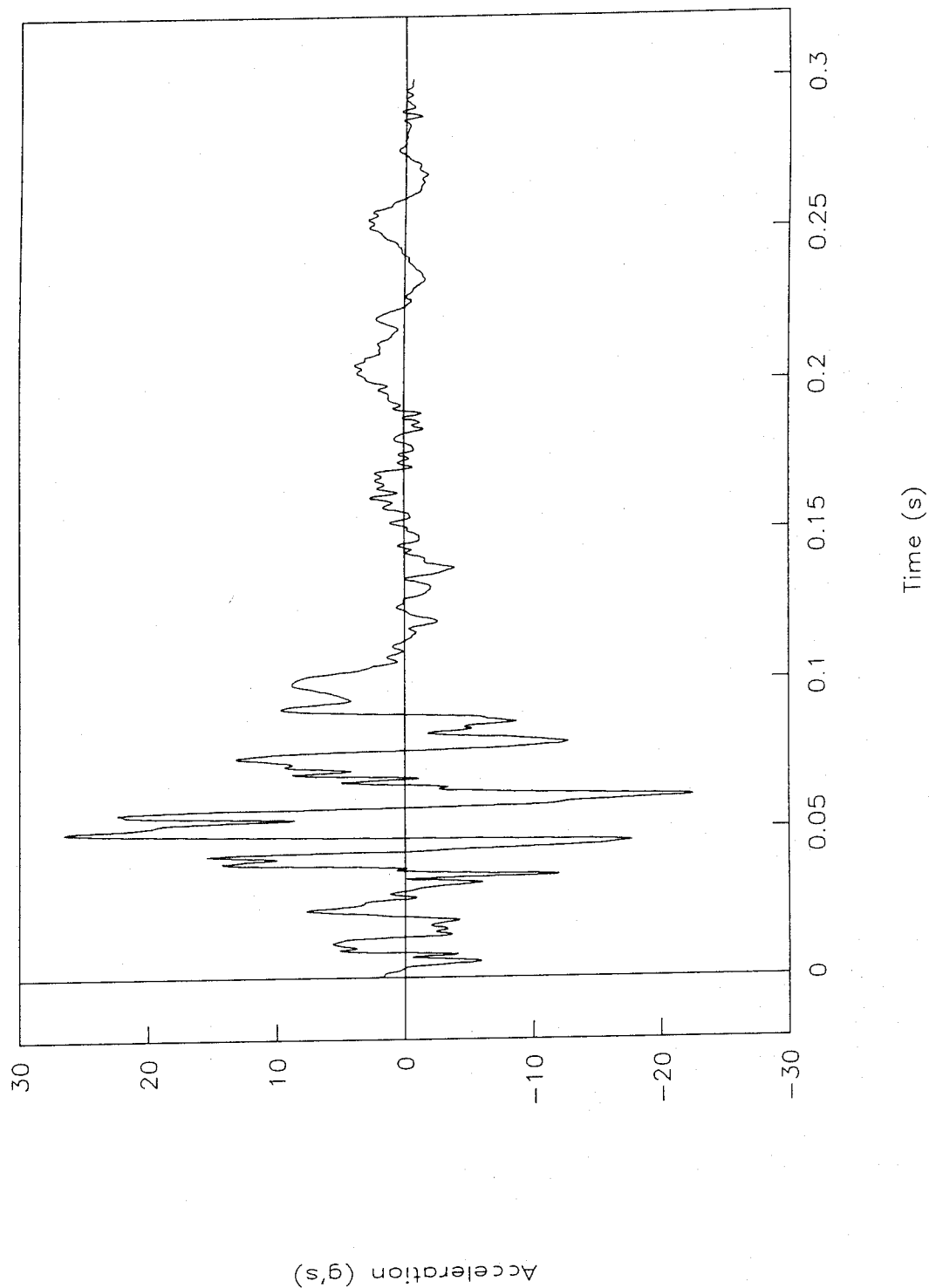


Figure 44. Acceleration vs. time, Z-axis, test 96F010.

Test No. 96F011

Acceleration vs. time

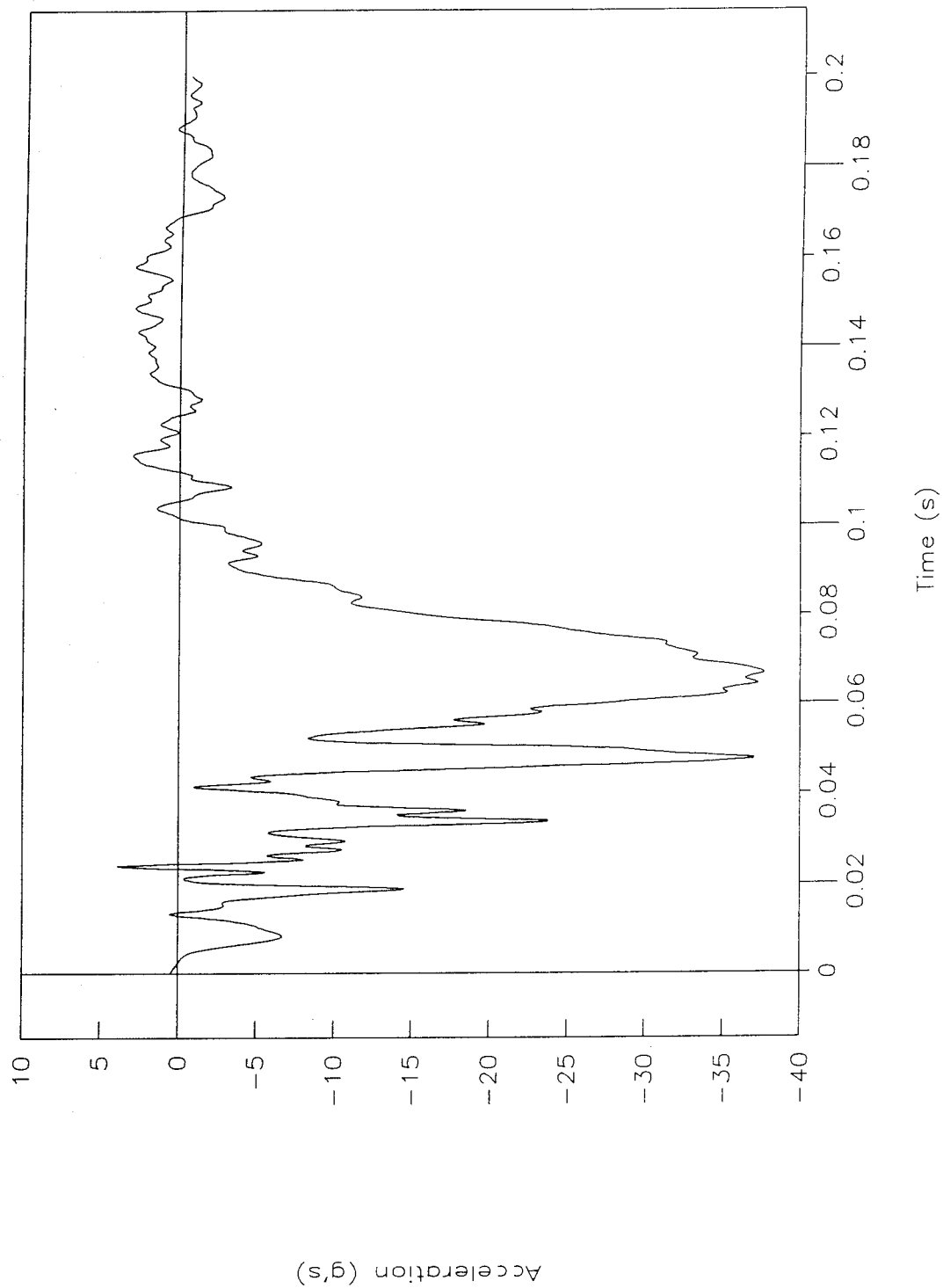


Figure 45. Acceleration vs. time, test 96F011.

Test No. 96F011

Velocity vs. time

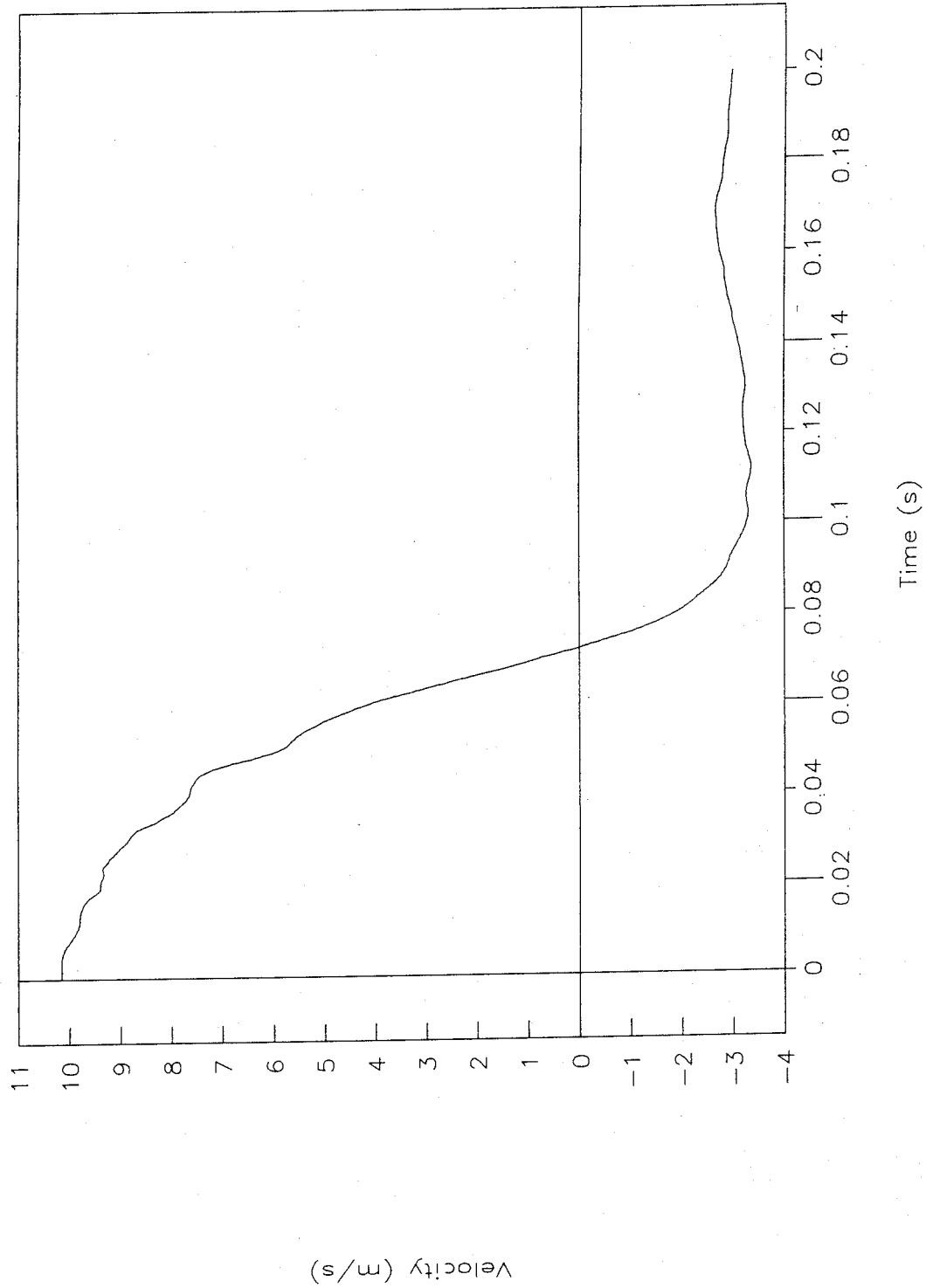


Figure 46. Velocity vs. time, test 96F011.

Test No. 96F011

Displacement vs. time

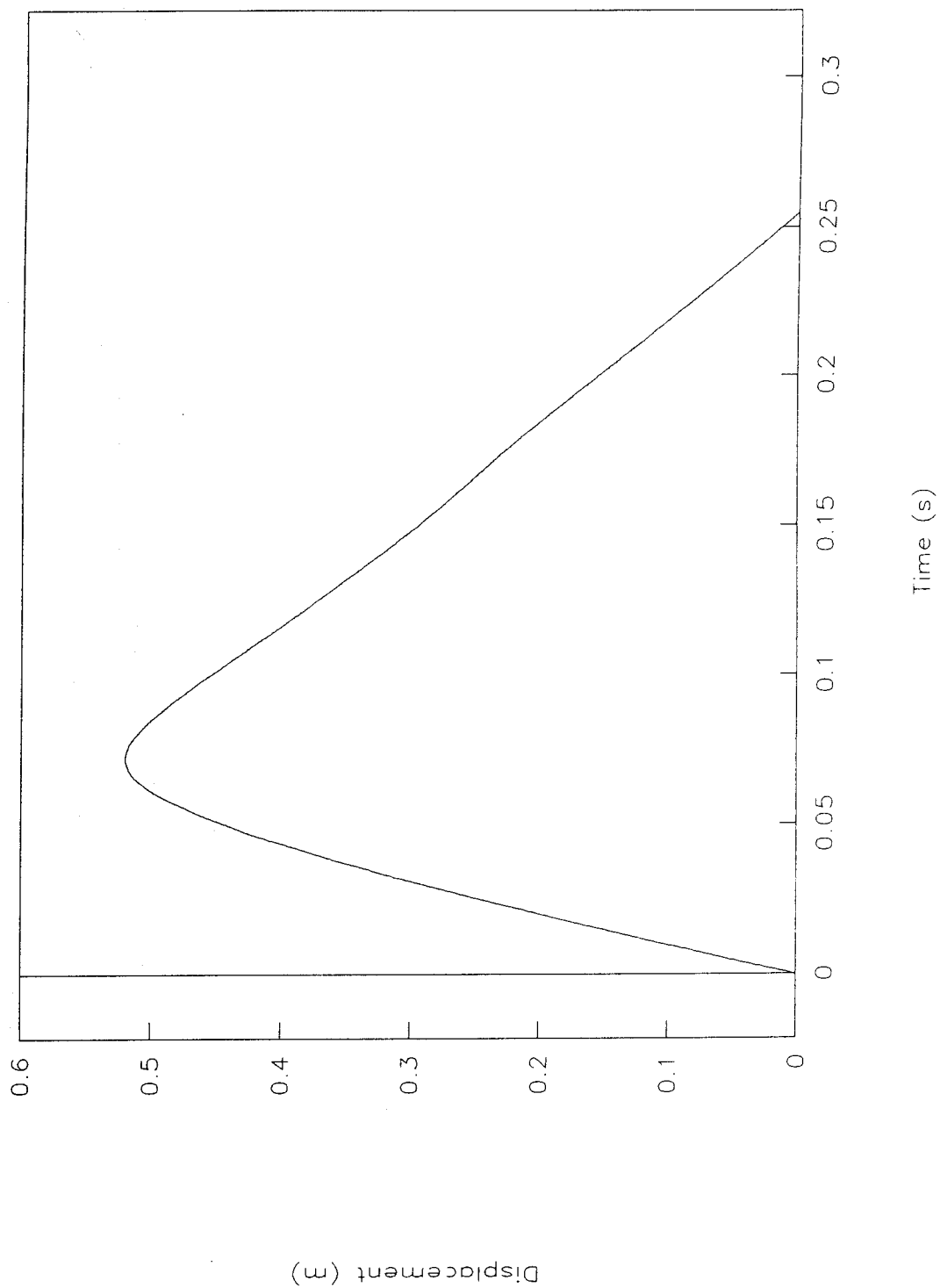


Figure 47. Displacement vs. time, test 96F011.

Test No. 96F011

Force vs. time, load-cell data

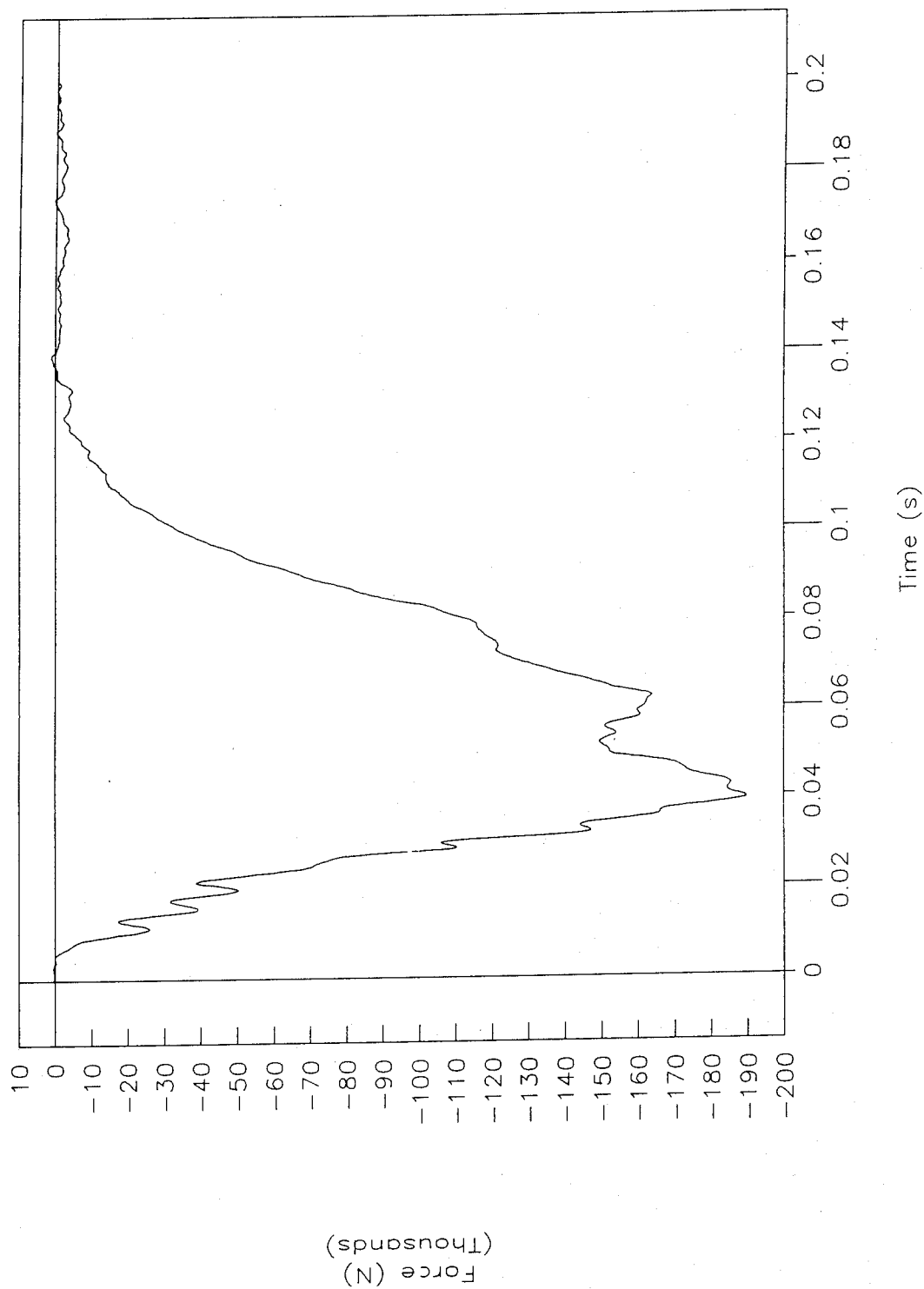


Figure 48. Force vs. time, load-cell data, test 96F011.

Test No. 96F011

Force vs. displacement

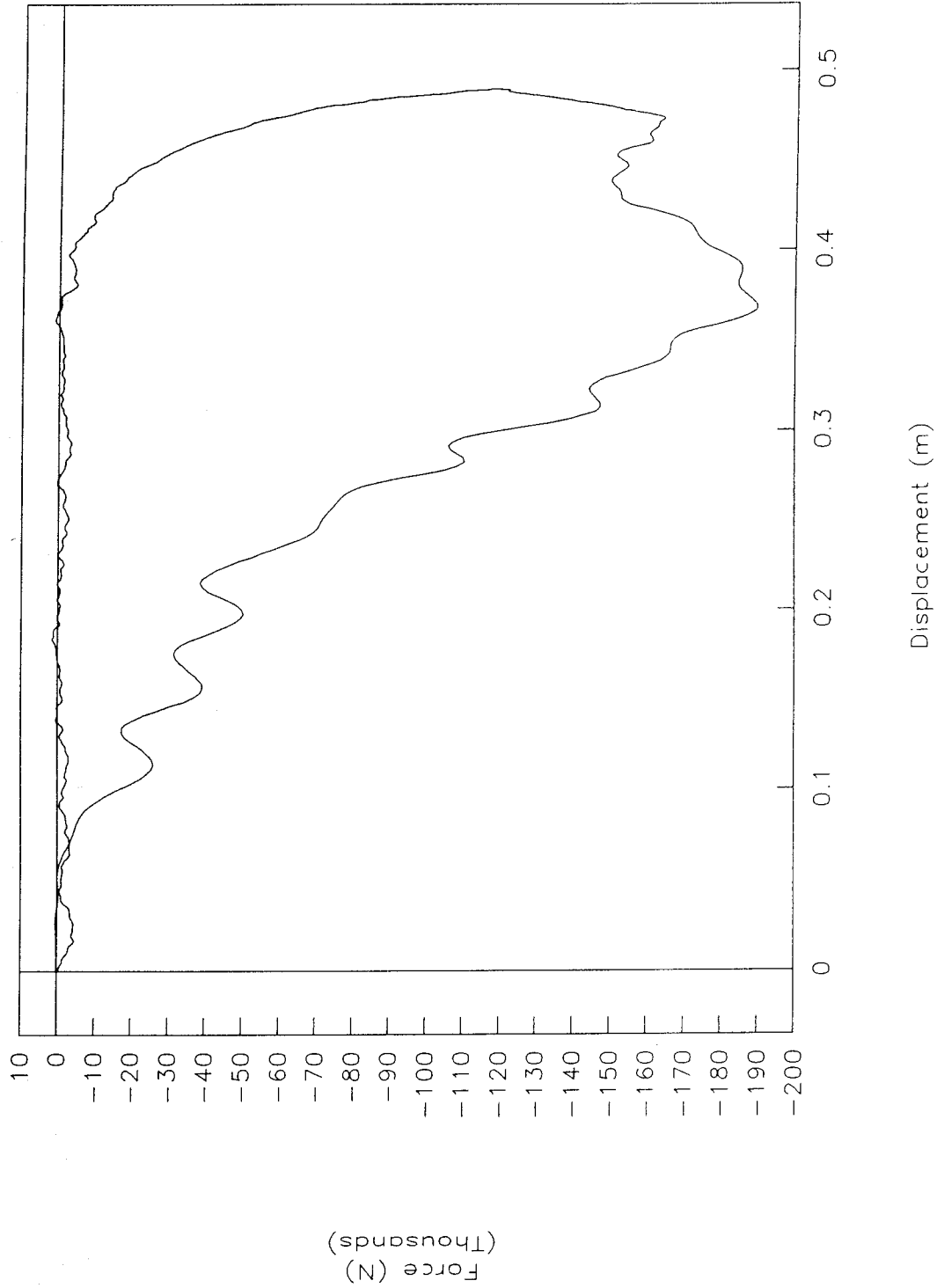


Figure 49. Force vs. displacement, test 96F011.

Test No. 96F011

Energy vs. displacement, load-cell data

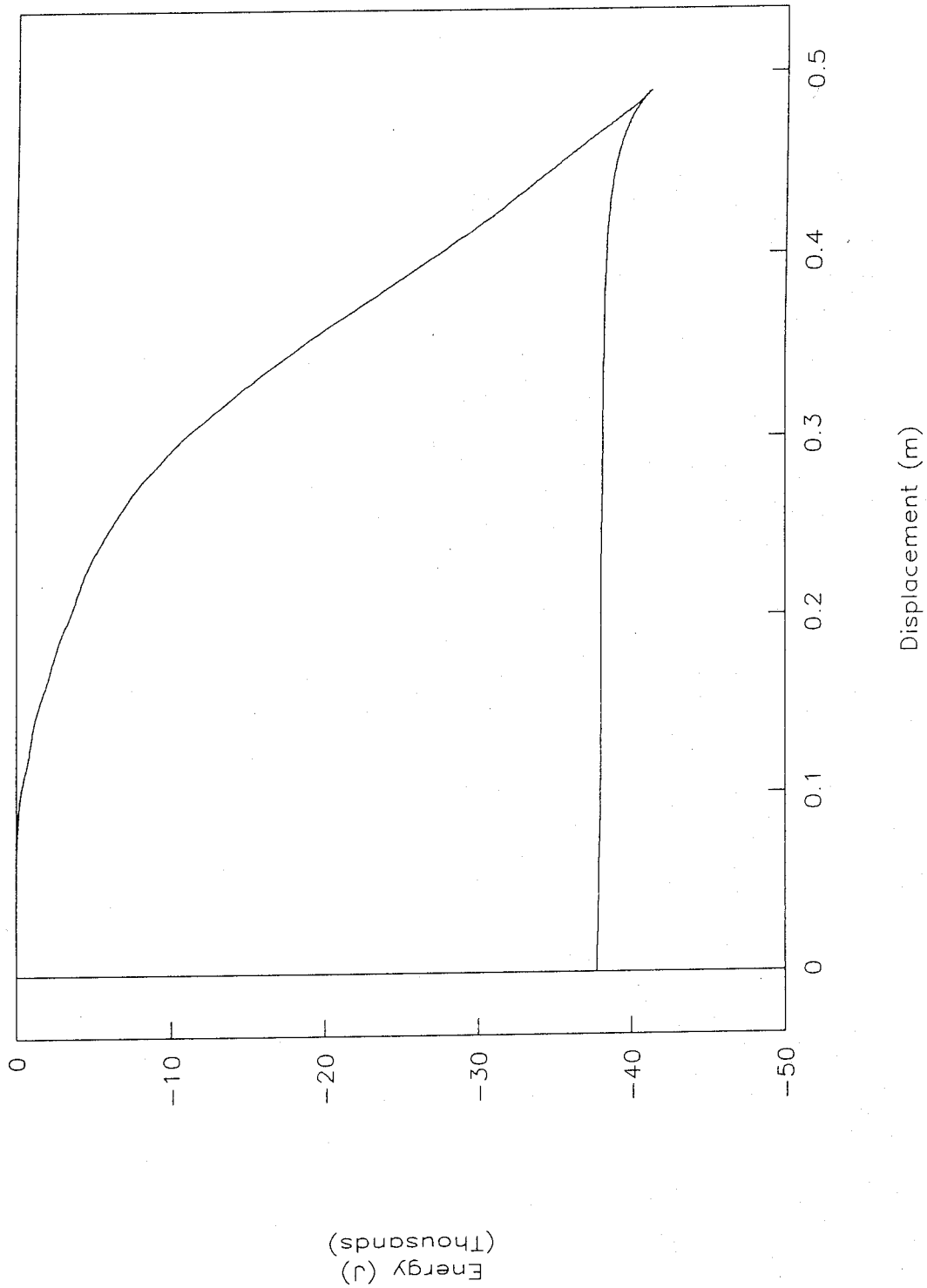


Figure 50. Energy vs. displacement, load-cell data, test 96F011.

Test No. 96F011

Acceleration vs. time, Y-axis

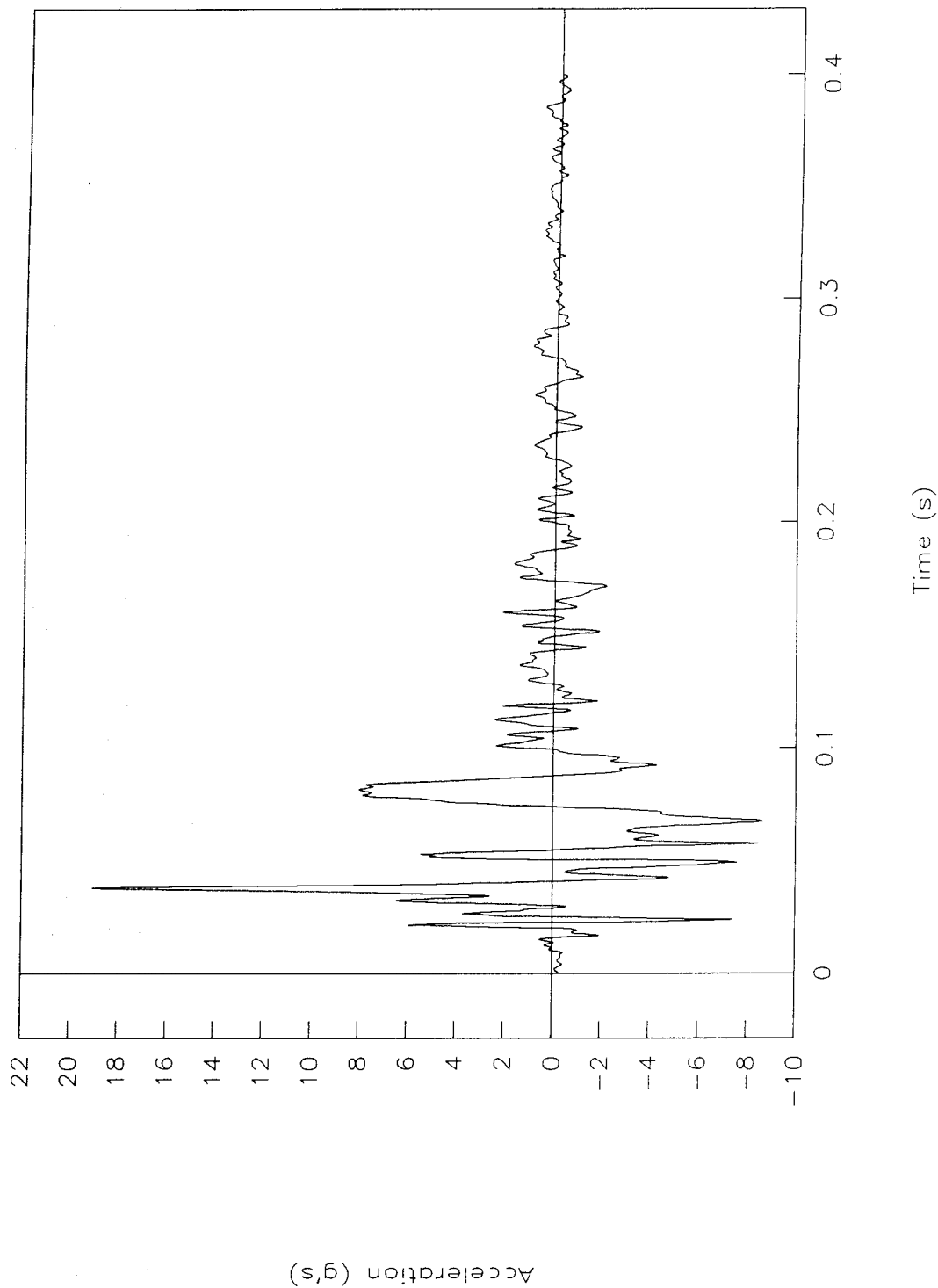


Figure 51. Acceleration vs. time, Y-axis, test 96F011.

Test No. 96F011

Acceleration vs. time, Z-axis

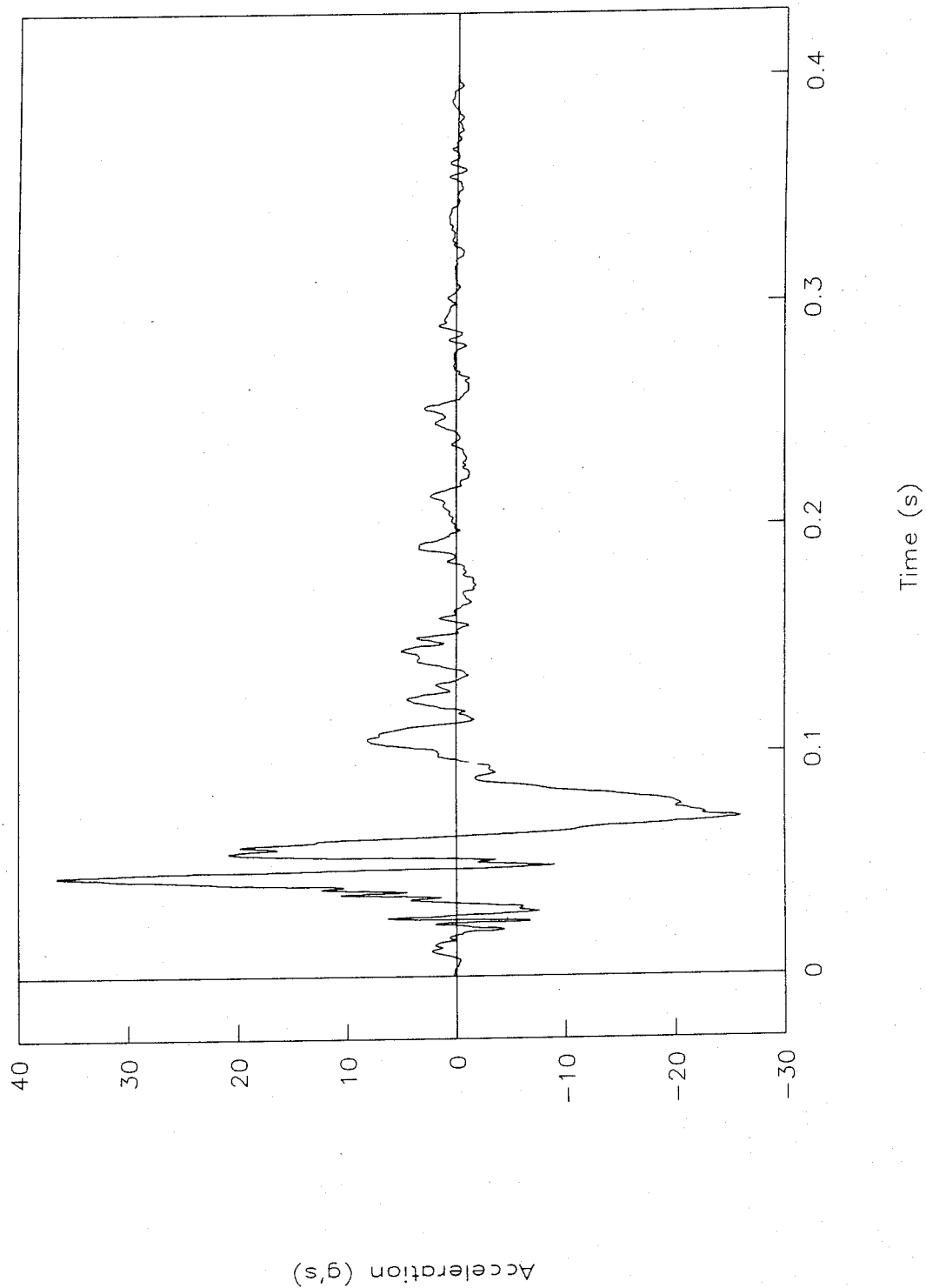


Figure 52. Acceleration vs. time, Z-axis, test 96F011.

Test No. 96F011

Resultant load height vs. time

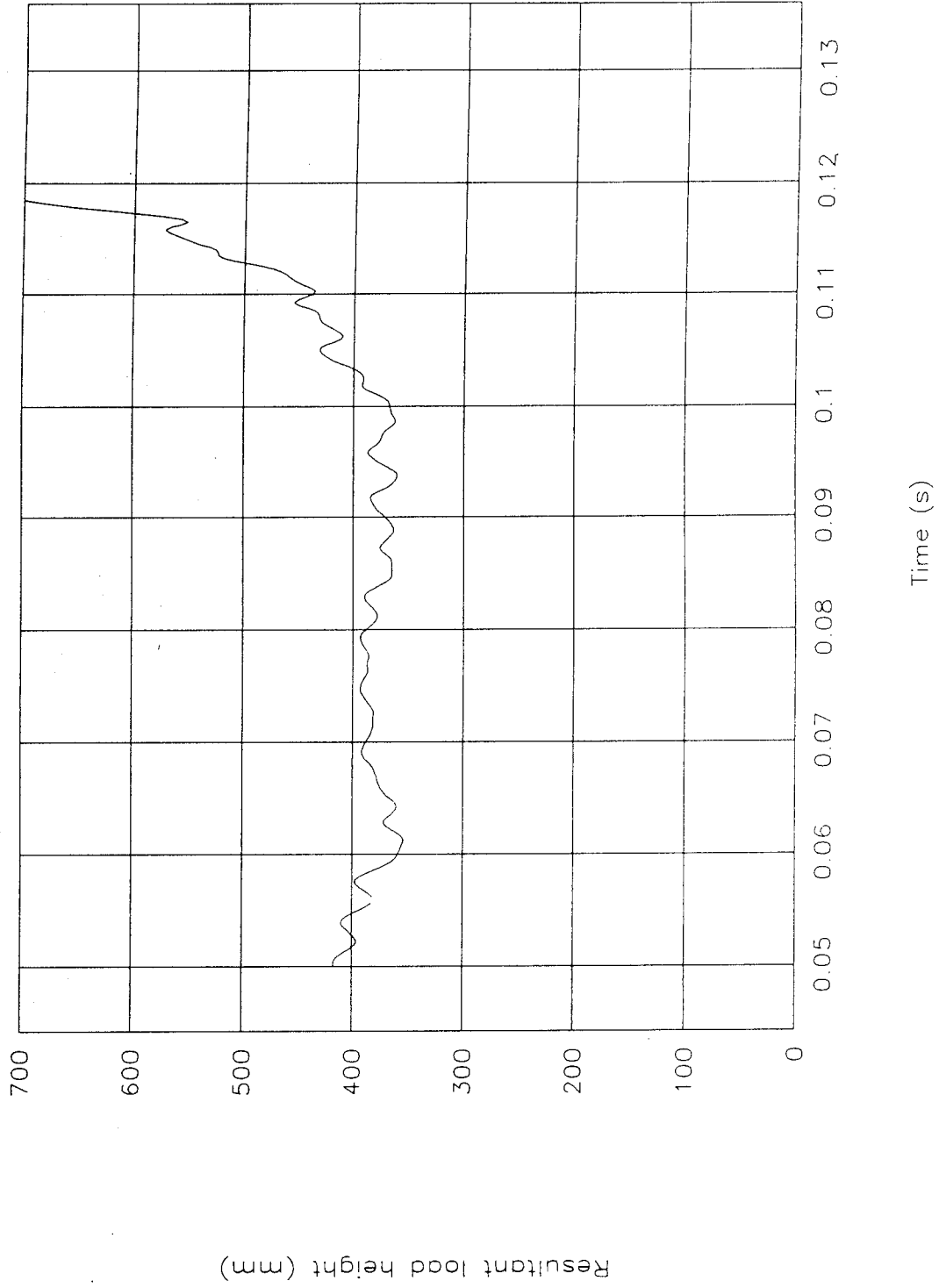


Figure 53. Resultant load height vs. time, test 96F011.

Test No. 96F011

Top of engine

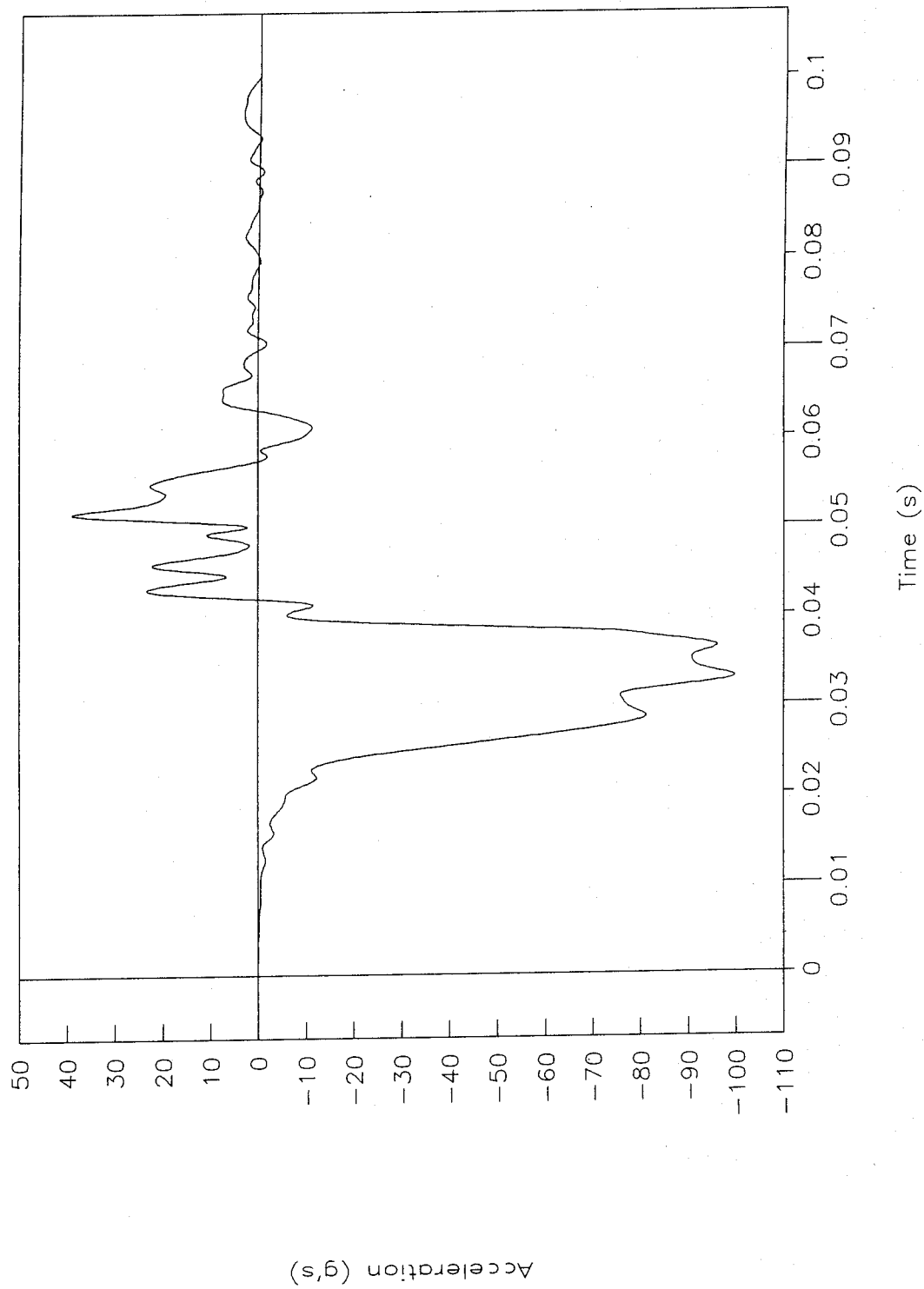


Figure 54. Acceleration vs. time, top of engine, test 96F011.

Test No. 96F011

Bottom of engine

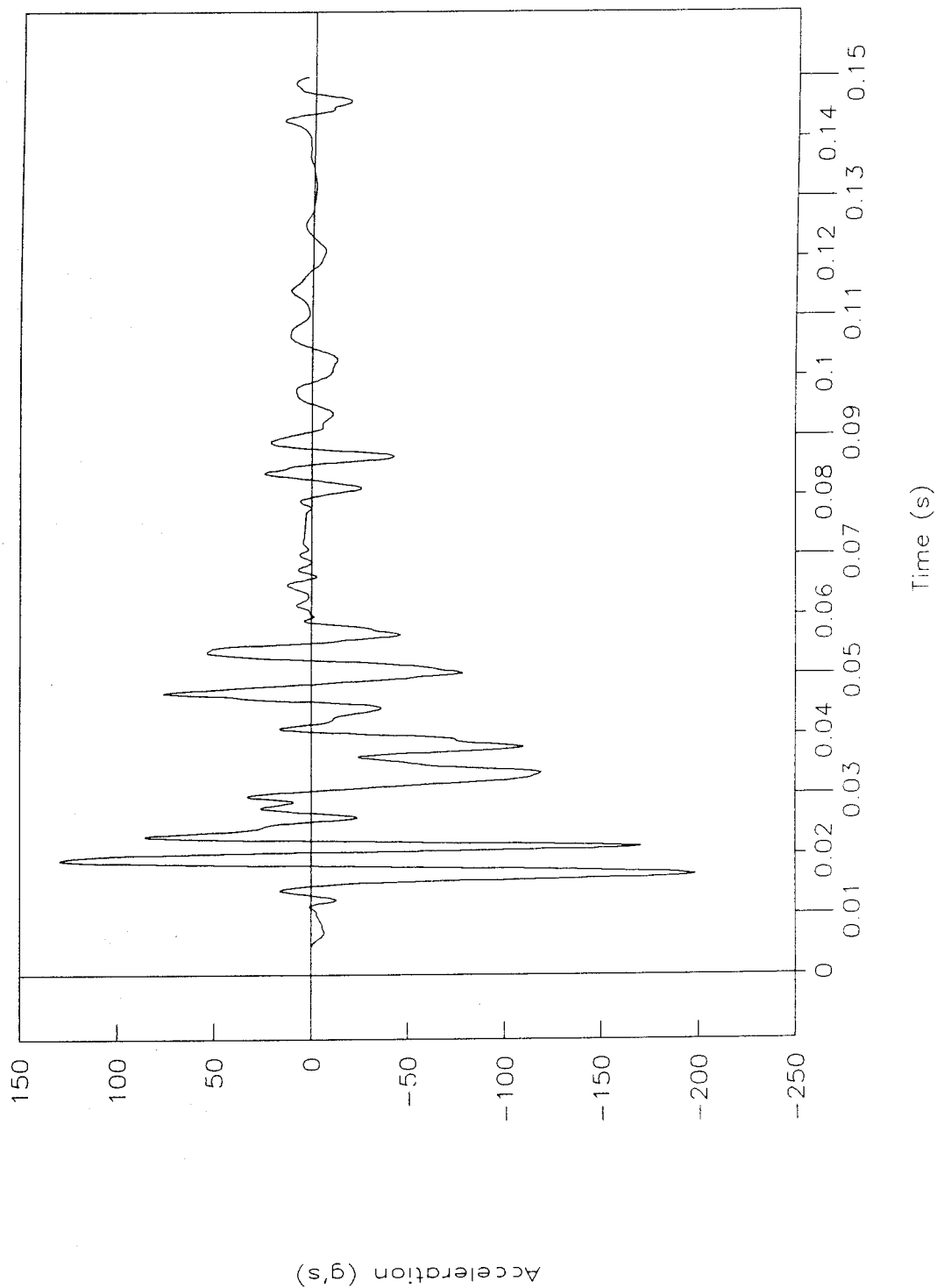


Figure 55. Acceleration vs. time, bottom of engine, test 96F011.

Test No. 96F011

Left control arm

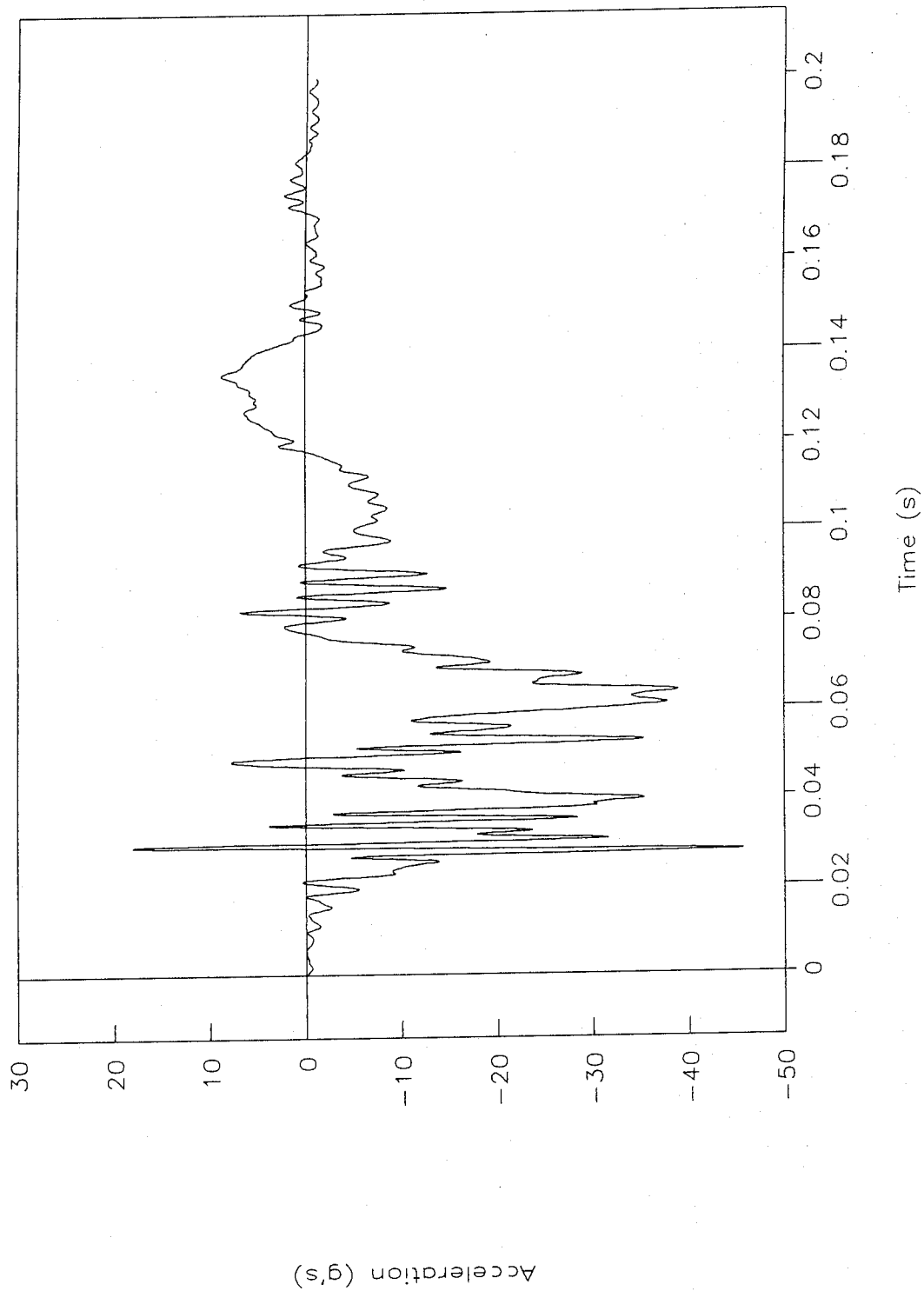


Figure 56. Acceleration vs. time, left control arm, test 96F011.

Test No. 96F011

Right control arm

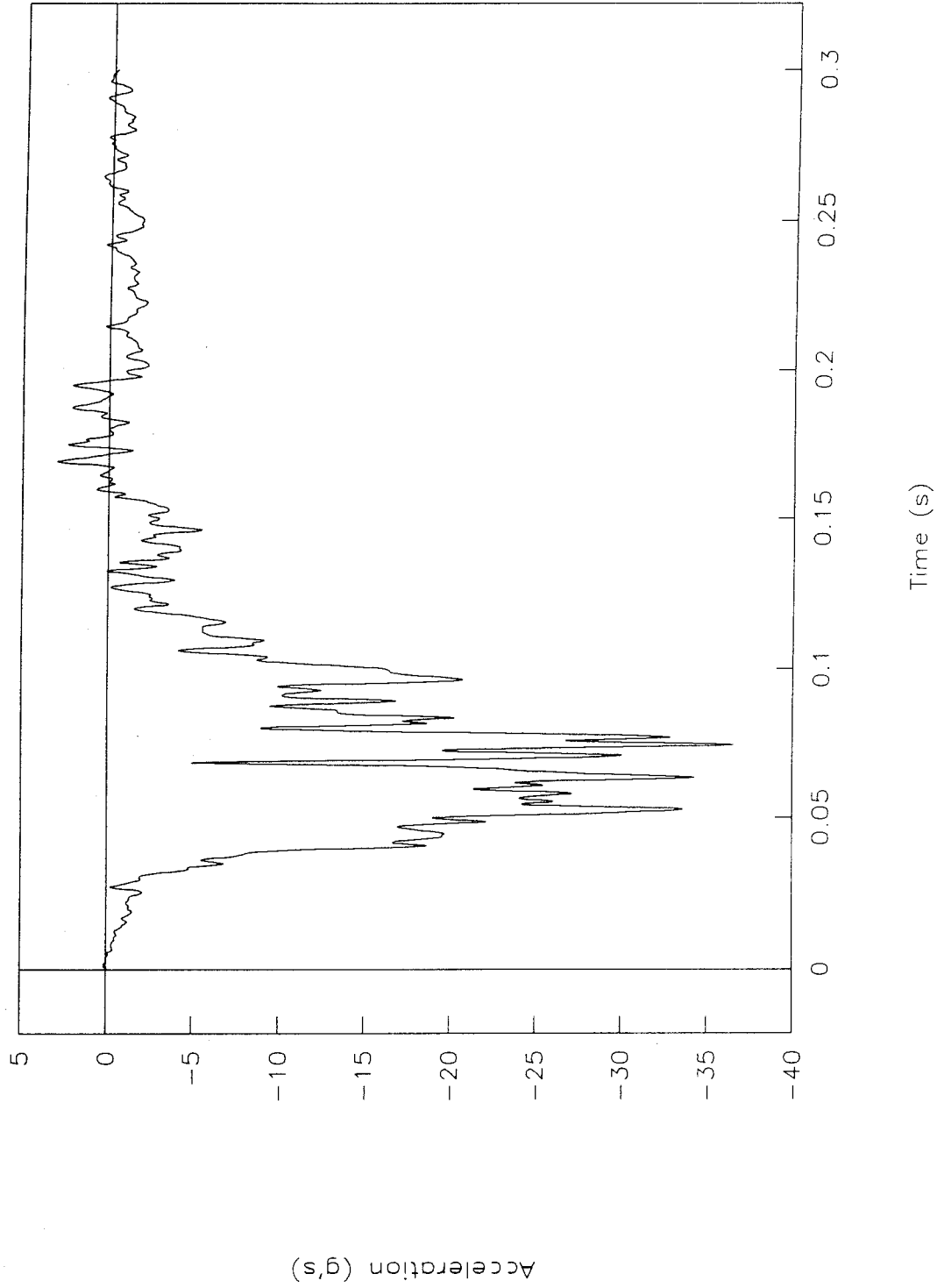


Figure 57. Acceleration vs. time, right control arm, test 96F011.

Test No. 96F011

Instrument panel

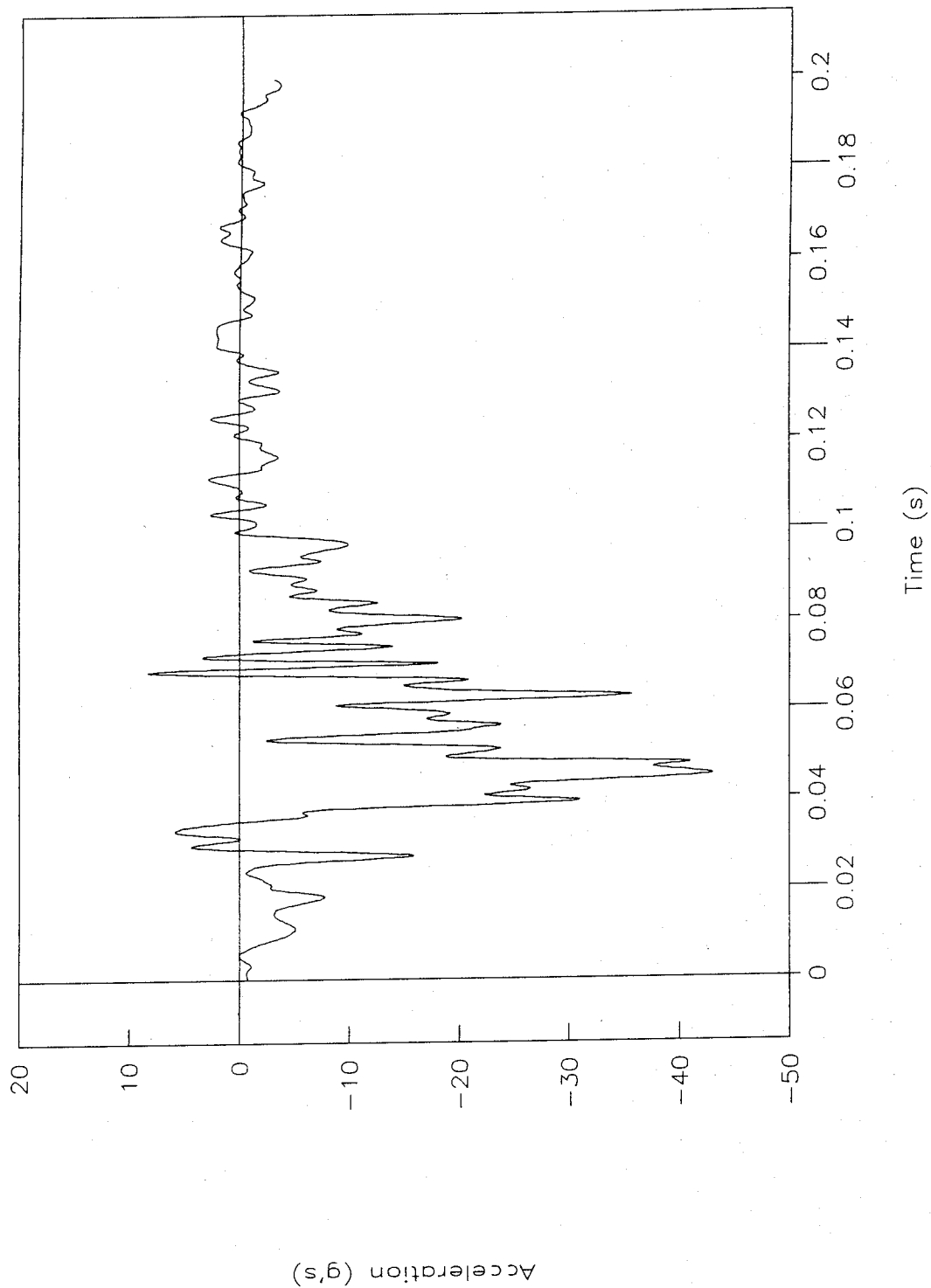


Figure 58. Acceleration vs. time, instrument panel, test 96F011.

Test No. 96F011

Left-rear seat

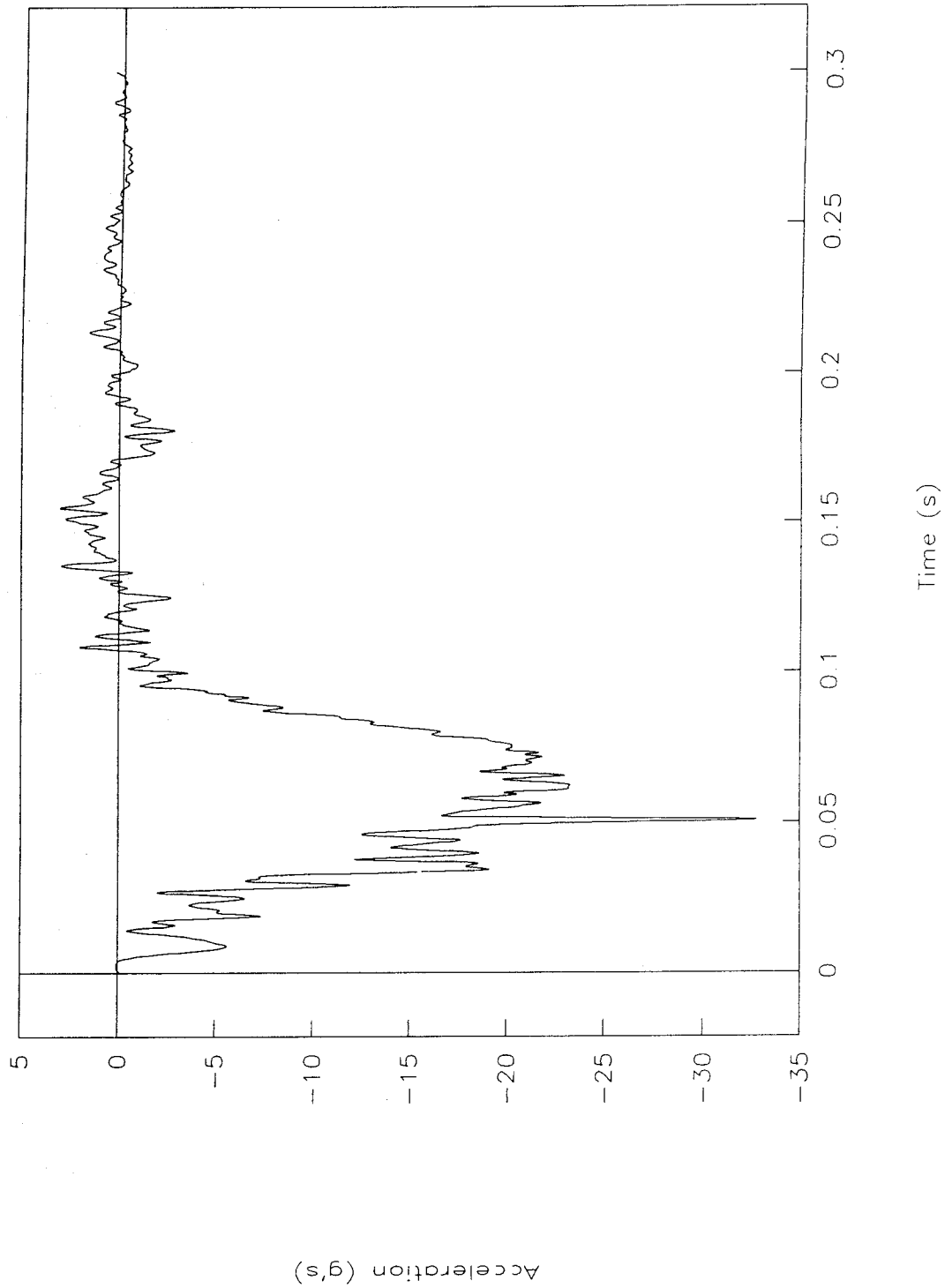


Figure 59. Acceleration vs. time, left-rear seat, test 96F011.

Test No. 96F011

Right-rear seat

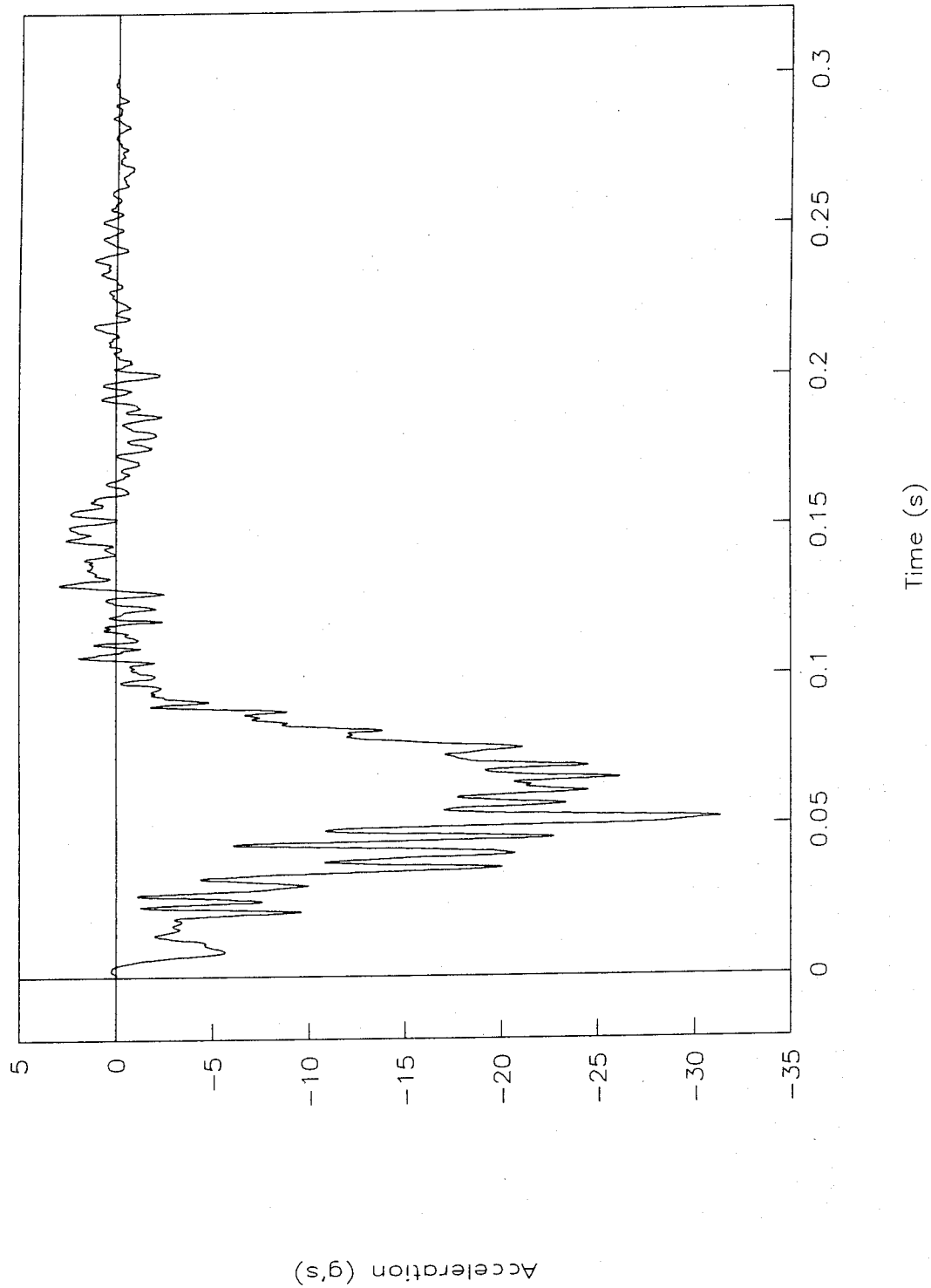


Figure 60. Acceleration vs. time, right-rear seat, test 96F011.

Test No. 96F012

Acceleration vs. time

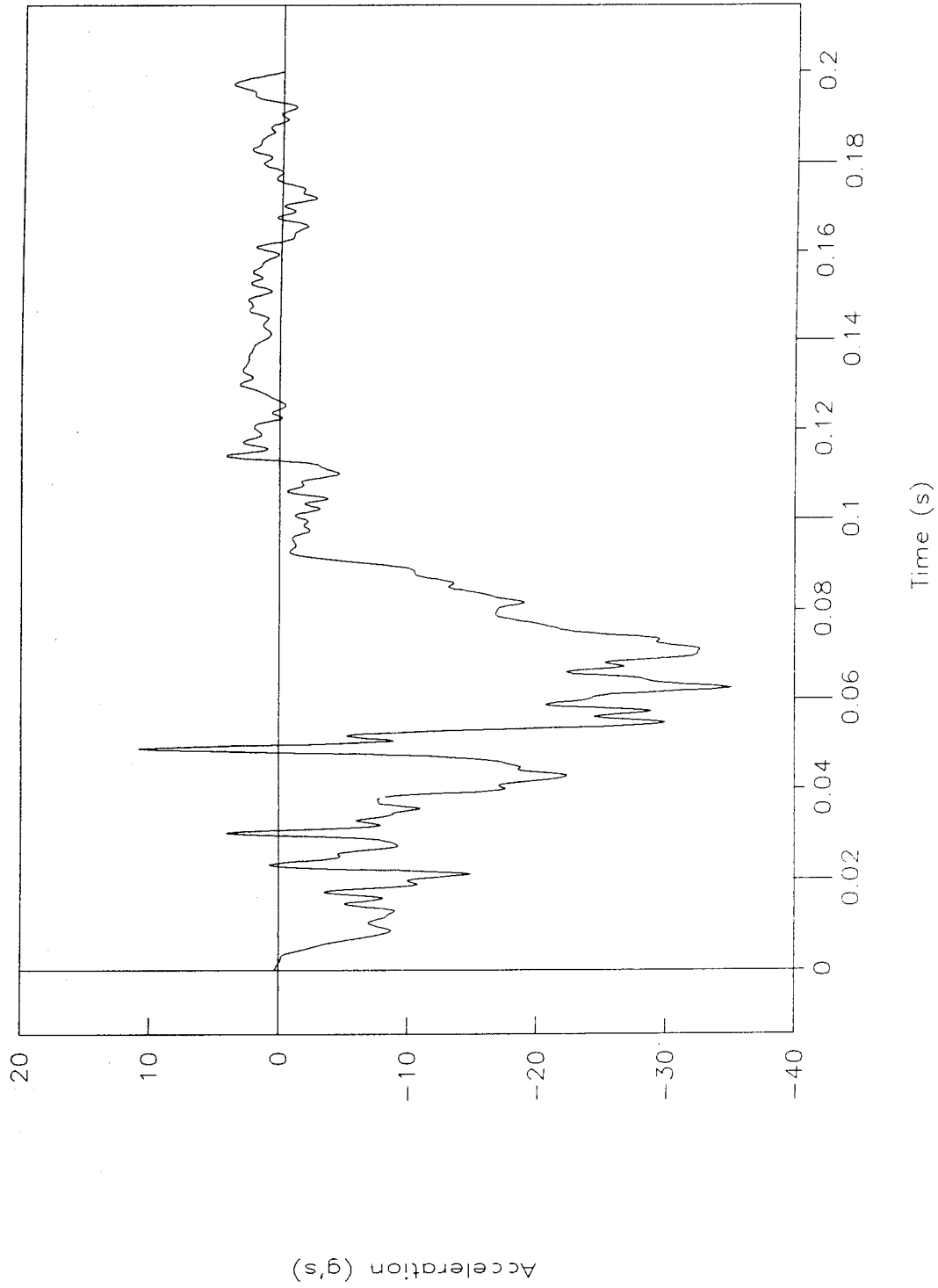


Figure 61. Acceleration vs. time, test 96F012.

Test No. 96F012

Velocity vs. time

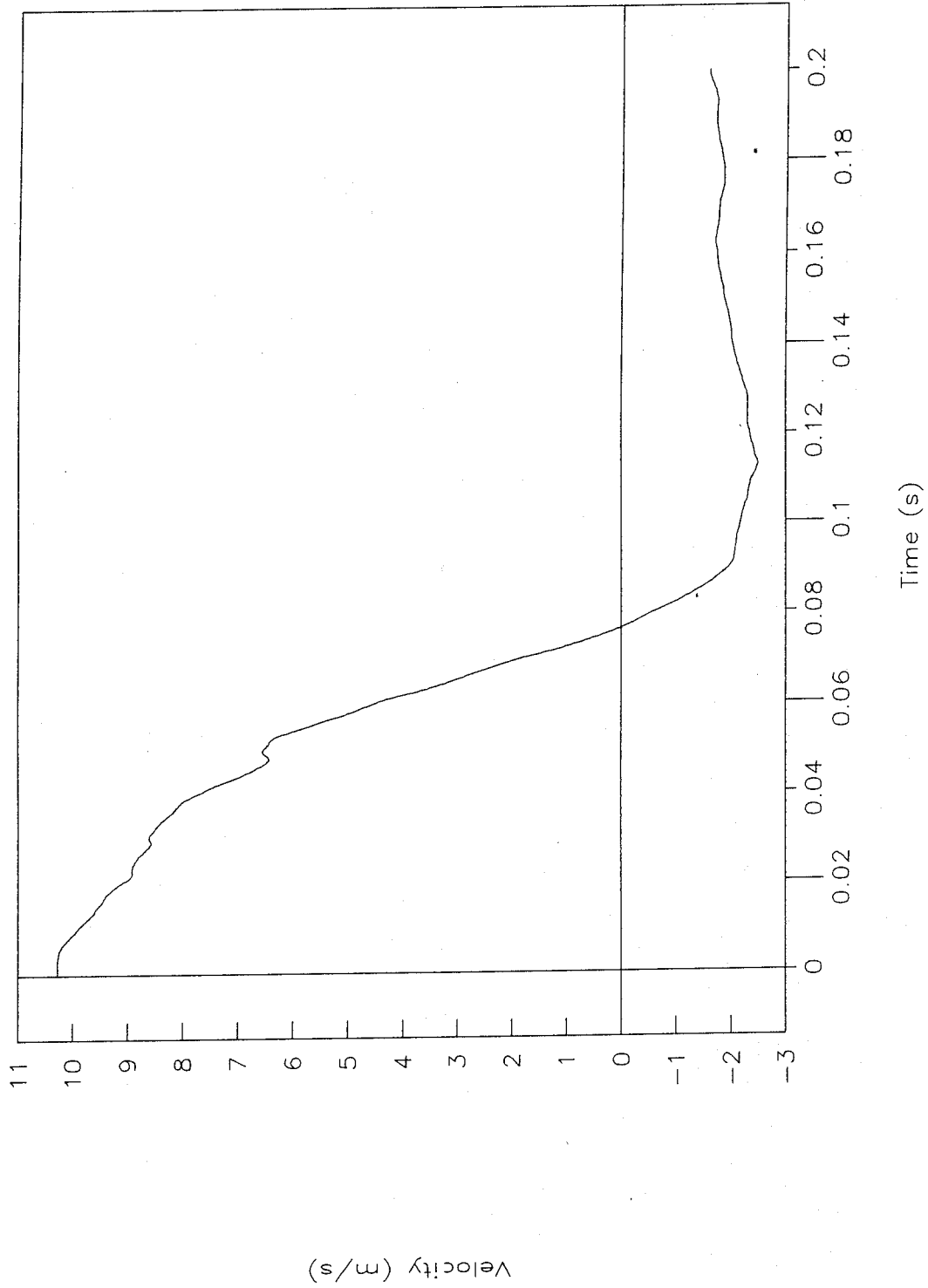


Figure 62. Velocity vs. time, test 96F012.

Test No. 96F012

Displacement vs. time

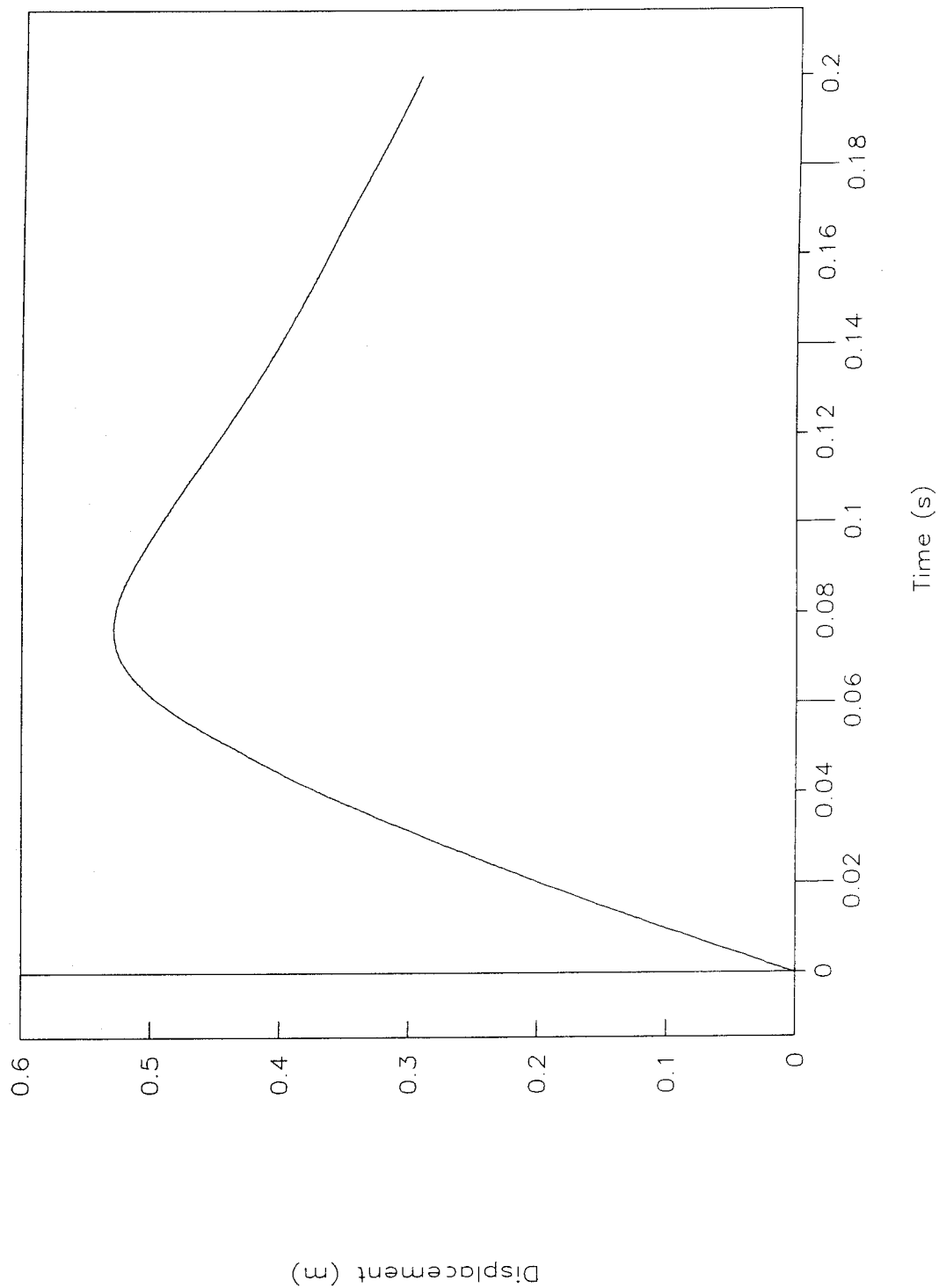


Figure 63. Displacement vs. time, test 96F012.

Test No. 96F012

Force vs. time, load-cell data

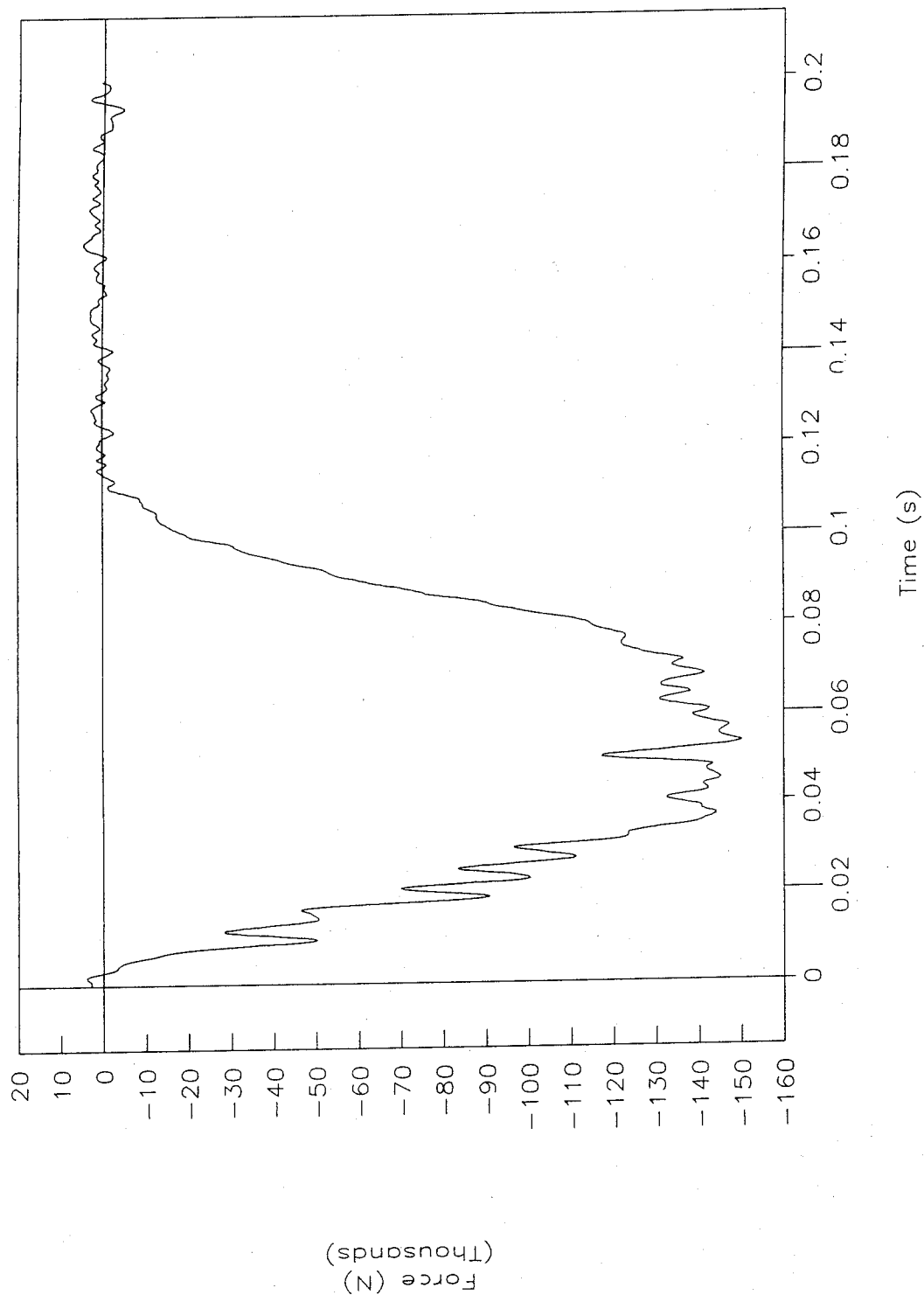


Figure 64. Force vs. time, load-cell data, test 96F012.

Test No. 96F012

Force vs. displacement, load-cell data

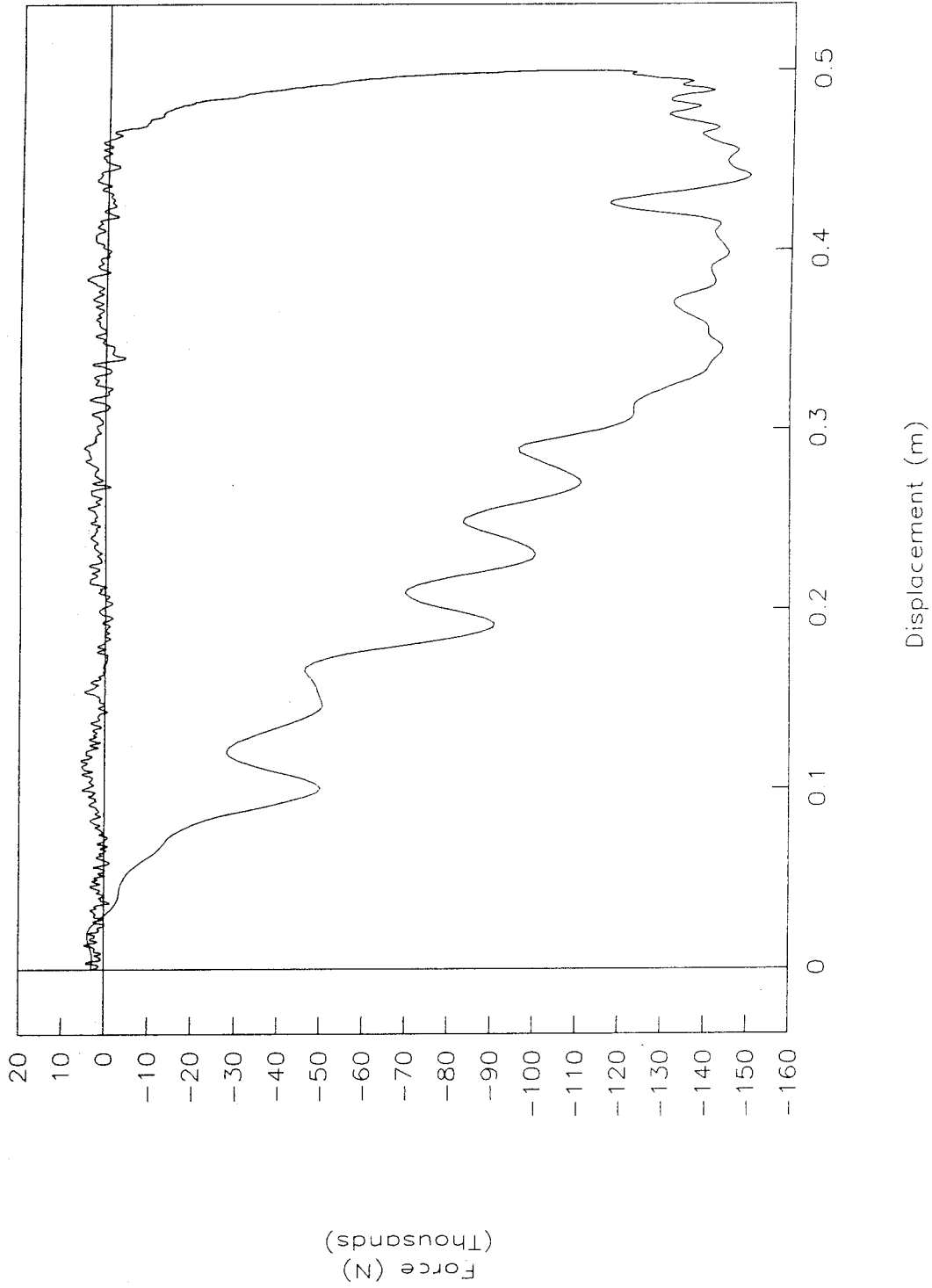


Figure 65. Force vs. displacement, load-cell data, test 96F012.

Test No. 96F012

Energy vs. displacement, load-cell data

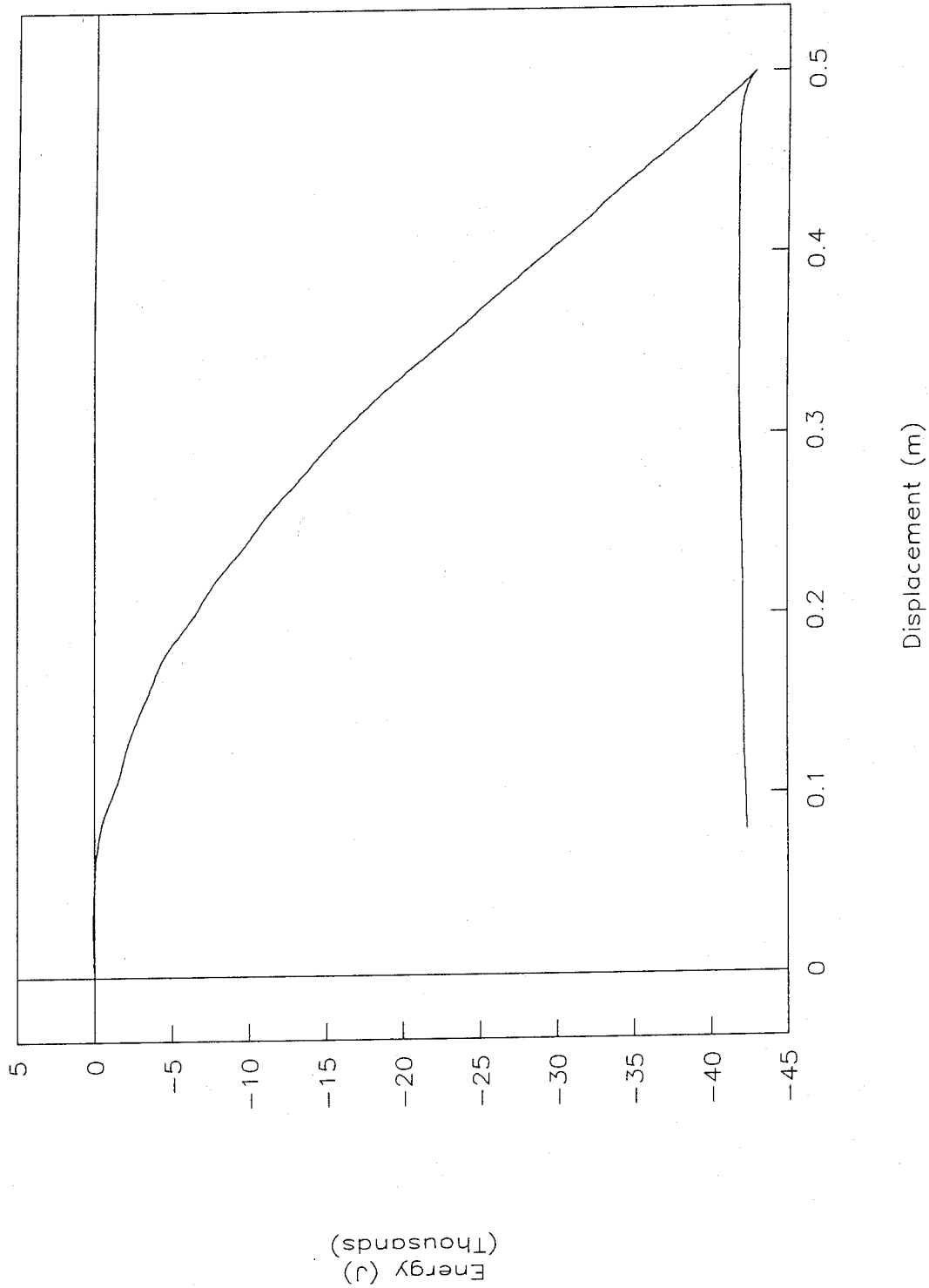


Figure 66. Energy vs. displacement, load-cell data, test 96F012.

Test No. 96F012

Acceleration vs. time, Y-axis

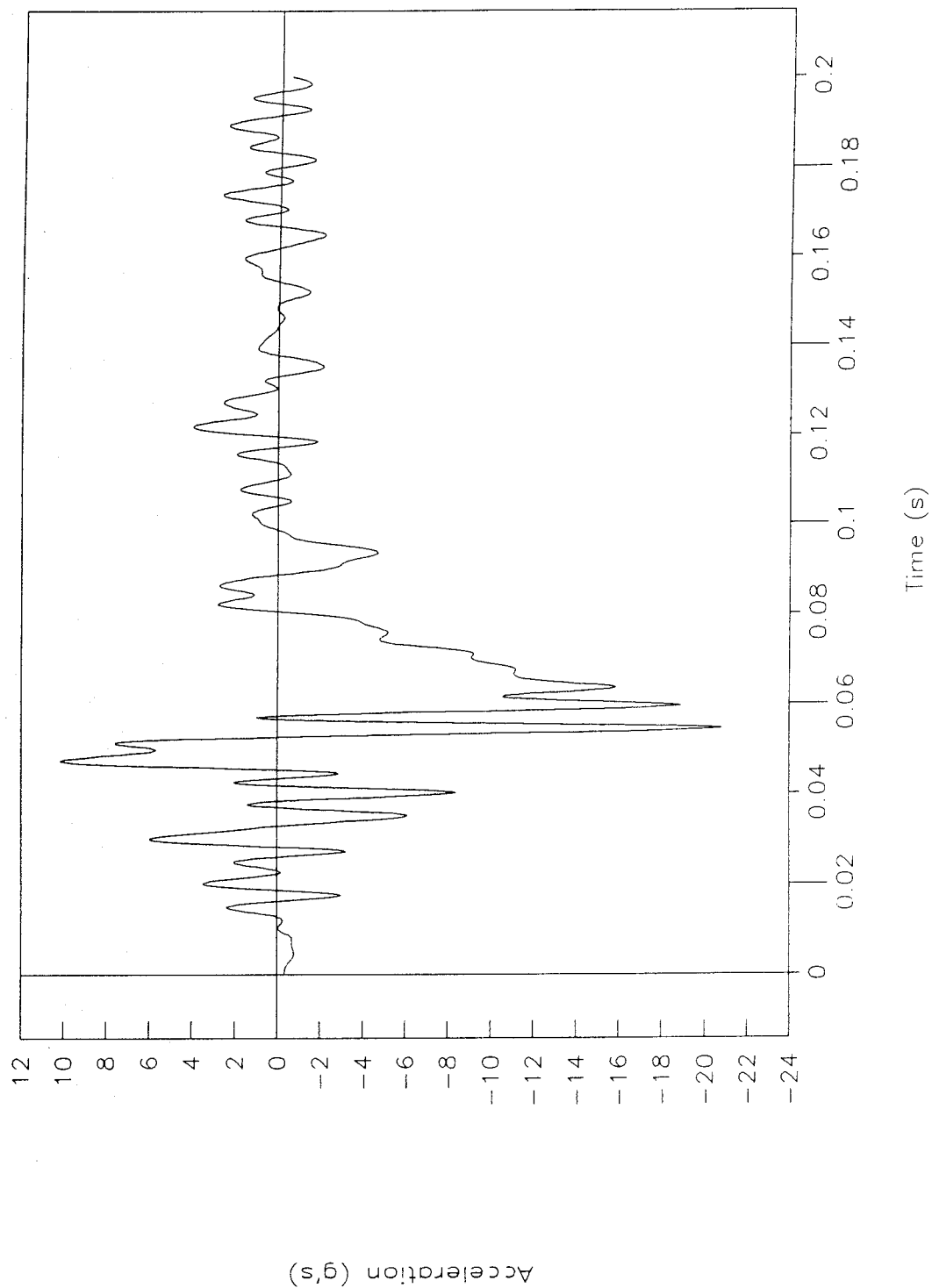


Figure 67. Acceleration vs. time, Y-axis, test 96F012.

Test No. 96F012

Acceleration vs. time, Z-axis

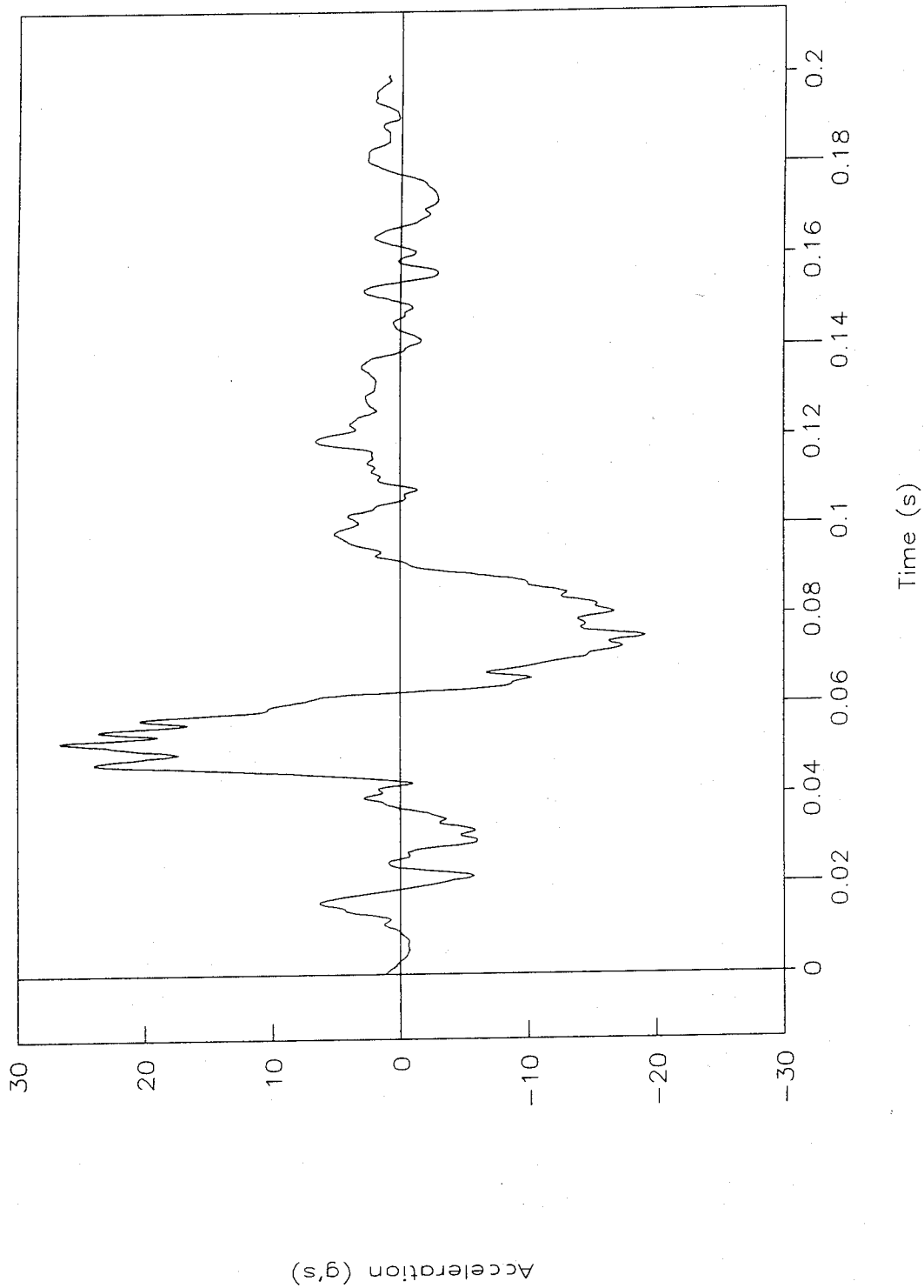


Figure 68. Acceleration vs. time, Z-axis, test 96F012.

Test No. 96F012

Resultant load height vs. time

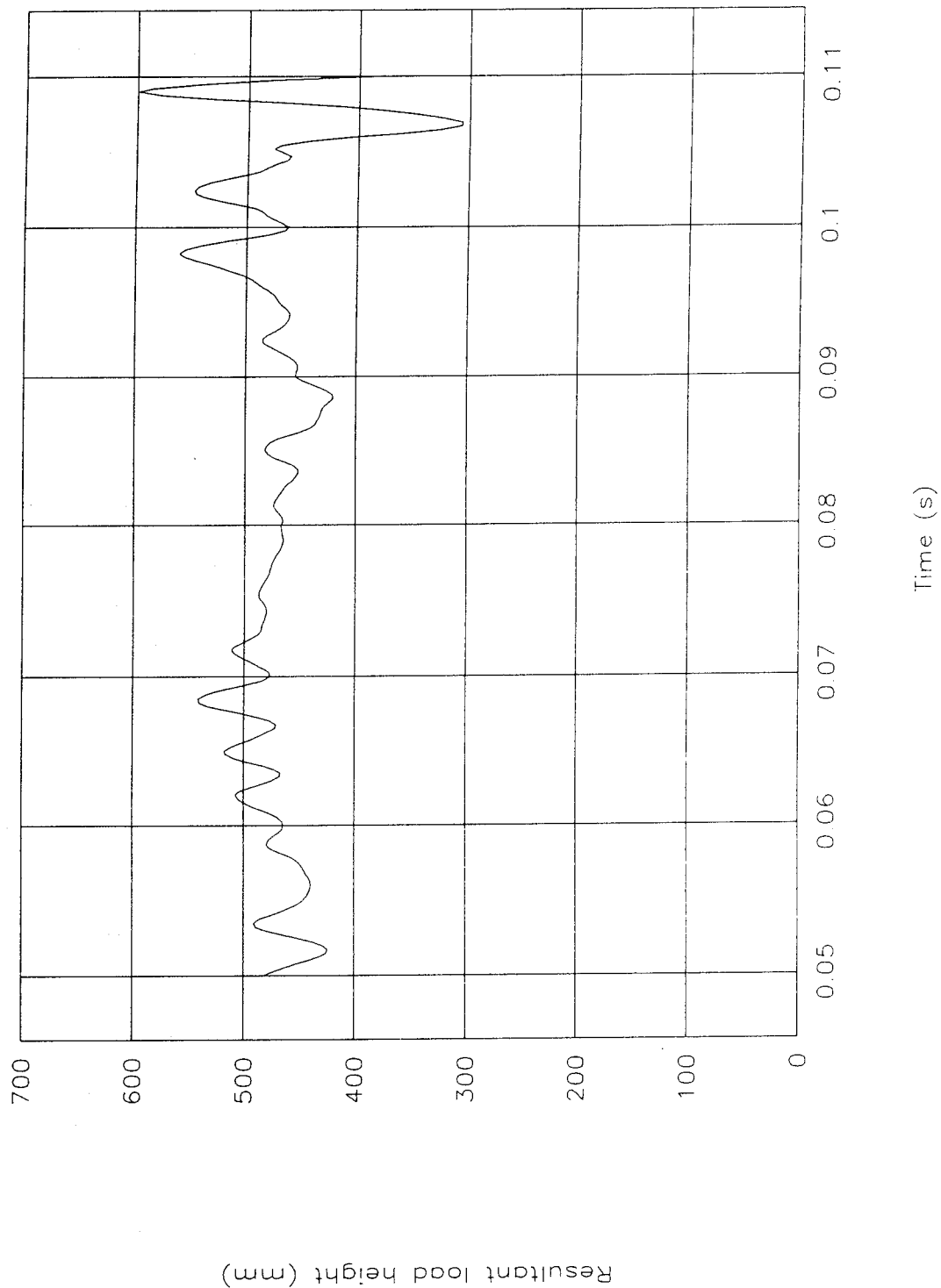


Figure 69. Resultant load height vs. time, test 96F012.

Test No. 96F012
Top of engine

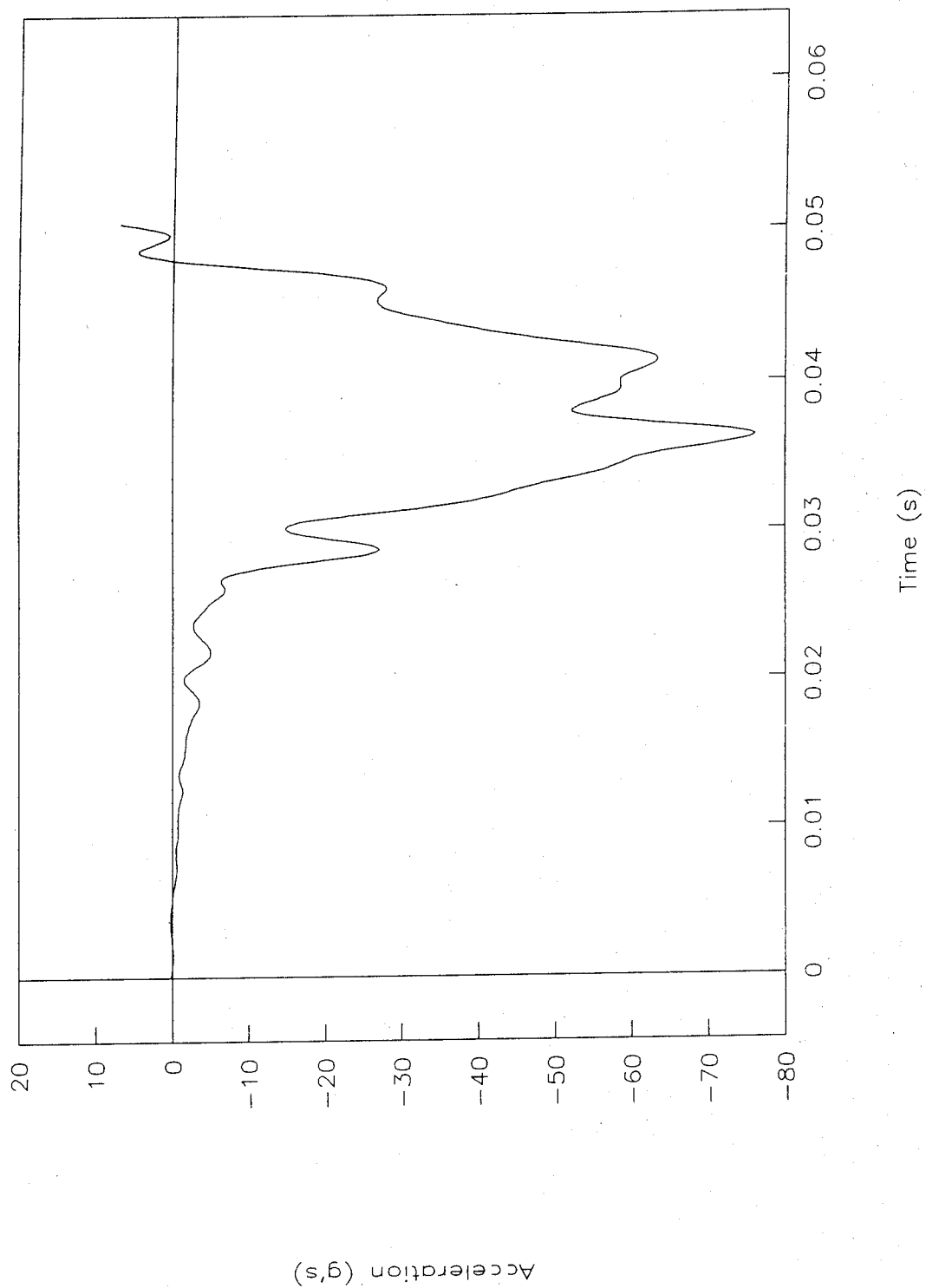


Figure 70. Acceleration vs. time, top of engine, test 96F012.

Test No. 96F012

Bottom of engine

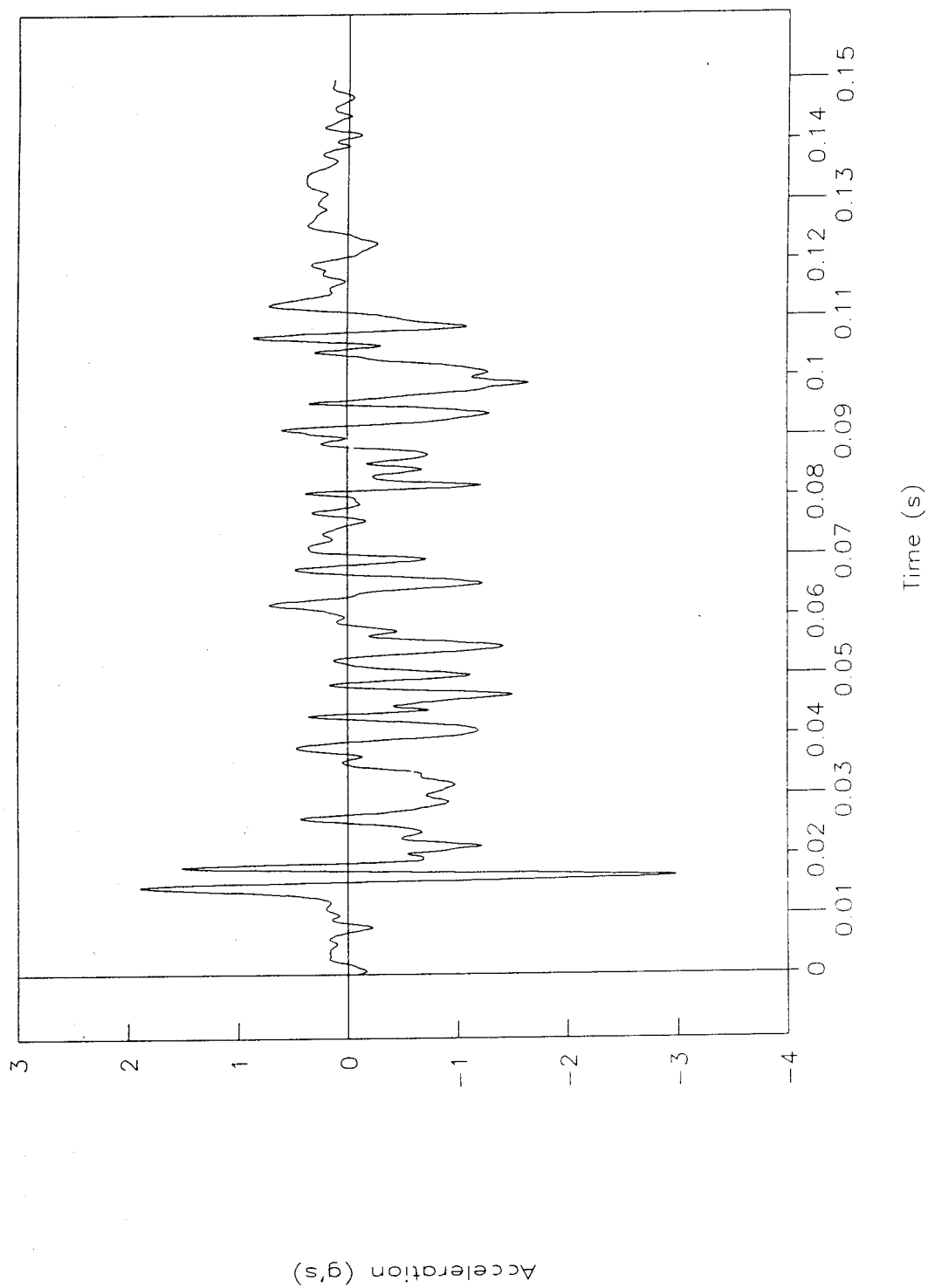


Figure 71. Acceleration vs. time, bottom of engine, test 96F012.

Test No. 96F012

Left control arm

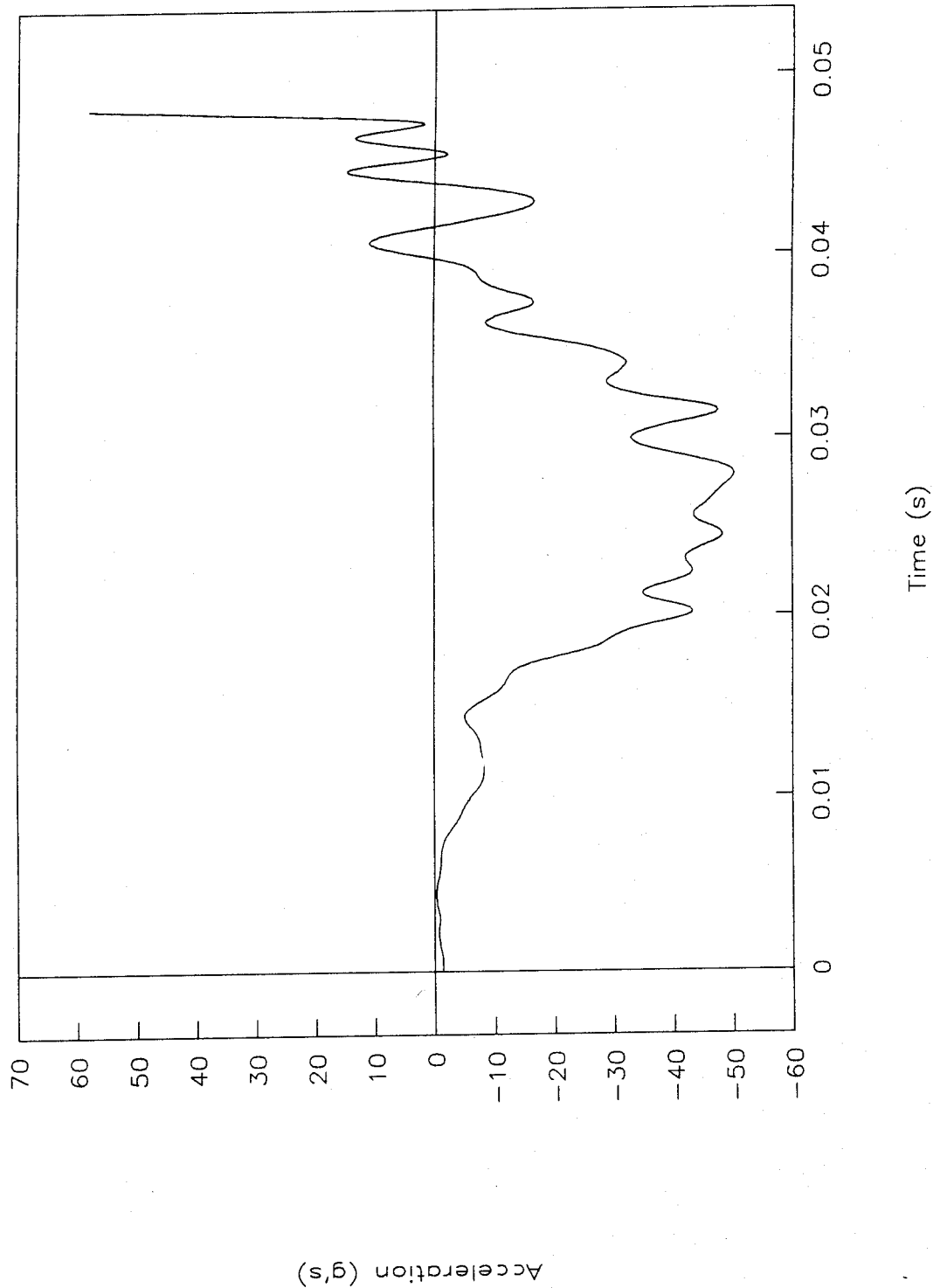


Figure 72. Acceleration vs. time, left control arm, test 96F012.

Test No. 96F012

Right control arm

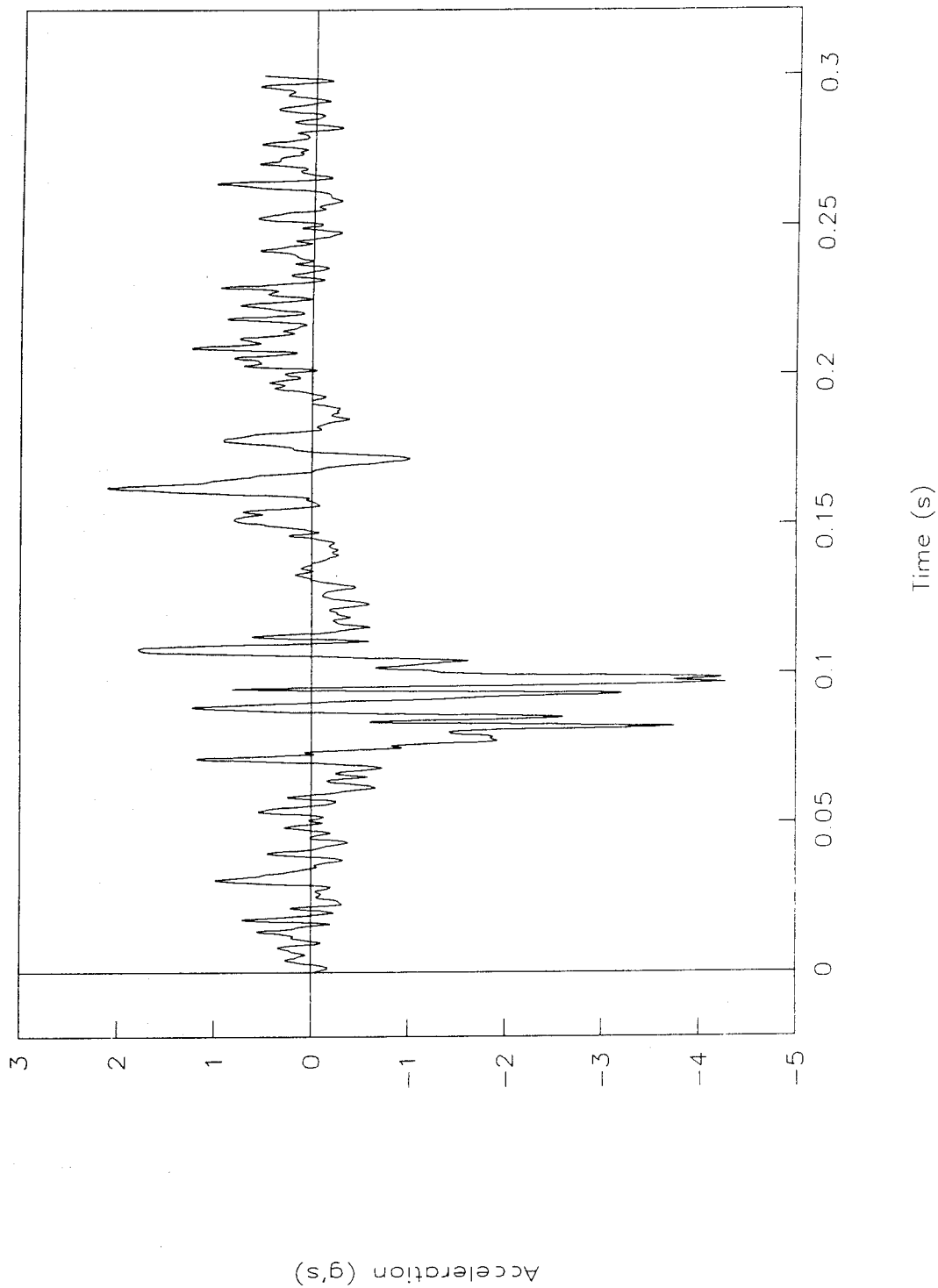


Figure 73. Acceleration vs. time, right control arm, test 96F012.

Test No. 96F012

Instrument panel

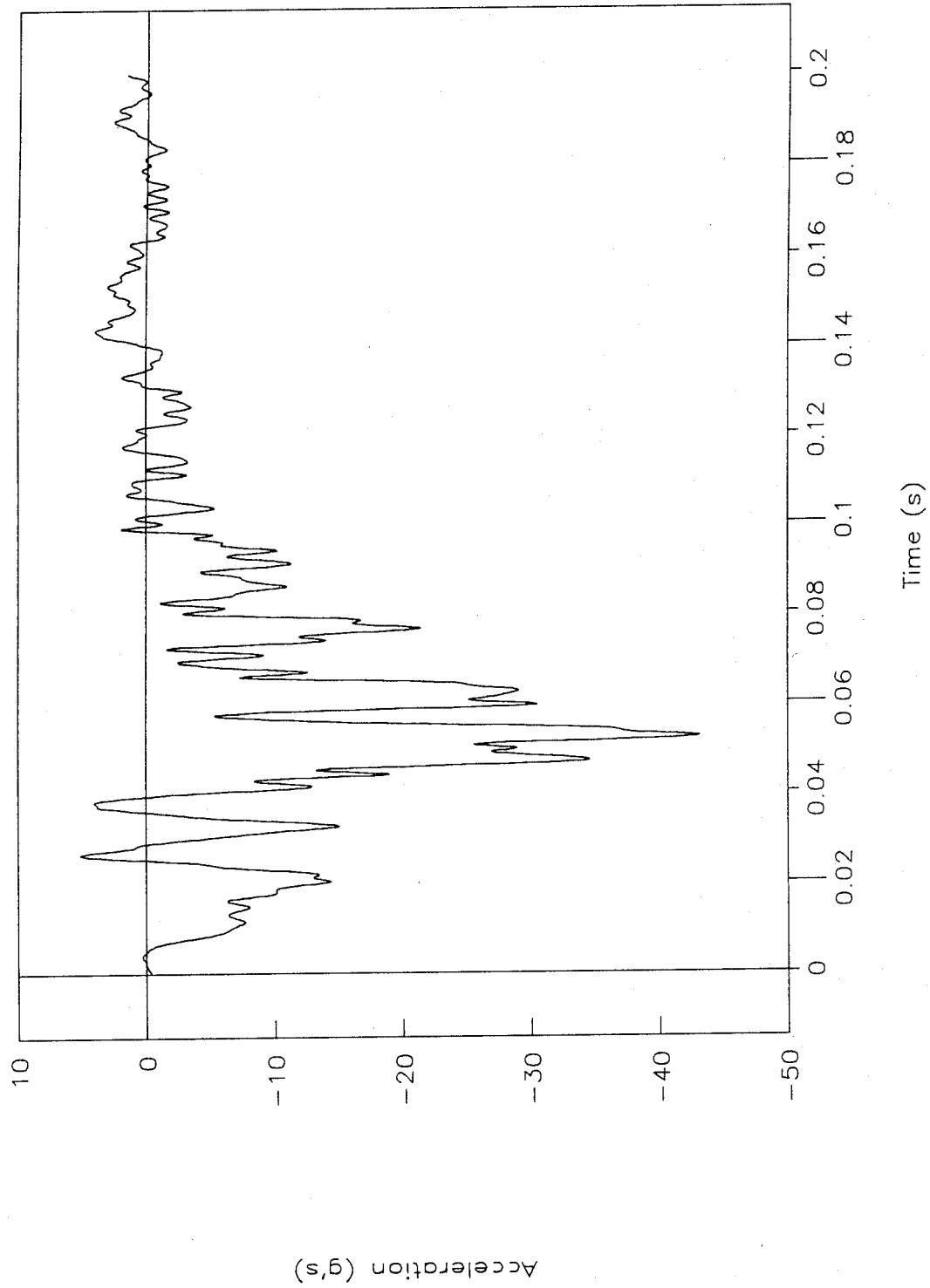


Figure 74. Acceleration vs. time, instrument panel, test 96F012.

Test No. 96F012
Left-rear seat

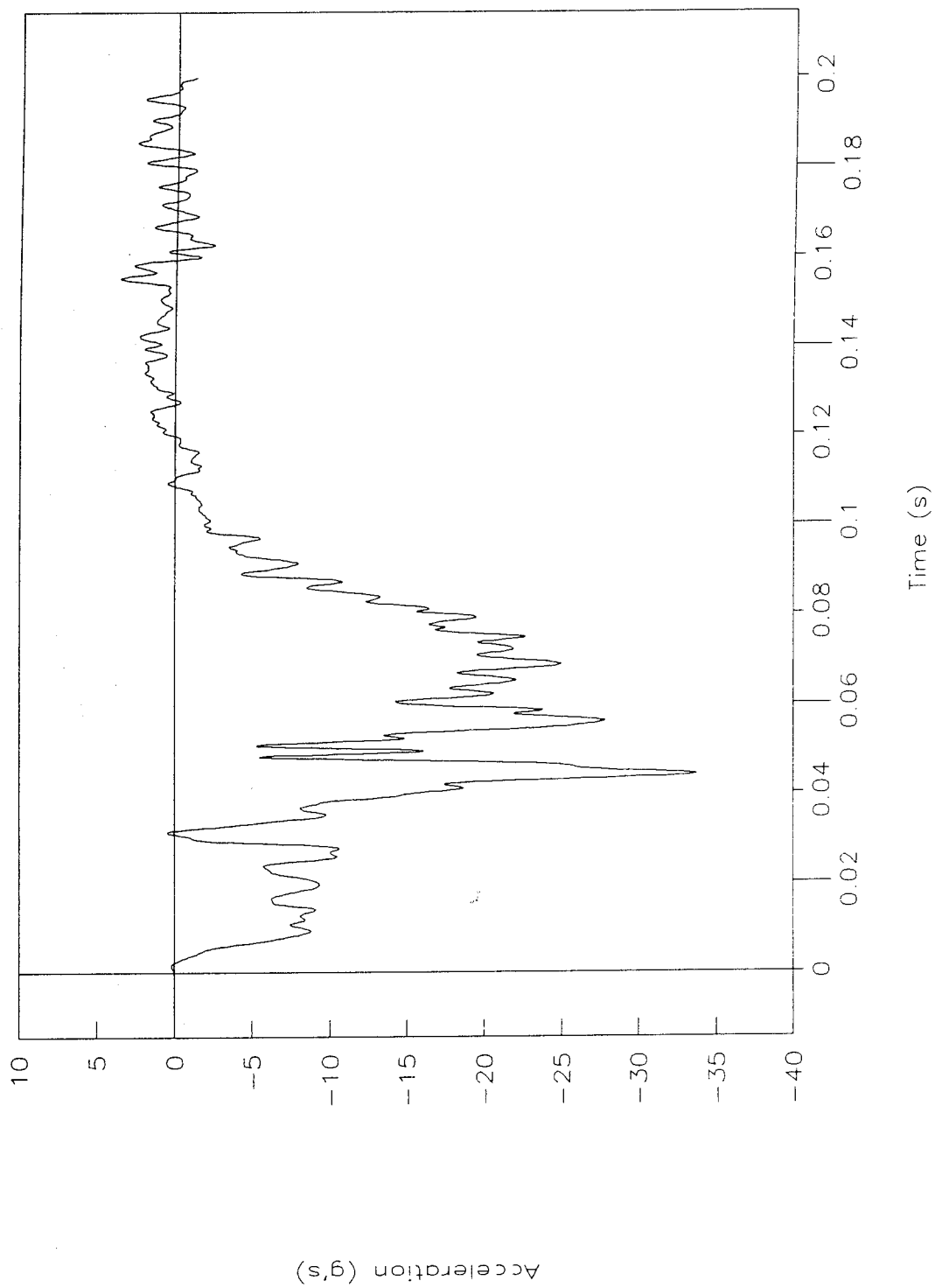


Figure 75. Acceleration vs. time, left-rear seat, test 96F012.

Test No. 96F012

Right-rear seat

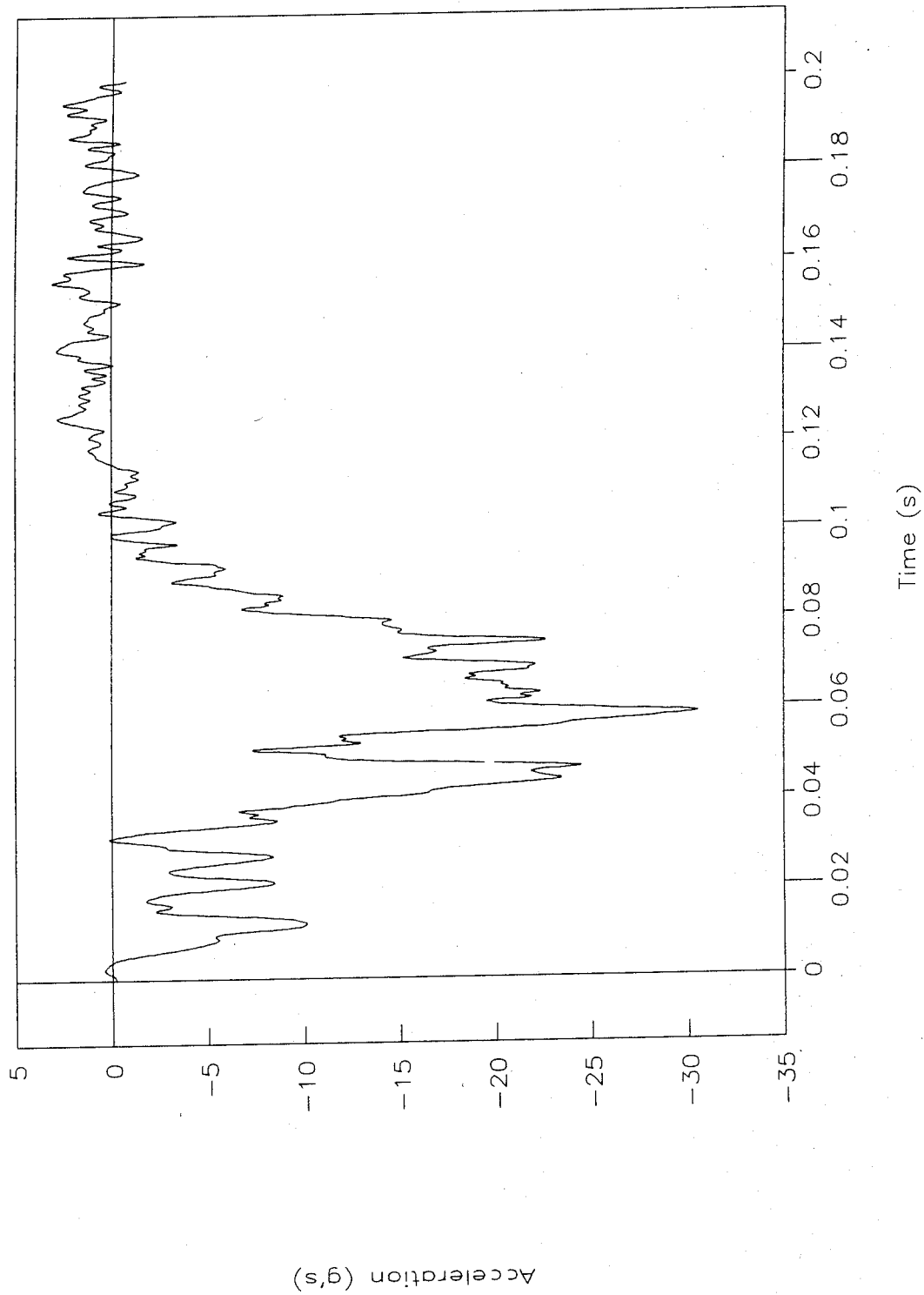


Figure 76. Acceleration vs. time, right-rear seat, 96F012.

Test No. 96F014

Acceleration vs. time

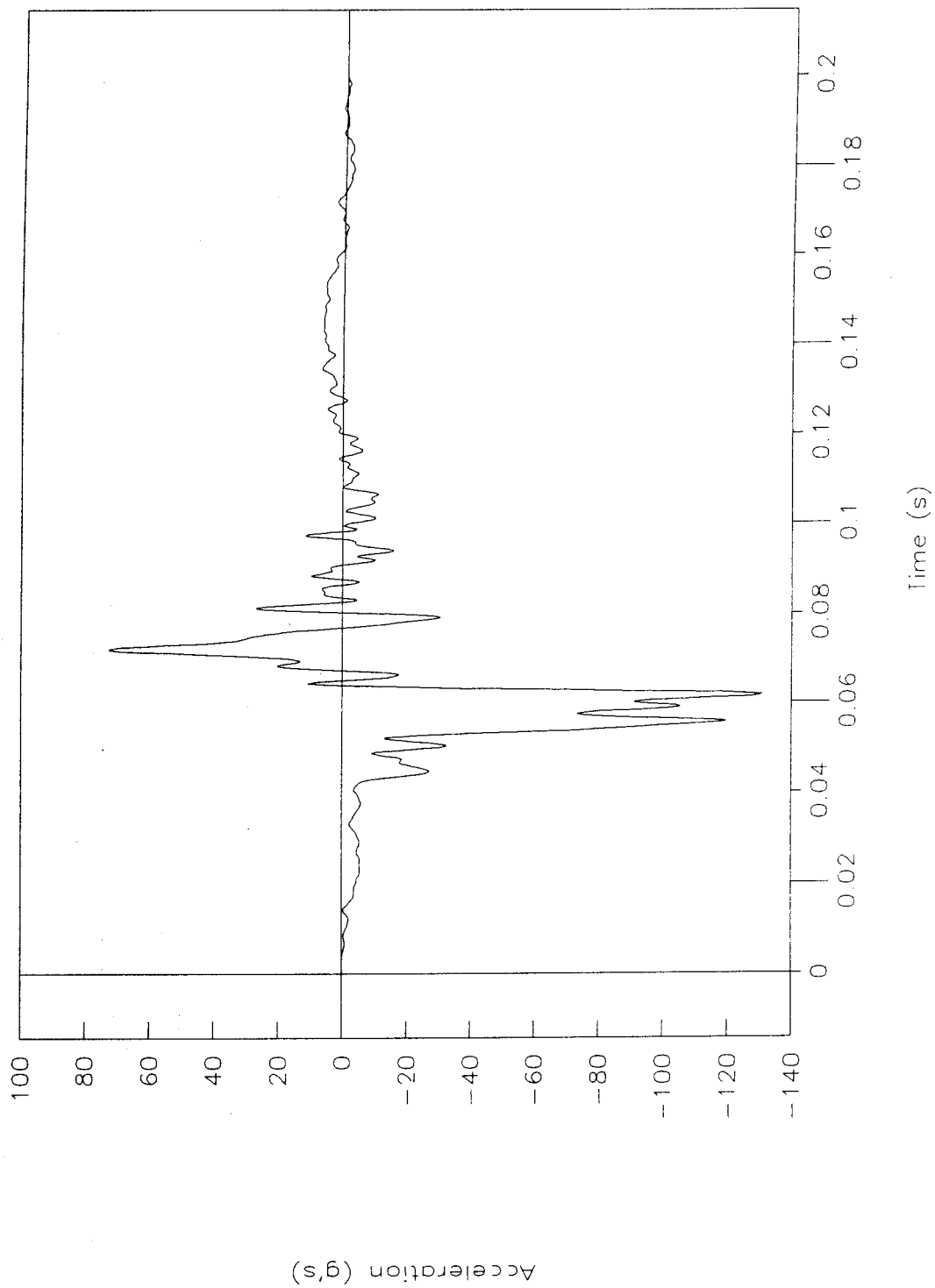


Figure 77. Acceleration vs. time, test 96F014.

Test No. 96F014

Velocity vs. time

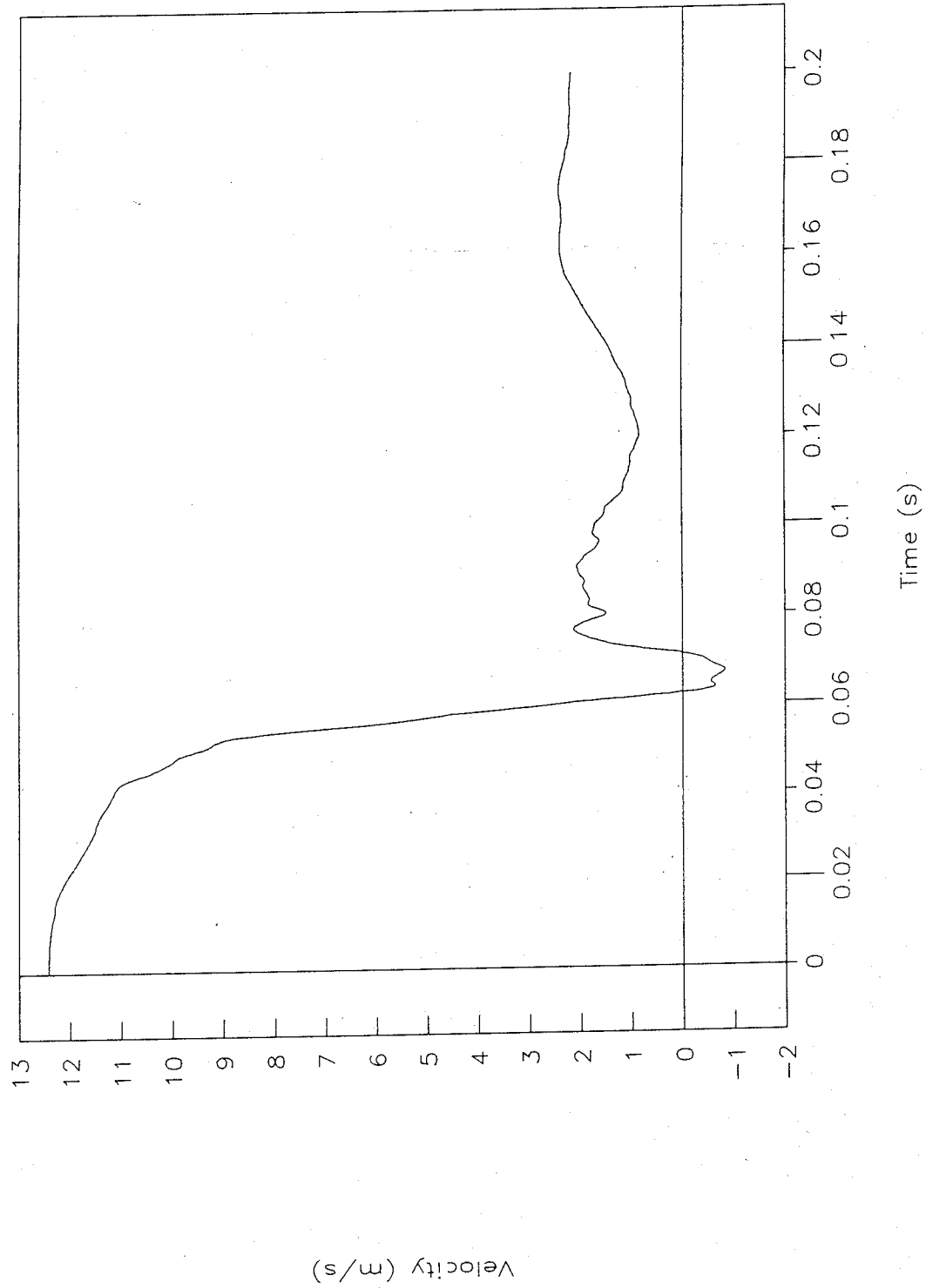


Figure 78. Velocity vs. time, test 96F014.

Test No. 96F014

Displacement vs. time

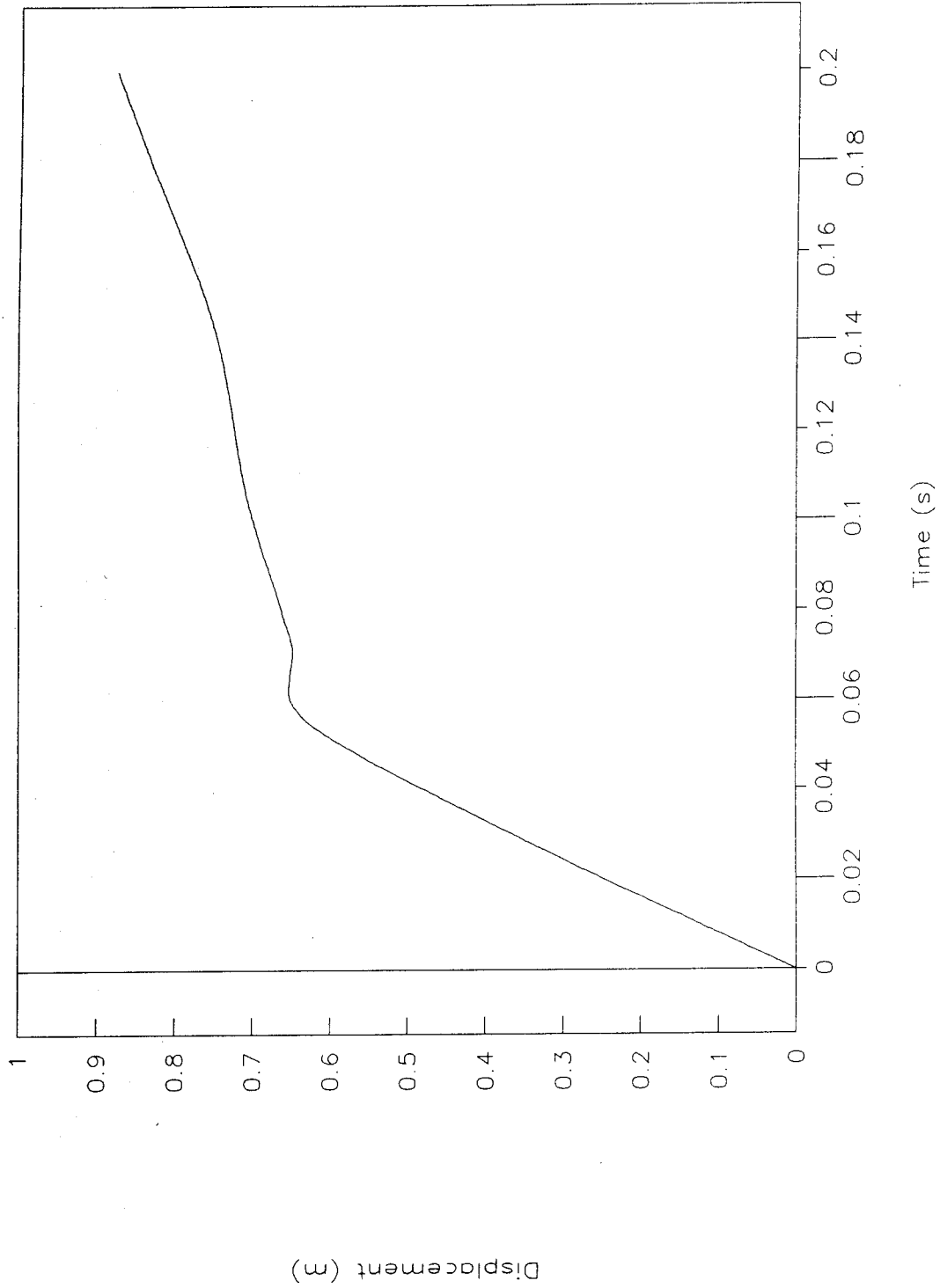


Figure 79. Displacement vs. time, test 96F014.

Test No. 96F014

Force vs. time, load-cell data

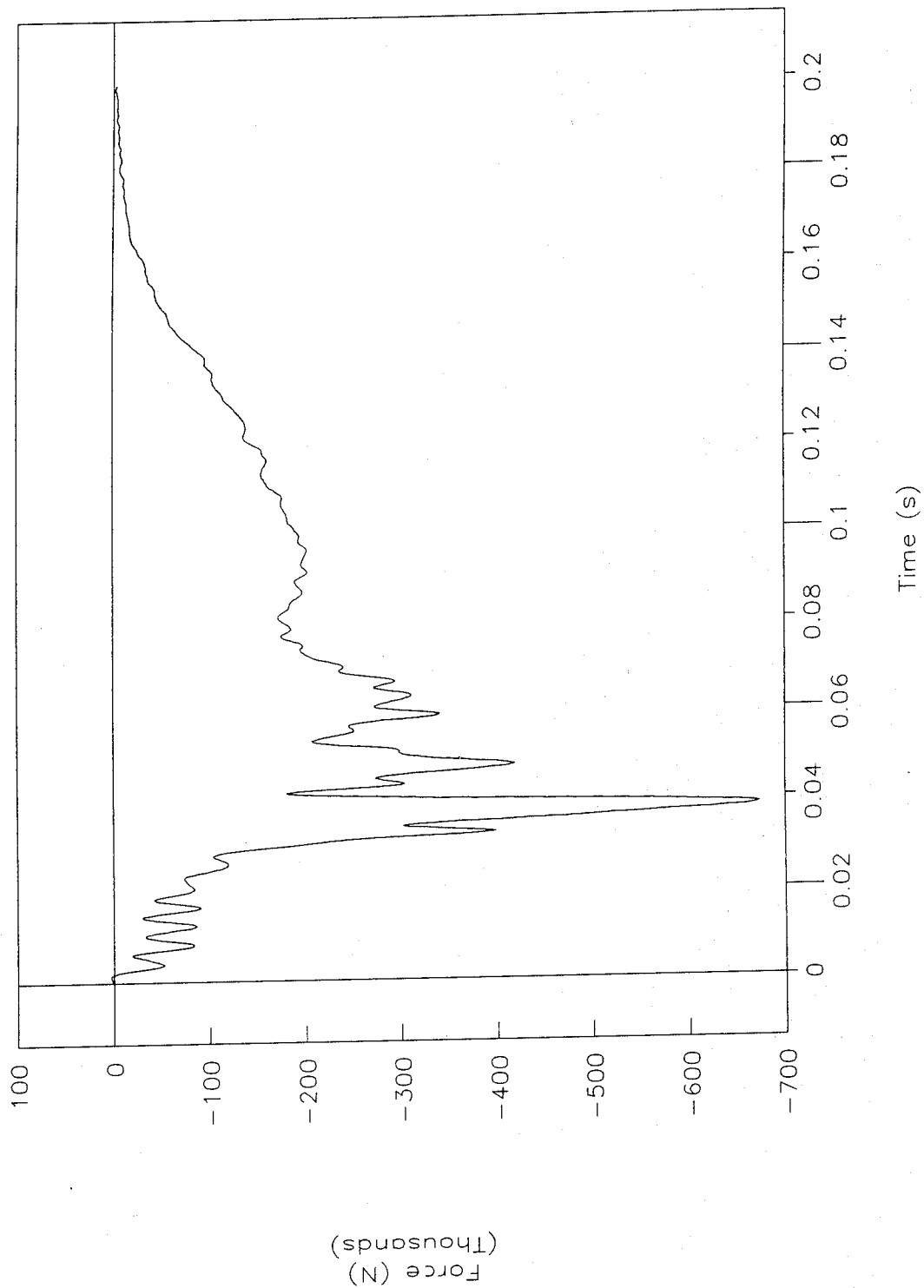


Figure 80. Force vs. time, load-cell data, test 96F014.

Test No. 96F014

Force vs. displacement, load-cell data

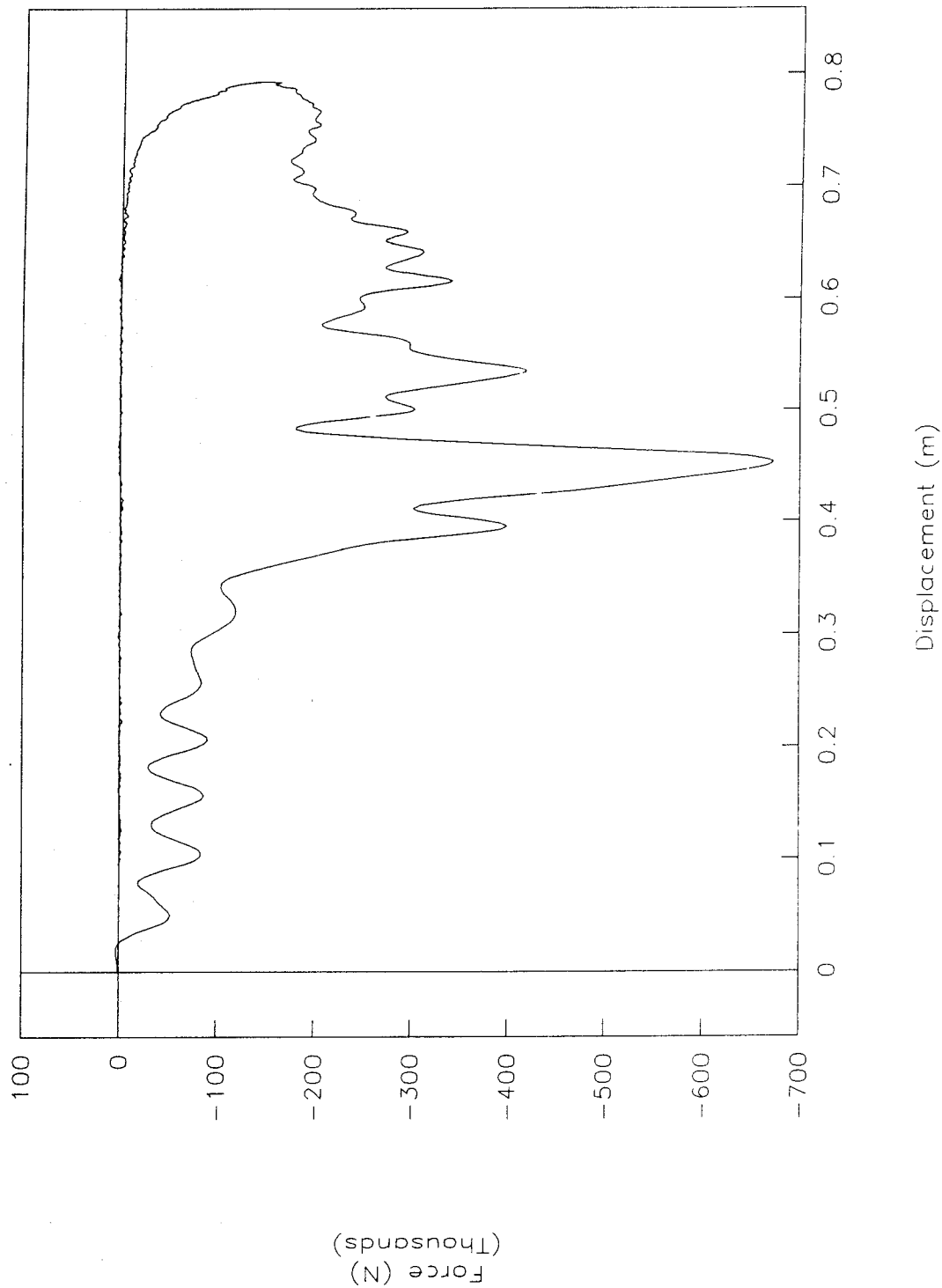


Figure 81. Force vs. displacement, load-cell data, test 96F014.

Test No. 96F014

Energy vs. displacement, load-cell data

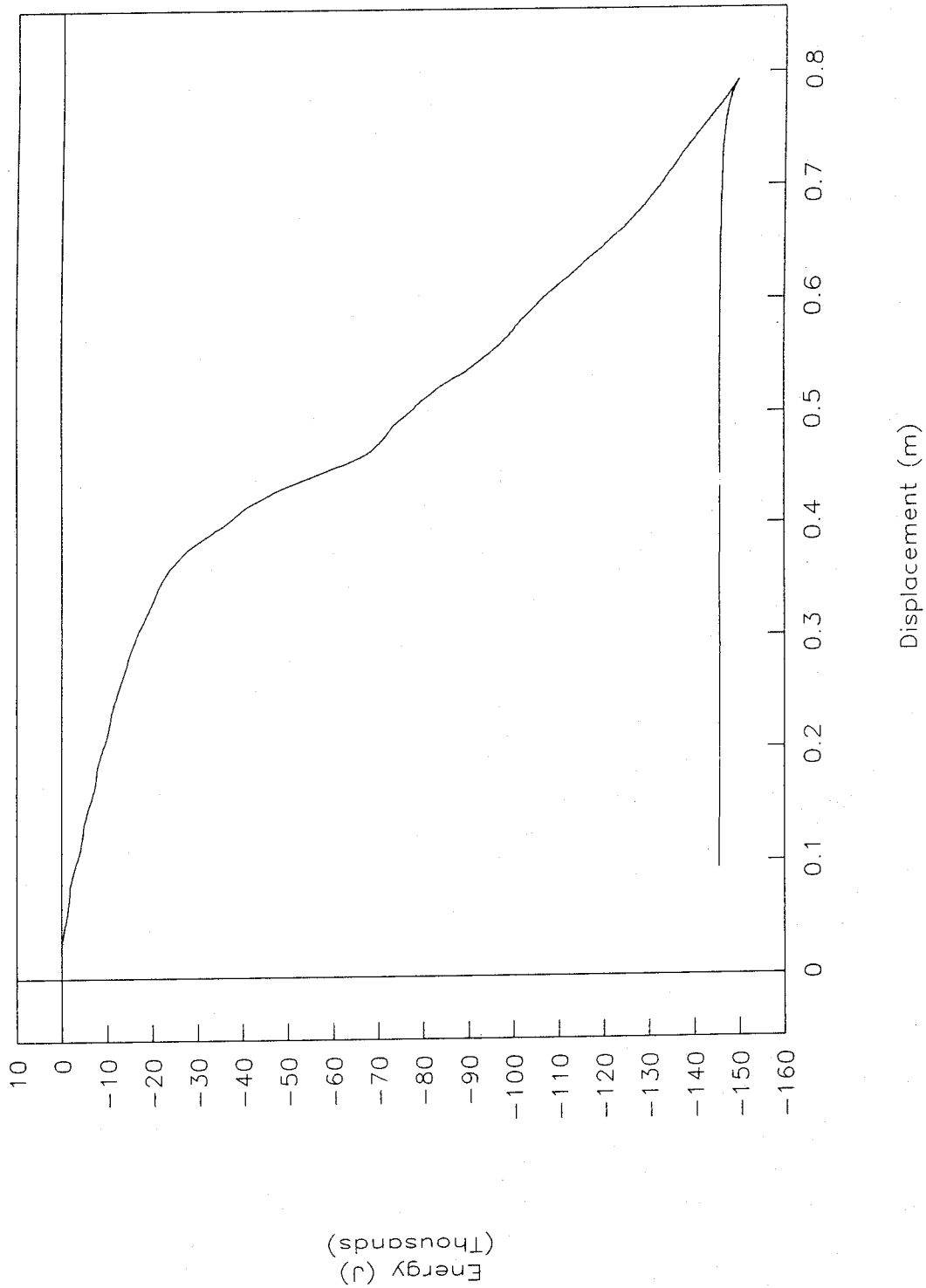


Figure 82. Energy vs. displacement, load-cell data, test 96F014.

Test No. 96F014

Acceleration vs. time, Y-axis

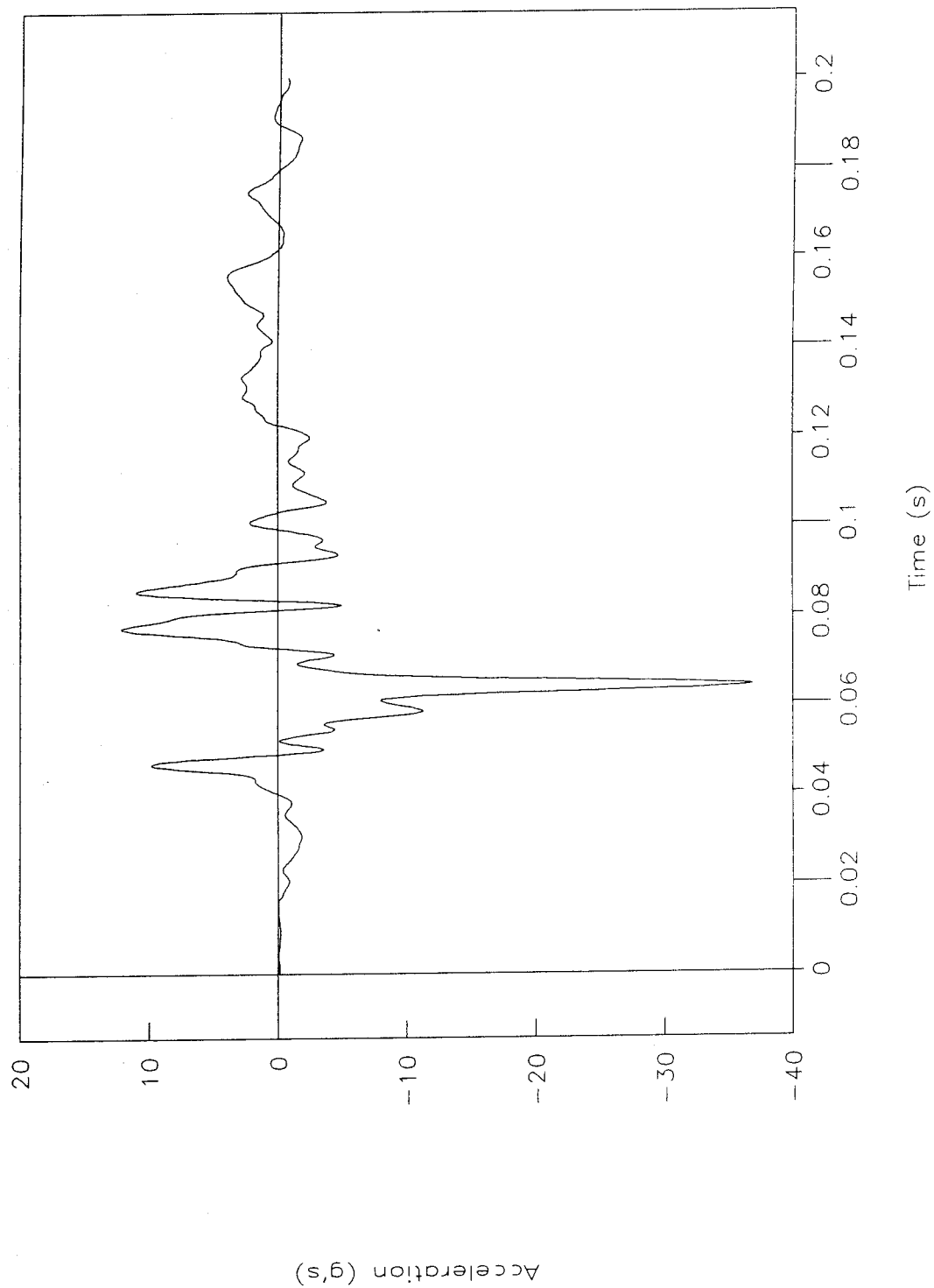


Figure 83. Acceleration vs. time, Y-axis, test 96F014.

Test No. 96F014

Acceleration vs. time, Z-axis

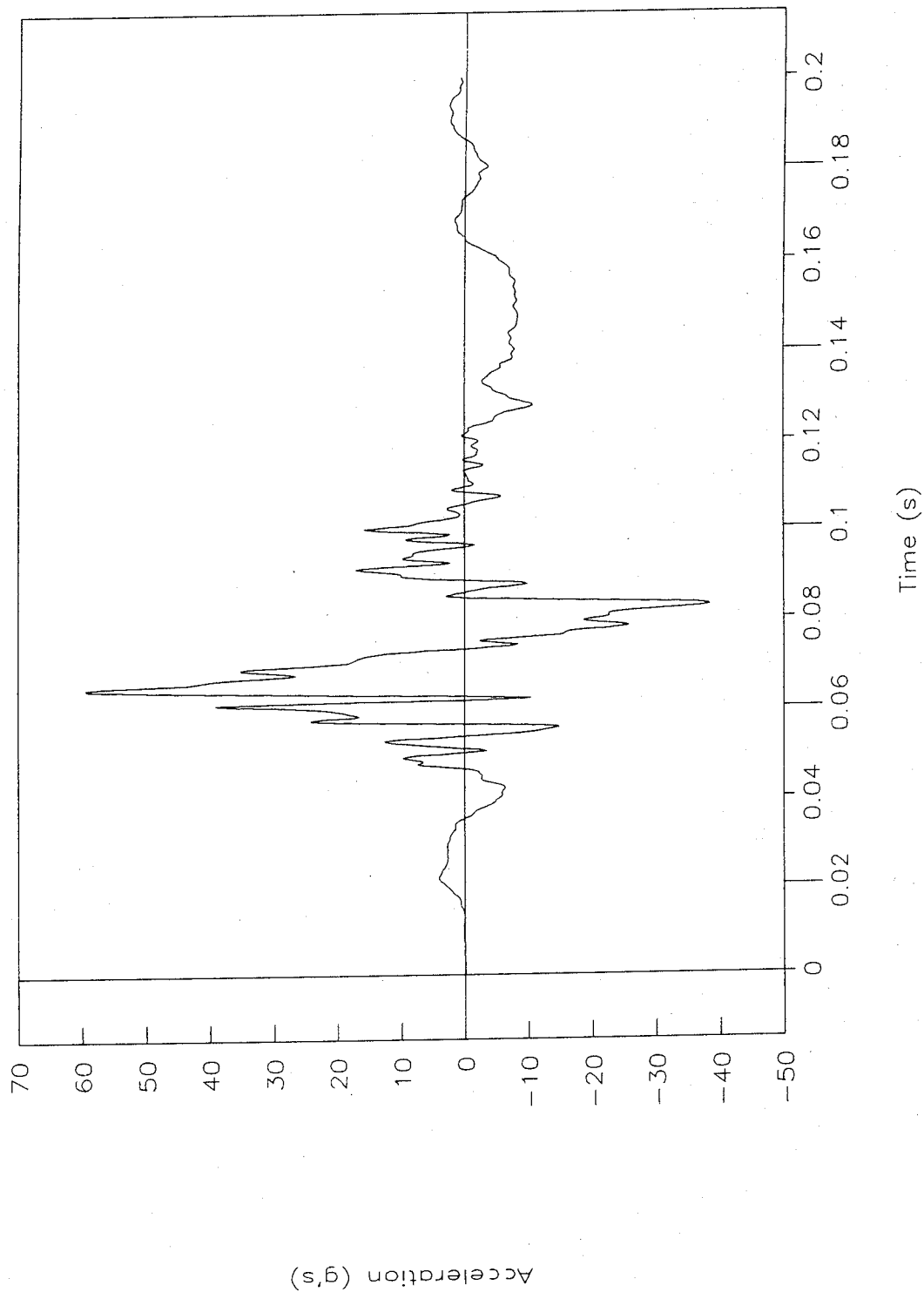


Figure 84. Acceleration vs. time, Z-axis, test 96F014.

Test No. 96F014

Resultant load height vs. time

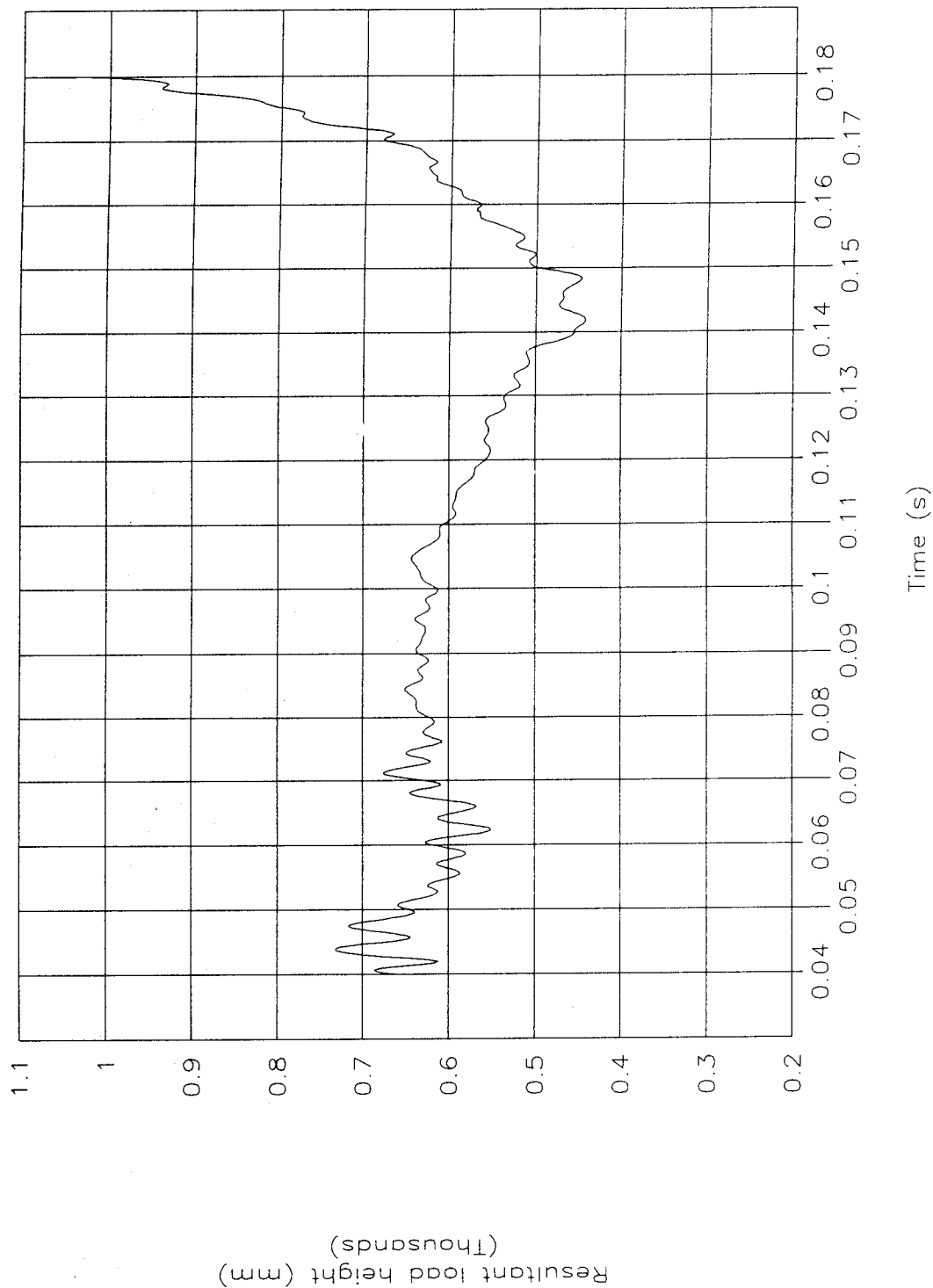


Figure 85. Resultant load height vs. time, test 96F014.

Test No. 96F014

Top of engine

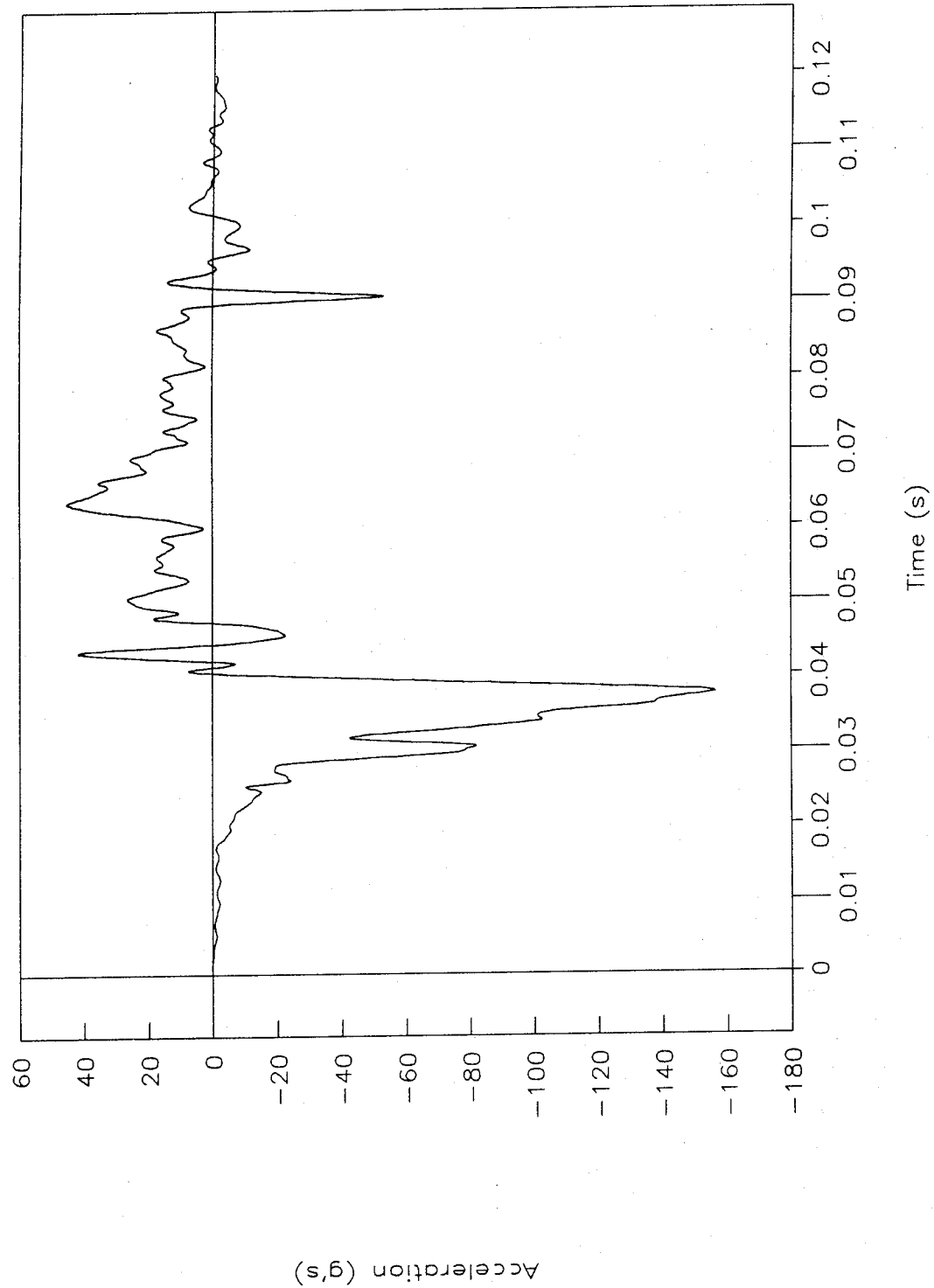


Figure 86. Acceleration vs. time, top of engine, test 96F014.

Test No. 96F014

Bottom of engine

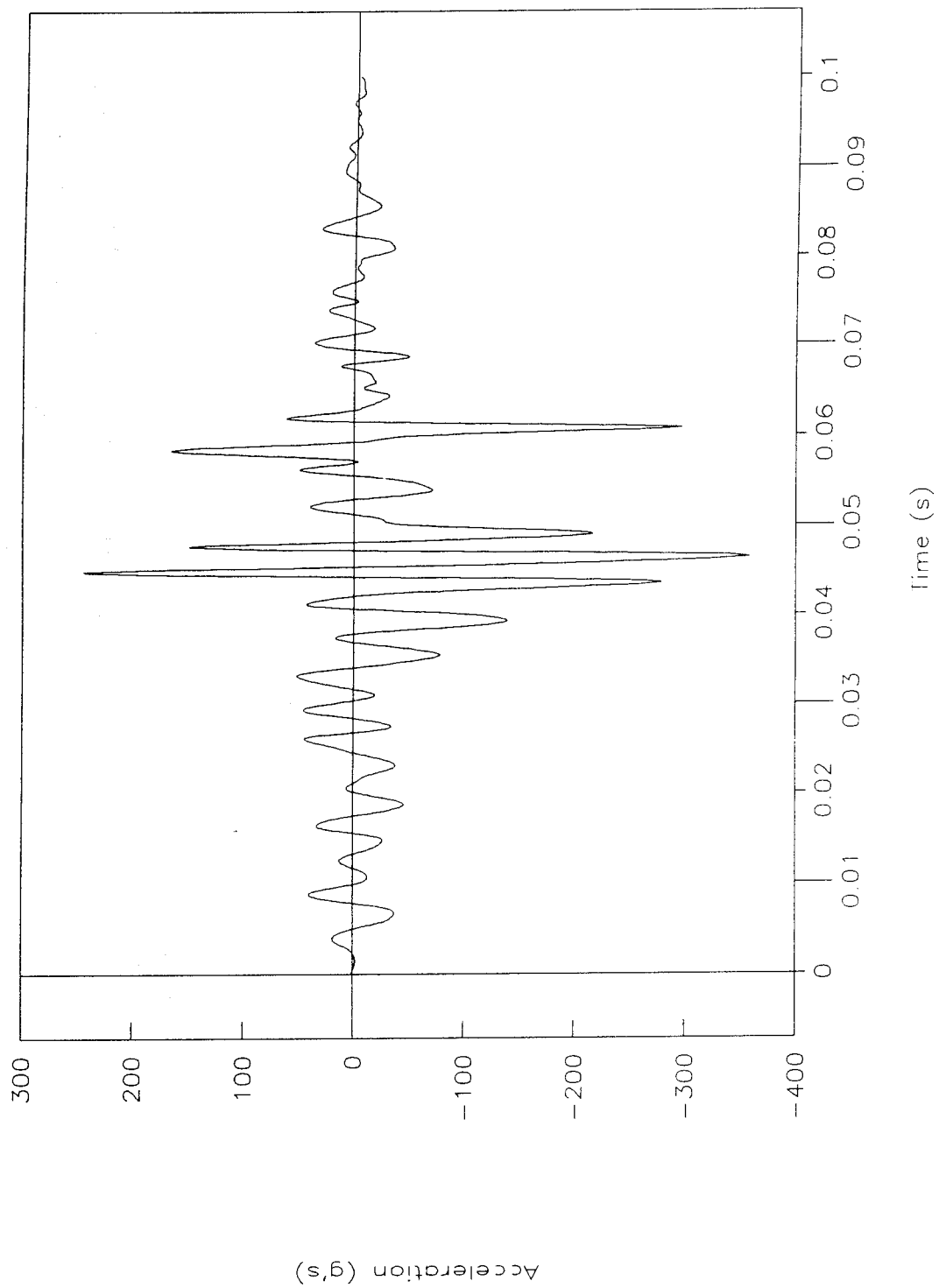


Figure 87. Acceleration vs. time, bottom of engine, test 96F014.

Test No. 96F014

Left control arm

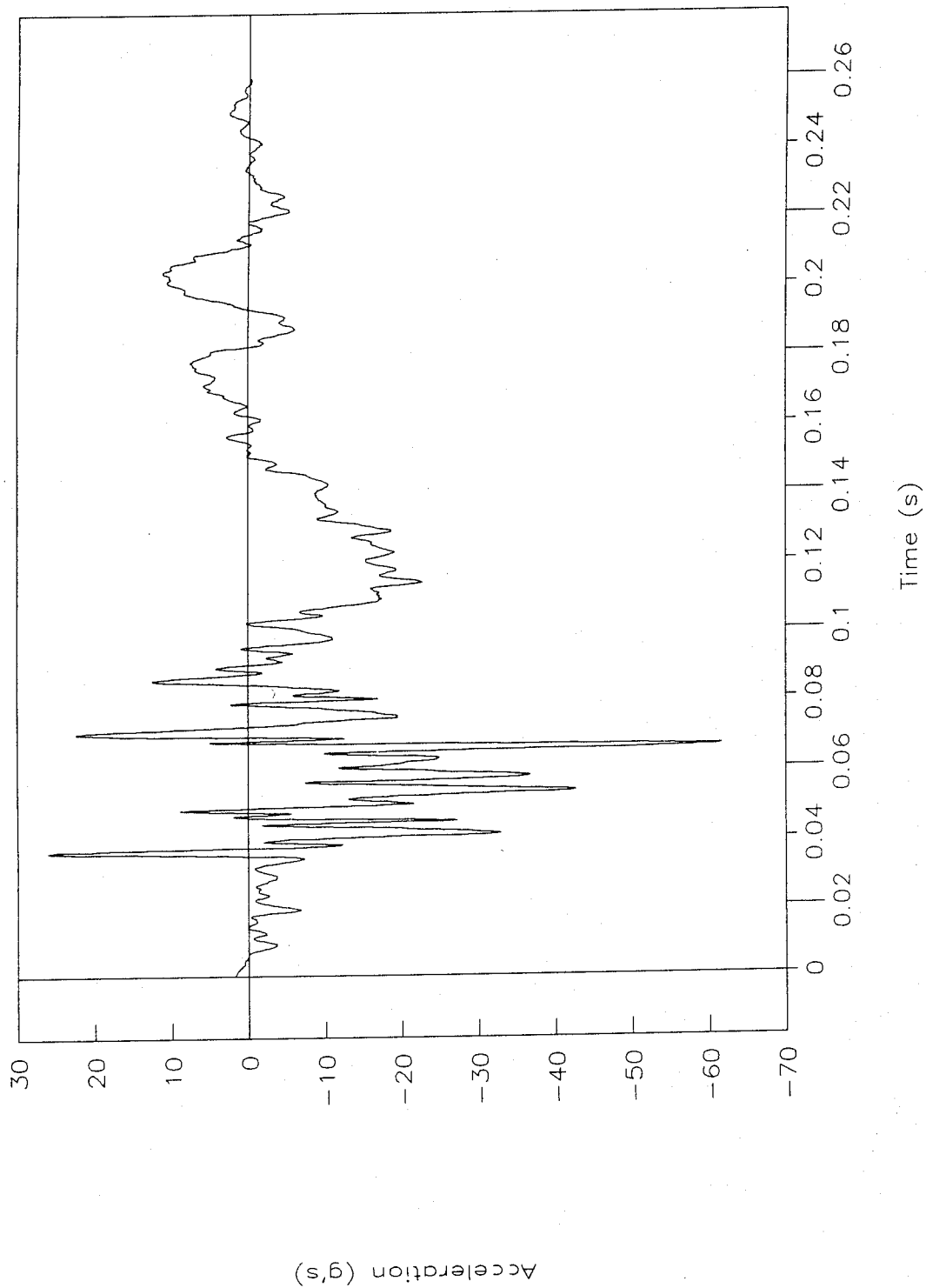


Figure 88. Acceleration vs. time, left control arm, test 96F014.

Test No. 96F014

Instrument panel

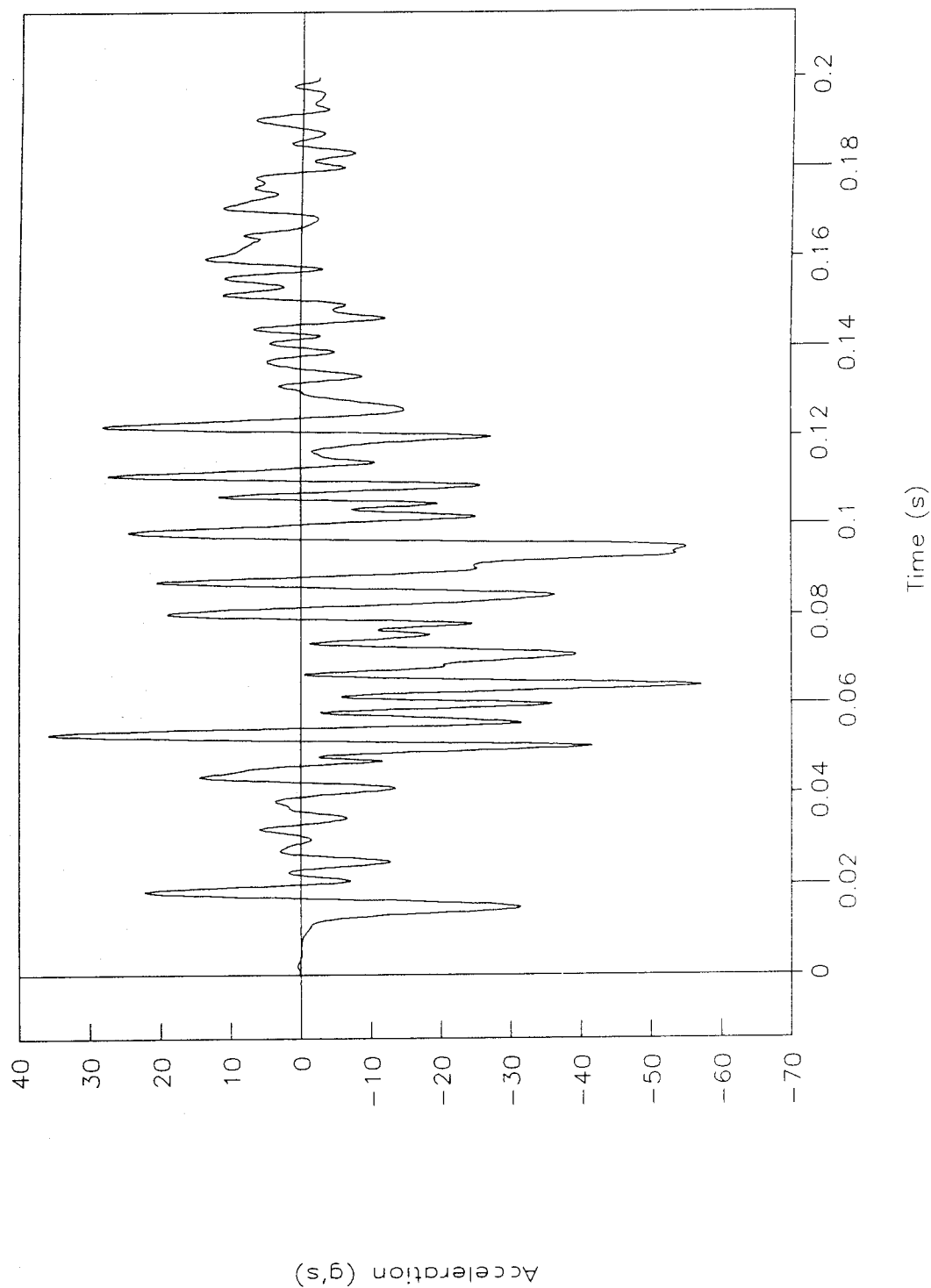


Figure 89. Acceleration vs. time, instrument panel, test 96F014.

Test No. 96F014

Left-rear seat

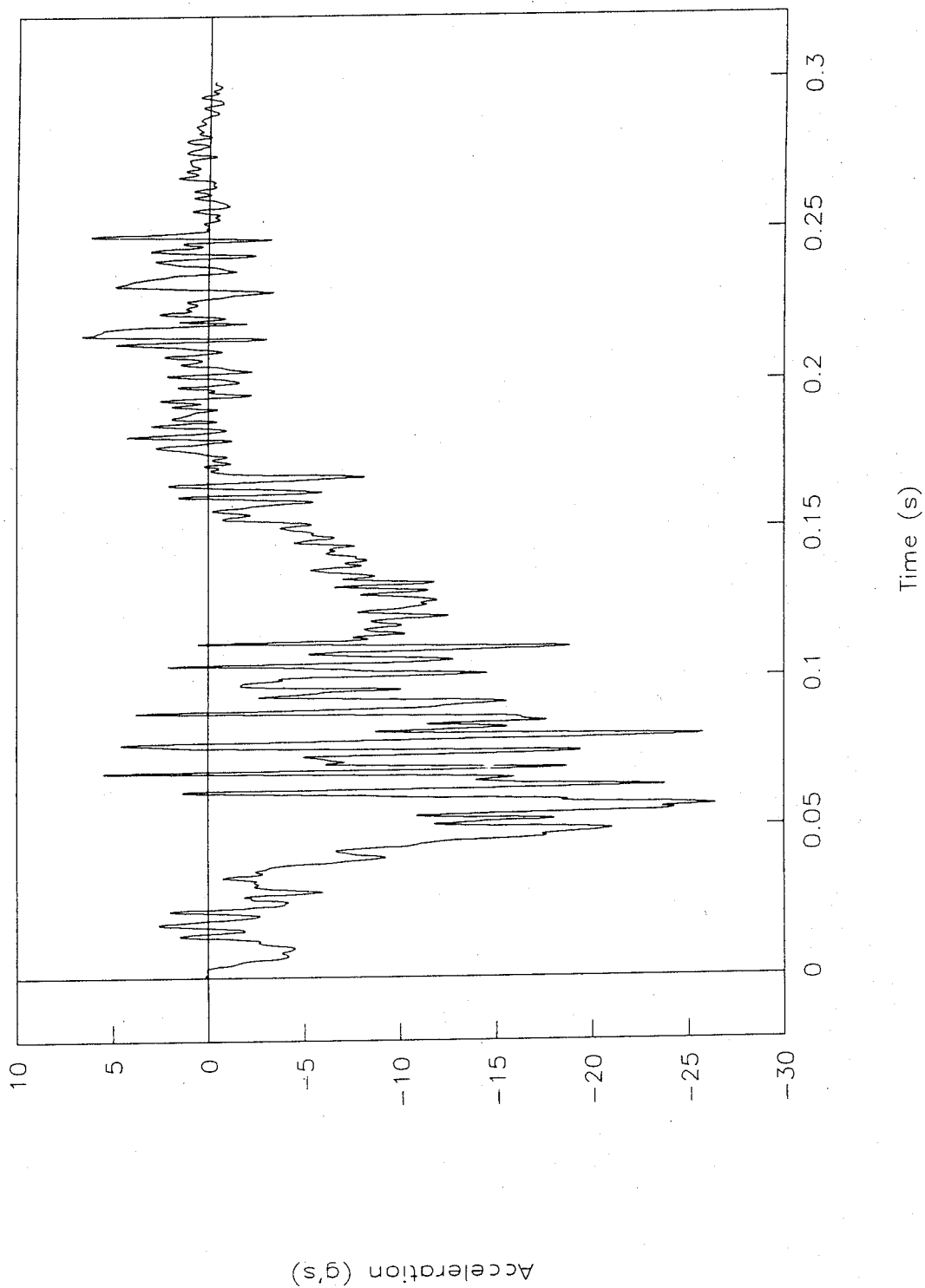


Figure 90. Acceleration vs. time, left-rear seat, test 96F014.

Test No. 96F014

Right-rear seat

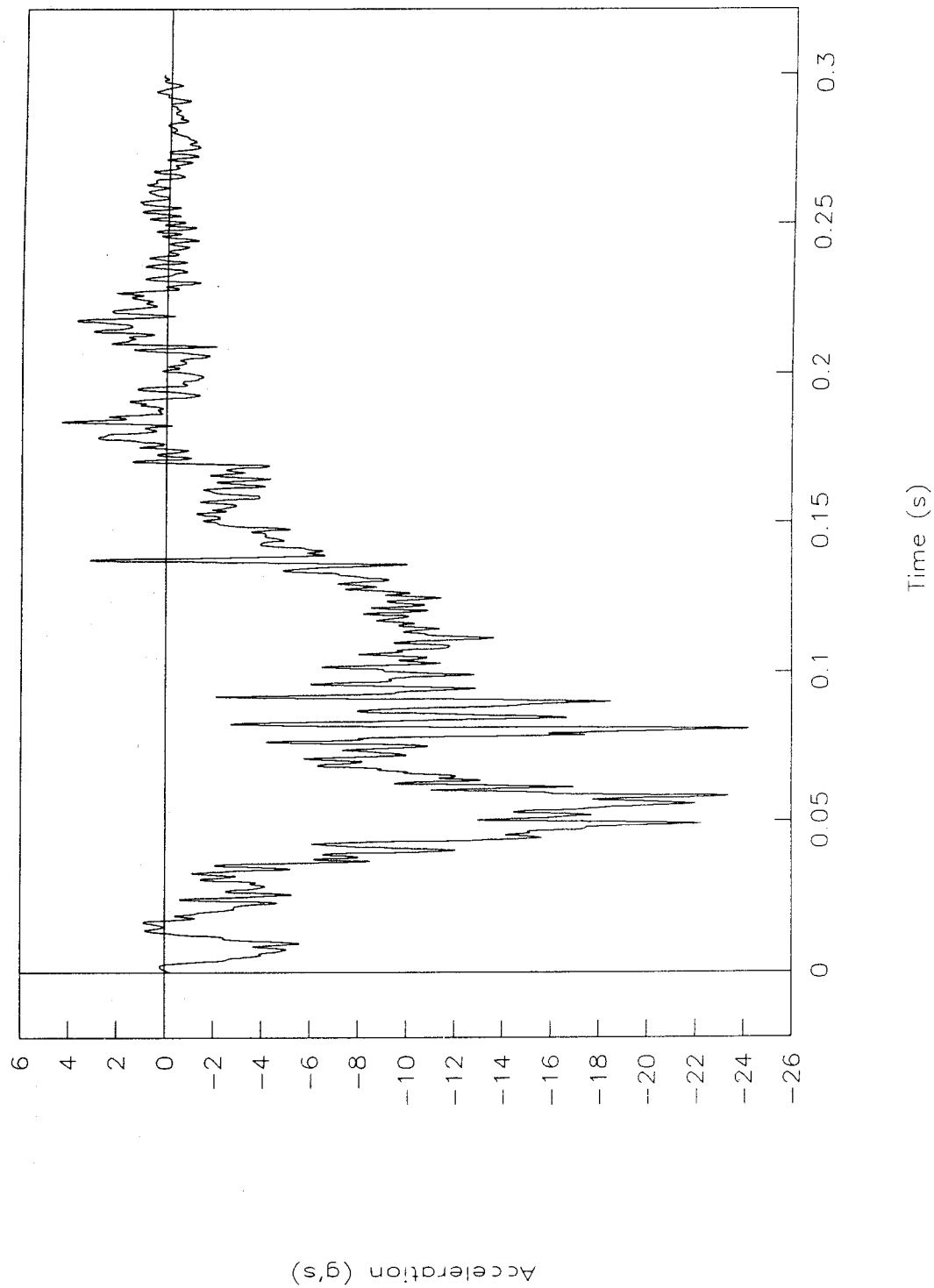


Figure 91. Acceleration vs. time, right-rear seat, test 96F014.

Test No. 96F015

Acceleration vs. time

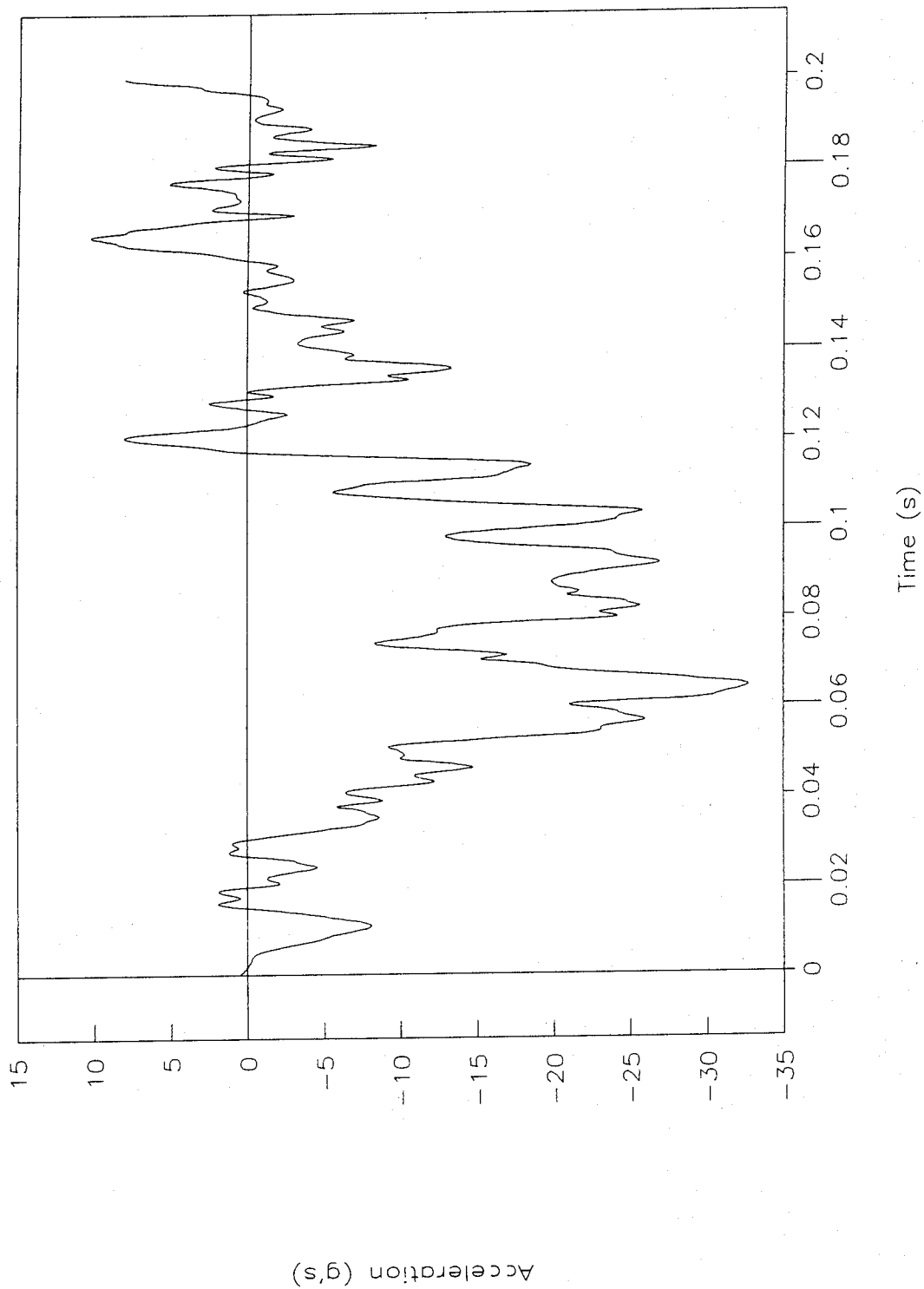


Figure 92. Acceleration vs. time, test 96F015.

Test No. 96F015

Velocity vs. time

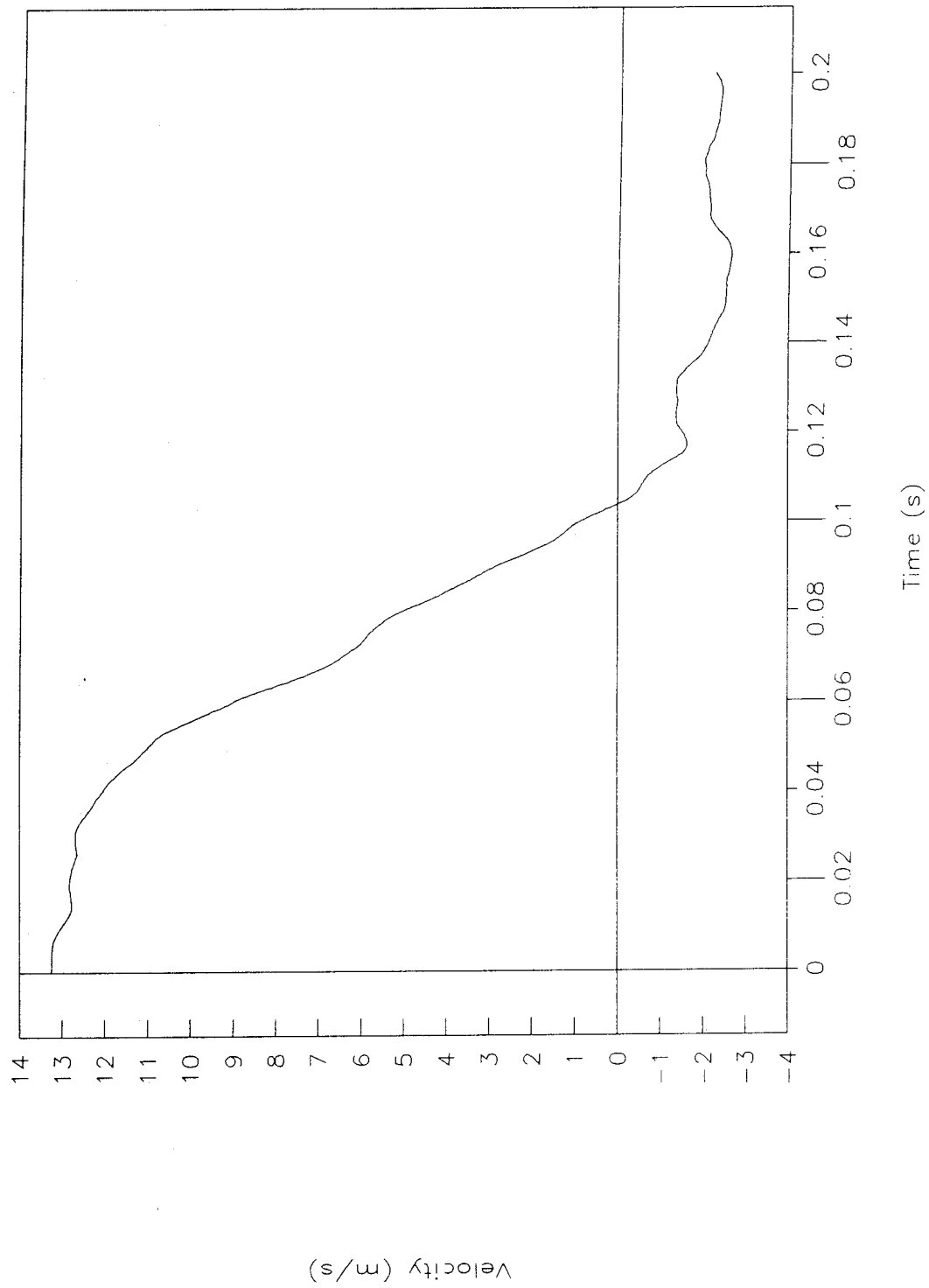


Figure 93. Velocity vs. time, test 96F015.

Test No. 96F015

Displacement vs. time

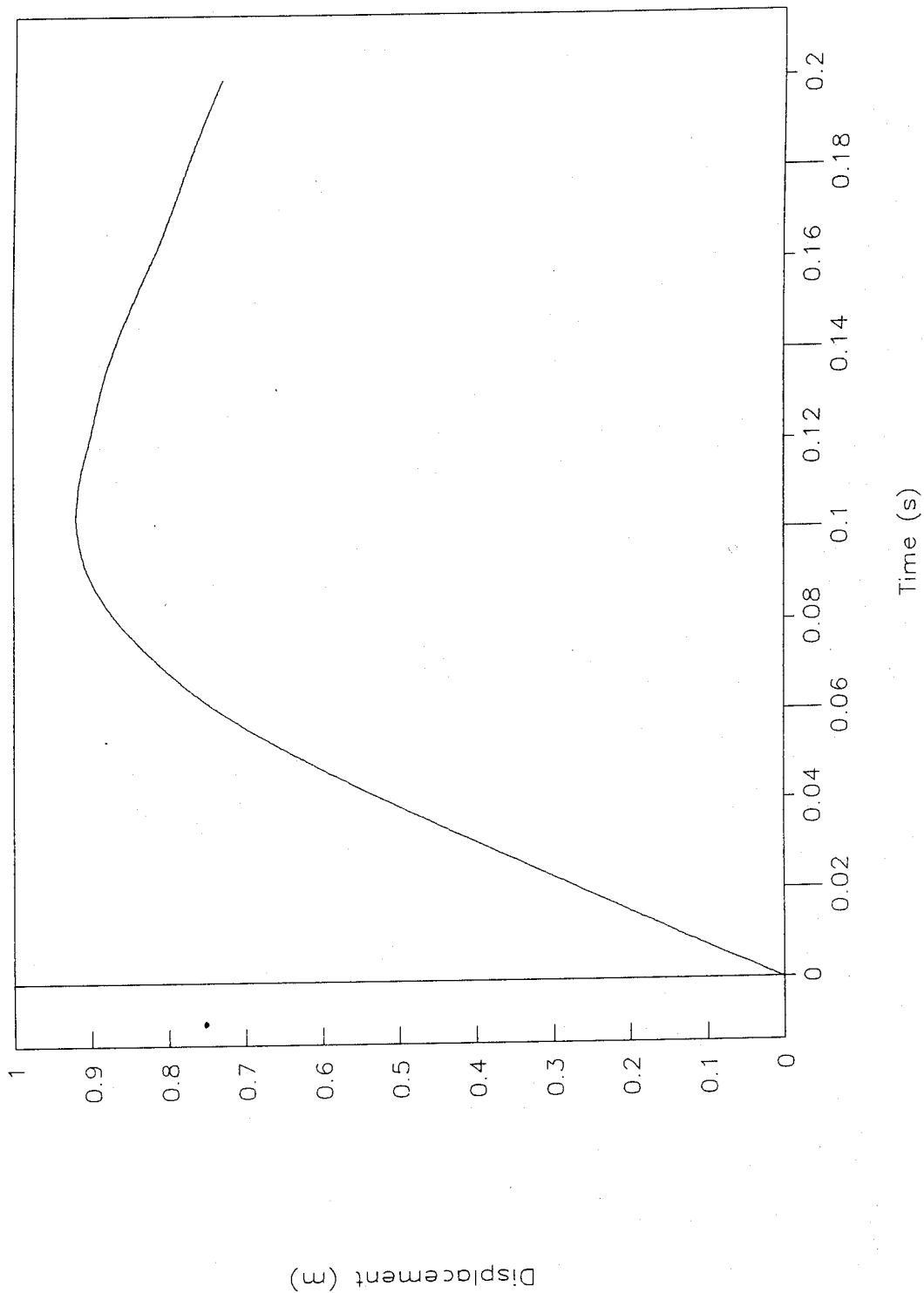


Figure 94. Displacement vs. time, test 96F015.

Test No. 96F015

Force vs. time, load-cell data

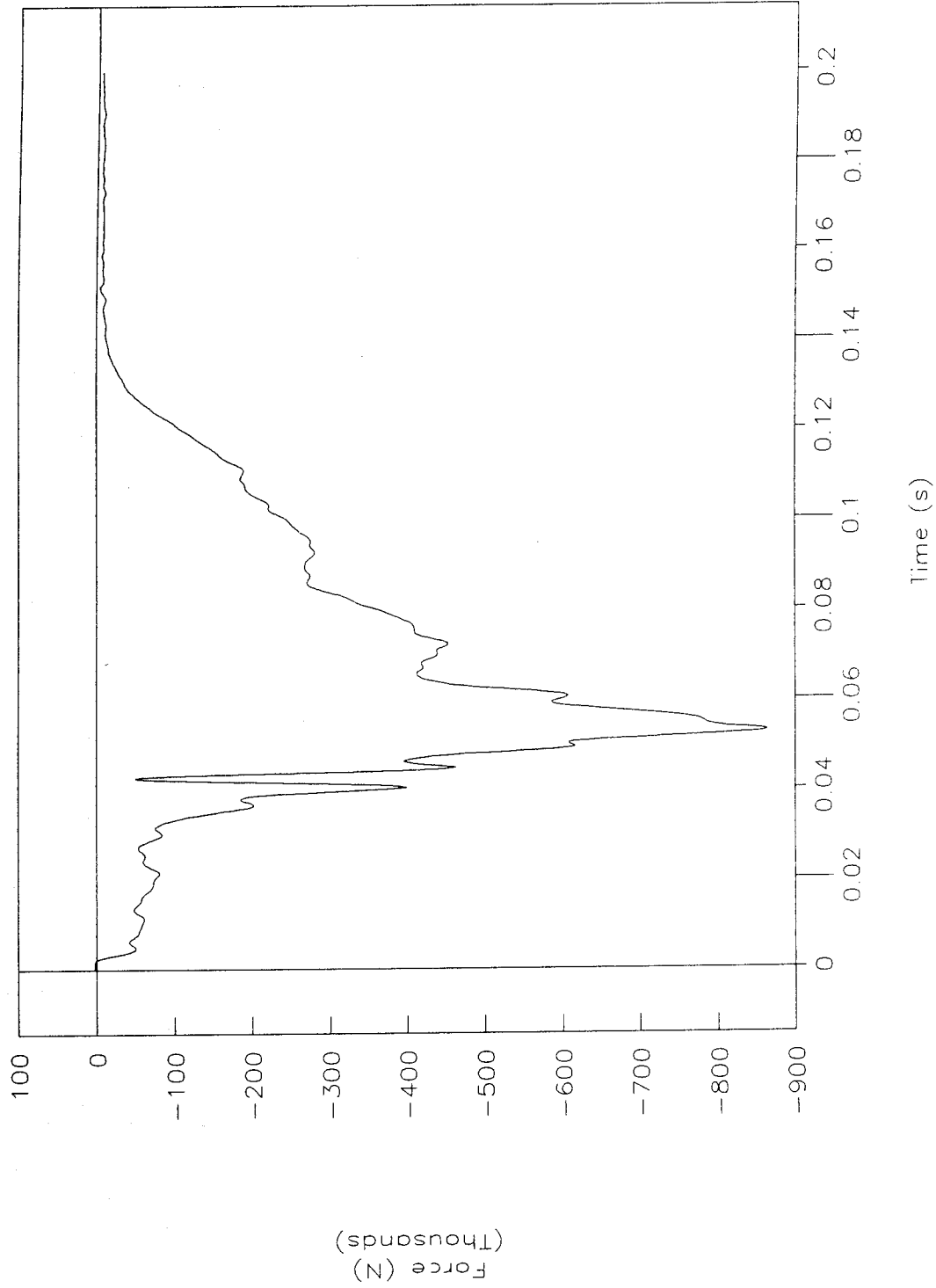


Figure 95. Force vs. time, load-cell data, test 96F015.

Test No. 96F015

Force vs. displacement, load-cell data

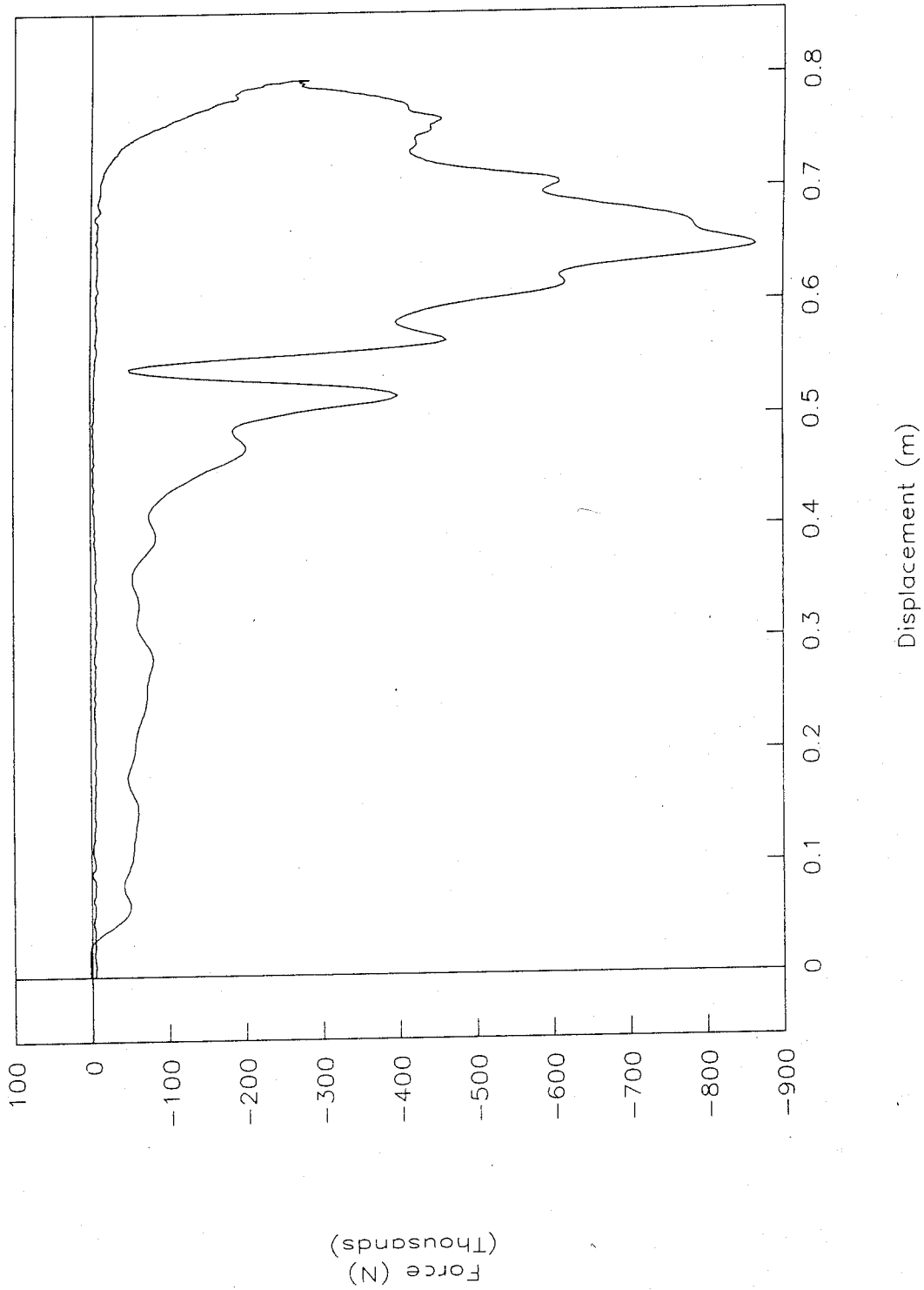


Figure 96. Force vs. displacement, load-cell data, test 96F015.

Test No. 96F015

Energy vs. displacement, load-cell data

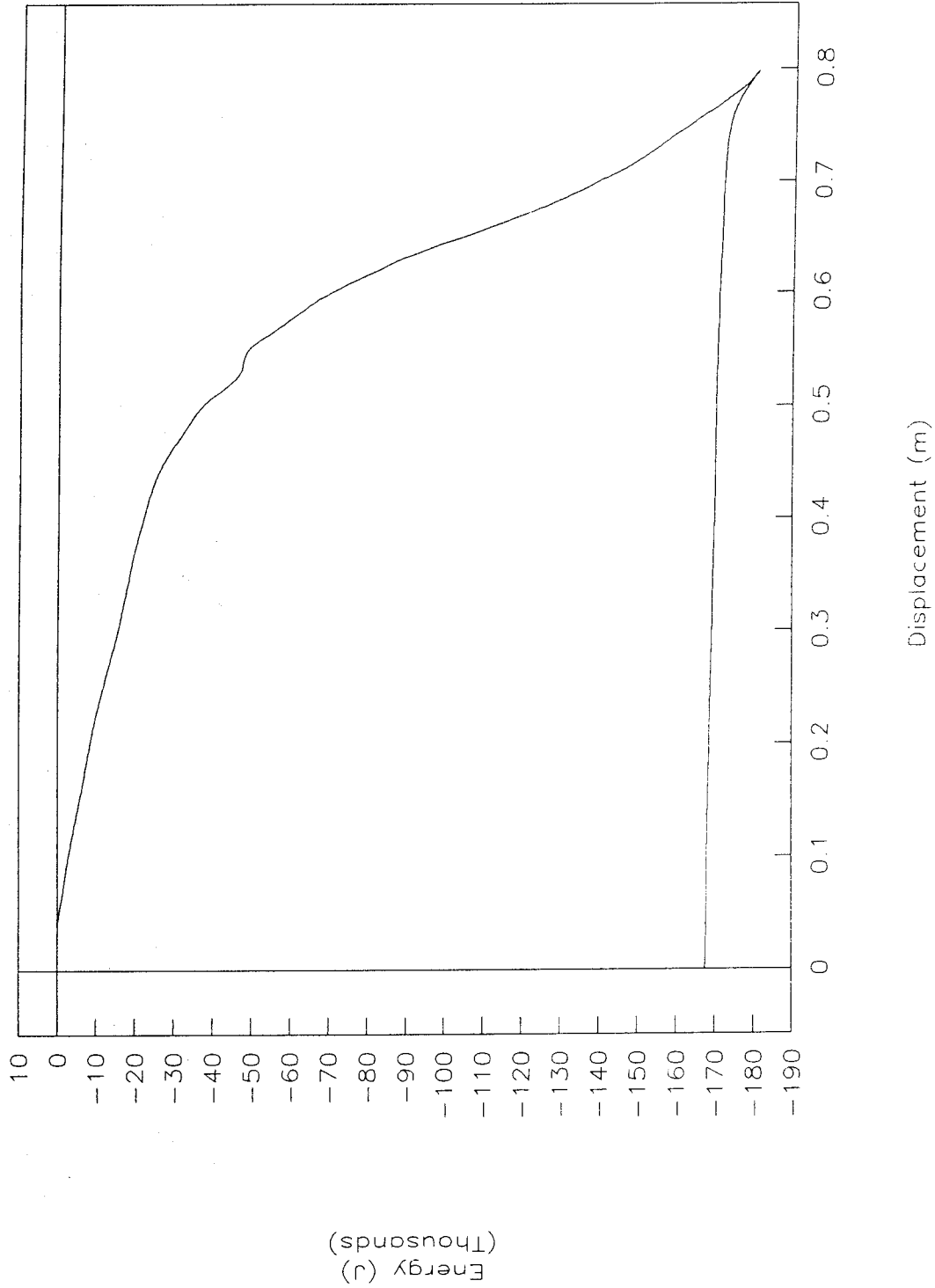


Figure 97. Energy vs. displacement, load-cell data, test 96F015.

Test No. 96F015

Acceleration vs. time, Y-axis

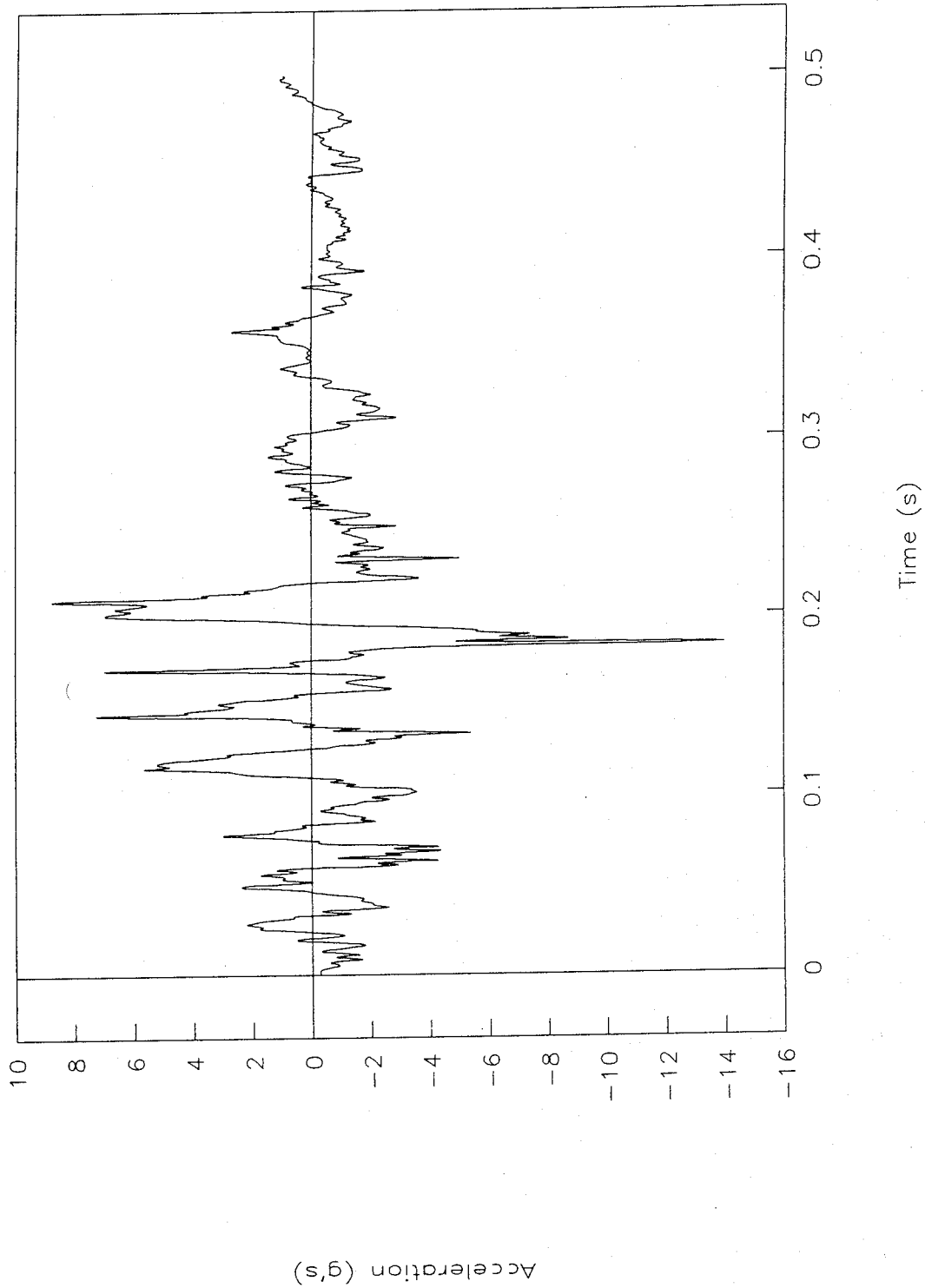


Figure 98. Acceleration vs. time, Y-axis, test 96F015.

Test No. 96F015

Acceleration vs. time, Z-axis

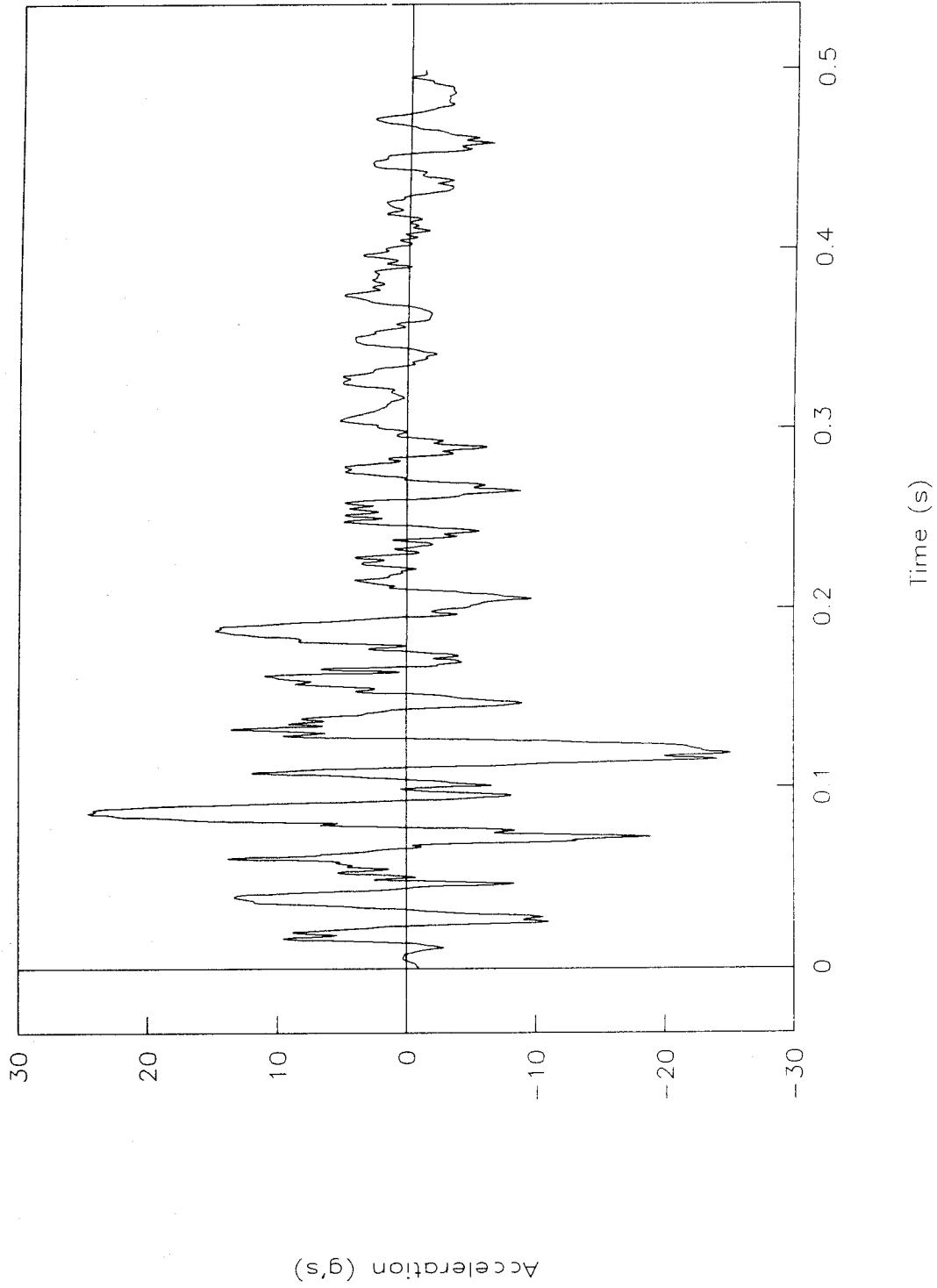


Figure 99. Acceleration vs. time, Z-axis, test 96F015.

Test No. 96F015

Resultant load height vs. time

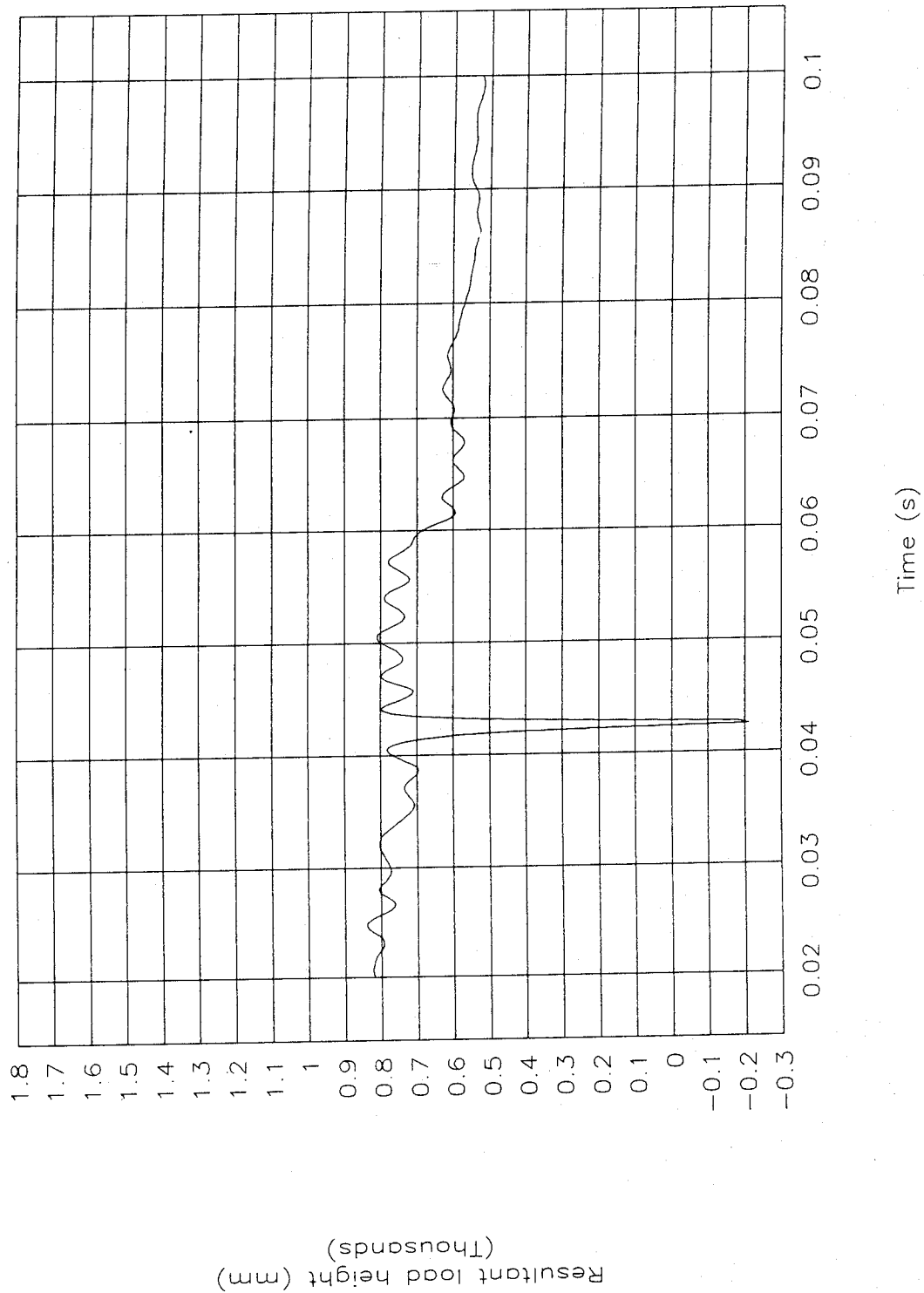


Figure 100. Resultant load height vs. time, test 96F015.

Test No. 96F015

Top of engine

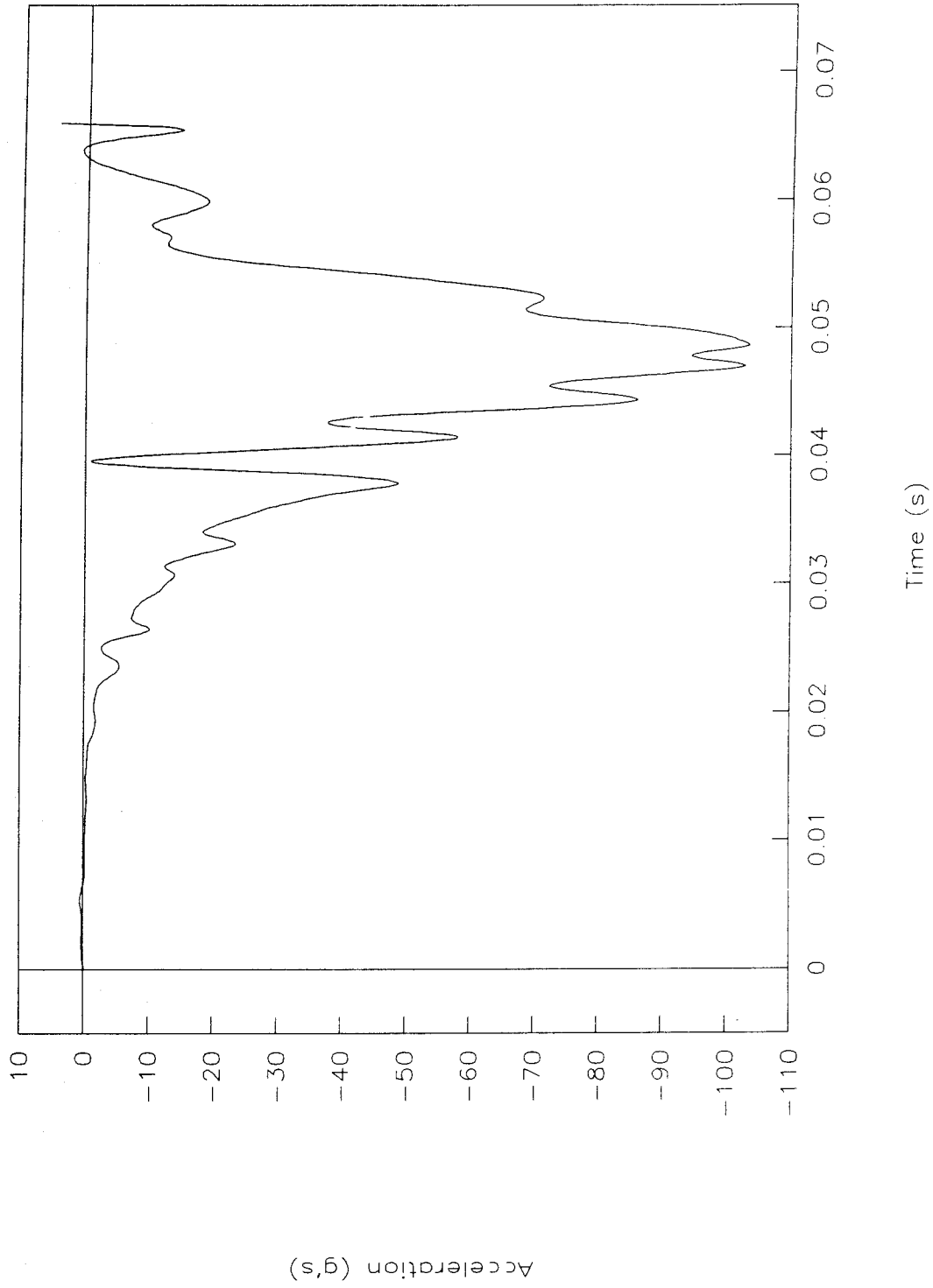


Figure 101. Acceleration vs. time, top of engine, test 96F015.

Test No. 96F015

Bottom of engine

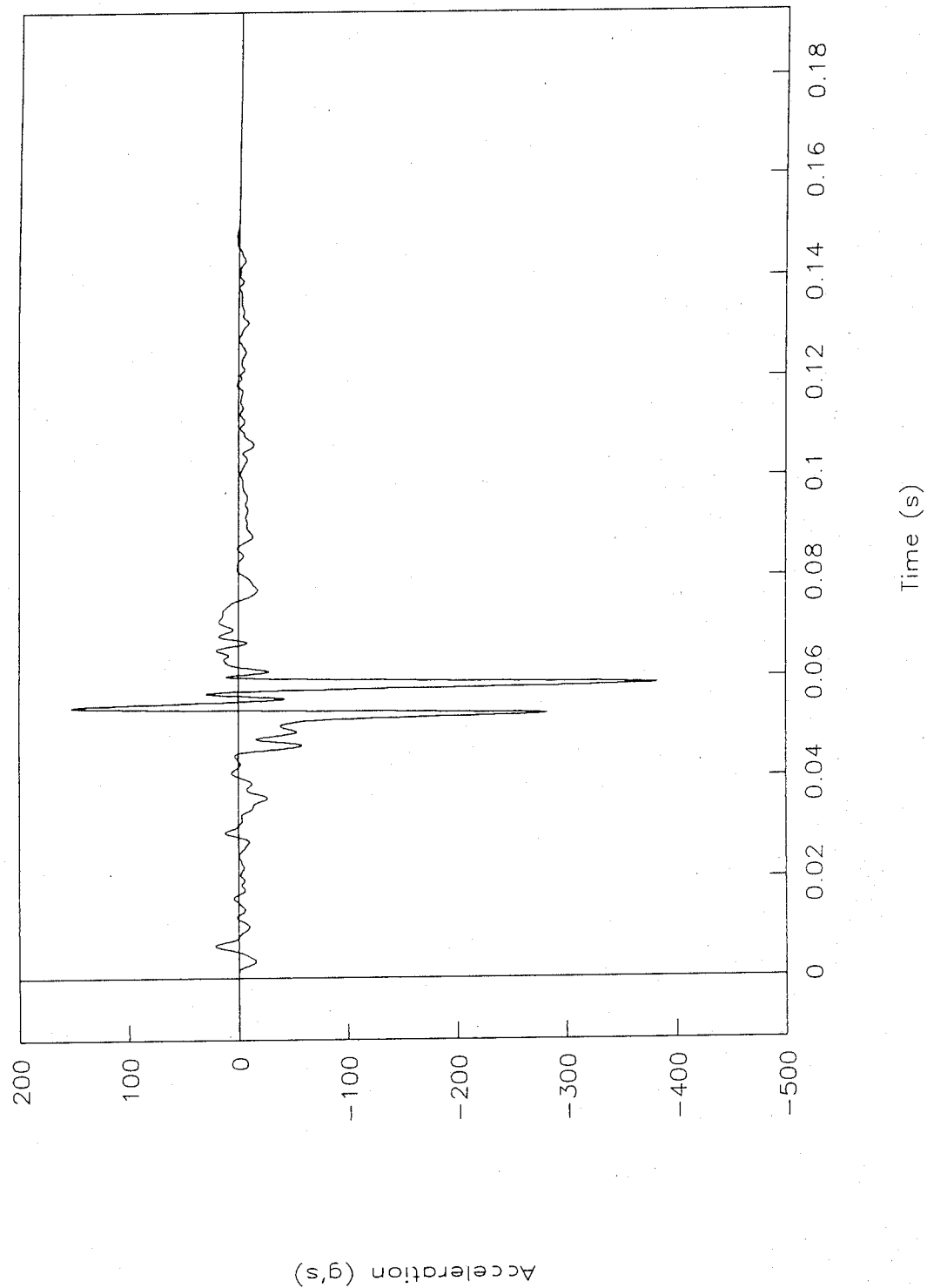


Figure 102. Acceleration vs. time, bottom of engine, test 96F015.

Test No. 96F015

Left control arm

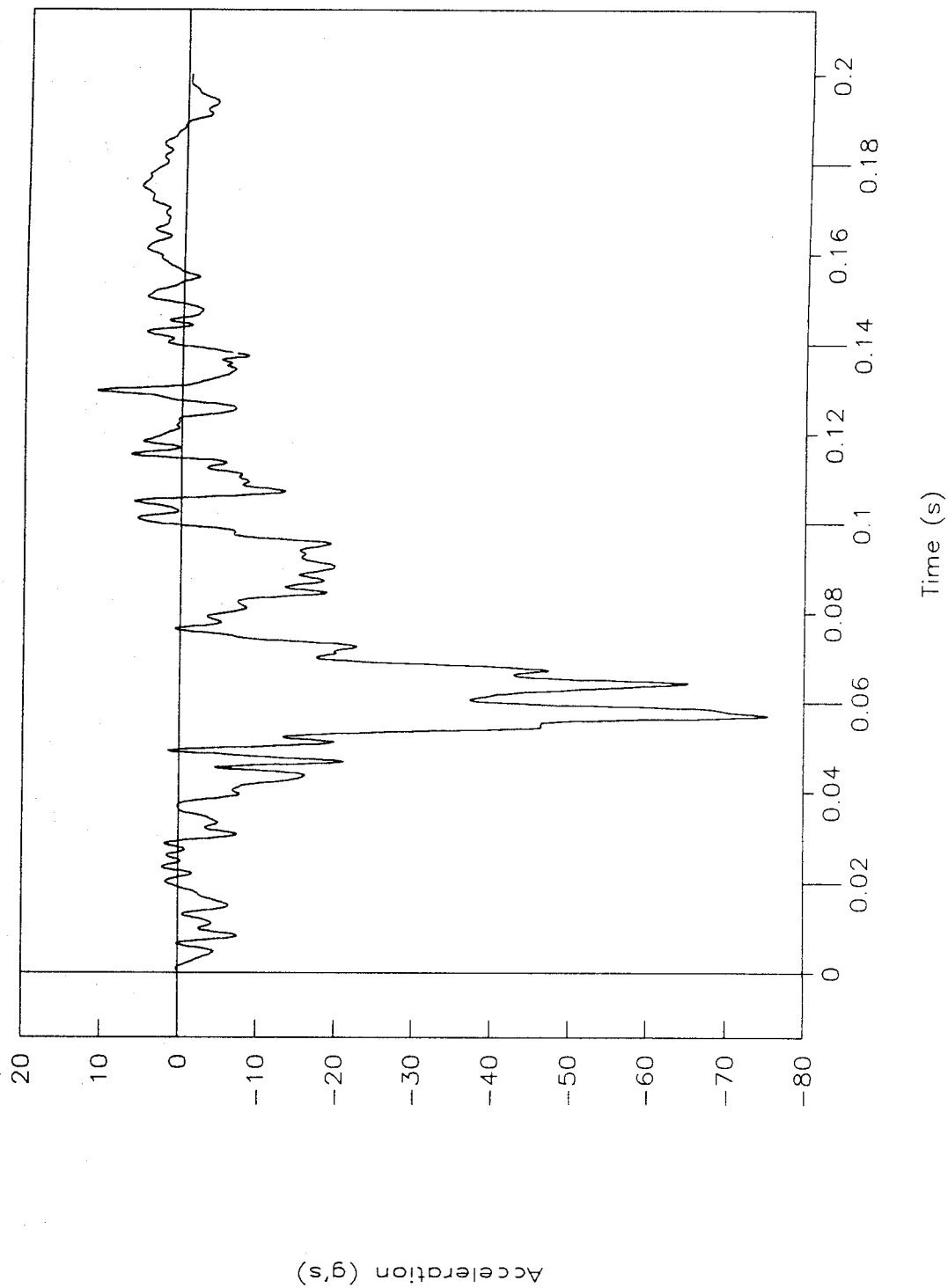


Figure 103. Acceleration vs. time, left control arm, test 96F015.

Test No. 96F015

Right control arm

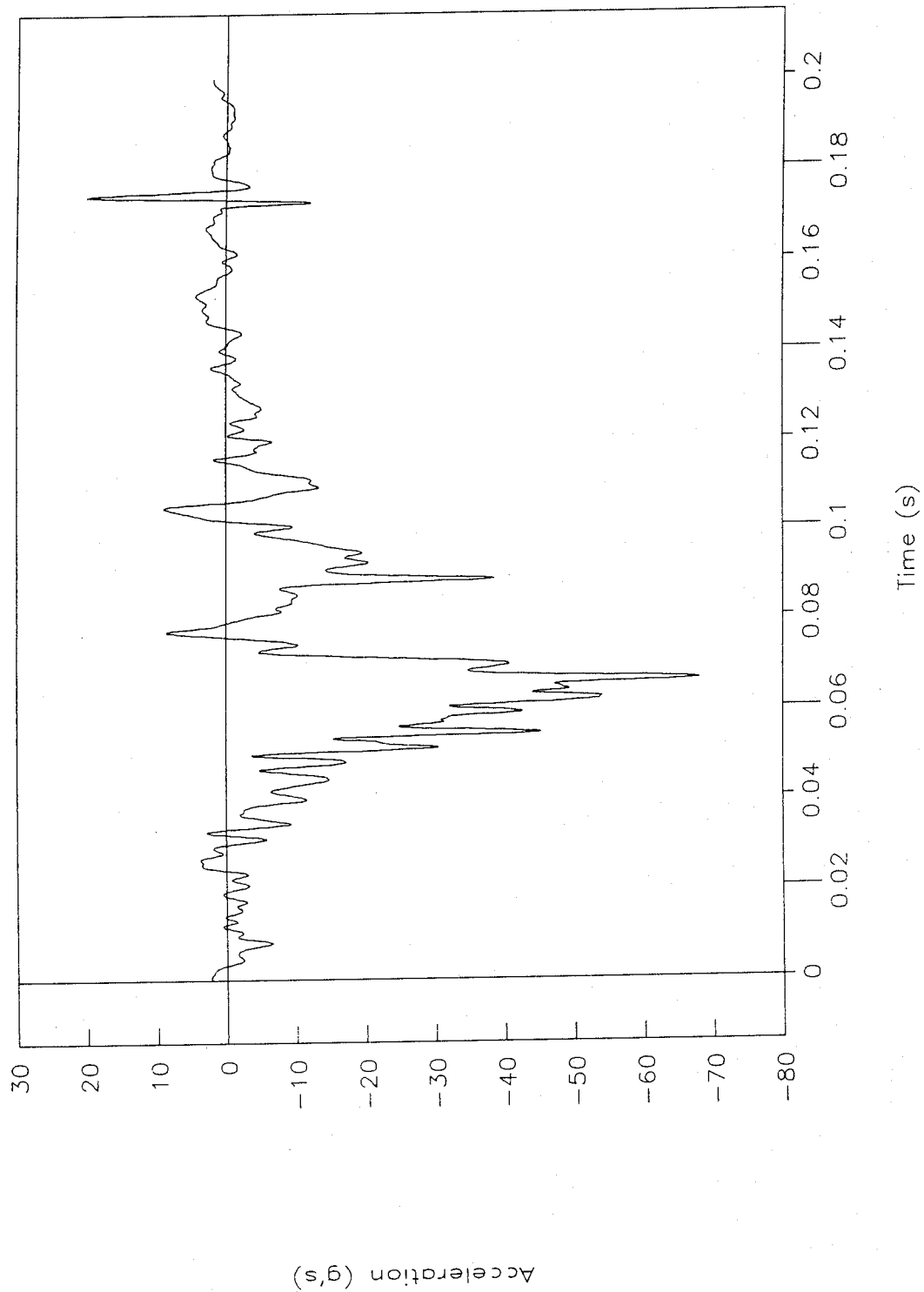


Figure 104. Acceleration vs. time, right control arm, test 96F015.

Test No. 96F015

Instrument panel

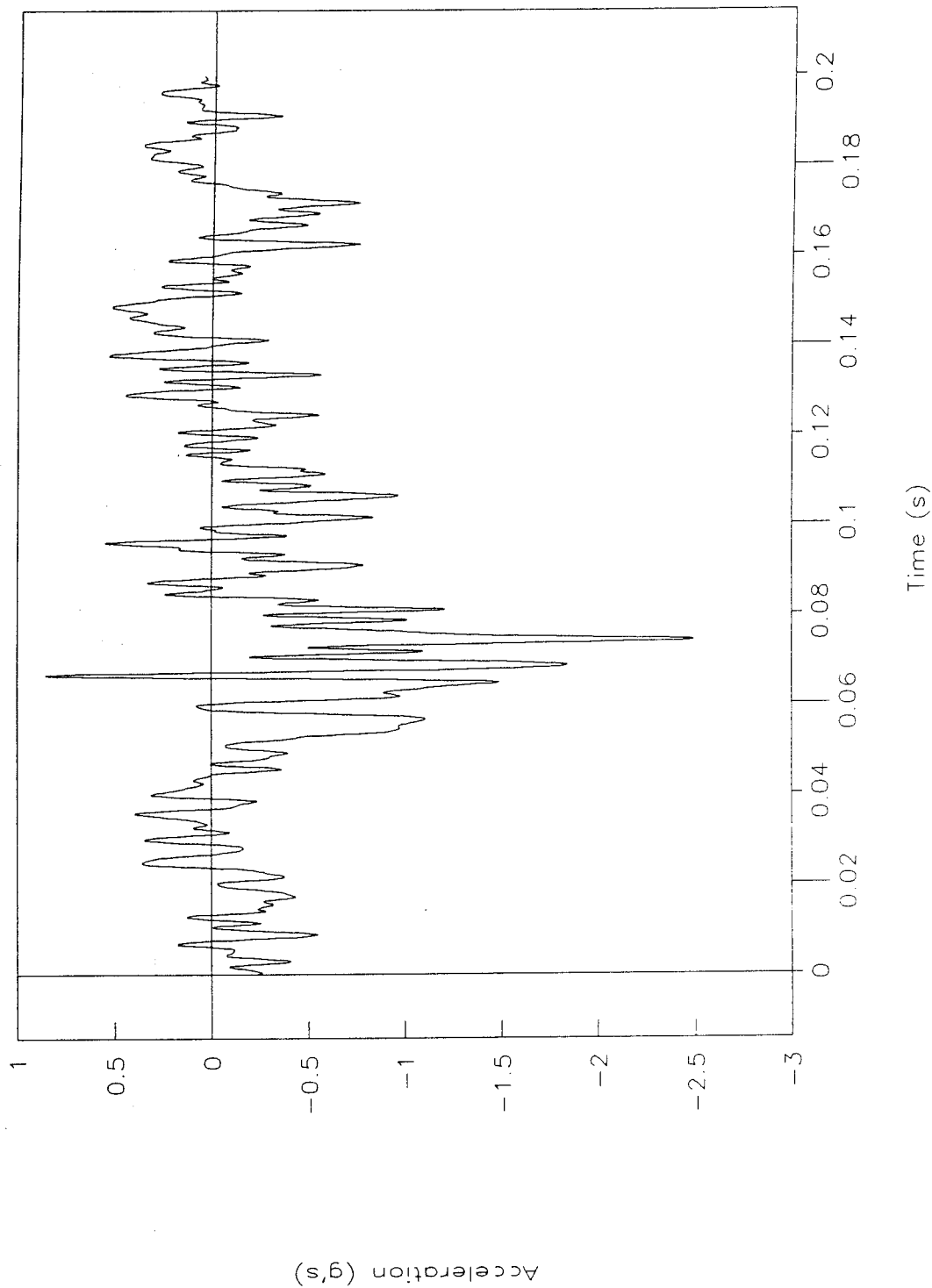


Figure 105. Acceleration vs. time, instrument panel, test 96F015.

Test No. 96F015

Left-rear seat

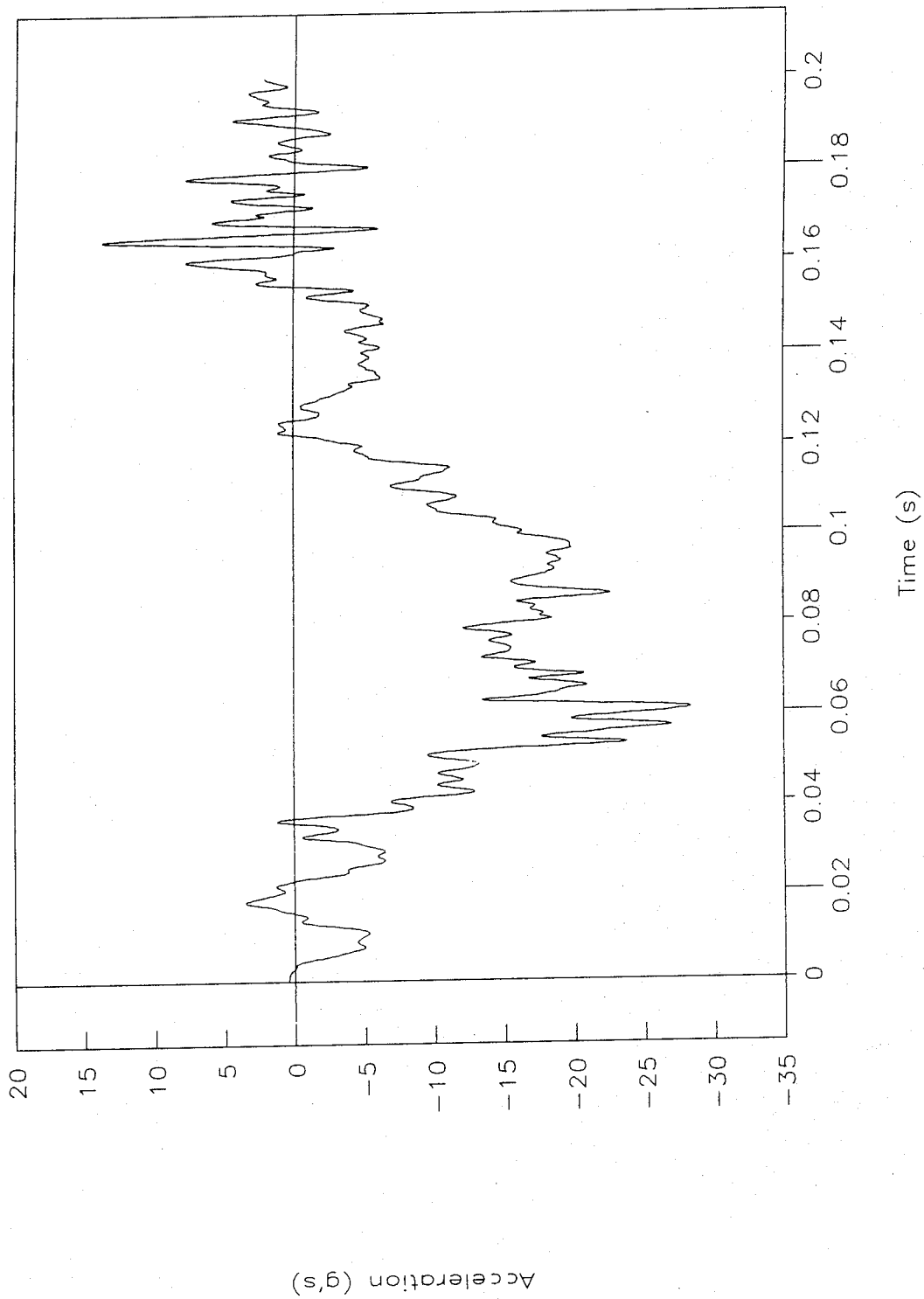
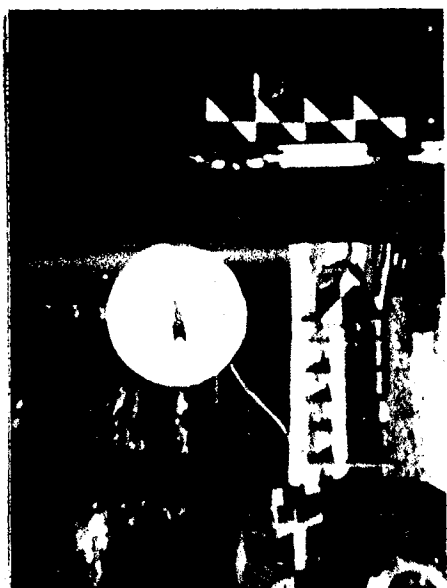
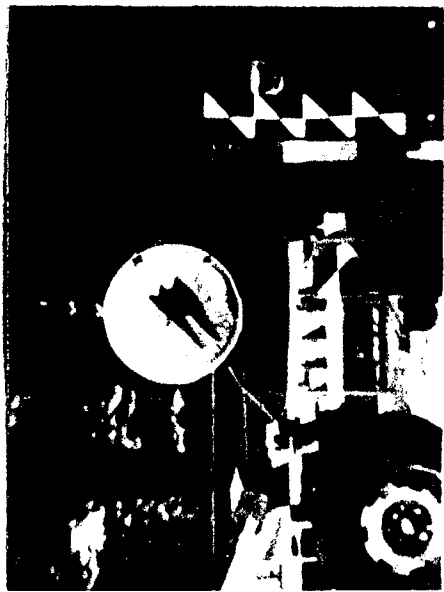


Figure 106. Acceleration vs. time, left-rear seat, test 96F015.

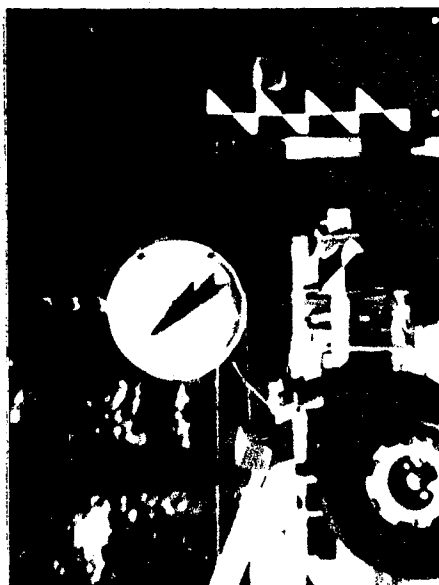
APPENDIX B. TEST PHOTOGRAPHS



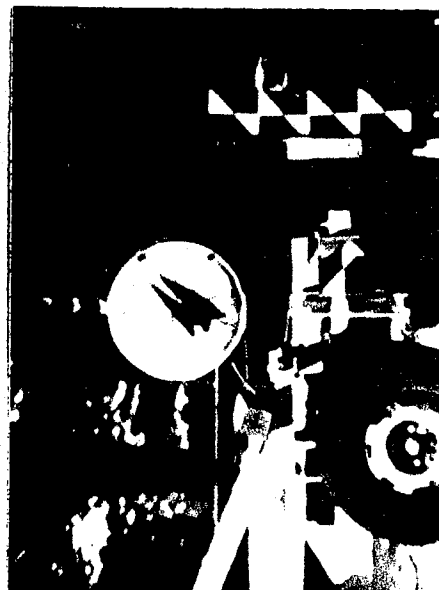
0.000 s



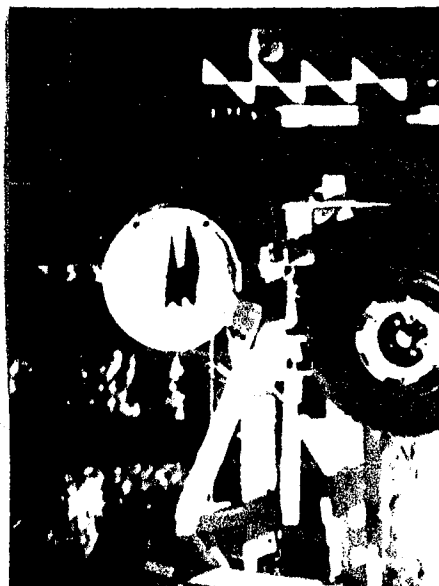
0.020 s



0.032 s

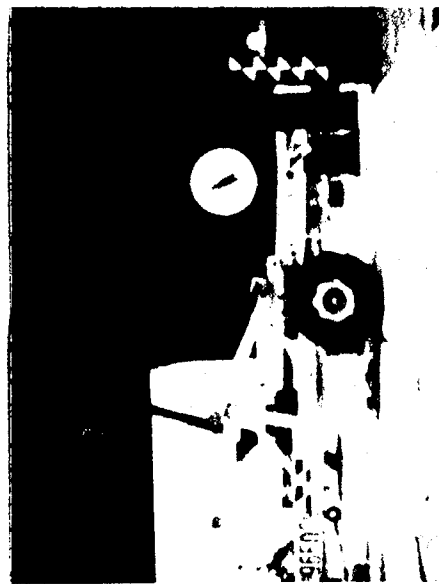


0.044 s

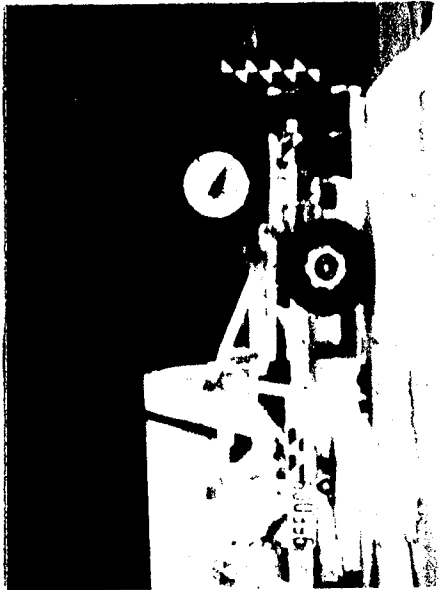


0.100 s

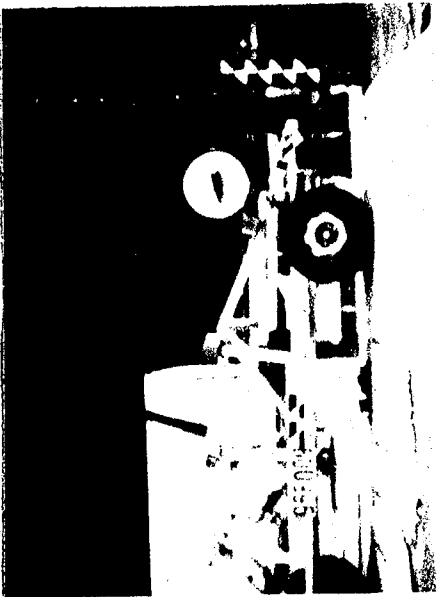
Figure 107. Test photographs during impact, test 96F008.



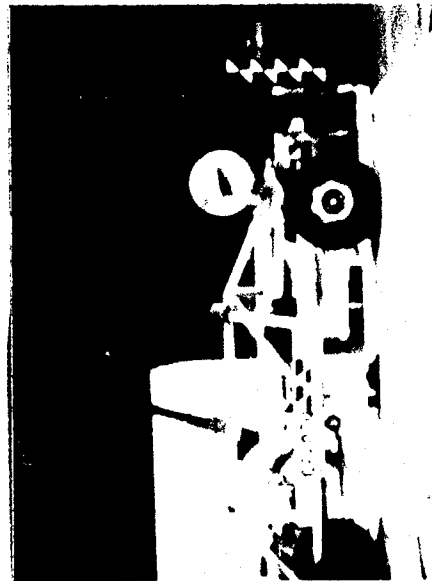
0.000 s



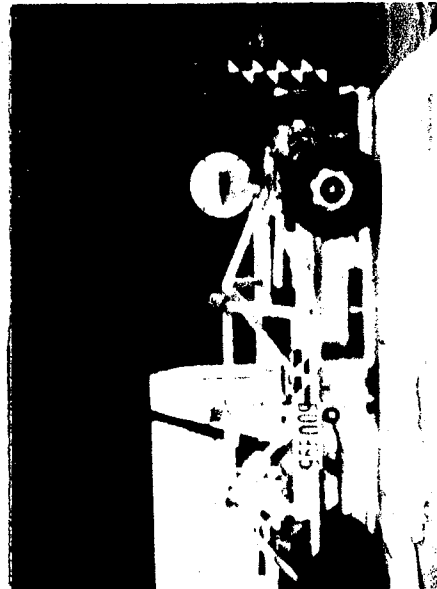
0.020 s



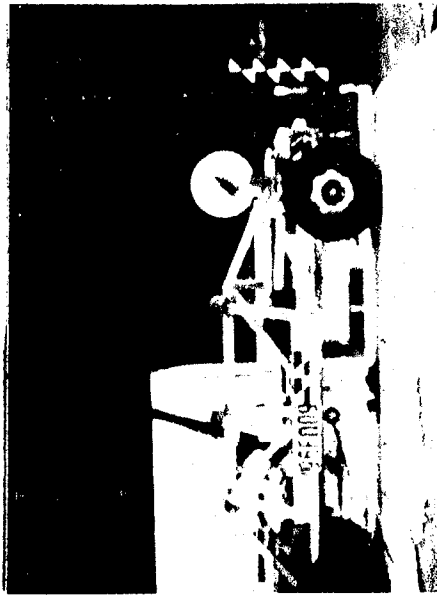
0.040 s



0.064 s

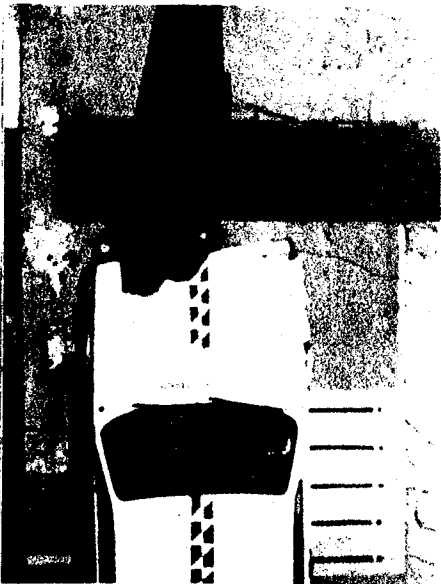


0.092 s

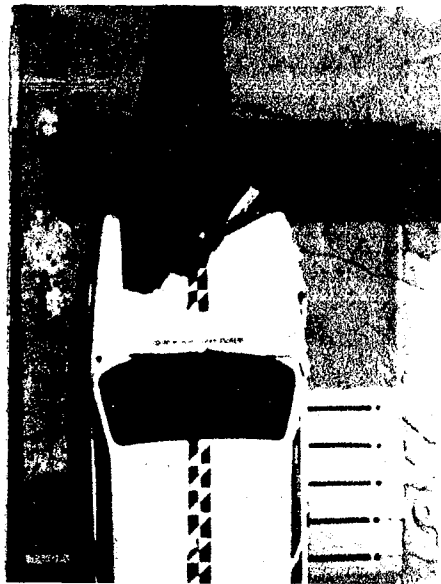


0.110 s

Figure 108. Test photographs during impact, test 96F009.



0.008 s



0.032 s



0.044 s



0.052 s



0.070 s



0.086 s

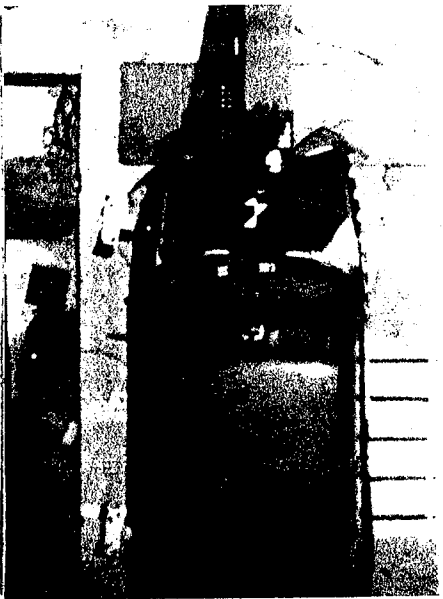
Figure 109. Test photographs during impact, test 96F010.



0.014 s



0.036 s



0.052 s



0.060 s

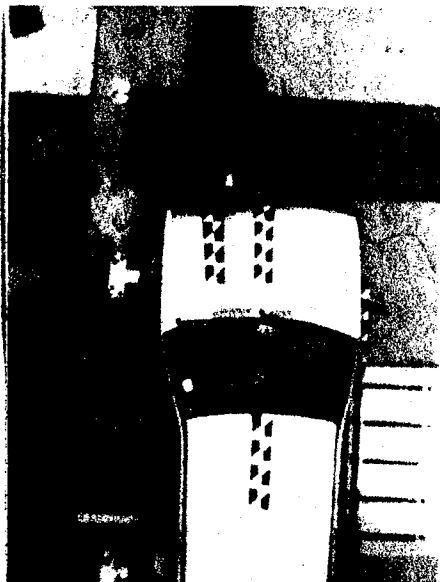


0.072 s

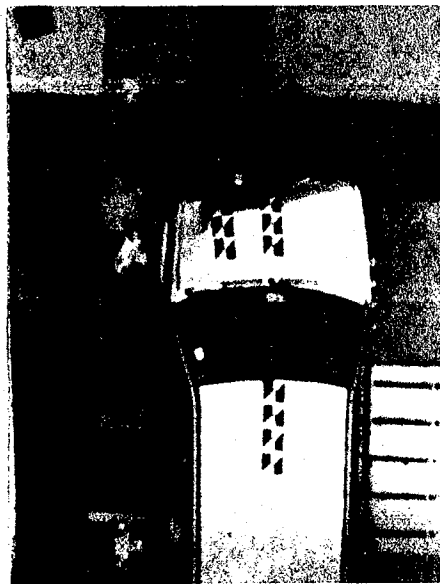


0.096 s

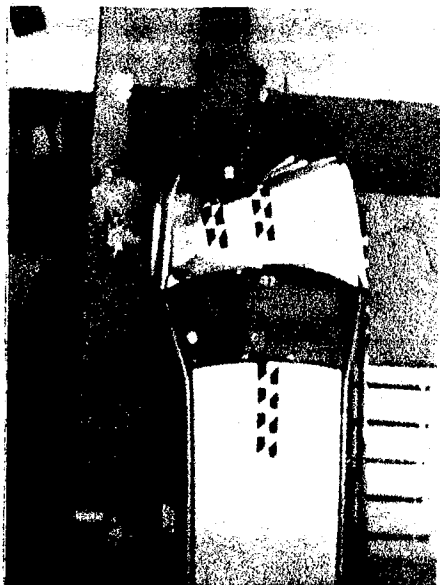
Figure 110. Test photographs during impact, test 96F011.



0.020 s



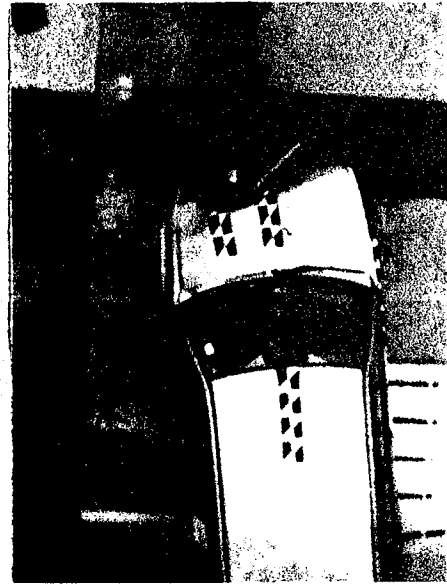
0.044 s



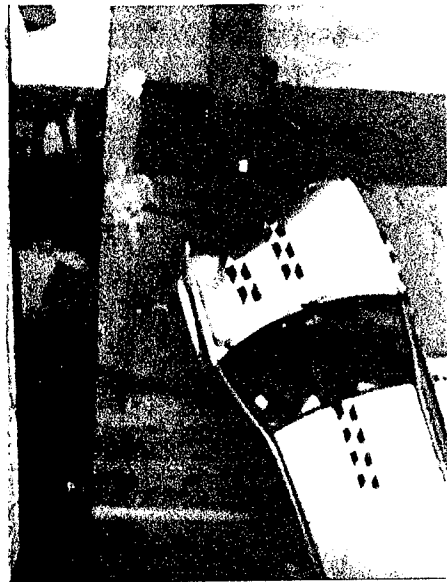
0.068 s



0.080 s

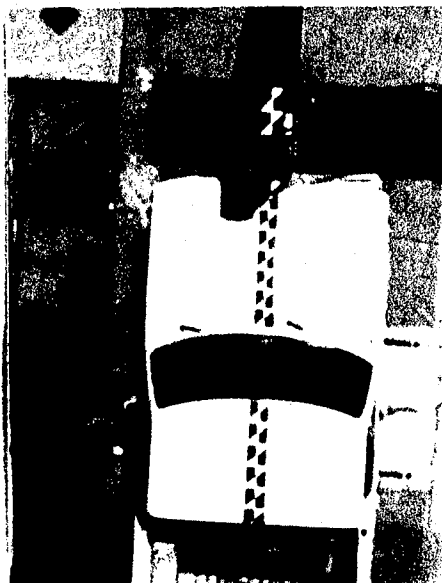


0.122 s

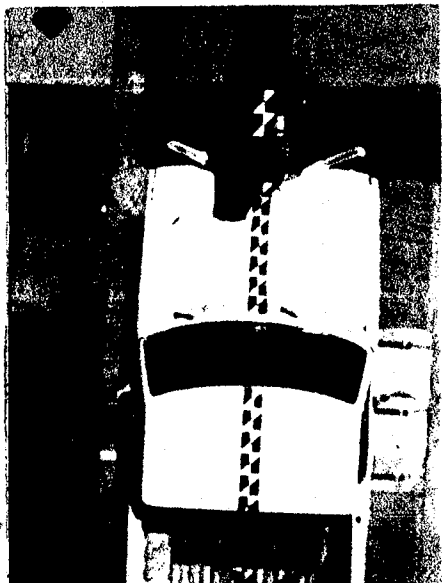


0.430 s

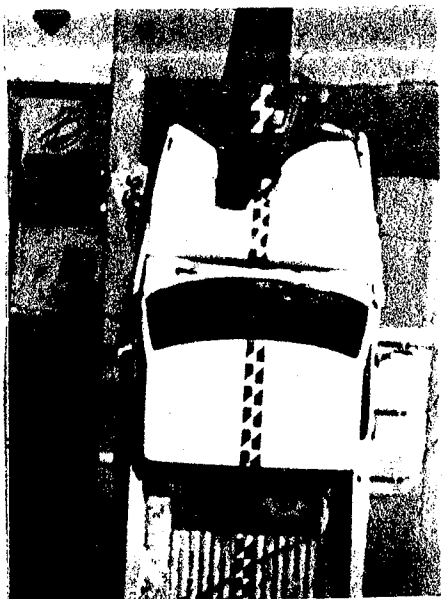
Figure 111. Test photographs during impact, test 96F012.



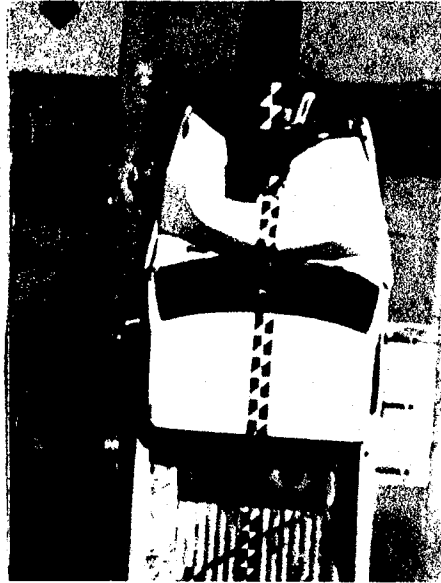
0.014 s



0.024 s



0.052 s



0.066 s

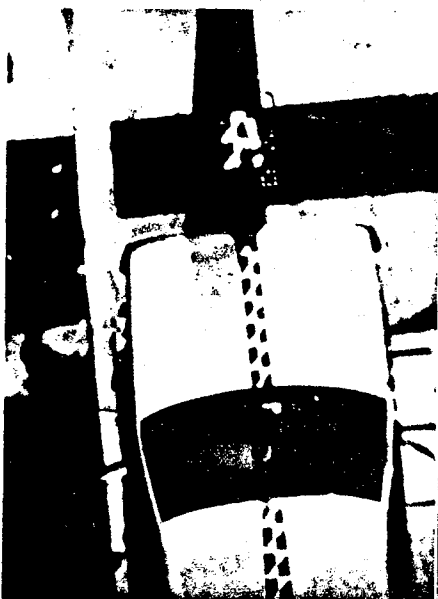


0.080 s

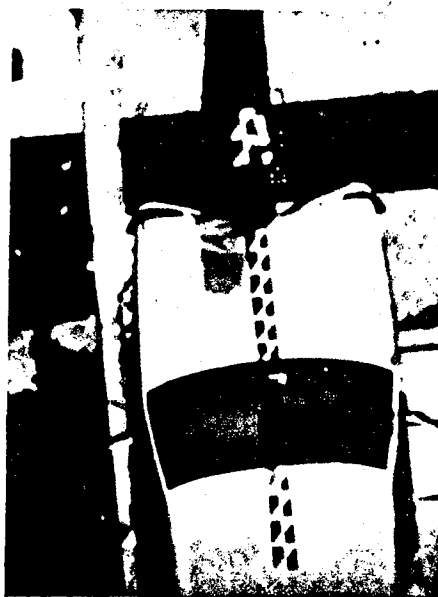


0.128 s

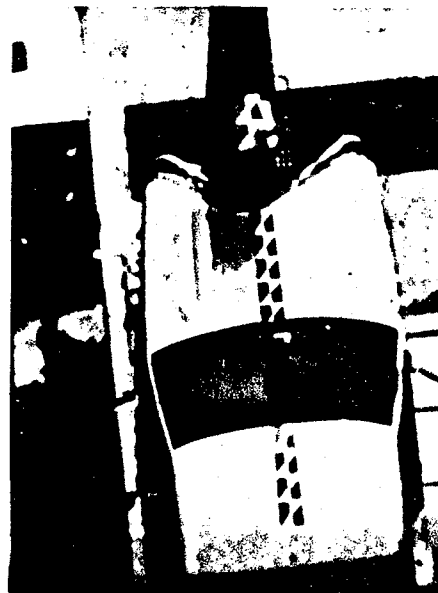
Figure 112. Test photographs during impact, test 96F014.



0.014 s



0.026 s



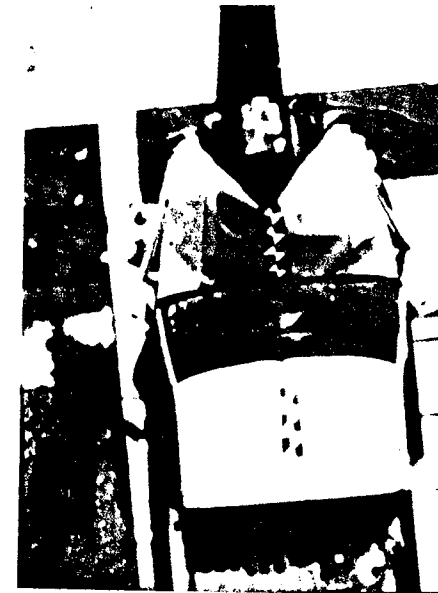
0.040 s



0.060 s



0.074 s



0.094 s

Figure 113. Test photographs during impact, test 96F015.

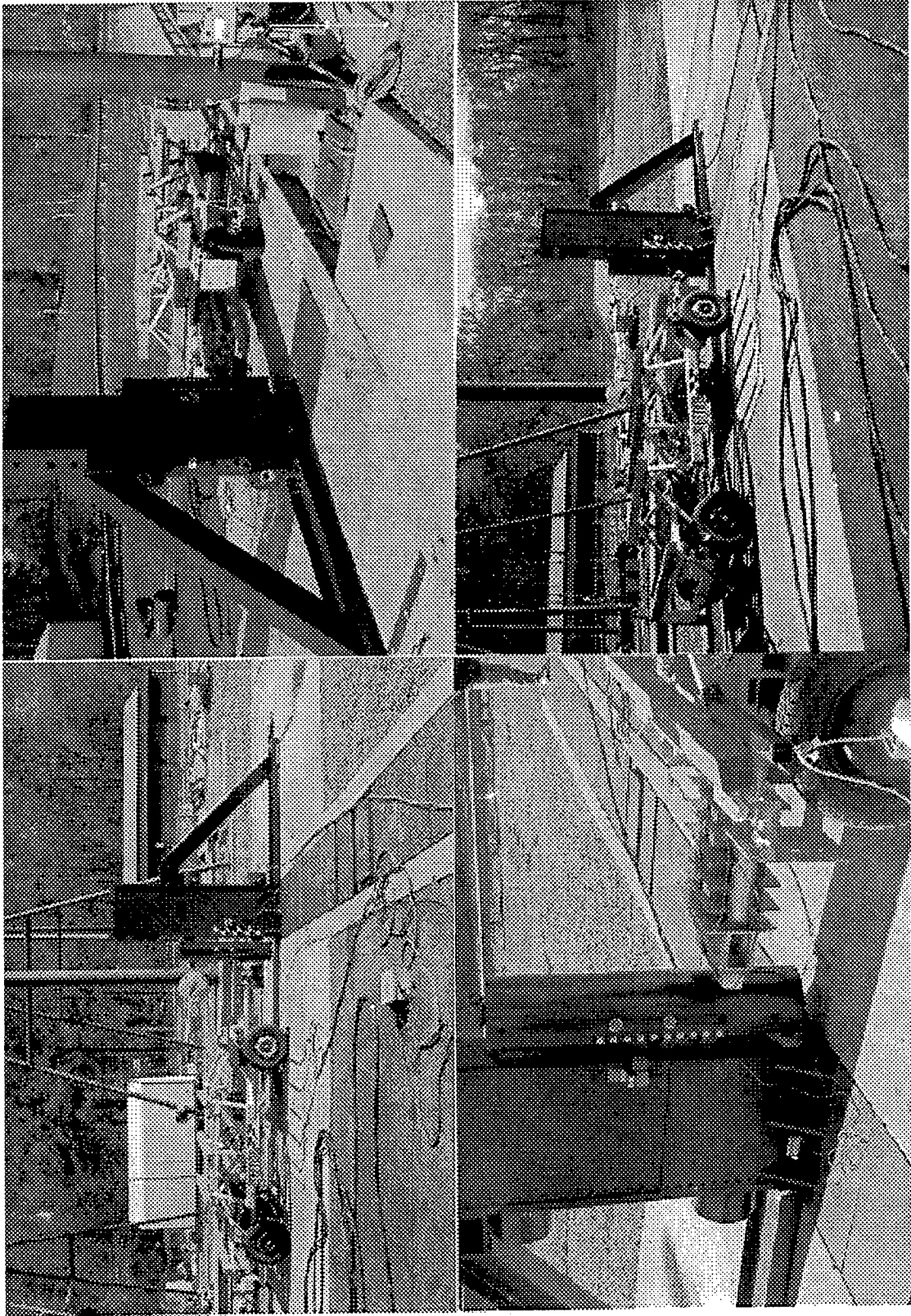


Figure 114. Pretest photographs, test 96F008.

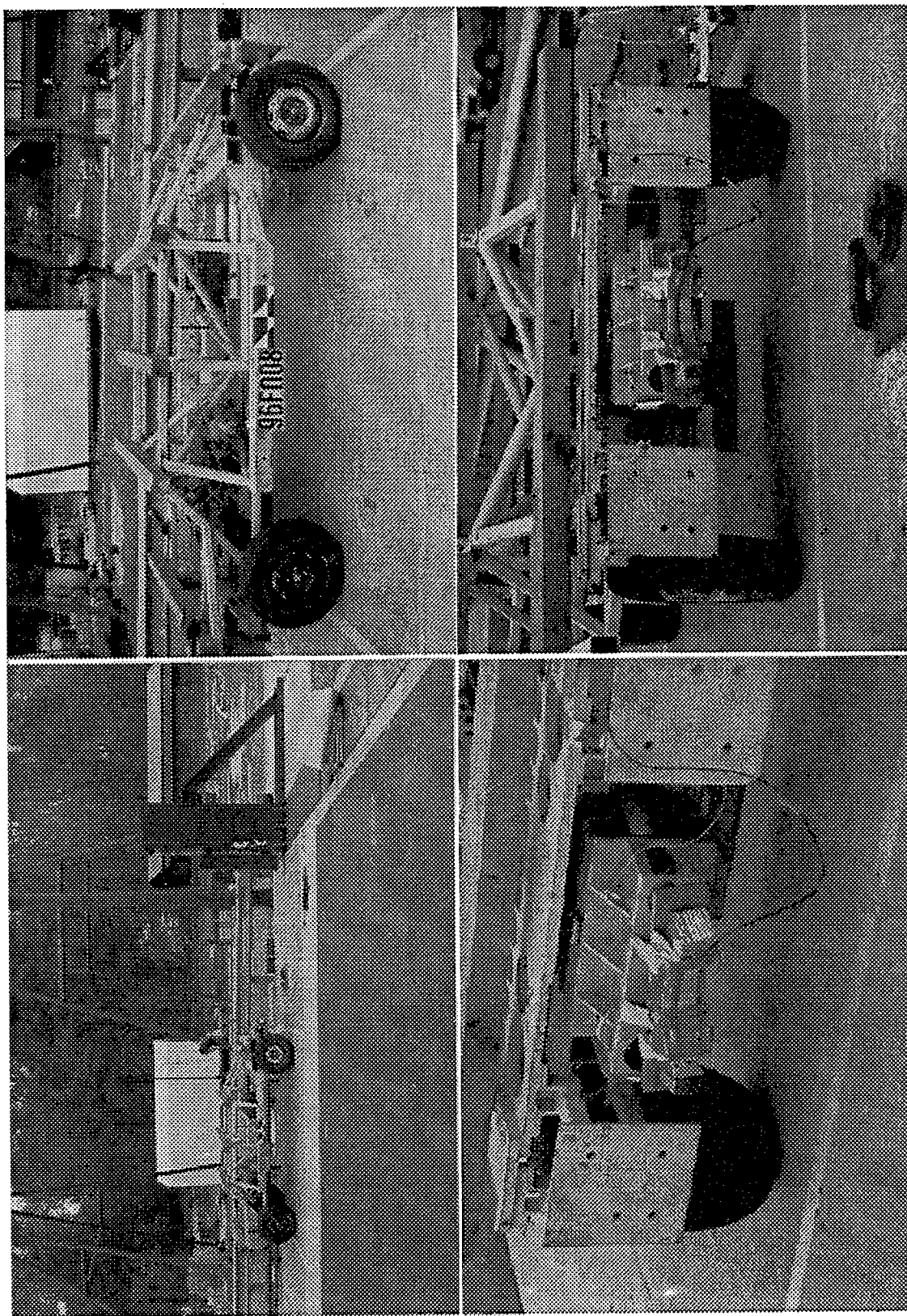


Figure 115. Post-test photographs, test 96F008.

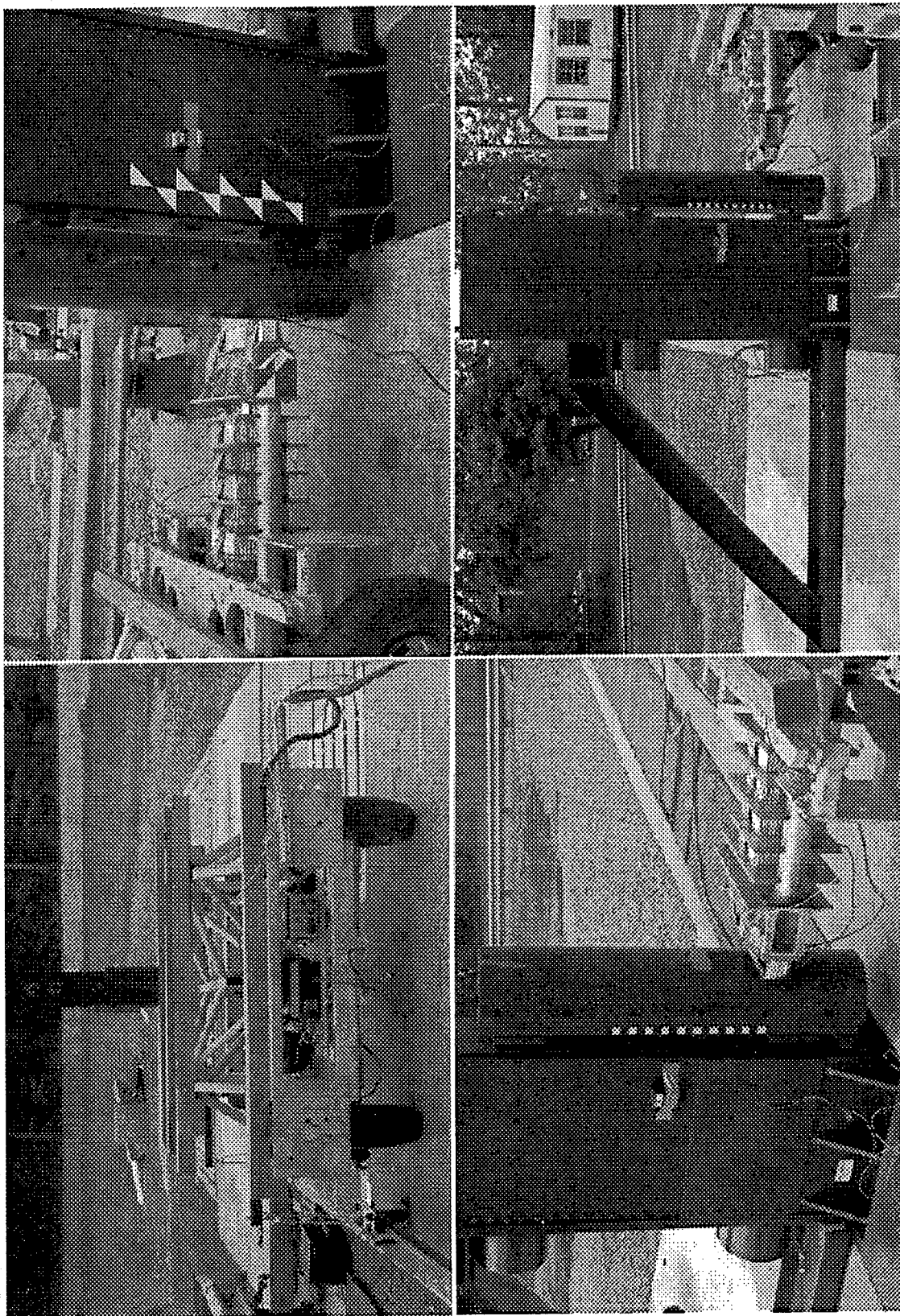


Figure 116. Pretest photographs, test 96F009.

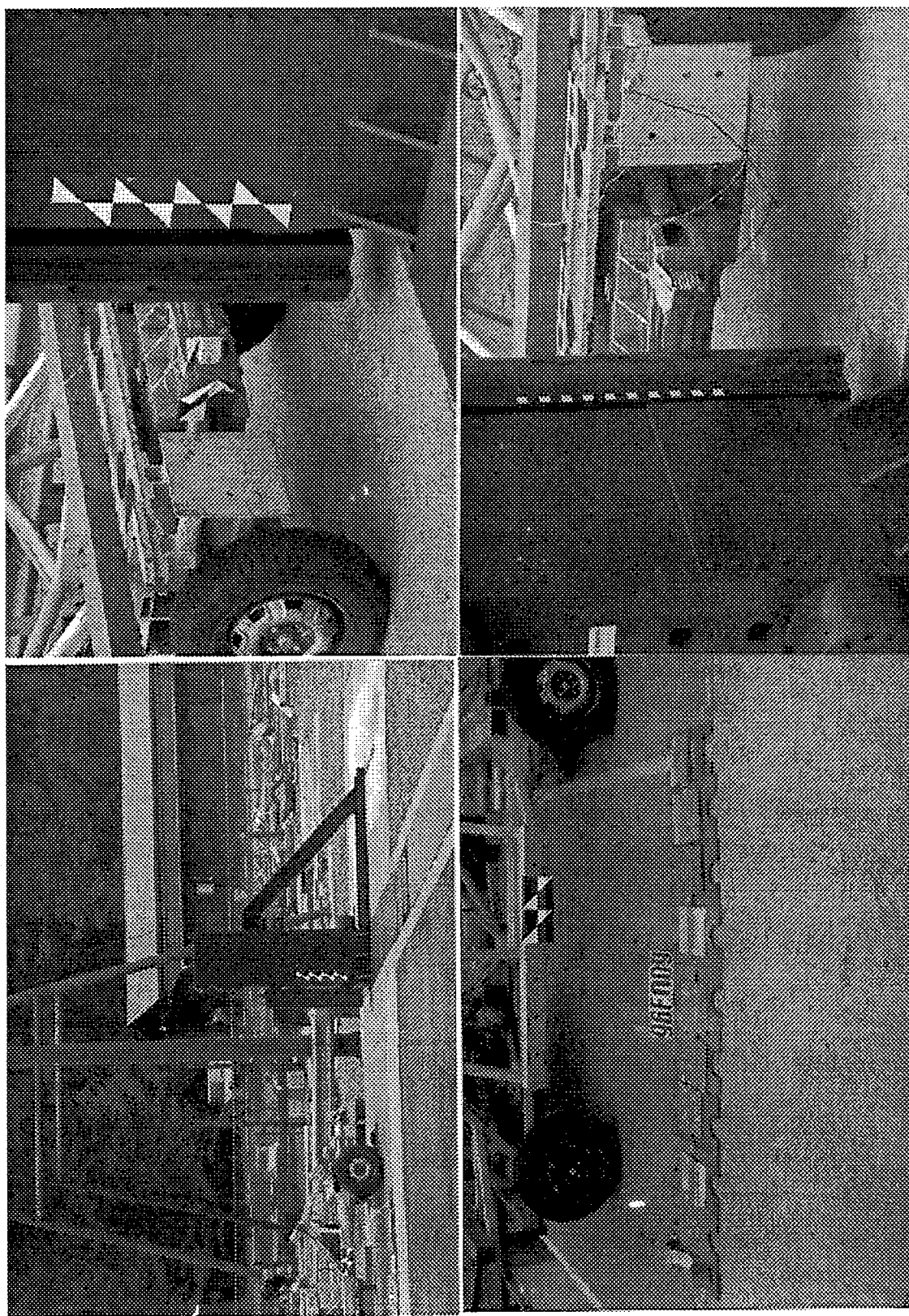


Figure 117. Post-test photographs, test 96F009.

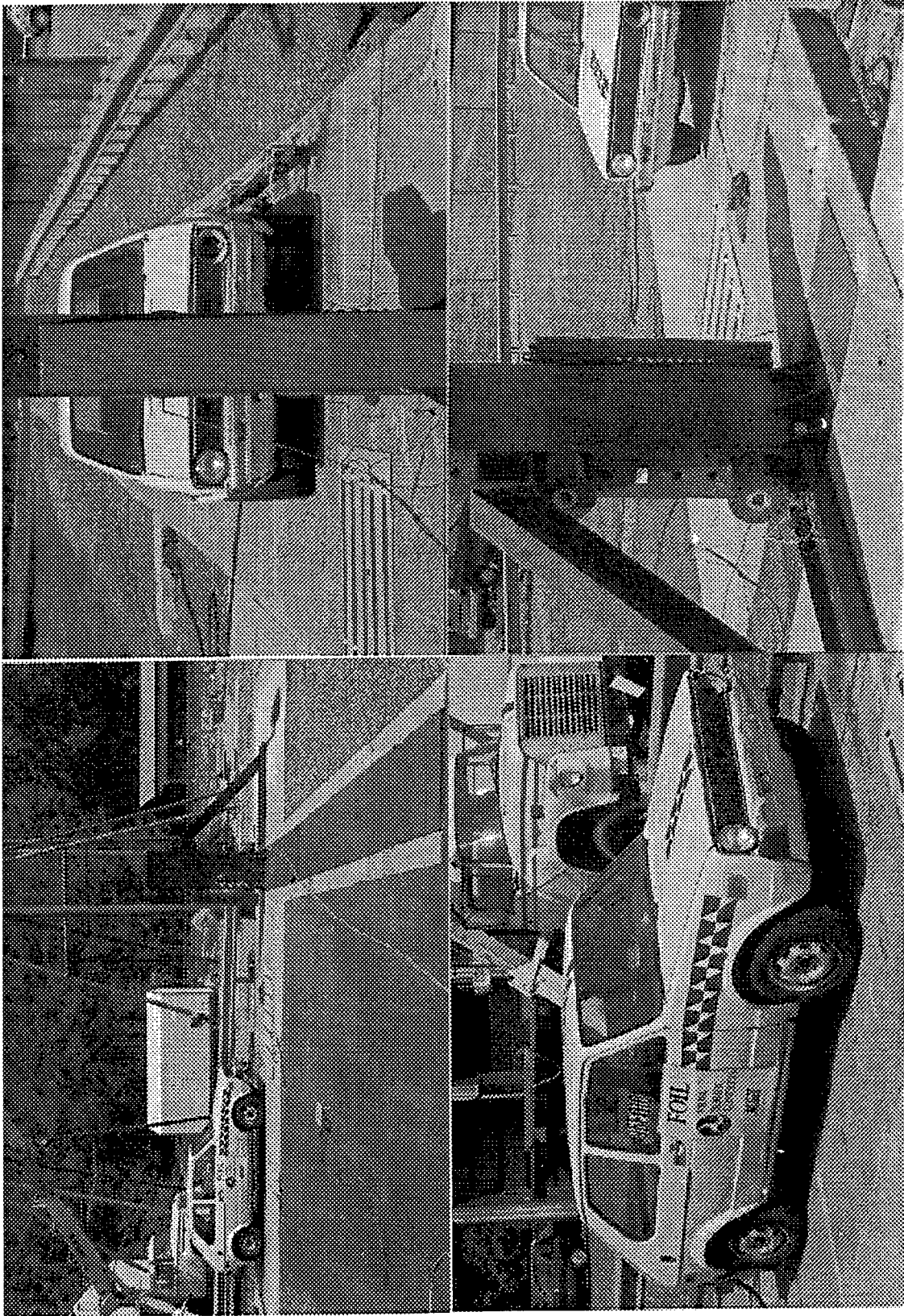


Figure 118. Pretest photographs, test 96F010.

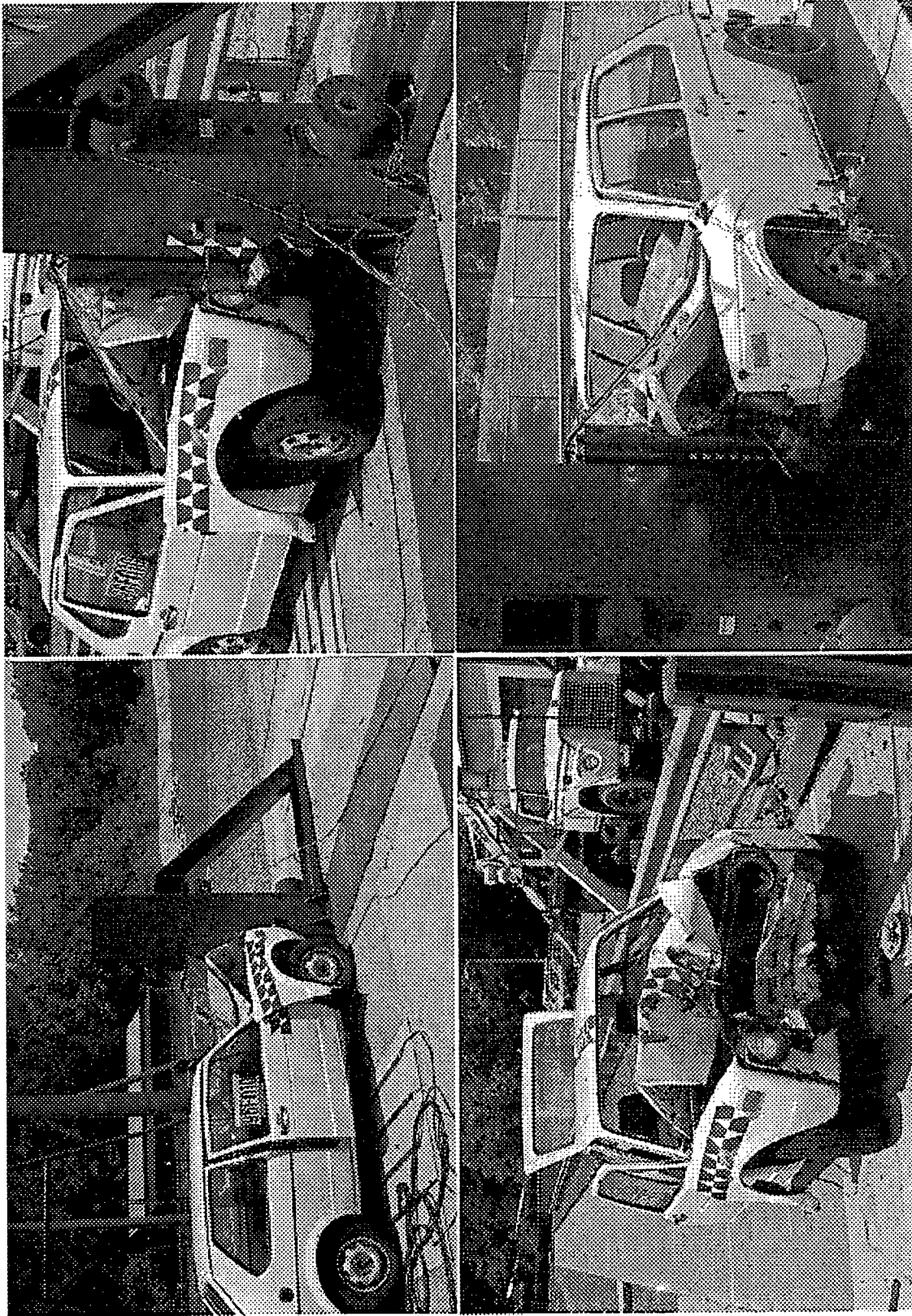


Figure 119. Post-test photographs, test 96F010.

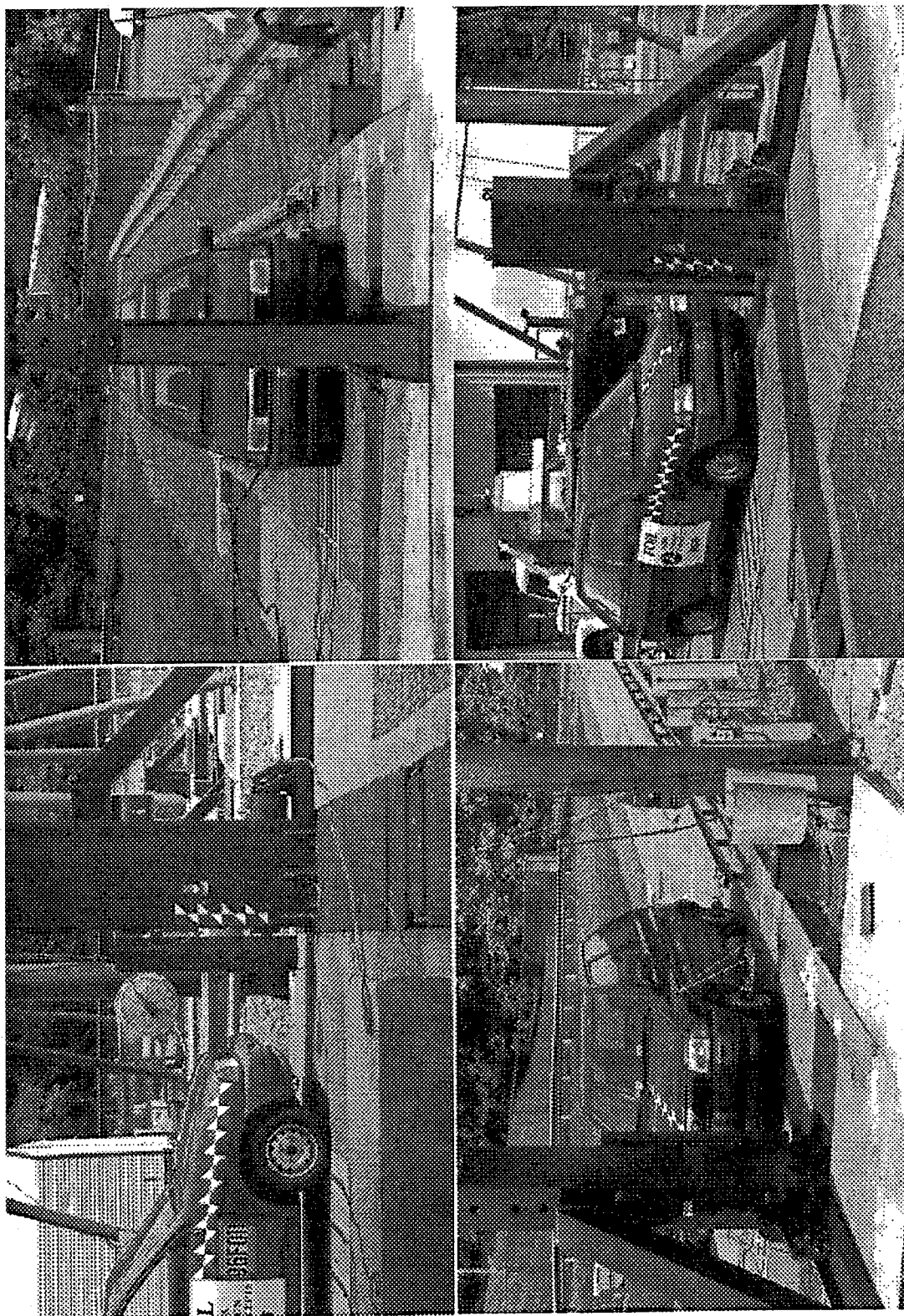


Figure 120. Pretest photographs, test 96F011.

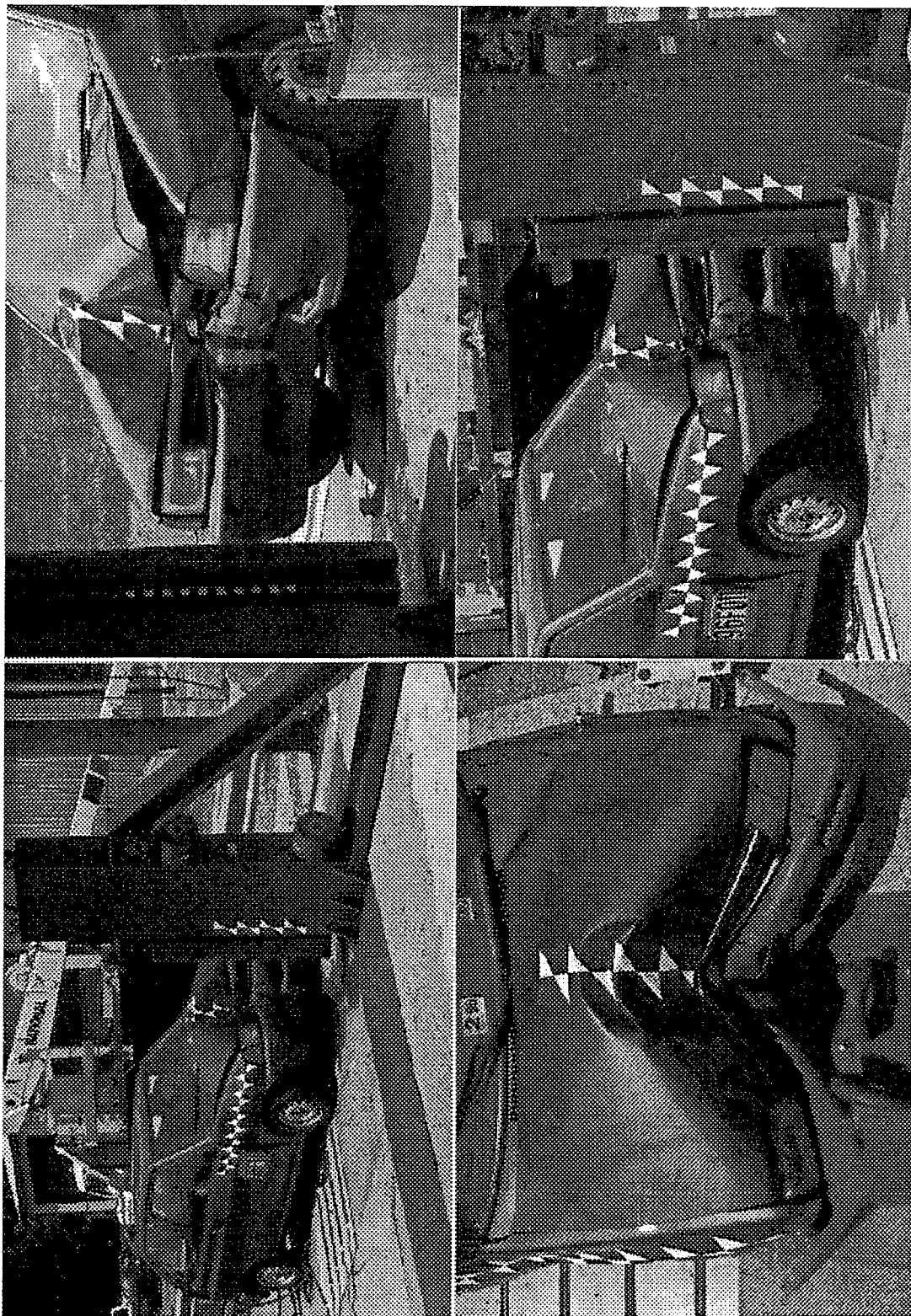


Figure 121. Post-test photographs, test 96F011.

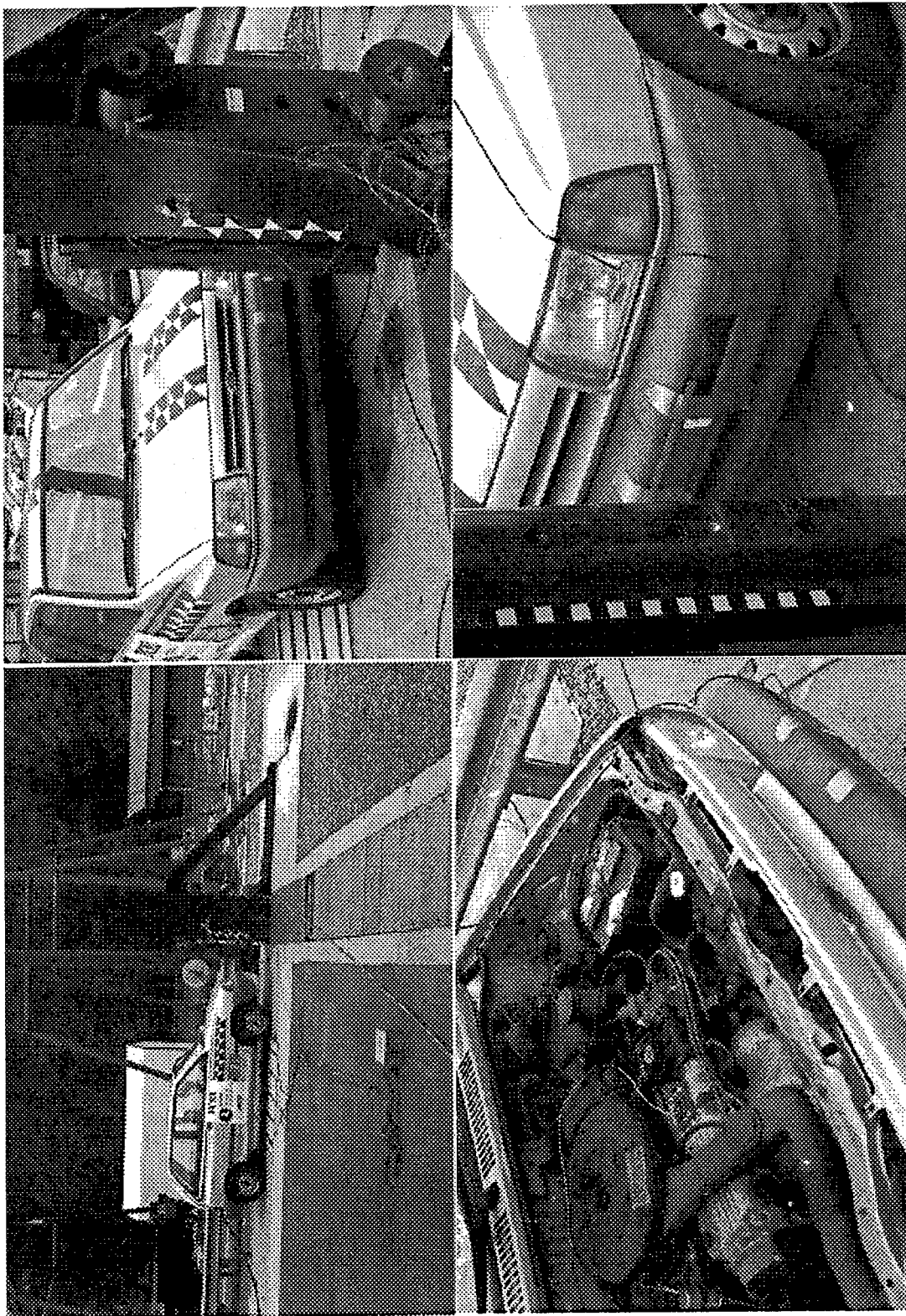


Figure 122. Pretest photographs, test 96F012.

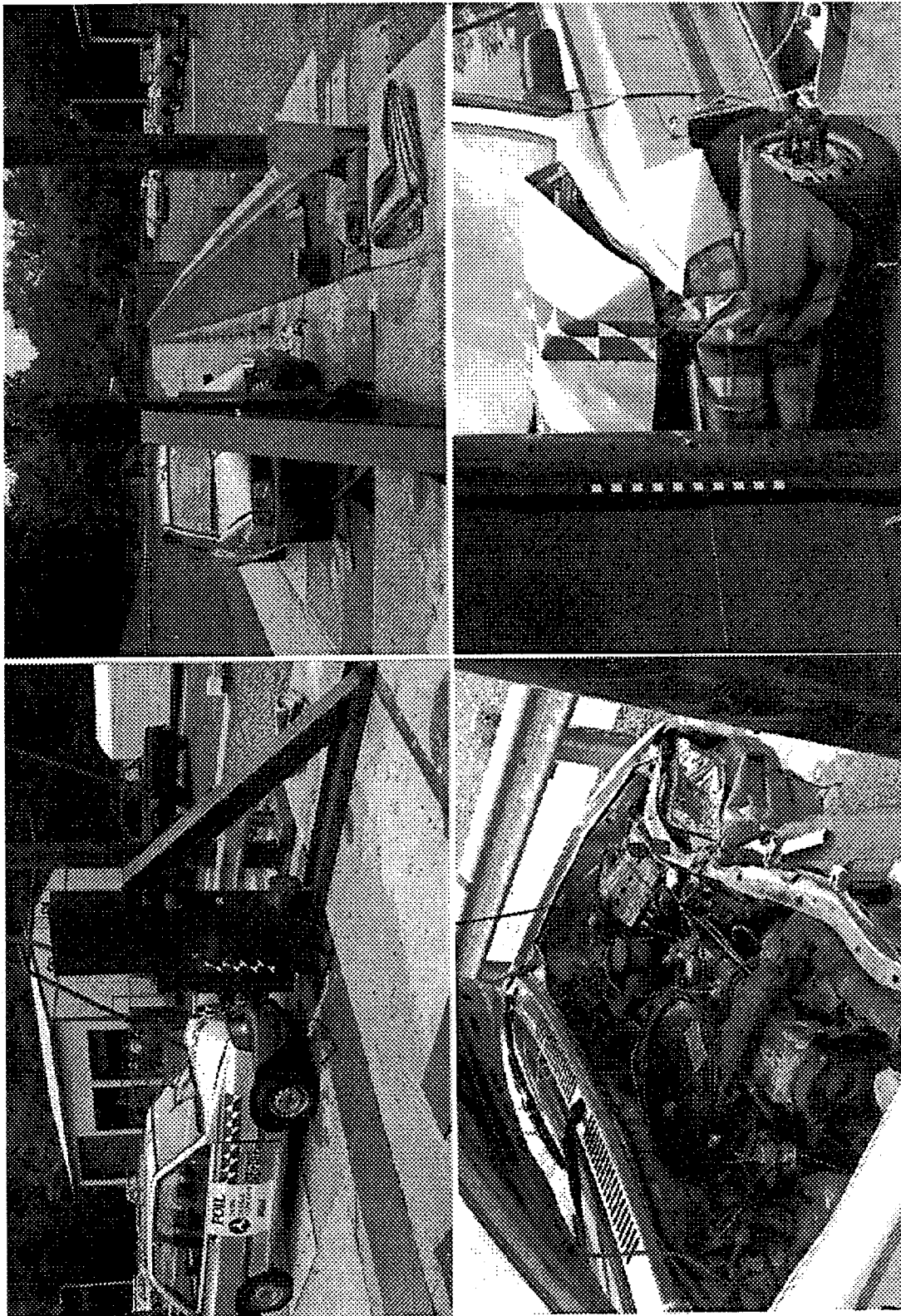


Figure 123. Post-test photographs, test 96F012.

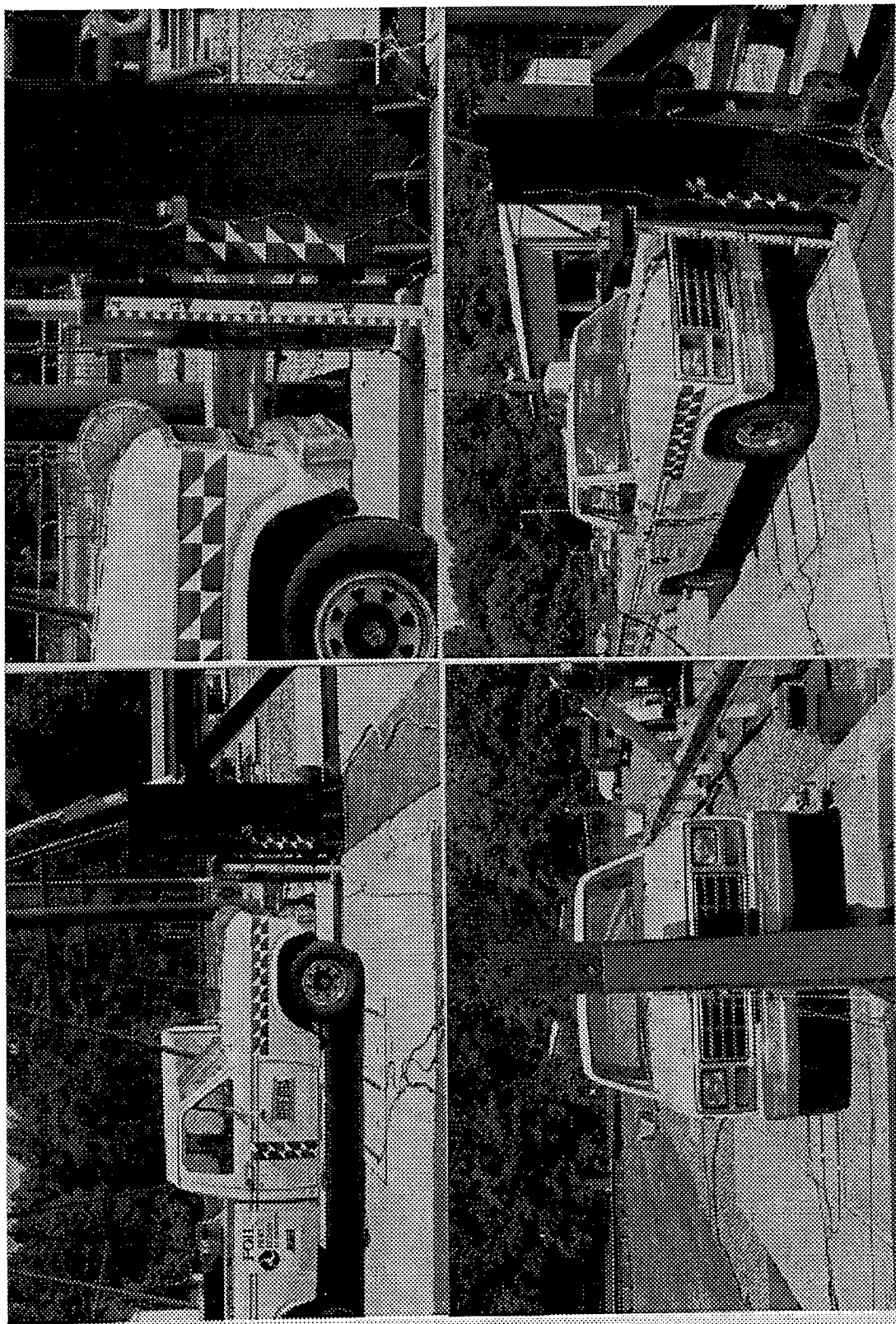


Figure 124. Pretest photographs, test 96F014.

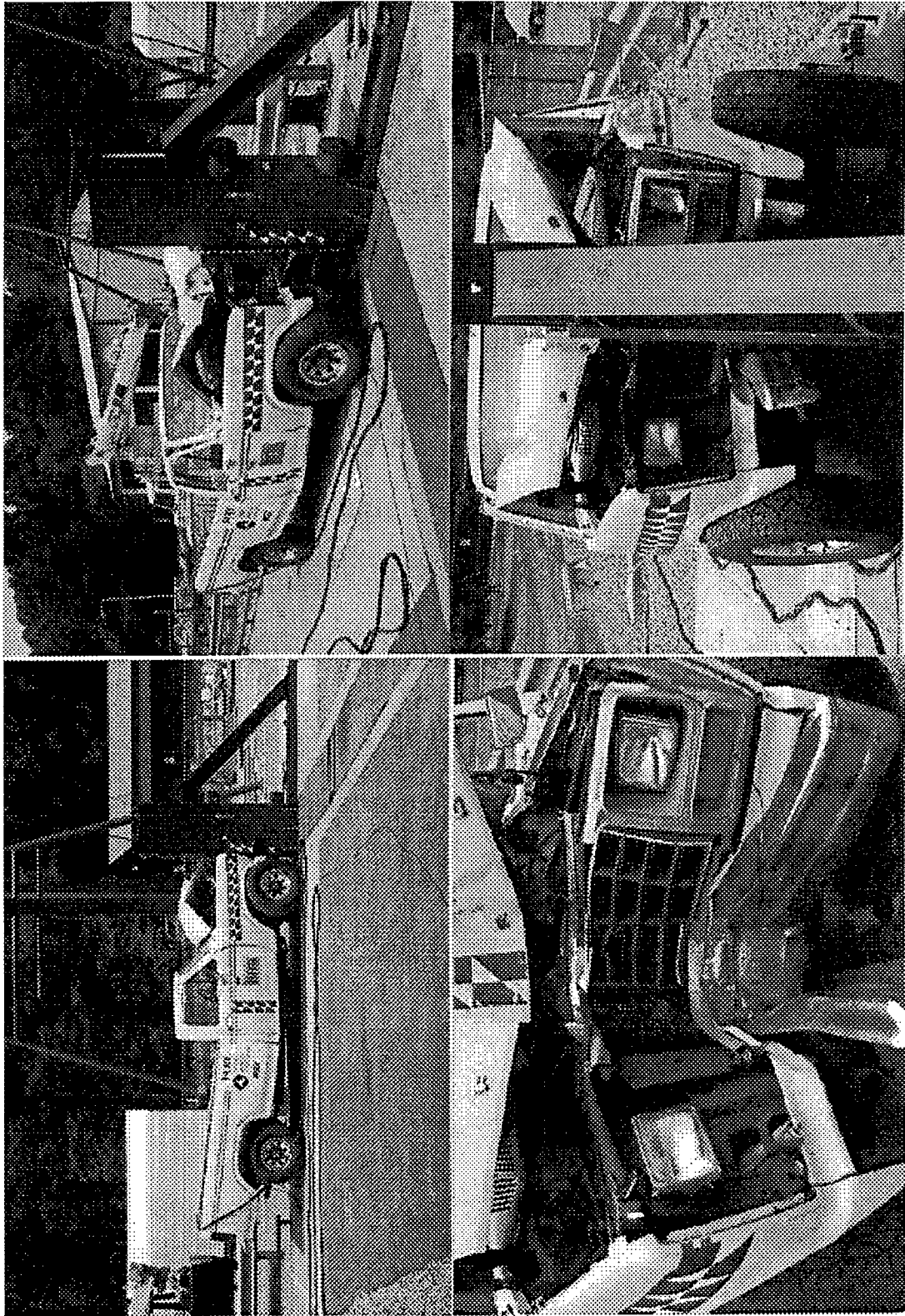


Figure 125. Post-test photographs, test 96F014.

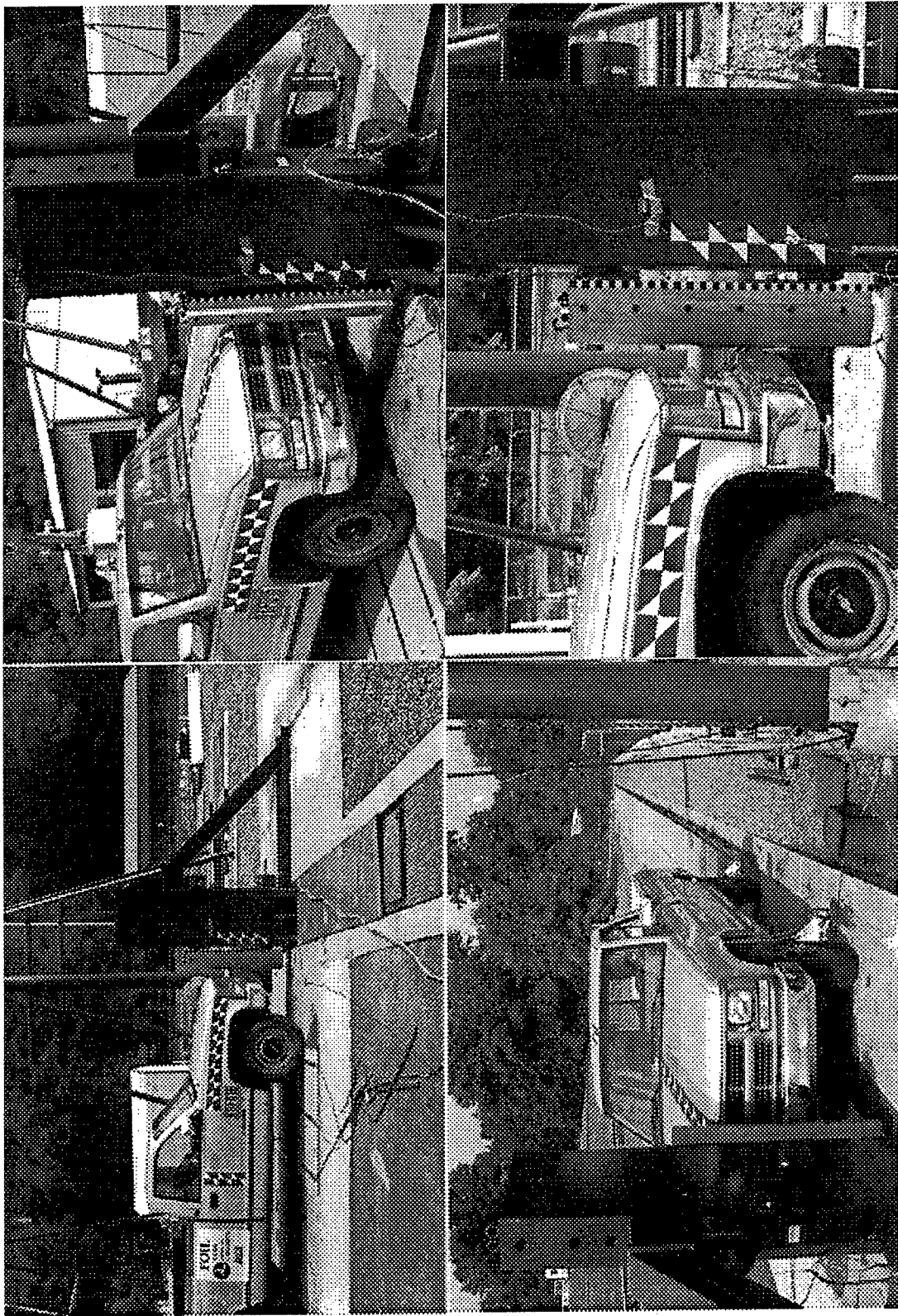


Figure 126. Pretest photographs, test 96F015.

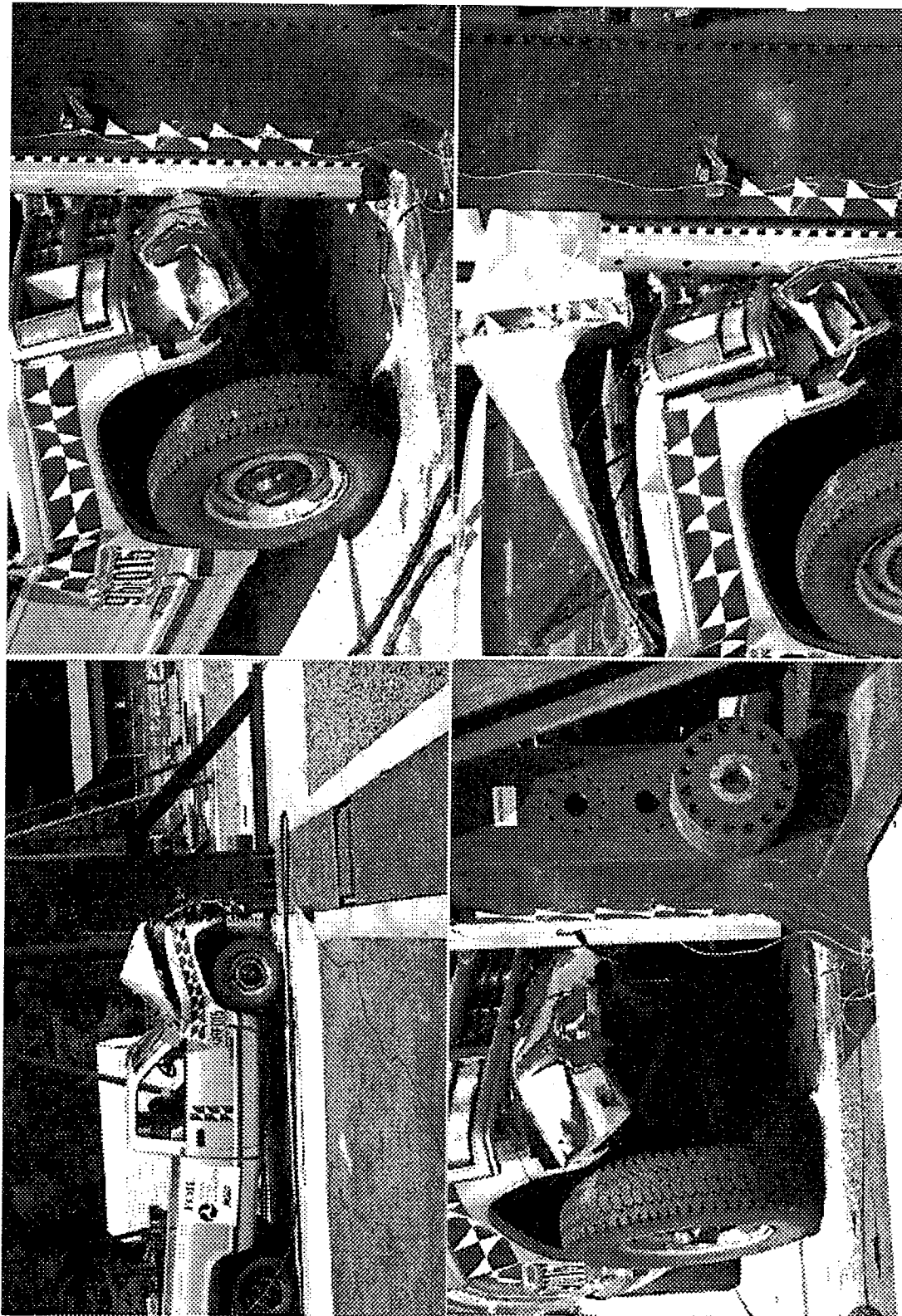


Figure 127. Post-test photographs, test 96F015.

REFERENCES

- (1) H. E. Ross, Jr., D. L. Sicking, R. A. Zimmer, and J.D. Michie, *Recommended Procedures for the Safety Performance Evaluation of Highway Features*, NCHRP Report 350, National Cooperative Highway Research Program, Transportation Research Board, Washington, DC, 1993.
- (2) C. Hott, C. Brown, N. Totani, and A. Hansen, *Crush Characteristics of the "Breakaway" Bogie*, Report No. FHWA-RD-89-107, Federal Highway Administration, Washington, DC, 1990.
- (3) NHTSA, *Laboratory Procedures for Federal Motor Vehicle Safety Standard 208*, National Highway Traffic Safety Administration, Washington, DC, May 1992.
- (4) Brown, Christopher M., *Validation of the ENSCO Surrogate Bogie Vehicle, FOIL Tests 92F028, 92F029, 92F030, and 92F031*, Report No. FHWA-RD-93-074, Federal Highway Administration, McLean, VA, January 1993.
- (5) Brown, Christopher M., *Ford Festiva Collisions With Narrow Objects*, Report No. FHWA-RD-96-129, Federal Highway Administration, McLean, VA, February 1997.

